Using a hierarchy of climate models to investigate snow processes influencing surface albedo

by

Chad William Thackeray

A thesis
presented to the University of Waterloo
in fulfillment of the
thesis requirement for the degree of
Doctor of Philosophy
in
Geography

Waterloo, Ontario, Canada, 2017

Examining Committee Membership

The following served on the Examining Committee for this thesis. The decision of the Examining Committee is by majority vote.

External Examiner	Dr. Aaron Berg Professor University of Guelph Department of Geography
Supervisor(s)	Dr. Christopher Fletcher Associate Professor Department of Geography and Environmental Management University of Waterloo
Internal Member	Dr. Richard Kelly Professor and Chair Department of Geography and Environmental Management University of Waterloo
Internal-external Member	Dr. Andrea Scott Assistant Professor Department of Systems Design Engineering University of Waterloo
Other Member(s)	Dr. Chris Derksen Research Scientist, Environment and Climate Change Canada Adjunct Faculty, University of Waterloo

Author's Declaration

This thesis consists of material all of which I authored or co-authored: see Statement of Contributions included in the thesis. This is a true copy of the thesis, including any required final revisions, as accepted by my examiners.

I understand that my thesis may be made electronically available to the public.

Statement of Contributions

This thesis contains a collection of journal articles that investigate climate interactions with terrestrial snow through changes to surface albedo. All of the manuscripts were a result of collaboration with colleagues, as credited below. For each article, my contribution was to carry out all analysis and write the first edition of the manuscript, along with editing subsequent drafts from the comments and writing of my coauthors (Christopher G. Fletcher; Chris Derksen, and Lawrence R. Mudryk).

The first paper (Chapter 2), published in *Progress in Physical Geography*, provides a detailed review of snow albedo feedback (SAF), while framing the current knowledge, global importance, and outstanding issues related to our understanding. A copyright waiver was not required from the publisher.

Thackeray, C. W., & Fletcher, C. G. (2016). Snow albedo feedback: Current knowledge, importance, outstanding issues and future directions. *Progress in Physical Geography*, *40*(3), 392–408. http://doi.org/10.1177/0309133315620999

The second paper (Chapter 3), published in the *Journal of Geophysical Research: Atmospheres*, uses a number of satellite-derived datasets to evaluate how well the current generation of global climate models simulate the seasonal cycle of climatological snow cover fraction (SCF) and surface albedo. A copyright waiver can be found in the backmatter of this document.

Thackeray, C. W., Fletcher, C. G., & Derksen, C. (2015). Quantifying the skill of CMIP5 models in simulating seasonal albedo and snow cover evolution. *Journal of Geophysical Research: Atmospheres*, *120*(12), 5831–5849. http://doi.org/10.1002/2015JD023325

The third paper (Chapter 4), in preparation for *Journal of Climate*, examines the impact of previously diagnosed model biases on simulated climate (i.e., temperature, snow cover, and atmospheric circulation).

Thackeray, C. W., Fletcher, C. G., & Derksen, C. The impact of simulated surface albedo biases on climate. *In preparation for Journal of Climate*.

The fourth paper (Chapter 5), published in *Journal of Climate*, utilizes a collection of observation-based snow and temperature products to evaluate model simulations of historical and future spring snow cover. A copyright waiver can be found in the backmatter.

Thackeray, C. W., Fletcher, C. G., Mudryk, L. R., & Derksen, C. (2016). Quantifying the Uncertainty in Historical and Future Simulations of Northern Hemisphere Spring Snow Cover. *Journal of Climate*, *29*(23), 8647–8663. http://doi.org/10.1175/JCLI-D-16-0341.1

Abstract

Northern Hemisphere (NH) extratropical land has experienced dramatic warming over the past century, a trend that is expected to continue in the coming decades. There is however, significant uncertainty surrounding projections of climate change. Warming has major impacts on the terrestrial cryosphere, particularly its largest component, snow cover. Snow is a significant climatological variable because of its role in the surface radiative and water balances. The combination of extensive snow cover and relatively high incoming radiation during spring make the NH climate system highly sensitive to concurrent changes in surface albedo, largely tied to snow albedo feedback (SAF). SAF is a positive feedback climate mechanism, whereby an initial warming is enhanced through a reduction in surface albedo resulting from melting snow (revealing a darker, less reflective surface). The current generation of global climate models (GCMs) accurately capture this process on average, but there is a large intermodel spread that arises because of differences in model design. Variability in SAF has been shown to account for 40-50% of the spread in projected NH land warming. To better synthesize the current state of knowledge regarding snow albedo feedback, a review article on the topic was published (Chapter 2). In this chapter, we summarize the importance of SAF, estimates from both models and observations, factors influencing the spread in SAF, and outstanding issues related to our understanding of the physical processes that control SAF.

The remainder of this thesis focuses on the critical evaluation of processes influencing simulated SAF (snow cover and surface albedo). Prior research has shown that a commonly used GCM (Community Climate System Model; CCSM) suffers from a weak bias in SAF over the boreal forest and links this to deficiencies in how it represents snow processes. This model bias is traced to the way snow interacts with the forest canopy layer causing snow-covered surface albedo to decrease prematurely. Following on from this work, we expand our analysis to evaluate all current GCMs to see if this issue is prevalent elsewhere. Using a variety of metrics, the models are shown to have substantial biases in simulated surface albedo over snow-covered land (especially boreal forest and non-boreal

tundra). Model biases are principally tied to either the timing (i.e., CCSM) or magnitude of seasonal changes in surface albedo.

Having demonstrated deficiencies in the simulation of surface albedo, we next determine the impact that these model biases have on climate (Chapter 4). The experimental design overrides the model's (biased) internal calculation of albedo and replaces it with prescribed albedo data, derived from satellite observations, or from another model. Results show that correcting the albedo in CESM (successor of CCSM) pushes the model further away from observed temperature (implying the presence of other biases), with robust cooling during winter and spring. It also induces a pattern reversal of climatological biases in winter sea level pressure, partially correcting the model's tendency towards a positive Arctic Oscillation. Furthermore, biases across the boreal forest region are found to be influential for both local and remote climate features. Models with large albedo magnitude biases are vulnerable to even greater climate impacts than CESM.

Lastly, in Chapter 5, we investigate the uncertainty in historical and future simulations of Northern Hemisphere spring snow cover using data from two climate model ensembles, seven observational snow products, and five temperature datasets. We find that the models underestimate the observed trend in historical snow cover, however, biases are much smaller than identified by previous studies that relied on a single observational dataset. The underestimation can be partially explained by biases in the climatological snow amount (i.e., starting the melt period with not enough snow cover) and a lack of sensitivity to warming in many models. The intermodel spread in future projections of snow cover can be largely explained by differences in simulated warming, and the amount of snow cover available for melt. The strong coupling between these features implies that by reducing the spread in projected NH land warming, uncertainty in snow cover would follow suit.

The overall aim of this research is to improve knowledge of terrestrial snow processes influencing climate through changes in albedo. This thesis encompasses the identification of issues related to the simulation of snow processes in GCMs, and the determination of their importance to climate with the long term aim of helping to reduce uncertainty in projections of climate change.

Acknowledgements

First, I would like to thank Dr. Chris Fletcher and Dr. Chris Derksen for their ongoing guidance and support of my research. I have thoroughly enjoyed our collaboration over the past five years. I would also like to express my appreciation to my current and prior committee members for their helpful comments, Dr. Richard Kelly, Dr. Andrea Scott, Dr. Aaron Berg, Dr. Claude Duguay, and Dr. Bryan Tolson. Thanks are also extended to the members of the Canadian Sea Ice and Snow Evolution (CanSISE) network for their support and constructive feedback over the years. Lastly, I would like to thank my family for everything.

Table of Contents

List of Figures

List of Tables

List of Abbreviations

AATSR – Advanced Along Track Scanning Radiometer

ACCESS – Australian Community Climate and Earth System Simulator

AMIP – Atmosphere Model Intercomparison Project

AO – Arctic Oscillation

APP-x – Polar Pathfinder extended

AVHRR – Advanced Very High Resolution Radiometer

BCC-CSM – Beijing Climate Center-Climate System Model

BNU-ESM – Beijing Normal University Earth System Model

BOR – Boreal albedo experiment

CAA – Canadian Arctic Archipelago

CAM – Community Atmosphere Model

CanESM – Canadian Earth System Model

CanESM-LE – Canadian Earth System Model large ensemble

CCSM – Community Climate System Model

CERES - Clouds and the Earth's Radiant Energy System

CESM – Community Earth System Model

CICE – Community Ice Model

CLM – Community Land Model

CMIP – Coupled Model Intercomparison Project

CNRM-CM - Centre National de Recherches Météorologiques-Climate Model

CO_2 – Carbon dioxide

CRUNCEP – forcing dataset combining CRU and NCEP data

CRUTEM – Climate Research Unit temperature dataset

CSIRO-Mk3.6 - Commonwealth Scientific and Industrial Research Organization Mark 3.6

DGVM – Dynamic Global Vegetation Model

DJF – December-January-February average

EASE – Equal-Area Scalable Earth grid

ERA-I-Land – ERA-Interim Land Reanalysis

ESM – Earth System Model

FGOALS-g2 - Flexible Global Ocean-Atmosphere-Land System model, Grid-point version 2

FMAMJ – February-March-April-May-June average

GCM – Global Climate Model

GCs – Grand Science Challenges

GFDL-ESM – Geophysical Fluid Dynamics Laboratory Earth System Model

GHCN – Global Historical Climatology Network

GHG – Greenhouse gas

GISS – Goddard Institute for Space Studies

GISS-E2-R – Goddard Institute for Space Studies Model E with Russell Ocean Model

GLC2000 – Global Land Cover dataset

GLDAS- Global Land Data Assimilation System

GPH – Geopotential height

HadISST – Hadley Centre Sea Ice and Sea Surface Temperature

HTESSEL – Hydrology Tiled ECMWF Scheme of Surface Exchanges over Land

ILAMB – International Land Model Benchmarking Project

IMS – Interactive Multisensor Snow and Ice Mapping System

INMCM - Institute for Numerical Mathematics Climate Model

IPCC AR5 – Intergovernmental Panel on Climate Change's Fifth Assessment Report

IPSL-CM – Insitut Pierre Simon Laplace Climate Model

IQR – Interquartile range

ISCCP – International Satellite Cloud Climatology Project

LAI – Leaf area index

LP DAAC – Land Processes Distributed Active Archive Center

MA – March-April average

MAMJ – March-April-May-June average

MERIS – Medium Resolution Imaging Spectroradiometer

MERRA – Modern Era Retrospective Analysis for Research and Applications

MIROC – Model for Interdisciplinary Research on Climate

MJ – May-June average

MM – Multi-model mean

MM_{med} – Multi-model median

MODIS – Moderate Resolution Imaging Spectroradiometer

MPI-ESM – Max Planck Institute for Meteorology Earth System Model

MRI-CGCM – Meteorological Research Institute Coupled General Circulation Model

NA – North American albedo experiment

NAO – North Atlantic Oscillation

NASA – National Aeronautics and Space Administration

NCAR – National Center for Atmospheric Research

NCDC – National Climatic Data Center

NCEP – National Centers for Environmental Prediction

NET – Total snow albedo feedback

NH – Northern Hemisphere

NH_{snow} – Northern Hemisphere snow covered region

NOAA CDR – National Oceanic and Atmospheric Administration climate data record

NorESM – Norwegian Earth System Model

OBS – Observed snow albedo feedback

OBS_{blend} – Blended surface albedo dataset from Thackeray et al., (2015)

PFT – Plant functional type

R – Correlation coefficient

RCP – Representative Concentration Pathway

SAF – Snow albedo feedback

SCE – Snow cover extent

SCF – Snow cover fraction

SH – Southern Hemisphere

SIE – Sea ice extent

SLP – Sea level pressure

SNC – Snow cover component of snow albedo feedback

SnowMIP – Snow Modeling Intercomparison Project

SON – September-October-November average

SPOT- Satellite pour l'observation de la terre

SS – Skill score

SST – Sea surface temperature

SWE – Snow water equivalent

SWM – Snow water mass

SZA – Solar zenith angle

TEM – Temperature metamorphism component of snow albedo feedback

TOA – Top of the atmosphere

WACE – Warm Arctic-Cold Eurasia

WEU – Western Eurasian albedo experiment

Chapter 1

Introduction

1.1 Background

Global mean surface temperature has increased drastically since the start of the industrial revolution, with a much more rapid rate of change over the last half century. The global warming trend is closely tied to a steep rise in greenhouse gas concentrations (Trenberth and Fasullo, 2013). According to a collection of independent observationally-based datasets (CRUTEM, GHCN, GISS and Berkeley), warming over recent decades (1979-2012) exceeds 0.25°C decade^{-1} (Hartmann et al., 2013). Moreover, this does not account for the three warmest years on record, which have all occurred since 2014 (GISTEMP Team, 2017; Hansen et al., 2010). Large regional variability exists within the temperature record, with enhanced warming over the Northern Hemisphere (NH) mid-high latitudes (Hartmann et al., 2013). Furthermore, the Arctic is experiencing the greatest rise in temperature, warming at double the rate of the global average (Figure 1-1; referred to as Arctic amplification). Heightened Arctic warming has major implications for several aspects of the climate system, particularly the cryosphere. One of the primary mechanisms driving Arctic amplification is the reduction of surface albedo (reflectivity) due to shrinking snow cover and sea ice (Serreze and Barry, 2011; Pithan and Mauritsen, 2014).

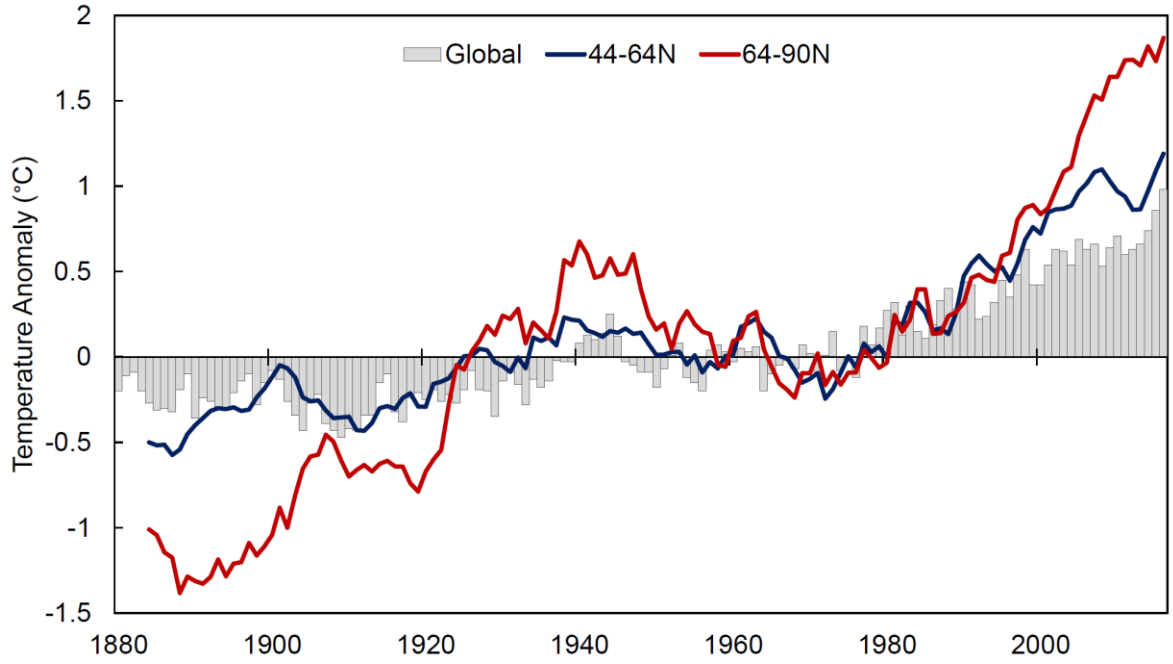

Figure 1-1: Change in annual global mean surface temperatures (°C) since 1880 (bars), and 5-year running mean regional temperature anomalies for the Northern mid-latitudes (blue line), and Arctic (red line). The changes are shown as differences from the 1951-1980 average values (data from GISTEMP Team, 2017; Hansen et al., 2010).

Snow cover plays an important role in the climate system, reducing incoming radiation absorbed at the surface through its extremely reflective nature. Fresh snow has an albedo of 0.8-0.9, and gradually becomes more absorbent as it ages (albedo of 0.4-0.5) (Wiscombe and Warren, 1980). This reduction in albedo can be attributed to several factors, including but not limited to grain size and shape, snow depth, and impurities such as aerosols or dust (Warren, 1984; Doherty et al., 2010). Snow metamorphism (change to grain size and shape) occurs because snow grains are highly sensitive to variations in temperature and liquid water content (Colbeck, 1982). Larger grain size makes it more likely that incoming radiation is absorbed by snow particles because a greater distance must be covered by incident energy (Warren et al., 1998).

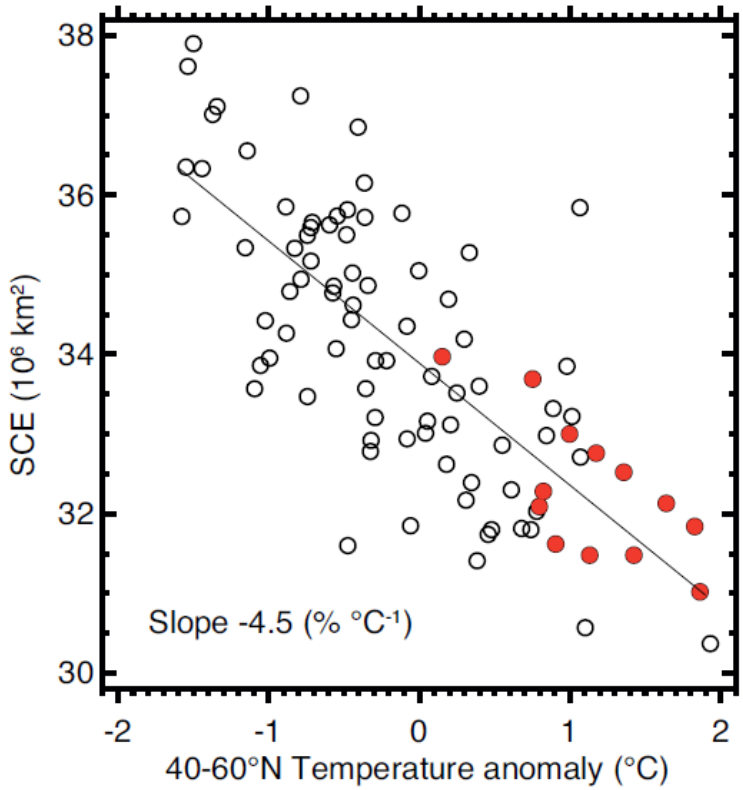

Figure 1-2: Relationship between NH April SCE and corresponding land air temperature anomalies over 40 to 60 from CRUTEM4. Red circles indicate 2000-2012. Updated from Brown and Robinson (2011), (Vaughan et al., 2013).

Snow cover extent (SCE) naturally varies from year-to-year depending on climatic conditions, but on average approximately 48 million km^2 of NH land is covered during late winter (Hall, 1988; Robinson and Frei, 2000). However, with recent warming, a sharp decline has been shown in SCE during spring (Brown et al., 2010; Brown and Robinson, 2011; Derksen and Brown, 2012; Figure 1-2). The greatest snow cover losses have occurred at higher latitudes because of stronger albedo feedbacks (Dery and Brown, 2007; Vaughan et al., 2013). It should be noted that prior estimates may have been slightly exaggerated because of the use of a single observational dataset (further discussed in Chapter 5 and Mudryk et al., 2017).

The impact of snow on surface fluxes can be strongly affected by vegetation. A significant piece of NH snow-covered area is heavily vegetated, creating an environment where complex interactions between snow and vegetation take place. The boreal forest occupies nearly 25% of this region (Bonan et al., 1992), and for much of it, snow is present for more than half of the year. It consists of three principal forest types; needleleaf evergreen, needleleaf deciduous, and broadleaf deciduous. The most expansive of these is the needleleaf evergreen boreal forest, which is somewhat unique in that it retains its canopy throughout the winter. This is climatologically important because snowfall over forests either reaches the surface or is intercepted by the canopy layer, canopy snow resides for some variable time before either being sublimated or dripping/falling to the surface (Hedstrom and Pomeroy, 1998; Storck et al., 2002; Rutter et al., 2009). Prior research has shown that half of cumulative snowfall is intercepted by the canopy layer during mid-winter (Pomeroy and Schmidt, 1993; Storck et al., 2002). However, the canopy (even when it holds intercepted snow) also acts to mask the underlying snow on the ground, reducing surface albedo, and warming the surface. The masking of underlying snow makes the circumpolar boreal forest stand out during the snow season due to its low albedo (~0.3) (Thomas and Rowntree, 1992; Barlage et al., 2005; Essery, 2013; Figure 1-3). This is also why the boreal region has a greater biogeophysical impact on temperatures than any other landcover type (Snyder et al., 2004; Bonan, 2008).

Seasonal snow cover also plays a key role in hydrological and land surface processes. Its low thermal conductivity also makes snow an effective insulator, which moderates soil

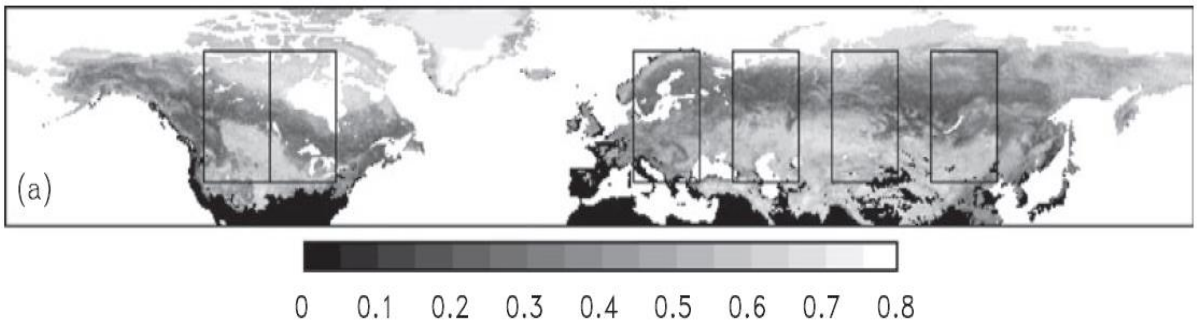

Figure 1-3: Average albedo for land with snow cover from MODIS. Black pixels have missing data or no observed snow cover for 2006-2010 (Essery, 2013).

temperatures and influences permafrost extent (Lawrence and Slater, 2010; Vaughan et al., 2013). The buildup of snow during winter is also a vital process in the terrestrial water balance. Snow acts as a natural reservoir, storing massive amounts of water that can be released during warmer months when demand is greatest (Gunther et al., 2007; Barnett et al., 2008). In fact, snowmelt generates a portion of the water supply for approximately one-sixth of Earth's population (Barnett et al. 2005; Mankin et al. 2015). Therefore, it is important that we fully understand the potential impacts of future climate warming on snow.

1.1.1 Global Climate Models

Rising greenhouse gas concentrations are expected to drive considerable changes to climate over the next century. It is anticipated that these alterations will vary dramatically by region, with diverse patterns of temperature and precipitation change around the world. Global Climate Models (GCMs) serve as the best tools for understanding the potential effects of climate change. GCMs are three-dimensional numerical depictions of the climate system used to examine the climate's response to past, present, and future external forcing (i.e., greenhouse gases). They represent the transfer of energy, mass, and momentum across the globe as well as interactions between the atmosphere, ocean, cryosphere, and land surface.

More recently, the incorporation of the biogeochemical processes (i.e. carbon, nitrogen cycling) has seen the transition to Earth System Models (ESMs; Flato, 2011). There is a hierarchy of models with varying degrees of complexity, which have different ways of simulating these natural processes. Climate models typically have a horizontal resolution of between 1-3 degrees, and a vertical structure made up of between 10 to 30 layers. The state of each layer and grid cell is calculated at every time-step (ranging from 15 minutes to a couple hours). Models are deemed as more reliable when providing projections of future climate if they can first demonstrate success at reproducing the past. Thus, it is important to examine whether models can accurately simulate observed climate features. This typically involves comparing model output to some observed quantity. In this thesis, we explore the use of numerous observation-based datasets to evaluate model performance.

There are however limitations to using climate models, many of which stem from issues with resolution or a lack of knowledge about certain processes. Uncertainty in climate model output comes from a variety of sources. First, there are many physical processes that must be parameterized because they occur at too fine of a spatial scale to be calculated by the models (i.e., snow metamorphism). This type of approximation is a key source of error. Uncertainty is also derived from the representation of complex climate feedback mechanisms related to warming, water vapor, oceans, clouds, and surface albedo. Differences in how each model represents certain phenomena and climate feedbacks can cause a wide range of responses to identical forcing. Projections of climate change are inherently more complicated because of the added influence of internal climate variability (climate noise) and the many unknowns regarding our future trajectory (i.e., population, policy). Climate projections are

generated for several greenhouse gas emissions scenarios (called Representative Concentration Pathways; RCPs), which produce various levels of radiative forcing by the end of the century (Moss et al., 2010; Collins et al., 2013). Using the output from many models in a multi-model ensemble framework allows for more reliable projections than using a single climate model (Bohn et al., 2010). Therefore, model output can be highly variable depending on the quantity of interest and the forcing pathway.

Much of the research contained within this thesis is designed to identify model biases that may contribute to uncertainty in future projections. The primary focus is on better understanding the model uncertainty stemming from surface albedo feedback as it relates to shrinking terrestrial snow cover, defined as the snow albedo feedback (SAF). SAF is a positive feedback mechanism, whereby rising air temperatures cause snow to recede and reveal a much less reflective land surface. The added absorption of incident radiation results in enhanced warming (Holland and Bitz, 2003; Hall, 2004). There is a considerable intermodel spread within the current generation of climate models regarding the strength of SAF (Qu and Hall, 2014; Fletcher et al., 2015), which can explain a large amount of variability in projected NH land temperatures (Qu and Hall, 2014). A more complete synthesis of this topic is provided in Chapter 2. Furthermore, to better understand simulated SAF, it is important to discuss how snow is represented in climate models.

1.1.2 Modeling of Snow

The land component of a GCM represents a wide array of biogeophysical processes characterizing the movement of energy, heat and moisture between vegetation, soil and snow

surfaces, and the atmosphere (i.e., Lawrence et al., 2011; Prentice et al., 2015). There has been extensive model development related to these processes in recent decades as knowledge of their importance to climate change (through feedbacks) grew stronger (Pitman, 2003; Flato et al., 2013; Clark et al., 2015). The snow surface can vary greatly by model (Slater et al., 2001; Boone et al., 2004), with different parameterizations for snow albedo, snow cover fraction, snow density, thermal conductivity, and evaporation, just to name a few. Some models represent the snow surface as one (Bartlett et al., 2006; Voldoire et al., 2013) or more (Schmidt et al., 2006; Oleson et al., 2010; Kowalczyk et al., 2013) distinct levels above the soil system, whereas less-sophisticated, so called zero-layer schemes adapt the characteristics of soil to match the properties of snow cover (de Rosnay and Polcher, 1998; Best et al., 2011). Moreover, there are differences in how models calculate snow albedo and its evolution with time. Some schemes allow snow albedo to change with temperature or snow age, whereas others elect to keep it constant (Slater et al., 2001; Bartlett et al., 2006; Qu and Hall, 2007; Essery et al., 2009; Kowalczyk et al., 2013). Simulated surface albedo also depends on the way in which fractional snow cover is parameterized. A common approach is to relate a given snow depth to snow cover fraction (in an empirical or conceptual way) through snow depletion curves (Essery et al., 2013).

Snowpack dynamics are extremely complicated and difficult to simulate, because what begins as a single snow layer with constant grain size and density, becomes a multi-layered object featuring ice lenses, wind crusts, and large variability in grain size (MacKay et al., 2006). Vegetation adds another dimension to the difficulty involved with simulating snow processes. The sizeable overlap between snow covered areas and forested landscapes

creates a variety of climatologically-important forest-snow interactions (i.e., interception, throughfall, drip, masking). Parameterizations of these processes are fairly rudimentary in many cases because of a lack of knowledge about the physical exchanges that take place within the canopy and between levels. Simulations of snow throughout the winter can diverge between models depending on how each model deals with forest-snow processes (Rutter et al., 2009). Despite intercepting nearly half of annual snowfall (Storck et al., 2002), the canopy layer masks the more reflective underlying snow surface. There are several ways in which this process can be illustrated, with differences linked to a large intermodel spread in SAF (Qu and Hall, 2007). Models with a simple forest representation (minimal canopy structure) tend to produce albedo values that are biased high and thus, a stronger SAF. On the other hand, models with a specific parameterization for individual canopy types tend to have albedo values that are biased low (Qu and Hall, 2007; Kuusinen et al., 2012). Further discussion of this topic can be found in Section 2.5.2.

Model intercomparison studies show that simulations of snow variables differ greatly in their accuracy. Despite differing levels of sophistication, there is a general consensus that no snow model consistently outperforms the rest, especially when considering several sites (Etchevers et al., 2004; Rutter et al., 2009; Essery et al., 2013). These studies also find that intermodel variance is greatest during the melt period. Following warming events (temperatures above freezing for more than two days), model divergence in simulated snow water equivalent (SWE) and albedo is greatest (Rutter et al., 2009). Some of this discrepancy is linked with mixed precipitation events and how rain/snow is partitioned (Rutter et al., 2009; Essery et al., 2013). This implies that models are most sensitive to differences in their

parameterizations during spring. Because of this fact and the greater importance of snow to climate in spring (Qu and Hall, 2007), much of the following research focuses on this time frame. Some of these topics are covered in greater detail by Thackeray (2014).

1.2 Motivation for Research

It is imperative to examine climate models in order to better understand aspects of the Earth system and direct future model improvements. In particular, snow processes must be evaluated because of their influence on regional climate through SAF. Evaluating simulated snow can be challenging because of sparse surface monitoring across the high latitudes (Brown, 2000; Slater et al., 2017) and a lack of confidence in satellite retrievals over snow-covered regions because of extensive winter cloud cover (Hall and Riggs, 2007). To combat these issues, a multi-observational approach is taken throughout this thesis. This prevents reliance on a single (possibly flawed) dataset.

The high-latitude and mountainous regions where snow resides are projected to experience some of the greatest changes due to global warming. We can gather some idea of how future changes to snow cover will occur by extrapolating the current seasonal evolution. This is because snow albedo feedback occurs similarly in the melt period and under future warming (Qu and Hall, 2007; Qu and Hall, 2014). However, there is a large intermodel spread in SAF strength under both contexts. This is important because variability in SAF explains 40-50% of the spread in projected NH land warming (Qu and Hall, 2014). Therefore, extensive evaluation of processes influencing SAF is needed. Chapter 2 serves to

synthesize recent progress regarding knowledge of SAF over recent decades, whereas the rest of this thesis looks at specific process-based analysis of models.

Much of the motivation for Chapter 3 comes from the findings of Thackeray et al., (2014). They show that a commonly used climate model (Community Climate System Model, version 4; CCSM4) suffers from a weak bias in SAF over the boreal forest because of deficiencies in how it represents snow processes. In particular, the model bias is traced to the way snow interacted with the forest canopy layer in the land model. A temperature switch within the parameterization for intercepted snow means that when temperatures rise above freezing, even for a single time step, all snow on the canopy is instantaneously melted. This results in an unrealistically early transition from a snow-covered to a snow-free canopy, and produces large differences between simulated and observed monthly albedo (Figure 1-4). This chapter (Thackeray et al., 2015) seeks to determine the prevalence of such issues within the current generation of global climate models. It is plausible that the same issues could exist elsewhere because many GCMs are related (Knutti, 2010), meaning that they share some parameterizations.

After biases in snow-covered surface albedo have been assessed within the CMIP5 ensemble, the importance of these biases is examined in Chapter 4. Biases of a certain magnitude likely have some impact on climate simulations as the albedo directly corresponds to the radiation absorbed at the surface. However, because of the coupled nature of climate simulations, the signal coming from albedo biases is impossible to isolate. Therefore, several model sensitivity experiments are needed to better understand the potential impacts that biases in snow-covered surface albedo can have on climate.

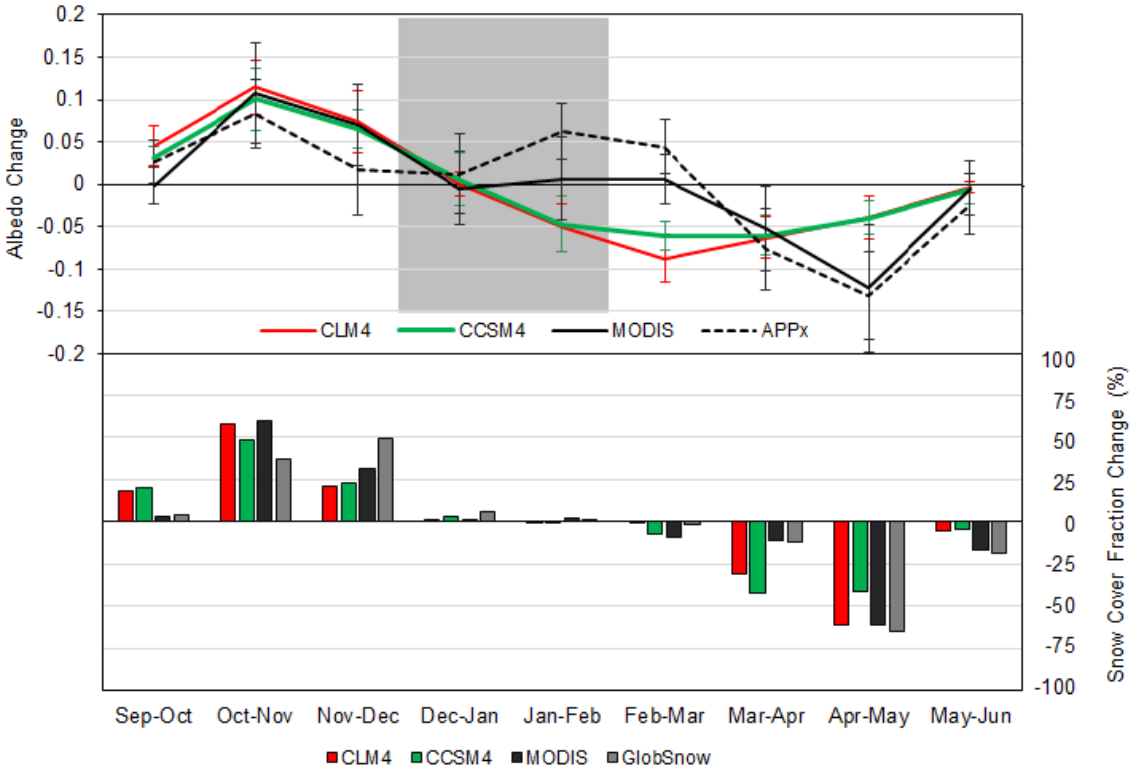

Figure 1-4: Monthly change in (a) albedo and (b) snow cover fraction (SCF) for boreal forest (>75%). Monthly changes are climatologies over the 2000-2004 period for CLM4, MODIS, and APP-x. Snow products used include CLM4, CCSM4, MODIS, and GlobSnow. The grey shaded region indicates months of the year when observational uncertainty is high due to large solar zenith angles (>75 degrees).

Chapter 5 looks at evaluating a different aspect of simulated snow in the Coupled Model Intercomparison Project Phase 5 (CMIP5) ensemble, spring trends in SCE. The motivation for this work stems from prior studies that have shown climate models to underestimate the rapidly declining Northern Hemisphere spring SCE over recent decades (Derksen and Brown, 2012; Brutel-Vuilmet et al., 2013). These studies used the National Oceanic and Atmospheric Administration climate data record (NOAA CDR) because of its length, but issues have since arisen regarding its inconsistent nature when compared to other datasets (Brown and Derksen, 2013; Mudryk et al., 2017). Therefore, a collection of seven observation-based estimates is used here to better understand the ability of climate models to

simulate spring snow cover trends. Moreover, there is a large intermodel spread in future projections of spring snow cover (Collins et al., 2013). Here, we investigate this spread to better understand the causes of uncertainty so that it can be reduced in future modeling efforts.

1.3 Research Objectives

The primary goal of this research is to improve our understanding of climate interactions with terrestrial snow through changes to surface albedo. The research strives to help with the long-term goal of reducing uncertainty in climate projections by highlighting deficiencies in the simulation of snow-covered surface albedo and snow cover (seasonality and trends). Model evaluation is a crucial step to understanding output and guiding future development. In this thesis, we aim to answer the following questions:

- What is the current state of knowledge with regards to interactions between snow cover and climate?
- Are previously identified model biases related to snow-covered surface albedo (as shown by Thackeray et al., 2014) prevalent in the current generation of global climate models?
- What is the ability of the CMIP5 models to accurately simulate the annual cycle of snow cover fraction (SCF) and snow-covered surface albedo over Northern Hemisphere extratropical land areas?

- What impact do model biases in snow-covered surface albedo have on simulated climate? Is this impact sensitive to the location, timing and/or magnitude of albedo biases?
- How well are trends in spring snow cover simulated when compared against an observational ensemble? What are the primary mechanisms driving the large intermodel spread in 21st century changes as projected by the CMIP5 suite of climate models?

1.4 Structure of Thesis

The structure of this manuscript-based thesis is broken into six chapters, the first of which describes necessary background information and provides motivation for this research. Background content includes discussion of the respective roles of snow and vegetation in controlling surface albedo, while also stating how modeling serves to improve our understanding of key climate processes. Chapters 2-5 encompass the body of this thesis, in the form of individual manuscripts. In Chapter 2 (Thackeray and Fletcher, 2016), a synthesis of research on snow albedo feedback is presented. This covers the importance of SAF to regional and global climate, estimates of its strength from both models and observations, and potential ways forward. Chapter 3 (Thackeray et al., 2015) provides a thorough evaluation of the seasonality of snow cover and albedo changes in current climate models. A skill metric is also utilized here as a method to track current and future model development. Chapter 4 (Thackeray et al., in prep) examines the impact of previously diagnosed model biases on climate through a series of novel model simulations. Chapter 5 (Thackeray et al., 2016)

explores the uncertainty in historical and future simulations of Northern Hemisphere spring snow cover. Lastly, the key findings of this research are summarized in Chapter 6, alongside some limitations to our approach and a number of recommendations for future work.

Chapter 2

Snow albedo feedback: current knowledge, importance, outstanding issues and future directions

2.1 Overview

Over the past decade, substantial progress has been made in improving our understanding of surface albedo feedbacks, where changes in surface albedo from warming (cooling) can cause increases (decreases) in absorbed solar radiation, amplifying the initial warming (cooling). The goal of this review is to synthesize and assess recent research into the feedback caused by changing continental snow cover, or snow albedo feedback (SAF). Four main topics are evaluated: (i) the importance of SAF to the global energy budget, (ii) estimates of SAF from various data sources, (iii) factors influencing the spread in SAF, and (iv) outstanding issues related to our understanding of the physical processes that control SAF (and their uncertainties). SAF is found to exert a small influence on a global scale, with an amplitude of ~ 0.1 $Wm^{-2}\,K^{-1}$, roughly 7% of the strength of water vapor feedback. However, SAF is an important driver of regional climate change over Northern Hemisphere (NH) extratropical land, where observation-based estimates show a peak feedback of around 1 % decrease in surface albedo per degree of warming during spring. Viewed collectively, the current generation of climate models represent this process accurately, but several models still use outdated parameterizations of snow and surface albedo that contribute to biases that impact the simulation of SAF. This discussion serves to synthesize and evaluate previously

published literature, while highlighting promising directions being taken at the forefront of research such as high-resolution modeling and the use of large ensembles.

2.2 Introduction

Changes in surface albedo that occur as a result of fluctuations in temperature through snow and ice cover gain/loss have long been known to have a strong influence on climate (Wexler, 1953). As the climate warms a subsequent reduction in snow and ice cover reveals a less reflective surface that absorbs more solar radiation, which further enhances the initial warming perturbation (Cess et al., 1991; Ingram et al., 1989; Robock, 1983; Schneider and Dickinson, 1974). This positive feedback mechanism is known as the surface albedo feedback. Surface albedo feedbacks have long been linked to enhanced climate sensitivity (the response of the climate system to a given forcing) at high latitudes (Budyko, 1969; Sellers, 1969). The early energy balance models of Budyko (1969) and Sellers (1969) showed that the coupling of planetary albedo and near-surface air temperature produces a strong positive feedback between ice/snow and temperature when an external forcing (i.e., increased solar radiation) is applied. These models were overly sensitive (roughly by a factor of five when compared with general circulation models) (Lian and Cess, 1977; Wetherald and Manabe, 1975), but they laid the groundwork for future progress in our understanding of surface albedo feedback.

The high albedo contrast between snow and ice-covered surfaces and snow and ice-free surfaces is a controlling factor in surface albedo feedback and polar climate (Robock, 1983). Early modeling studies found that prolonged temperature fluctuations of a few degrees could cause a complete loss of polar ice sheets (Schneider and Dickinson, 1974).

They also showed that warming does not occur equally everywhere at all times; instead the greatest warming occurs during winter at high latitudes (Manabe and Wetherald, 1975; Robock, 1983). At this time there was a general consensus that the surface albedo feedback was one of the most important climate feedbacks that could affect climate change (Lian and Cess, 1977; Manabe and Stouffer, 1980).

A second snow/ice feedback initially referred to as the snow/ice-meltwater feedback (more commonly known as the snow-metamorphosis component of SAF) was also shown to be an important mechanism. This process is characterized by an increase in meltwater and snow grain size that occurs when near-surface air temperature rises causing a decrease in snow albedo (Robock, 1980, 1983). The very simplified models of Budyko and Sellers did not include this or many other processes, such as albedo that varied with land cover type (leading to an overestimate of snow-covered surface albedo because this neglects forests, which have a much lower winter albedo than other land cover types), which contributed to their overly high climate sensitivity (Lian and Cess, 1977; Robock, 1983).

An early attempt to link observed snow cover evolution with global warming and its influence on the Earth's energy balance was made by Groisman et al. (1994). They showed that spring surface warming is enhanced by corresponding snow cover loss (from 1972-1992: mean snow cover extent decreased by 10%). Much of this snow loss occurs in so-called 'temperature-sensitive regions', where changes in snow cover are strongly correlated to temperature variations (Karl et al., 1993) and changes to snow extent in spring have the greatest impact on the radiation budget (Groisman et al., 1994). More recently, Déry and Brown (2007) confirmed these findings that the climate system is most sensitive to changes

in snow cover during spring. Changes during fall are of less importance because of decreasing insolation across the Northern Hemisphere.

The surface albedo feedback follows the classical framework for climate feedbacks, and can be calculated by relating changes in temperature and albedo to changes in incoming/outgoing shortwave radiation (Cess and Potter, 1988; Hall, 2004; Qu and Hall, 2007). There are two primary terms controlling surface albedo feedback strength in the models. The first term is the ratio of variations in planetary albedo with surface albedo changes ($\partial\alpha_p/\partial\alpha_s$) (Qu and Hall, 2006, 2014). The second is the relationship between changes in surface albedo and near surface air temperature ($\Delta\alpha_s/\Delta T_s$) (Equation 2-1) (Qu and Hall, 2007).

$$\frac{\partial Q_{net}}{\partial T_s} = \frac{\partial Q_{net}}{\partial \alpha_s}\frac{\Delta \alpha_p}{\Delta T_s} = -Q\frac{\partial \alpha_p}{\partial \alpha_s}\frac{\Delta \alpha_s}{\Delta T_s} \quad . \tag{2-1}$$

The equation states that surface albedo feedback represents the additional (reduced) amount of net shortwave radiation (Q_{net}) at the top of the atmosphere (TOA) associated with decreases (increases) in surface albedo (α_s) caused by changes in surface air temperature (T_s). The α_p term is the planetary albedo, and Q is the incoming shortwave radiation. Another method that is commonly used for calculating climate feedbacks involves the use of radiative kernels (see Shell et al., 2008; Soden et al., 2008). This approach is computationally simple as the kernels do not differ much between models, meaning that intermodel comparisons can be easily performed. However, we will primarily focus on the approach described above.

This review will focus on snow albedo feedback (SAF). SAF is at its strongest during the Northern Hemisphere (NH) spring, as this is a time when continental snow cover is large,

incoming radiation is rather intense, and there is large month-to-month change in albedo (Hall, 2004; Ingram et al., 1989; Manabe and Stouffer, 1980). Even though there is more snow in January over the Northern Hemisphere, the lack of incident radiation means that warming-induced snow loss is limited to southerly latitudes (Cess et al., 1991). Hall (2004) showed that about 50% of the total NH SAF caused by global warming occurs during NH spring. This is also the time when SAF spread between models is largest (Qu and Hall, 2014). SAF has also been shown to be capable of driving enhanced warming over areas that are sensitive to temperature variability, such as at high elevations (Fyfe and Flato, 1999; Hernández-Henríquez et al., 2015). The goal of this review is to synthesize and evaluate recent progress in our understanding of snow albedo feedback. In Section 2.3, the importance of SAF is put into a broader context with a brief review of how it compares to other climate feedbacks. Section 2.4 contains a discussion on estimates of SAF from climate models and observations. Factors influencing the variability in simulated SAF are described in Section 2.5, while Section 2.6 contains a discussion of the outstanding issues in the field and potential avenues for future research.

2.3 Global/Northern Hemisphere importance of SAF

Climate model projections of global mean warming by the end of the 21st century (2081-2100) range from 1° to 5°C relative to present under all forcing scenarios combined (Flato et al., 2013; Knutti and Sedláček, 2013). The strength of simulated warming is closely linked to intermodel variation in the simulation of various climate feedback mechanisms, which are complex functions of both time and spatial scales (Bony et al., 2006; Colman, 2003, 2013; Randall and Wood, 2007; Shell et al., 2008). Determining the physical processes responsible

for the range in climate feedback strength, and improving their simulation on the full range of scales, are expected to improve projections of future climate (Bony et al., 2006; Shell et al., 2008).

Colman et al. (2013) showed that global surface albedo feedback among models varies by nearly an order of magnitude (0.1-0.85 $Wm^{-2}K^{-1}$). Estimates from various studies have shown that the annual global ensemble mean surface albedo feedback strength is approximately 0.25-0.4 $Wm^{-2}K^{-1}$ (Colman, 2003; Dessler, 2013; Hall, 2004; Shell et al., 2008; Soden and Held, 2006; Soden et al., 2008; Zelinka and Hartmann, 2012) and is made up of nearly equal contributions from NH snow, and NH and SH sea ice (Colman, 2013). For comparison, the ensemble mean water vapor and cloud feedback strengths have been calculated as between 1.2-2.2 $Wm^{-2}K^{-1}$ (Dessler, 2013; Soden and Held, 2006; Soden et al., 2008; Zelinka and Hartmann, 2012) and 0.5-0.7 $Wm^{-2}K^{-1}$ (ensemble range of -0.1 – 1.35 $Wm^{-2}K^{-1}$), respectively (Dessler, 2013; Soden and Held, 2006; Zelinka and Hartmann, 2012). Therefore, in terms of global importance, surface albedo feedback is substantially weaker than both the water vapor and cloud feedbacks (Bony et al., 2006; Colman, 2003; Zelinka and Hartmann, 2012). The contribution from Northern Hemisphere snow is even smaller, as shown by a global-mean SAF estimate of approximately 0.08 $Wm^{-2}K^{-1}$ (ranging from 0.03 to 0.16 $Wm^{-2}K^{-1}$) in the current generation of climate models (Qu and Hall, 2014). This estimate is much weaker than the dominant climate feedbacks listed above but these global measures do not capture the local importance of SAF to climate change over the terrestrial NH.

Interestingly, surface albedo feedback is known to be very important for regional climate change, playing a significant role in Arctic amplification (Bony et al., 2006; Déry and Brown, 2007; Hall, 2004; Holland and Bitz, 2003). Pithan and Mauritsen (2014) found that the contribution to Arctic warming from surface albedo feedback due to snow and ice loss is second largest, only slightly weaker than the lapse rate feedback. However, there is some debate on the level of importance of SAF for Arctic amplification (Déry and Brown, 2007; Graversen and Wang, 2009; Graversen et al., 2014). For example, Graversen et al. (2014), using simulations from a single GCM, found that albedo feedback is responsible for only ~40% of the Arctic warming amplification, leaving more than half to be explained by other processes, such as thermal advection.

SAF can be defined on a variety of timescales as there is no implicit time information contained in the partial derivatives (Eq. 2-1), which can be evaluated over any time period. A very useful property of SAF is that it can be evaluated over the seasonal cycle and in the context of climate change (Hall and Qu, 2006). However, there are certain physical constraints; for example, SAF is commonly calculated as either a seasonal or annual mean. In the current seasonal cycle, NH snow cover retreats from its peak in late winter in response to greater insolation and warmer temperatures (Robinson et al., 1993), thus decreasing surface albedo and amplifying the warming. Similarly, simulations show that climate warming will reduce snow cover extent, decreasing surface albedo, and amplifying the warming through greater radiation absorbed at the surface (Cess et al., 1991; Hall and Qu, 2006). On seasonal timescales, surface albedo feedback is dominated by contributions from NH snow (SAF), which physically makes sense because of the large changes in terrestrial snow cover that

occur during the snow melt period (Colman, 2013). Studies have shown that SAF is the largest positive feedback over NH high-latitudes (Zelinka and Hartmann, 2012), particularly during the winter-to-spring transition (Qu and Hall, 2014). The best estimate of SAF based on the observed seasonal cycle (Feb to Jun) is 0.87 $Wm^{-2}K^{-1}$, while the fifth Coupled Model Intercomparison Project (CMIP5) ensemble has a significant intermodel spread (0.50 – 1.35 $Wm^{-2}K^{-1}$) (Qu and Hall, 2014).

The importance of SAF is perhaps best exemplified by the findings of Qu and Hall (2014) that show SAF variability in the CMIP5 models accounts for 40-50% of the spread in warming over Northern Hemisphere extratropical land (Figure 2-1). In fact, there was shown to be a strong positive correlation between annual-mean SAF strength and projected zonal mean temperature change (~0.6-0.7) in springtime, and a slightly weaker correlation throughout summer (Qu and Hall, 2014).

In recent decades, NH melt season snow cover has shown a dramatic negative trend (i.e., -21% per decade for June) (Derksen and Brown, 2012), which is larger in magnitude than the well-publicised declining trend in Arctic sea ice (-13% per decade for September) (Stroeve et al., 2007, 2012). In fact, melt season continental warming in the NH has likely been enhanced by SAF (Groisman et al., 1994). Multiple studies have shown that warming across much of the terrestrial Arctic is a key driver behind a lengthening of the snow-free season because the snow is being melted earlier (i.e., Brown et al., 2010; Chapin et al., 2005). Hall et al. (2008) also demonstrated that SAF strength and summertime temperature are correlated through changes in water storage as a result of SAF. In summary, it is likely that changes to snow extent and snow cover duration have triggered a series of climate feedbacks

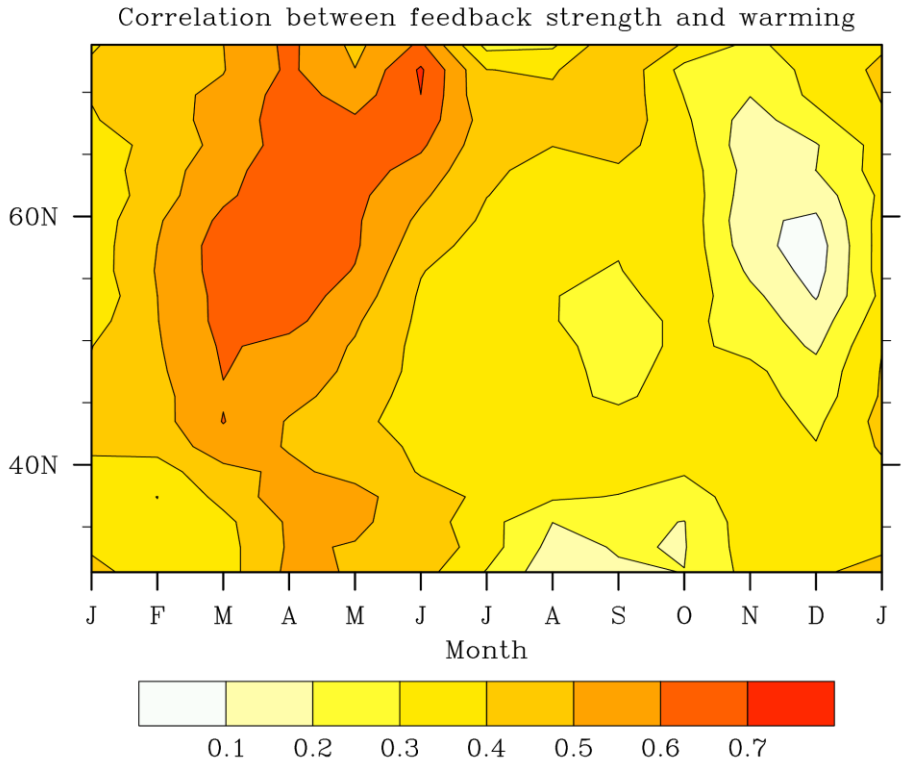

Figure 2-1: Cross-model correlation between the annual-mean SAF strength and zonal-mean surface warming over land areas, for each month. Surface warming is quantified as the difference between the T_s climatologies in the periods 1980-1999 and 2080-2099 (from Qu and Hall, 2014). Reprinted with permission from Springer.

that are enhancing, and will continue to enhance, warming of the NH land (Chapin et al., 2005; Déry and Brown, 2007).

2.4 Estimates of SAF from various data sources

2.4.1 Simulated SAF in climate models

The recent observed changes to the cryosphere are largely underestimated by the CMIP5 models (Derksen and Brown, 2012; Stroeve et al., 2012). For example, the annual mean NH snow and ice albedo feedbacks are much greater (~2.5 times) in observations than models (Crook and Forster, 2014; Flanner et al., 2011). The motivation for looking at SAF in models extends well beyond this disagreement between models and observations, because we know

that both the models and observations are likely deficient. However, the models are a crucial tool for understanding the observations as well as for making future projections. Therefore it is important to better understand the processes behind this feedback mechanism, and how well they are simulated by models.

Early studies of climate sensitivity involving general circulation models (GCMs) demonstrated that with increased CO_2 (or incoming radiation) forcing there was greater warming at high latitude regions as a result of less snow cover and subsequently a lower surface albedo and more absorbed radiation (Manabe and Stouffer, 1980; Manabe and Wetherald, 1975; Wetherald and Manabe, 1975). The enhanced polar warming due to SAF was approximately two to three times greater than the global average in a CO_2 doubling experiment by Manabe and Wetherald (1975). The first model intercomparison of SAF using multiple GCMs dates back to Cess et al. (1991). They examined simulations with climate warming imposed through specified sea surface temperature (SST) perturbations, but which were able to generate their own surface feedback response over land. These early results demonstrated a large intermodel spread in the global "snow feedback parameter" (0.9-1.9 $Wm^{-2}K^{-1}$) (Cess et al., 1991; Randall et al., 1994).

There are two common ways to quantify SAF, through changes in TOA shortwave flux with warming/cooling (Eq. 2-1), and through changes in surface albedo with warming/cooling ($\Delta\alpha_s/\Delta T_s$). Of the two partial derivatives in the SAF equation (Eq. 2-1), the first term ($\partial\alpha_p/\partial\alpha_s$) was always thought to be about 0.5, but recent research has reduced this estimate to ~0.35, meaning that variations in surface albedo have slightly less impact on planetary albedo than first estimated (Donohoe and Battisti, 2011; Qu and Hall, 2014).

However, this parameter has been shown to exhibit very little intermodel variability among the Coupled Model Intercomparison Project phase 3 (CMIP3) (Donohoe and Battisti, 2011; Qu and Hall, 2006) and CMIP5 models (Qu and Hall, 2014), meaning it is not a factor in SAF variability. By contrast, several studies have shown that intermodel variations in SAF are highly correlated with the simulated strength of the second term ($\Delta\alpha_s/\Delta T_s$), which describes the sensitivity of surface albedo to temperature changes (Qu and Hall, 2007). This term explains more than 80 % of the multimodel spread in SAF (Qu and Hall, 2007, 2014), and so it is commonly used as a proxy for SAF strength (Fernandes et al., 2009; Fletcher et al., 2012).

SAF in the CMIP3 climate models has been investigated in numerous studies (i.e., Fletcher et al., 2012; Qu and Hall, 2006, 2007; Winton, 2006). In terms of total feedback strength, the CMIP3 ensemble has a multi-model mean SAF of -1.20 % K^{-1} (percent change in albedo per degree Kelvin of warming) in March-April-May-June (MAMJ; calculated for 1982-1999) and a spread of approximately -0.72 to -1.57 % K^{-1} (Fletcher et al., 2012). Despite a large focus on land model development since CMIP3 (Brovkin et al., 2013; Oleson et al., 2010), the current generation of models (CMIP5) have not shown much progress related to SAF. Qu and Hall (2014) found that the intermodel variance in the sensitivity of surface albedo to changes in temperature ($\Delta\alpha_s/\Delta T_s$), and in turn SAF, remains largely unchanged from CMIP3 to CMIP5. The median model feedback strength (Interquartile range) is approximately -1.20 % K^{-1} (-0.90 to -1.70 % K^{-1}) in the seasonal cycle over the Northern Hemisphere extratropics (Fletcher et al., 2015). Qu and Hall (2014) calculated SAF as an annual mean over NH extratropical land and showed that a fourfold spread exists

within the CMIP5 ensemble (range: 0.18-0.78 $Wm^{-2}K^{-1}$). To better understand the similarities between these two calculations, we use data from Figure 1(c) of Qu and Hall (2014) to isolate for only the winter-to-spring transition (MAMJ), which results in a mean SAF of ~0.89 $Wm^{-2}K^{-1}$ (0.81 $Wm^{-2}K^{-1}$ for FMAMJ).

The large spread tells us that several models have an unrealistic SAF in the current seasonal cycle, but despite these biases (SAF and surface albedo) the model simulated temperature is on average consistent with observations over the recent historical period (Thackeray et al., 2015). This is important because SAF in the seasonal cycle forms an excellent predictor for SAF strength under future climate change (Figure 2-2) (Hall and Qu, 2006; Qu and Hall, 2014). This property can be exploited by using available observational data to constrain future projections of SAF (Qu and Hall, 2014), and thus of surface temperature, and possibly of circulation (Fletcher et al., 2009). Although this feedback is restricted to high latitudes it may influence the global energy budget through an impact on the poleward transport of energy (Zelinka and Hartmann, 2012). Therefore, if a model cannot accurately represent seasonal snow cover changes, then it is not likely to capture how snow cover will recede in a warmer climate. Levis et al. (2007) showed that the extent of present day snow cover is positively correlated with SAF strength, whereby a model with greater snow extent has a larger "SAF potential" (the strength of SAF that a model can produce for a given warming) because there is more snow-covered area that can be exposed revealing a less reflective underlying surface.

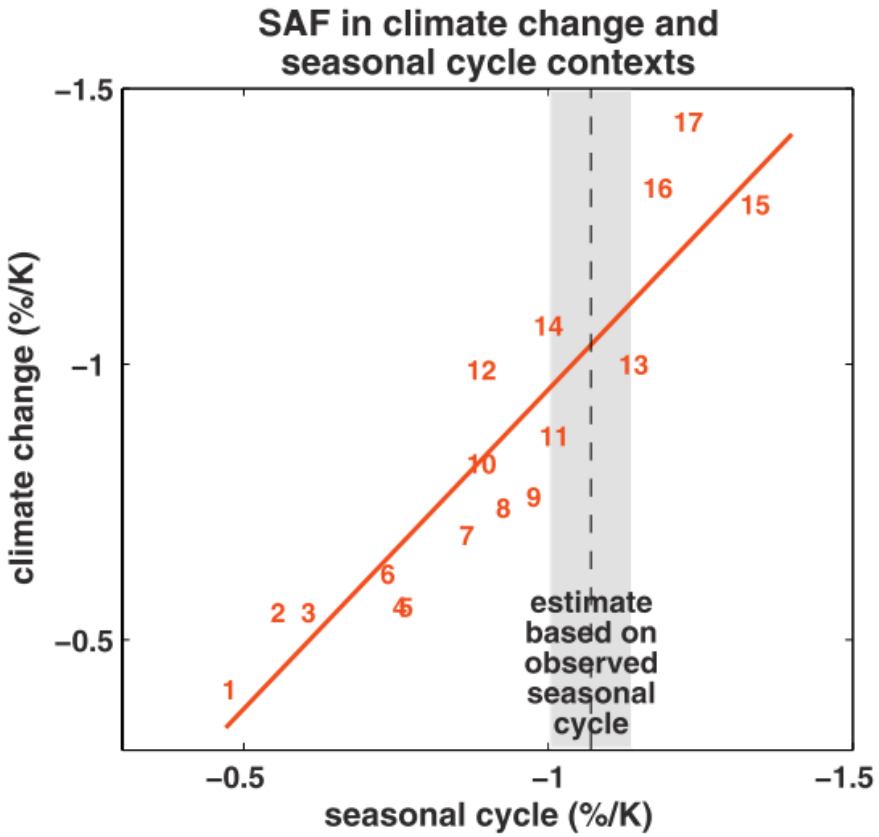

Figure 2-2: Scatterplot of simulated springtime SAF values in climate change and in the seasonal cycle. Each number represents an individual model. A least-squares fit regression line for the simulations is also shown. The two parameters are highly correlated ($r^2 = 0.92$). The observed springtime value based on ISCCP and the ERA40 reanalysis is plotted as a dashed vertical line (from Hall and Qu, 2006). Reprinted with permission from John Wiley and Sons.

2.4.2 Observation-based SAF

The satellite data record allows for monitoring of large-scale changes to the cryosphere, and these data can be used to derive an observational estimate of SAF due to the seasonal cycle. The large intermodel spread in SAF (Section 2.4.1) also helped drive a push to quantify the observed SAF strength, with the hope that observational constraints could help to reduce the spread in projected warming (Fernandes et al., 2009; Hall et al., 2008). Early attempts to calculate SAF using satellite-derived albedo, snow cover, and temperature found a total strength that varied slightly depending on the data sources used. Hall et al. (2008) found that

spring SAF over the Northern Hemisphere extratropics was larger than the multi-model ensemble mean from 18 models. They estimated observational SAF using surface albedo from the International Satellite Cloud Climatology Project (ISCCP) to be -1.13 +/- 0.13 $\%K^{-1}$ (Table 2-1). This is approximately 20% stronger than an estimate of -0.93 +/- 0.06 % K^{-1} that used surface albedo from the Advanced Very High Resolution Radiometer (AVHRR) Polar Pathfinder extended (APP-x) project (Fernandes et al., 2009). This ~1% reduction in albedo per degree Kelvin of warming equates to a global mean strength of approximately 0.1 $Wm^{-2}K^{-1}$ (Qu and Hall, 2014). A similar approach was used by Fletcher et al., (2012) in an attempt to update the observational estimate of SAF in the seasonal cycle (MAMJ). The authors showed a total feedback strength of -1.11 % K^{-1}, an increase from Fernandes et al. (2009), where a different methodology but same study area (AVHRR subset of EASE grid) was utilized. These observational differences are primarily linked to the various albedo and temperature datasets used, and their methodological differences (retrieval algorithms, spatial domain, temporal domain, etc.).

More recently, Qu and Hall (2014) used surface albedo data from the Moderate Resolution Imaging Spectroradiometer (MODIS) to estimate an observed SAF strength of 0.87 +/- 0.09 % K^{-1} in a shortened seasonal cycle (Apr-May). Fletcher et al. (2015) chose to employ a multiple observation approach using all available data to produce a best estimate of SAF strength. The calculation of NET SAF using a variety of observational products was consistently around -1.22 % K^{-1} over NH land polewards of 45°N. The weaker SAF strength calculated by Qu and Hall (2014) may stem from differences in methodology, study area, and observational data used. It has been suggested that observed SAF in the seasonal cycle could

Table 2-1: Strength of observational estimates of snow albedo feedback as reported by various studies. Studies using the APP-x albedo dataset are limited to a smaller spatial domain (NH45; polewards of 45°N) than those using other products that cover the entire Northern Hemisphere extratropics (NH30). The time frame is represented by the first letter of each month (i.e., MAM = March-April-May).

SAF Strength	Spatial/Temporal Domain	Albedo Dataset	Reference
-1.13 % K^{-1}	NH30/MAM	ISCCP	Hall et al., 2008
-0.93 % K^{-1}	NH45/MAM	APP-x	Fernandes et al., 2009
-1.11 % K^{-1}	NH45/MAMJ	APP-x	Fletcher et al., 2012
-0.87 % K^{-1}	NH30/AM	MODIS	Qu and Hall, 2014
-1.22 % K^{-1}	NH45/MAMJ	MODIS & APP-x	Fletcher et al., 2015

be used to constrain SAF in climate change in order to narrow the spread in projections of warming (Qu and Hall, 2014). Qu and Hall (2014) showed that this would eliminate approximately half of the intermodel range in SAF strength during climate change, from 0.3-1.4 $Wm^{-2}K^{-}1$ to 0.5-1.0 $Wm^{-2}K^{-1}$.

With regards to its spatial distribution, seasonal SAF strength typically falls between 0 and -1 % K^{-1} over the Northern Hemisphere, except for a region just north of the boreal forest where SAF locally reaches between -1 to -5 % K^{-1} (Fernandes et al., 2009). The stronger SAF seen here is largely due to a greater surface albedo contrast (α_{sfc_snow} - α_{land}) because vegetation is either sparse or easily masked by snow (i.e. grass, shrub). A subsequent analysis of the regional variations in observed SAF found local maxima across northern Canada, northern Siberia, and southwest Eurasia (Fletcher et al., 2012). The CMIP5 ensemble is biased high over the boreal forest, and biased low over the Arctic (Fletcher et al., 2015). Model biases in SAF over these land cover types have been shown to be strongly linked to biases in climatological snow-covered surface albedo (Thackeray et al., 2015). Therefore the current generation of climate models has some success replicating the spatial distribution of SAF, but shows local biases over the boreal forest and Arctic tundra.

2.5 Factors influencing the spread in simulated SAF

2.5.1 SAF components

The sensitivity of surface albedo to temperature changes ($\Delta\alpha_s/\Delta T_s$; henceforth NET, corresponding to its role in describing the total SAF) is controlled by two mechanisms: (i) reduction of snow cover (S) revealing a darker surface, decreasing surface albedo (SNC; Eq. 2-2), (ii) physical changes to the snowpack with warmer temperatures (T_s) occurring with constant S (TEM; Eq. 2-3) (Fletcher et al., 2012; Qu and Hall, 2007).

$$SNC = (\overline{\alpha_{sfc\_snow}} - \alpha_{land})\Delta S/\langle \Delta T_s \rangle \quad (2\text{-}2)$$

$$TEM = \overline{S}.\ \Delta\alpha_{sfc\_snow}/\langle \Delta T_s \rangle \quad , \quad (2\text{-}3)$$

where α_{sfc_snow} is the snow-covered surface albedo, α_{land} is the snow-free land albedo, deltas represent the change in a quantity (either month-to-month in the seasonal cycle context, or future minus past in the climate change context), overbars represent the seasonal mean, and the angle brackets around temperature indicate the use of a NH extratropical mean.

The SNC component dominates SAF (>50% of NET) in 14/17 CMIP3 models (Qu and Hall, 2007; Fletcher et al., 2012). However, there has been some disagreement about the contributions from the SNC and TEM terms to total (NET) SAF (Fletcher et al., 2015). Fletcher et al. (2012) used this methodology (Eq. 2-2, 2-3) to determine that SAF in the seasonal cycle context had a 60/40 (SNC/TEM) breakdown in CMIP3 models (for reference, observations showed a 70/30 split; but this split is highly sensitive to the choice of SCF dataset (Fletcher et al., 2015)). On the other hand, Qu and Hall (2007) showed that the difference in albedo between a snow-covered and snow-free surface accounts for ~80% of the intermodel variance in the snow cover component of SAF. Subsequently, more than 80%

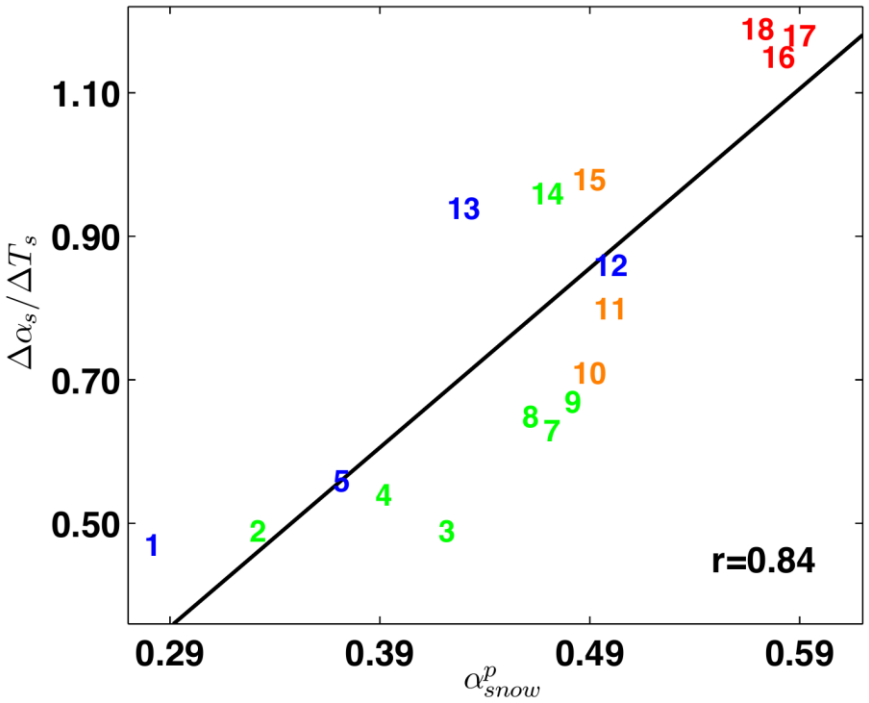

Figure 2-3: Scatterplot of Δαs/ΔTs (units % K^{-1}) vs mean albedo of fully snow-covered regions (dimensionless) for the current climate in 17 CMIP3 simulations. The numbers of the 17 simulations are from Table 1 of Qu and Hall (2007). The numbers are color coded by the way vegetation/albedo is parameterized in that model: blue = Type 1, green = Type 2, orange = Type 3, and red = Type 4 (from Qu and Hall, 2007). See Section 2.5.2 for definition of the four types listed here. Reprinted with permission from the American Meteorological Society.

of the spread in albedo contrast can be accounted for by variability in α_{sfc_snow} (Figure 2-3). Simulated snow albedo is therefore found to be highly correlated (r>0.8) with SAF strength (Qu and Hall, 2007), implying that correcting biases in simulated α_{sfc_snow} could provide strong constraints on SAF, and therefore future surface albedo and temperature changes, over NH land. SAF in the CMIP5 models continues to be dominated by the snow cover component (SNC; -0.75% K^{-1}), while the temperature dependent component (TEM; -0.45% K^{-1}) plays a slightly lesser role (Figure 2-4) (Fletcher et al., 2015). In terms of their snow and land albedos there are signs of improvement, as the multi-model median has moved closer to observations, but as previously noted a large spread still lingers for both of these terms (Fletcher et al., 2015).

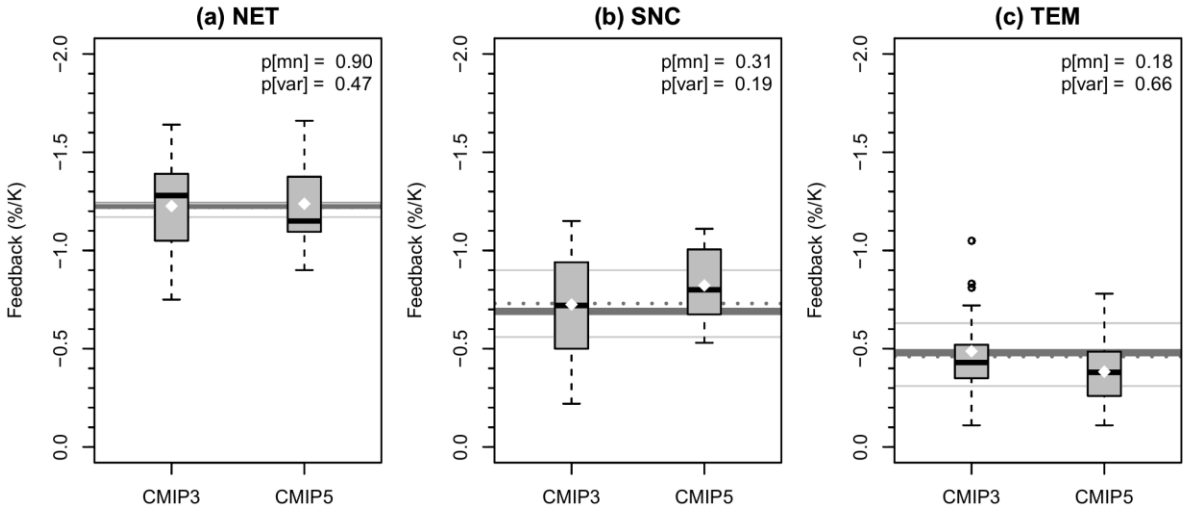

Figure 2-4: Boxplots showing the spread of the MAMJ mean SAF terms in CMIP3 and CMIP5 models (a) NET, (b) SNC, (c) TEM. For each box the grey shaded region shows the 25th-75th percentile range, the black horizontal line shows the median, and the white diamond shows the multimodel mean. The dashed fences indicate 1.5x the interquartile range (IQR), and outlier models are shown by open circles. The longer grey horizontal lines behind the boxes denote the observation-based estimates (from Fletcher et al., 2015). Reprinted with permission from John Wiley and Sons.

Additivity of the two terms that comprise SAF (i.e., SNC+TEM = NET) would illustrate that the components fully capture the physical processes controlling the total feedback. This has been shown to hold up quite well in observations and models, to within a few percent for the NH land area as a whole (Fletcher et al., 2012). However, when looking at SAF averaged as a function of latitude, additivity is not well satisfied for observationally-derived estimates (although the relationship is still satisfied in models). This lack of additivity implies that the SNC/TEM decomposition is not capturing all SAF processes at a sub-hemispheric scale (Fletcher et al., 2015). We speculate that this may be tied to inaccuracies with satellite based snow cover estimates (Fernandes et al., 2009), as the derivation of these terms, particularly SNC, is sensitive to biases in the snow cover product used. Over regions that contain a high fraction of sub-pixel water cover (for example the lake-rich regions of Northern Canada and Siberia) there is a tendency for satellite-derived

snow melt to be delayed (Frei and Lee, 2010; Zhao and Fernandes, 2009). Therefore our understanding continues to be limited by a lack of confidence in our observational products that are used to derive estimates of SAF and its components.

2.5.2 Land cover types and vegetation masking

A large range in the simulated albedo of fully snow-covered surfaces plays an integral role in SAF spread. The snow-covered surface albedo (α_{sfc_snow}) in GCMs is primarily linked to the type of surface albedo parameterization and vegetation masking scheme in place. Simulating snow and albedo over forested regions is challenging because of the interactions between the canopy layer and the ground surface. In dense evergreen forests, the snowpack is often largely shaded by the forest canopy at higher solar zenith angles in winter (Wang et al., 2014), but this process is often poorly represented in GCMs. The type of vegetation/snow masking scheme employed by a model plays an important role in albedo evolution (Essery, 2013; Loranty et al., 2014). Qu and Hall (2007) defined four distinct types of snow albedo masking schemes in the CMIP3 ensemble, with varying degrees of complexity. The simplest approach (Type 4) uses an albedo that is independent of land cover and is only tied to the snow depth. The Type 3 models calculate albedo as a weighted average of snow-free surface albedo and snow albedo, dependent on snow cover fraction. Type 2 models, on the other hand, calculate albedo as a weighted average of canopy and ground albedo, dependent on land cover type. The most complex approach (Type 1) uses a full canopy radiative transfer model that uses two-stream approximations (Essery, 2013; Qu and Hall, 2007). The wide variety of parameterization types contributes to a large spread in snow-covered surface albedo (~0.25-0.60) and SAF over forested regions (Loranty et al., 2014; Thackeray et al.,

2015). It should be noted that more sophisticated representations are not necessarily the best; as the five CMIP3 models with the lowest α_{sfc_snow} over the NH all use either type 1 or 2 parameterizations (Qu and Hall, 2007). Furthermore, the way in which a model represents snow in the canopy layer has also been shown to influence SAF (Thackeray et al., 2014). For these reasons it has been suggested that observations should be used to constrain simulated wintertime albedo over heavily vegetated landscapes (Qu and Hall, 2014).

It is well known that snow albedo is sensitive to changes in near-surface air temperature and that albedo decreases with snow age through metamorphosis processes (Robock, 1983; Wiscombe and Warren, 1980). These snowpack evolution processes tend to be parameterized in GCMs with a dependence on either snow age or temperature, and it is this dependency that largely controls the seasonal evolution of α_{sfc_snow} (Qu and Hall, 2007). Pedersen and Winther (2005) showed that temperature dependent schemes had a tendency to decrease in albedo too early in the melt season and this change occurred more rapidly than in situ observations at temperate sites (where T_s rises above 0°C several times during winter). Therefore the chosen parameterizations relating to snow and vegetation can have a strong influence on simulated SAF.

2.6 Discussion and conclusions

This review has summarized recent progress in the understanding of snow albedo feedback (SAF) and its importance to the climate system. There is a consensus that SAF is a relatively weak climate feedback in the global context, but it plays an important role in regional climate change over the Northern Hemisphere (NH) extratropics (Déry and Brown, 2007; Hall, 2004). In these regions SAF is strongest during the winter-to-spring transition months (Feb-

Jun), when the seasonal mean strength is characterized by approximately a 1 % reduction in surface albedo per degree of warming (Fletcher et al., 2012; Hall et al., 2008; Qu and Hall, 2014). SAF can be decomposed into two components, one related to the presence/absence of snow cover (SNC), and the other to temperature-mediated changes in the snowpack occurring in the presence of snow cover (TEM). The total SAF strength is controlled primarily by SNC, which in models is strongly tied to the simulated albedo of a fully snow-covered surface (Qu and Hall, 2007). However, there is some discrepancy with regards to how strong of an influence these terms have on SAF (Fletcher et al., 2015). In the most recent generation of climate models there has been an improvement in simulated surface albedo and mean climate (Fletcher et al., 2015).

2.6.1 Limitations associated with observational data products

Several pressing issues still limit our understanding of SAF. First, there remains a lack of reliable observational data over much of the cryosphere (Liston, 2004; MacKay et al., 2006), in particular over northern Canada, Siberia, and Greenland, where there is a low density of coastal and interior land weather stations (Rigor et al., 2000). This is particularly important when it comes to measurements of surface temperature, which may require spatial interpolation to be applied where *in situ* measurements are sparse (Mortin et al., 2014). Satellite-derived products provide much better spatial coverage but still contain uncertainties. Satellite retrievals of snow cover and albedo can be particularly difficult to confidently acquire at large solar zenith angles (i.e. during winter, at high latitudes) (Schaaf et al., 2002; Wang et al., 2014) and over complex terrain (i.e. mountainous regions). Furthermore, many global satellite-derived products are not available at spatial and temporal resolutions that are

comparable with output from GCMs, which limits our ability to use these data for model validation and improvement. Most satellite-derived products are distributed with spatial grid resolutions of ~1 km, whereas GCM resolutions are of the order ~100 km, meaning that grid interpolation must be applied to ensure sound comparison. These products are also seldom available at a daily temporal resolution, causing key processes during the melt season—when the snowpack is in a state of rapid change and albedo can decrease dramatically in a matter of days—to be undersampled (Loth et al., 1993). For example, the current 16-day mean surface albedo product from MODIS has been shown to have decreased accuracy during rapid melt events (Wang et al., 2014).

Increasing availability of observational products at higher temporal resolution should allow for the evaluation of SAF, and other cryosphere-relevant processes, at the critical daily and weekly timescales. A demonstration of the impact of timescale on SAF is presented in Figure 2-5, where SAF computed from an offline simulation of the Community Land Model version 4 (CLM4) (Figure 2-5a) is compared with an observationally-derived estimate on a weekly (Figure 2-5b) and a monthly timescale (Figure 2-5c). The SAF strength peaks at ~-8 % K^{-1} in weeks 12/13 just south of 70°N in the model and observational estimate, and then further north during weeks 14-16. The weekly SAF calculation reveals much more detail about the seasonal evolution than the current protocol of aggregating the data over a month (comparing panels (b) and (c)), and provides a visible signal of the timing of snow cover retreat across the Northern Hemisphere (particularly through the boreal forest). A similar type of analysis could be performed on the individual SAF components to get a better

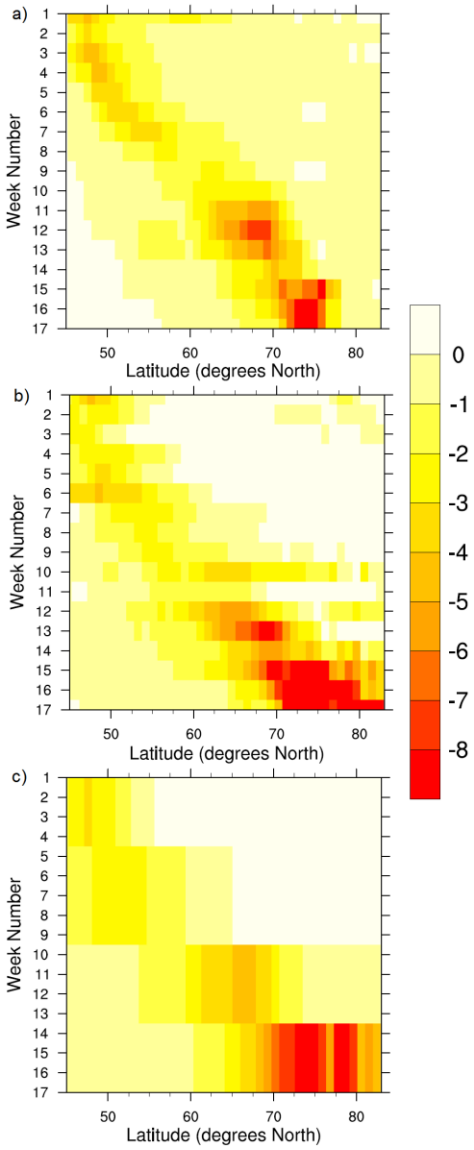

Figure 2-5: Hovmöller diagrams showing NET SAF (units % K^{-1}) as a function of latitude and time (in weeks) over the winter-to-spring transition (March-April-May-June). Week 1 is March 1-7, while week 17 is June 21-27. In panels (a) and (b) the SAF values are computed using weekly mean surface albedo, snow cover, and temperature data extracted from (a) an offline simulation using the land model NCAR-CLM4, (b) satellite observations (APP-x albedo, IMS snow cover). In panel c the SAF values are computed as in Fletcher et al. (2015), using monthly mean observational data, covering the four months March-June.

understanding of short-timescale processes related to snow cover and albedo change that may be undersampled in monthly mean data.

The bias and uncertainty in the observed snow cover record can influence the breakdown of SAF components (Eq. 2-2, Eq. 2-3). Fletcher et al. (2015) showed a large spread in calculations of observed SNC and TEM as a result of dissimilarities in snow cover datasets. In particular, it was the discrepancy between MODIS and the IMS/NOAA products, whereby SNC is weaker when snow cover persists for longer. The observational uncertainty associated with various datasets of the same geophysical variable can limit our confidence in its application. To address this issue there has recently been a shift to using multiple independent observationally based estimates as a way to demonstrate observational uncertainty and for model evaluation over the cryosphere (Brown and Derksen, 2013; Fletcher et al., 2015; Mudryk et al., 2015; Thackeray et al., 2015). The thinking behind this approach is that each observational estimate has its own inherent uncertainty and this can be limited, but not entirely eliminated, by using multiple datasets (Flato et al., 2013). Individual sources of snow cover data can be influenced by alterations to mapping methodology over time, biases in satellite retrievals, and changes to satellite sensors (Brown et al., 2010). Brown and Derksen (2013) showed that one commonly used snow cover dataset, the NOAA climate data record, has an increasing trend (over the 1982-2005 period) in Eurasian October snow in contrast to a significant negative trend in four other independent datasets. Similarly, analysis of several snow water equivalent datasets has revealed large observational spread in snow mass and SWE trends over recent decades (Mudryk et al., 2015). A new project called the Satellite Snow Products Intercomparison & Evaluation Exercise (SnowPEX) hopes to evaluate the various observational snow cover products and derive their relative uncertainties

for climate change monitoring. This will provide the community with a much better sense of the variability within observationally based estimates of snow.

2.6.2 Potential to improve model projections

The persistence of the large intermodel spread in simulated SAF within the current generation of climate models remains another important limitation (Qu and Hall, 2014). This means that SAF is still a crucial source of uncertainty for projections of climate warming over Northern Hemisphere land areas. Qu and Hall (2014) showed that the use of observational constraints would eliminate approximately half of the intermodel range in SAF strength during climate change, from 0.3-1.4 $Wm^{-2}K^{-1}$ to 0.5-1.0 $Wm^{-2}K^{-1}$. Extending their approach to the intermodel spread in surface temperature, we can estimate how much observational constraints could narrow projections of NH land warming. Under the RCP8.5 scenario the range in 21st century warming (2080-2099 minus 2006-2025) over the NH extratropics is 3.1-7.4°C across 24 CMIP5 models. Taking the mean from only the "best" models (defined as those with SAF in the seasonal cycle context that lies within the range of observational uncertainty, based on Fig. 4 and Table 1 from Qu and Hall (2014)) we find a range of projected warming 4.4-6.9°C, which represents a reduction in intermodel spread of ~40 %. This type of analysis serves as a demonstration of how a reduction in process-level model biases (for example in simulated snow albedo), might help to reduce the uncertainty in projections of climate change over large areas.

There are several streams of emergent research which show promise and are expected to lead to substantial changes in our understanding or representation of SAF. A few of them are discussed here. Much of this research is tied to model development, but as previously

mentioned there is still a large amount of potential for improving observational datasets. One area where improvements are ongoing is across the boreal forest, where the models overestimate SAF strength on average (Fletcher et al., 2015). The recent evaluation of vegetation parameterization and distributions has revealed that many models have an unrealistic representation of forested regions (i.e., tree cover fraction distribution) (Essery, 2013; Loranty et al., 2014). Excluding the models with unrealistic vegetation schemes from model intercomparison studies has been shown to dramatically limit the spread in snow-covered albedo (Essery, 2013). Thackeray et al. (2014) showed that issues with the representation of canopy snow in one model (Community Climate System Model version 4; CCSM4) had a knock-on effect that caused albedo to decrease too early in the winter, producing a 40% weaker than observed SAF. Development to improve the simulation of canopy snow interception/offloading and reduce associated albedo biases in the CCSM4 is ongoing (J. Perket, personal communication, 2015).

Also, in the near-future we should expect to see the incorporation of observational estimates to improve model simulations; such as using observed SAF to constrain how snow cover evolves in a warmer climate (Qu and Hall, 2014), or applying observationally based albedo/vegetation relationships (Loranty et al., 2014). Perturbed physics ensembles, where key model parameters are varied across their full range of observational/empirical uncertainty, provide a pathway toward improvement in overall model quality (Fischer et al., 2011; Sanderson, 2011). Also, as computational power continues to increase we can expect to see higher resolution modeling and larger model ensembles. For CMIP5, most models were run at resolutions between 100-300 km, but more recently there has been an increased

use of higher resolutions (0.25-0.5°) that allow for better representation of small-scale processes (Jia et al., 2015; Roberts et al., 2015). Meanwhile, the number of historical simulations for each model ranged from 1-10 for CMIP5, but this is often too low to properly separate forced from internal climate variability. In response, a new push in the community is the production of large ensembles, which contain upwards of 30 realizations of historical and future scenario runs (i.e. Kay et al., 2014). These advancements should reduce our need to upscale observational data for model evaluation, and provide a better understanding of the role of internal variability in various simulated processes, particularly in the cryosphere (i.e. Screen et al., 2014; Wettstein and Deser, 2014).

2.7 Acknowledgements

We would like to thank Xin Qu and Alex Hall for providing their original figures, and to two anonymous reviewers for their constructive comments.

Chapter 3

Quantifying the skill of CMIP5 models in simulating seasonal albedo and snow cover evolution

3.1 Overview

Effectively modeling the influence of terrestrial snow on climate in general circulation models (GCMs) is limited by imperfect knowledge and parameterization of arctic and sub-arctic climate processes, and a lack of reliable observations for model evaluation and improvement. This study uses a number of satellite-derived datasets to evaluate how well the current generation of climate models from the fifth Coupled Model Intercomparison Project (CMIP5) simulate the seasonal cycle of climatological snow cover fraction (SCF) and surface albedo over the Northern Hemisphere snow season (September – June). Using a variety of metrics, the CMIP5 models are found to simulate SCF evolution better than that of albedo. The seasonal cycle of SCF is well reproduced despite substantial biases in simulated surface albedo of snow-covered land (α_{sfc_snow}), which affect both the magnitude and timing of the seasonal peak in α_{sfc_snow} during the fall snow accumulation period, and the springtime snow ablation period. Insolation-weighting demonstrates that the biases in α_{sfc_snow} during spring are of greater importance for the surface energy budget. Albedo biases are largest across the boreal forest, where the simulated seasonal cycle of albedo is biased high in 14/16 CMIP5 models. This bias is explained primarily by unrealistic treatment of vegetation masking and subsequent overestimation (more than 50% in some cases) of peak α_{sfc_snow}, rather than by biases in SCF. While seemingly straightforward corrections to peak α_{sfc_snow} could yield

significant improvements to simulated snow albedo feedbacks, changes in α_{sfc_snow} could potentially introduce biases in other important model variables such as surface temperature.

3.2 Introduction

Snow is a crucial component of the climate system, interacting with the energy budget of the atmosphere and the land surface. It has a very strong influence on surface albedo (α_{sfc}), controlling the timing of peak reflectivity and its evolution through the snow season. The observed seasonal evolution of albedo has been shown to increase throughout the winter, peaking in March on average in the Northern Hemisphere (NH) (Fang et al., 2007; He et al., 2014). He et al. (2014) suggested that this late winter maximum albedo is due to weak insolation during winter, and the increasing influence of snow and ice-covered surfaces on the shortwave radiation budget during the winter-to-spring transition. This peak albedo is strongly tied to land cover, with forested regions being the least reflective, even with high snow cover, because the forest canopy masks the surface (Jin et al., 2002; Barlage et al., 2005; Fang et al., 2007). We define the quantity α_{sfc_snow} to represent the albedo of a snow-covered surface, meaning that α_{sfc_snow} is influenced by a combination of factors including snow cover fraction (SCF), the albedo of pure snow, the albedo of the underlying surface and/or vegetation, and the confounding effect of snow lying on the vegetation.

The impact of snow on climate in general circulation models (GCMs) has proven difficult to effectively model because of imperfect knowledge and parameterization of arctic and sub-arctic climate processes, and a shortage of reliable observations for model assessment and development (Liston, 2004; MacKay et al., 2006). Qu and Hall (2007) showed that the Coupled Model Intercomparison Project phase 3 (CMIP3) models had a

large spread (~0.28 – 0.59) in the mean α_{sfc_snow}, and a spread of this magnitude still exists in the more recent generation of models from phase 5 (CMIP5) (Qu and Hall, 2014). Models with a high α_{sfc_snow} also tend to have a large surface albedo contrast (snow-covered minus snow-free albedo), and in turn a stronger snow albedo feedback (SAF) (Qu and Hall, 2007; Fletcher et al., 2012). SAF is an important positive feedback mechanism that enhances surface warming through a reduction in surface albedo resulting from receding snow cover and snow metamorphism. A fivefold spread in SAF strength among the CMIP5 models explains 40-50% of the spread in predicted future warming over NH land (Qu and Hall, 2014).

A significant factor in the intermodel spread in SAF is the number of different ways in which the models parameterize snow, vegetation masking, the albedo of pure snow, and the interactions between these variables. Slater et al. (2001) showed that there are four primary model structures for representing snow cover in land models. The least sophisticated model structure is an "implicit" scheme, which assumes an equal distribution of snow mass across a grid cell. A "composite layer" structure monitors the fraction of a grid cell that is covered by snow on the ground (snow cover fraction; SCF), while its snow temperature is the same as the uppermost soil layer. The other two structures track SCF, while also simulating the snowpack above the soil surface as either a single layer ("bulk layer") or multiple layers ("multi-layer"). The albedo of pure snow is typically parameterized to evolve following snowfall through a dependence on either snow age or surface temperature (Qu and Hall, 2007). There are also differences in how mixed precipitation events are parameterized, with

the partitioning between rain and snow critical to snowpack evolution (Rutter et al., 2009; Essery et al., 2013).

An important portion of the NH snow-covered region is forested, so accurate simulation of canopy-snow interactions and vegetation masking are critical for the NH energy budget and water balance. Qu and Hall (2007) classified the various snow albedo masking schemes in the CMIP3 models. They found four distinct groups of models, each with increasing complexity, that were also employed in the newer CMIP5 models. The simplest and least sophisticated approach (referred to as "type 4" models) employs an albedo that is independent of land cover type and is instead related only to snow depth. The "type 3" group calculates albedo via the weighted average of snow-free surface albedo and snow albedo, as a function of SCF, while "type 2" models include the weighted average of canopy albedo and ground albedo, as a function of vegetation cover. The most sophisticated approach ("type 1") uses two-stream approximations for radiative transfer between (a potentially snow-filled) canopy and the surface (Qu and Hall, 2007; Essery, 2013). The type of snow vegetation masking scheme employed by models and the details of the vegetation masking schemes (i.e., simulated tree cover fraction, parameter values related to snow interception/unloading, etc.) play an important role in the seasonal evolution of albedo.

The primary goal of this work is to quantify the ability of CMIP5 models to accurately simulate the annual cycle of SCF and α_{sfc} over Northern Hemisphere land areas. This will allow different models to be directly compared in a standardized fashion, and provides a framework for the assessment of future improvements in simulated albedo and other snow processes. The simulation of month-to-month changes in α_{sfc} and SCF are

compared to satellite derived datasets for the NH as a whole, and over specific biomes (boreal forest and Arctic tundra) in order to identify land cover specific uncertainties in the simulations. The methodology and data are described in Section 3.3. In Section 3.4, we evaluate monthly changes in snow cover and albedo from climate models and satellite observations, while we quantify the model performance using a normalized skill score in Section 3.5. Section 3.6 contains a discussion of the importance of these findings, and how improvements can be made.

3.3 Data and Methods

3.3.1 Climate Model Data

We used monthly mean output for the period 1980-2005 from the suite of *historical* simulations from the CMIP5 archive (Taylor et al., 2012) to evaluate 16 models for albedo (Table 3-1), and 14/16 that provided snow data (i.e., archived either of the variables snc (SCF) or snw (snow mass)). For models where SCF was not provided, a conversion from snow mass (units kg m^{-2}) to SCF (units %) was applied, consistent with Qu and Hall, (2007) and Fletcher et al. (2012). This method was also applied to the satellite derived snow water equivalent (SWE) data described in Section 3.3.2. This estimate of SCF from snow mass was previously shown to agree very well with direct outputs of snow cover (see Appendix of Qu and Hall, 2007). All model output was regridded to a common grid using bilinear interpolation; for simplicity, we interpolate to the grid from the Community Climate System Model, version 4 (CCSM4), with spatial resolution 1.25° longitude x 0.95° latitude.

For a given model *i*, and a given variable X, the month-to-month change in climatological α_{sfc} and SCF was calculated as $\Delta X_i = X_{i,month2} - X_{i,month1}$. To simplify the

Table 3-1: List of models analyzed in this study with their institution, number of realizations (*n*) and Arctic SCF melt group. The right-hand column denotes the group that each model belongs to based on the pattern of snow melt over the Arctic (see Section 3.4.1).

Model	Institute	*n*	Arctic SCF Melt
ACCESS1-0	CSIRO-BOM	2	N/A
BCC-CSM1.1	BCC	3	Group 2
CanESM2	CCCMA	5	Group 1
CCSM4	NCAR	6	Group 1
CNRM-CM5	CNRM-CERFACS	10	Group 1
CSIRO-Mk3-6-0	CSIRO-QCCCE	10	Group 2
FGOALS-g2	LASG-CESS	5	Group 1
GFDL-ESM2M	NOAA GFDL	1	Group 2
GISS-E2-R	NASA GISS	6	Group 1
HadGEM2-ES	MOHC	5	Group 2
INM-CM4	INM	1	Group 2
IPSL-CM5A-MR	IPSL	3	N/A
MIROC5	MIROC	5	Group 1
MPI-ESM-MR	MPI-M	3	Group 2
MRI-CGCM3	MRI	3	Group 1
NorESM1-ME	NCC	1	Group 1
CLM4-QIAN	NCAR		
CLM4.5-QIAN	NCAR		
CLM4.5-CRUNCEP	NCAR		

interpretation of our results, in cases where institutes provided simulations from multiple versions of their models, one model (either the most recent version, or the version that was run at the highest horizontal resolution) was selected for the analysis. We have verified (not shown) that results from the other model configurations submitted from the same institute do not vary significantly from the single model selected. The ensemble mean of all available realizations (n=1 to 10; Table 3-1) was calculated for each model prior to beginning the analysis, which emphasizes deterministic over natural (internal) variability.

A series of offline simulations using the land component of CCSM4 (Community Land Model version 4.0; henceforth CLM4-OFF) (Oleson et al., 2010) were also utilized to help isolate the influence of biases in the simulated mean climate (Table 3-1). The first

simulation was forced for the period 1982-2004 by observation-based meteorological fields (precipitation, temperature, specific humidity, wind speed, surface pressure, and surface downward solar radiation) derived from a reanalysis product (Qian et al. 2006). For consistency with the other observational products used in this study (see below), we analyze only the period 2000-2004 from CLM4-OFF; we have verified that in this simulation there is minimal change in the seasonal cycle between 1982 and 2000 (not shown). A more recent version of the Community Land Model, version 4.5 (Oleson et al., 2013) includes improvements to the terrestrial snow parameterizations. The time evolution of SCF in CLM4.5 is calculated differently for accumulation and melt periods because of the complex relationship between snow water equivalent (SWE) and SCF during these times (Swenson and Lawrence, 2012). We evaluated two offline simulations using CLM4.5 to determine the impact of these model developments on the simulated seasonal evolution of the terrestrial cryosphere. The two CLM4.5 simulations were forced by, respectively, the same Qian et al (2006) dataset as CLM4-OFF, and an updated forcing dataset called CRUNCEP (Viovy, 2011).

3.3.2 Observational Data

We use satellite retrievals of albedo from the Moderate Resolution Imaging Spectroradiometer (MODIS) MCD43C3 product (Schaaf et al., 2002), the extended Advanced Very High Resolution Radiometer (AVHRR) Polar Pathfinder (APP-x) project (Wang and Key, 2005), and a suite of optical sensors synthesized within the GlobAlbedo project (Muller, 2013). Time series of albedo for the periods of 2000-2005 (MODIS, and GlobAlbedo) and 1982-2005 (APP-x) over the snow season were taken from these three

observational products from which a multi-dataset month-to-month climatological change in albedo was calculated.

A quality filter was applied to MODIS white-sky shortwave albedo (0.05° resolution; upscaled by aggregating the native 500m product) such that only high-quality (grade 2 or better) retrievals were included in our analysis. This quality measure is determined by how many cloud-free observations were acquired over a 16-day period. When observations are limited, a backup model produces albedo estimates using prior knowledge of the surface (Strugnell and Lucht, 2001; Jin et al., 2002). In the case of grade 2 data, 25% or less of the data is in-filled by this backup model (Schaaf et al., 2002).

APP-x daily blue-sky albedo (the weighted average of black- and white-sky, as a function of cloud cover (Wang and Key, 2005)) data was acquired on an Equal-Area Scalable Earth Grid (EASE-Grid) at a spatial resolution of 25 km. This instrument has an orbital configuration centered on the North Pole, which limits the spatial domain of the NH to areas polewards of ~50° N. This domain still captures a majority of seasonally snow-covered regions and significantly lengthens our climatological study period, by using all available data from 1982-2005.

Lastly, we use monthly mean white-sky shortwave albedo from GlobAlbedo (Muller, 2013) at a 0.05° resolution. GlobAlbedo uses measurements from the Advanced Along Track Scanning Radiometer (AATSR), SPOT4-VEGETATION, SPOT5-VEGETATION2, and the Medium Resolution Imaging Spectrometer (MERIS) to get an optimal estimation of albedo, while surface anisotropy data from MODIS is used to help gap fill (Lewis et al., 2013; Muller, 2013). There are, however, documented issues related to snow detection and large

solar zenith angles (SZA) at high latitudes (~70°N) which cause some artefacts (Muller, 2013; He et al., 2014).

A multiple observational approach was used to mitigate the uncertainty associated with each product individually (Brown and Derksen, 2013; Fletcher et al., 2015). For example, data gaps exist in the quality filtered MODIS albedo, despite its 16-day retrieval window, because of persistent winter cloud coverage (Barlage et al., 2005). This extensive winter cloud coverage also means that the diffuse component of albedo (white-sky) dominates the direct component (black-sky) for much of our study period and makes the greater contribution to the actual albedo for ambient sky conditions (blue-sky). Therefore we assume that any differences due to our use of blue-sky (APP-x) and white-sky albedo (MODIS, GlobAlbedo) are minor. It should also be noted that Wang et al. (2004) suggested white-sky albedo is better suited for model comparison than black-sky because it uses the integral of black-sky albedo across all SZAs. Despite the methodological differences and the independent sources of satellite measurements (MODIS; AVHRR; AATSR), we find good agreement between the observational albedo products, as illustrated by their temporal correlations computed using monthly mean climatological albedo (MODIS/APP-x $R^2 = 0.99$ over the NH_{snow} region, MODIS/GlobAlbedo $R^2 = 0.84$, APP-x/GlobAlbedo $R^2 = 0.82$; possible reasons for why they differ are discussed in He et al. (2014)). Therefore, we evaluate the models against a blended observational dataset (henceforth, OBS_{blend}) that is the mean of the monthly climatologies from the three albedo products. The observational agreement is also demonstrated by a low mean albedo bias (MODIS = -0.002, APP-x = -0.007, GlobAlbedo = 0.009) and mean absolute error (MODIS = 0.011, APP-x = 0.017,

GlobAlbedo = 0.028) relative to OBS_{blend} over the snow season. The weaker agreement for GlobAlbedo is largely due to a tendency to reach its maximum albedo earlier in the winter than the other products (see Fig. 2b and Fig. 3a of He et al. (2014)). In terms of location, the observational differences are largest at high latitudes (60-75°N), which we speculate is linked to retrieval uncertainty as a result of very large SZA during winter. We take the approach that including all available products is better than excluding one because of slight differences from the average. In any case, removing the least certain product does not affect our conclusions. The use of a multi-dataset mean mitigates the impact of individual product biases in the absence of an evaluation of the albedo products, and in the future more datasets could be added.

Uncertainties with satellite-derived albedo products can be large at high latitudes during winter because of extensive cloud coverage (Fang et al., 2007) and high solar zenith angles (Schaaf et al., 2002). However, polar night presents an even bigger challenge, because as the area covered by polar darkness expands during early winter—peaking around the winter solstice—the NH mean albedo decreases artificially. The reason is that a progressively larger swath of snow-covered land over the Arctic (including much of the tundra, which has very high mean albedo ~ 0.7) is excluded from the calculation, because all areas under polar darkness are set to missing values (by definition, albedo cannot be defined when incoming solar radiation is zero). The problem is most acute in December (hereafter, all months will be abbreviated by their first three letters, i.e., Dec), when the area of polar darkness is largest and we found a decreasing trend in NH mean albedo at a time when snow extent is still expanding. To correct for this artefact, we estimate NH mean albedo (and non-boreal Arctic

albedo) in Dec using a linear interpolation between mean values from the two neighboring months (Nov and Jan). This method allows us to compare albedo values over the same land area in all months, while also retaining the important Arctic tundra region in our analysis domain (see Section 3.3.3).

SCF data are drawn from two satellite-derived products. Monthly SCF from version 5 (http://dx.doi.org/10.5067/IPPLURB6RPCN) of the MODIS MOD10CM product (2000-2005) is output on a 0.05° global grid through aggregation of the native 500 m resolution (Hall et al., 2002; Hall et al., 2006). Daily SWE taken from the GlobSnow data record (Takala et al., 2011) was also converted to SCF (2000-2005). A snow mass threshold of 60 kg m^{-2} was used to assign a pixel as fully snow-covered, and a value less than this was divided by the threshold to give a fractional value (as described in Thackeray et al., 2014). Using a fixed threshold value in this calculation does not account for seasonal changes in snow density or snow patchiness (snow cover tends to be patchier during melt). MODIS SCF was used to fill in alpine areas where GlobSnow data is not provided; however, the MODIS snow product can be susceptible to some of the same issues affecting retrievals of albedo, such as extensive cloud cover during the accumulation period (Klein et al., 1998; Hall et al., 2002). All of the satellite-derived products described here were regridded to the same spatial grid as the model output using bilinear interpolation.

3.3.3 Study Area

Our analysis was conducted over an area we refer to as the "NH snow covered region" (henceforth NH_{snow}), which is represented by colored shading in Fig. 3-1. The NH_{snow} region

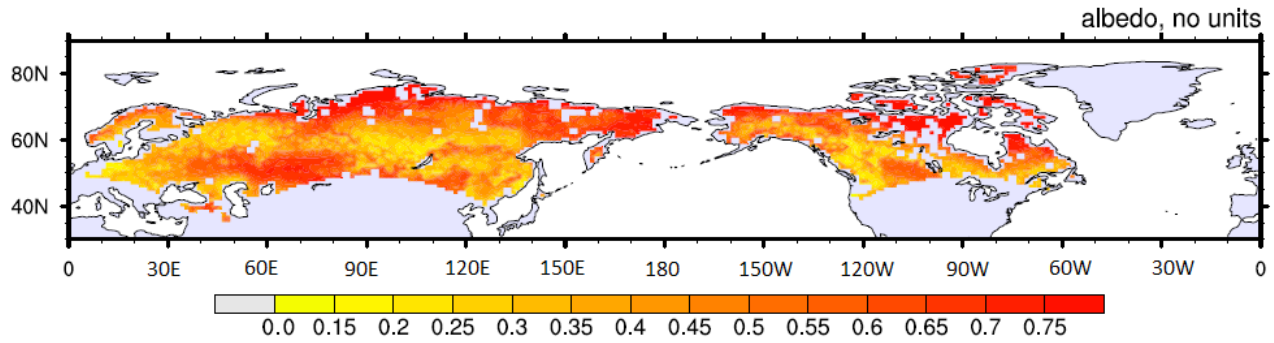

Figure 3-1: Maximum monthly mean surface albedo from the blended observational dataset over the Northern Hemisphere snow-covered region. Missing data (gray) either falls outside of the APP-x domain or is not classified as being snow covered by MODIS (not enough snow on average or missing in all years).

includes only grid cells over NH land (excluding Greenland) with at least 25% snow cover in their February MODIS climatological SCF (Fig. 3-1). The use of an observed snow mask means that we are excluding areas where the models may overpredict snow cover, but this is likely to be a small effect that is restricted to low-latitude areas with ephemeral snow cover. In addition, NH_{snow} is further reduced to match the EASE grid projection of the APP-x data product (Wang and Key, 2005). One limitation is that certain grid cells (primarily over central Canada and Siberia) are classified as missing in NH_{snow} because their underlying landscape has a high lake fraction, over which MODIS does not retrieve snow cover. The extent of the APP-x domain means that areas like the Tibetan Plateau were omitted; however, APP-x provided a much longer climatological period to evaluate albedo than is provided by MODIS or GlobAlbedo.

We also identified two specific land cover classes that pose unique challenges for model simulations of snow processes: the boreal forest and the non-boreal Arctic. The boreal forest is an expansive portion of the terrestrial Northern Hemisphere that has an extensive snow cover season and is primarily made up of needleleaf evergreen trees (Bonan et al.,

2002). In an effort to eliminate biases from other land cover types, we isolated this area by defining the boreal forest region as all grid cells where the MODIS plant functional type (PFT) (Friedl et al., 2002) boreal needleleaf evergreen exceeds 75 %. This threshold allows for a sufficiently large study area [~4.9 x 10^6 km^2], while simultaneously limiting the influence from non-boreal PFTs.

The non-boreal Arctic region was isolated by combining the area covered by at least 75% of the three MODIS Arctic PFTs (Arctic shrub, Arctic grass, and bare land/tundra) north of 60°N. However, it should be noted that observational uncertainty for retrievals of albedo is much larger in this region because of higher solar zenith angles (Schaaf et al., 2002). Also, the analysis for this more northerly region was conducted over an extended snow season (Aug-Jul) to fully capture the evolution of snow onset and ablation. This high latitude region is important because it is expected to be a bellwether for cryospheric impacts of climate change (Chapin et al., 2005; Vavrus et al., 2012; Cohen et al., 2014). Furthermore, fundamental snow processes unique to the Arctic, such as wind-driven snow redistribution and sublimation loss, are currently not adequately represented in most models (Essery and Pomeroy, 2004; Turner et al., 2006). Lastly, the suite of CMIP5 models use a number of different land cover classification systems (many models use MODIS derived land cover, but others use Global Land Cover 2000 (GLC2000) data (Bartholome and Belward, 2005)). In addition, two models evaluated here (HadGEM2-ES and MPI-ESM-MR; both of which underestimate tree cover fraction over the Northern Hemisphere (Loranty et al., 2014)) are run with Dynamic Global Vegetation Models (DGVMs), meaning that the simulated distribution of vegetation evolves in response to climate changes (Collins et al., 2011;

Brovkin et al., 2013). The boreal and non-boreal Arctic regions defined above using the MODIS PFT data may not, therefore, correspond precisely to the boundaries of the boreal forest, or tundra/grass, in all models. However, visual inspection of GLC2000 data verifies that differences between the land cover classification systems is small. This indicates that using another product, for example GLC2000, to formulate the analysis regions would not significantly alter our conclusions.

3.4 Results

3.4.1 Seasonal Biases in Snow Cover Fraction

We first evaluate the CMIP5 representation of the seasonal cycle of SCF over the Northern Hemisphere snow-covered region (NH_{snow}), during the complete snow season (Sep-Jun). This is of interest because the evolution of the snowpack during onset/melt periods is important for cryosphere-climate influence and feedbacks which vary with land cover. Figure 3-2 shows that the observed seasonal evolution is marked by a steady increase in SCF over the fall, a stable peak during mid-winter, and a dramatic melt in the spring. Simulated SCF agrees closely with observations during the majority of the snow season (Nov-Apr), with larger biases and spread at the start and end. The timing of snow advance and retreat are also both accurately captured by the models. There is, however, a low bias (Model – OBS) in the magnitude of these changes in Sep-Oct and May-Jun, which are underestimated by ~5% SCF in the multi-model ensemble median (MM_{Med}) (equal to 17% of the relative change in OBS_{blend}).

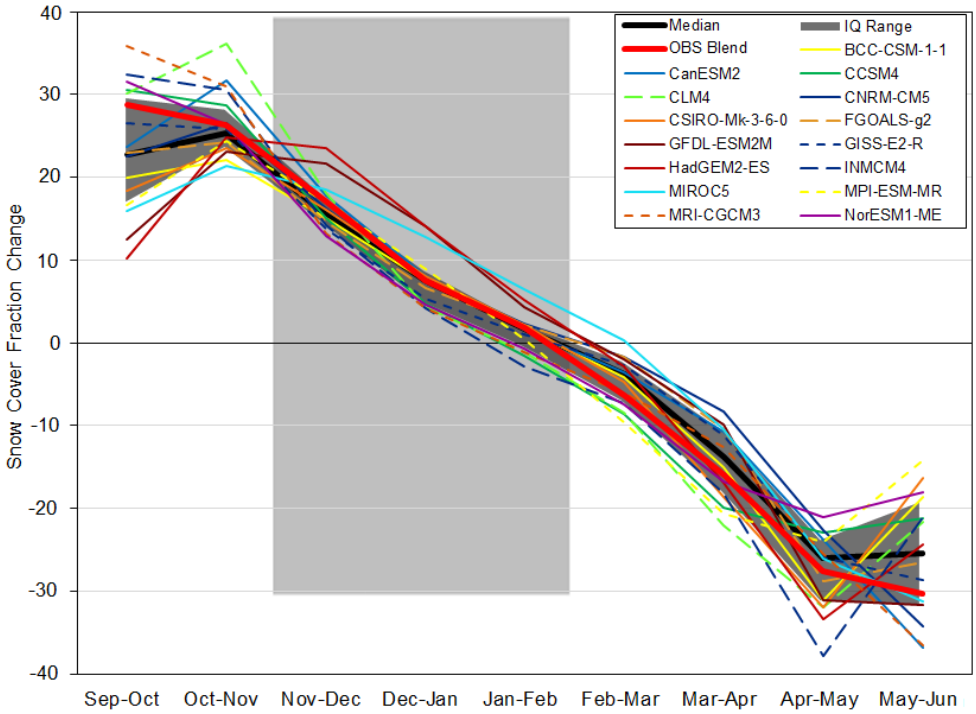

Figure 3-2: Monthly change in snow cover fraction (%) for Northern Hemisphere snow-covered land (excluding Greenland). Monthly changes are climatologies over the 1980-2005 period for CMIP5 models. The ensemble median (black line) is the median SCF change amongst all CMIP5 models, while the dark-gray region captures the interquartile range. The light-gray shaded region indicates months of the year when observational uncertainty is high due to large solar zenith angle (>75°).

In general, the models agree quite well with each other, as demonstrated by the small interquartile range (IQR); we define this envelope as the "zone of model consensus" (dark gray shading in Fig. 3-2). Intermodel spread (maximum value - minimum value) in the fall is likely related to snowfall sensitivity to small temperature biases (which influences the phase of precipitation) and the modeled relationship between SWE and SCF (i.e., how much snow mass is required to change SCF), whereas in the spring it is likely more related to how snow melt is parameterized within the models. Figure 3-2 also indicates that the CMIP5 ensemble median better agrees with observations during the snow accumulation period than the snow ablation period. On average, the models realistically reproduce the NH_{snow} region seasonal

cycle of SCF. This conclusion agrees well with Brutel-Vuilmet et al. (2013), who examined a slightly different subset of CMIP5 models over the entire Northern Hemisphere.

The month-to-month changes in SCF over the boreal region in all models show larger biases than for the entire NH_{snow} region (Fig. 3-3a). There are seven models that show a relatively rapid melt during Mar-Apr, one month before observations. Despite this bias, the MM_{Med} accurately captures the timing of snow accumulation and melt on a month-to-month basis. However, the amplitude of the simulated changes in SCF is much smaller than in observations, which lie outside the zone of model consensus in both Sep-Dec and Apr-May. It is important to point out that this Apr-May low bias (~15% ΔSCF) occurs primarily because the previously noted group of seven models melt too much snow in the month prior, and not because SCF persists for too long. At least two of these models (MPI-ESM-MR and HadGEM-ES) underestimate tree cover fraction across the boreal region (Loranty et al., 2014), which we speculate could be influencing their simulated SCF evolution through a lack of snowpack masking.

Over the non-boreal Arctic region snow cover persists for an additional 1-2 months compared to lower latitudes (Fig. 3-3b). Snow onset occurs rapidly at these latitudes and its timing is realistically represented by the MM_{Med}, which captures the magnitude of this change in Sept-Oct (~6% difference in ΔSCF). The period Dec-Apr, with SCF in a steady state, is well simulated by all models. The Arctic land surface remains completely snow covered at this time, due to mean ambient temperatures that are typically well below freezing. On average, the models capture the loss of snow cover accurately in Apr-May

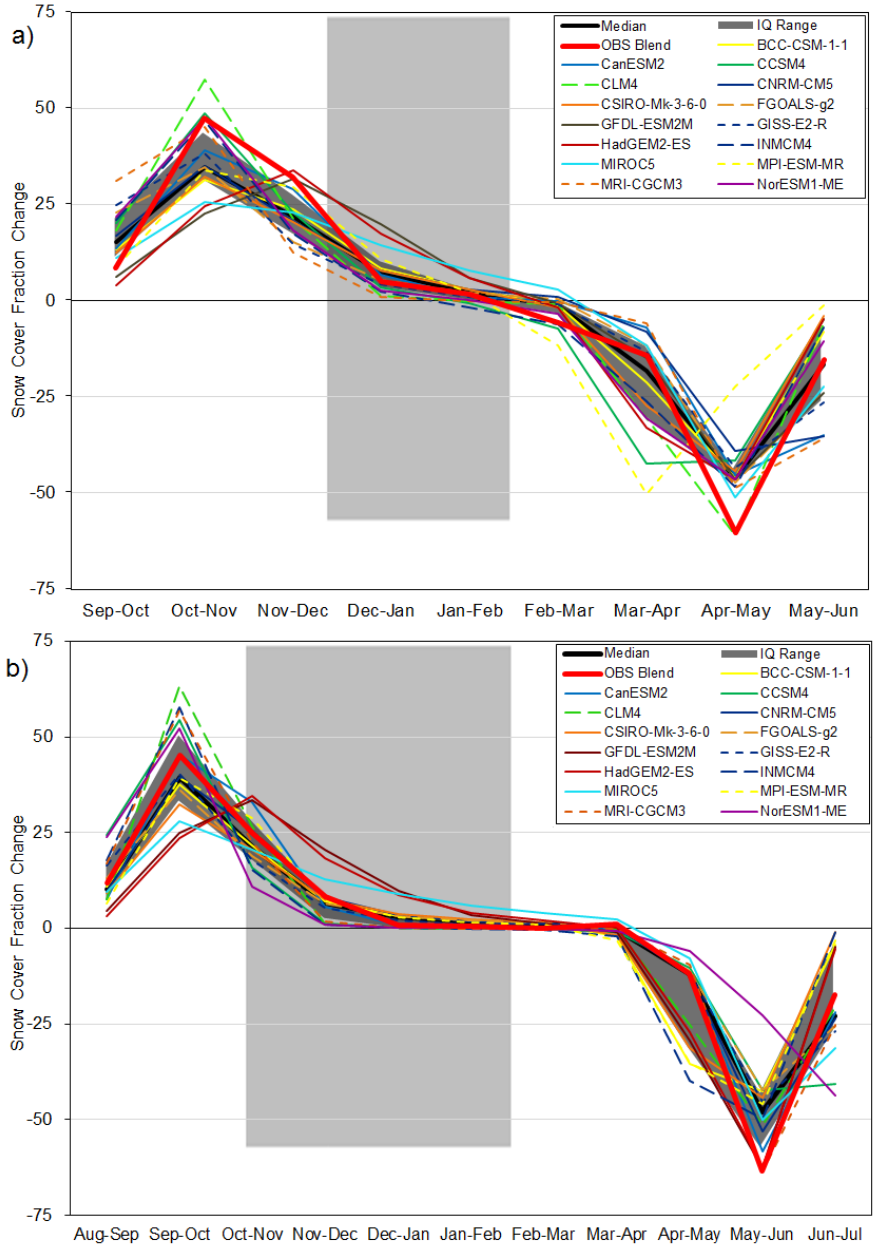

Figure 3-3: (a) Same as Fig. 3-2, but for the Boreal forest region (>75% boreal evergreen needleleaf PFT). (b) Same as Fig. 3-2, but for the non-boreal Arctic region (>75%) and showing an extended snow season (Aug-Jul).

(CMIP5: -12% ΔSCF, OBS_{blend}: -12% ΔSCF), but underestimate the median melt rate in May-Jun (CMIP5: -49% ΔSCF, OBS_{blend}: -63% ΔSCF) due to an apparent bimodal distribution in melt rates. The CMIP5 models can be divided into two groups, based on their

snow cover melt rates over the Arctic. A subset of eight models loses less than 10% SCF in Apr-May (Group 1; Table 3-1), whereas the remainder loses between 30-40% SCF during the same period (Group 2). Overestimated melt rates in the Group 2 models leave them with unrealistically low mean SCF by June (< 5% SCF compared to 19% in the observations; Fig. 3-3b). We associated the low SCF biases with biases in mean springtime air temperature: the six Group 2 models are, on average, 3.4°C warmer over the Arctic sector during May than the eight Group 1 models. This temperature bias causes a low bias in the MM_{Med} ΔSCF for May-Jun. Again, this is the result of stronger simulated snow melt early in the melt season causing significantly reduced mean SCF in Jun, because much of the snow has already melted.

3.4.2 Seasonal Biases in Albedo over the NH

The observed seasonal cycle of climatological albedo is marked by a steady increase in fall that occurs with the expansion of snow cover; α_{sfc} increases gradually throughout winter to a peak in Mar, then begins to decline as the snow melts. Over the entire NH_{snow} region, simulated α_{sfc} shows generally larger biases than for SCF (Fig. 3-4a). On average, the models tend to overestimate the magnitude of albedo increase during the accumulation period (Sep-Oct-Nov), which leads to the models having a larger peak albedo than observations (CMIP5: 0.51, OBS_{blend}: 0.46). The timing of α_{sfc} changes is also somewhat different in the models, which reach their maximum albedo earlier with obvious implications on the absorbed shortwave radiation at the surface. A fundamental question is whether the α_{sfc} biases are related to snowfall biases during these months. To investigate this we calculate the inter-model correlation between biases in these two variables. We find a very weak positive inter-

model correlation between mean absolute SCF biases and mean absolute albedo biases during the accumulation period ($R^2 = 0.02$). Therefore, we conclude that factors other than biases in SCF are responsible for the albedo biases.

There are also model biases in the timing of the decrease in α_{sfc} coincident with snow melt. It should be noted that since we are looking at the NH average, the decrease is when the albedo over this snow-covered region begins to decline more than it is increasing as there are regional variations in the transition from increasing to decreasing albedo. The peak simulated albedo occurs at peak snow cover extent (Fig. 3-4a), whereas in the observations α_{sfc} increases throughout the winter, suggesting that SCF is not the only controlling factor. The ensemble mean simulated month-to-month changes in albedo and SCF are very strongly correlated ($R^2 = 0.99$), while a slightly weaker positive correlation exists for the observations ($R^2 = 0.86$). We speculate that the excessive correlation in the models is a result of many models having albedo parameterizations that are too dependent on the fraction of ground that is snow-covered and not enough dependent on snow aging or snow-vegetation interactions (see Qu and Hall, 2007; Essery, 2013).

We elect to normalize the change in albedo bias across regions because unlike SCF, the seasonal maximum albedo varies strongly with land cover type. In Fig. 3-5 we are therefore showing the fractional contribution of the bias, relative to the observed peak value (α_{max}) at a location (Eq. 3-1):

$$NBias = Bias / \alpha_{max} \quad . \qquad (3\text{-}1)$$

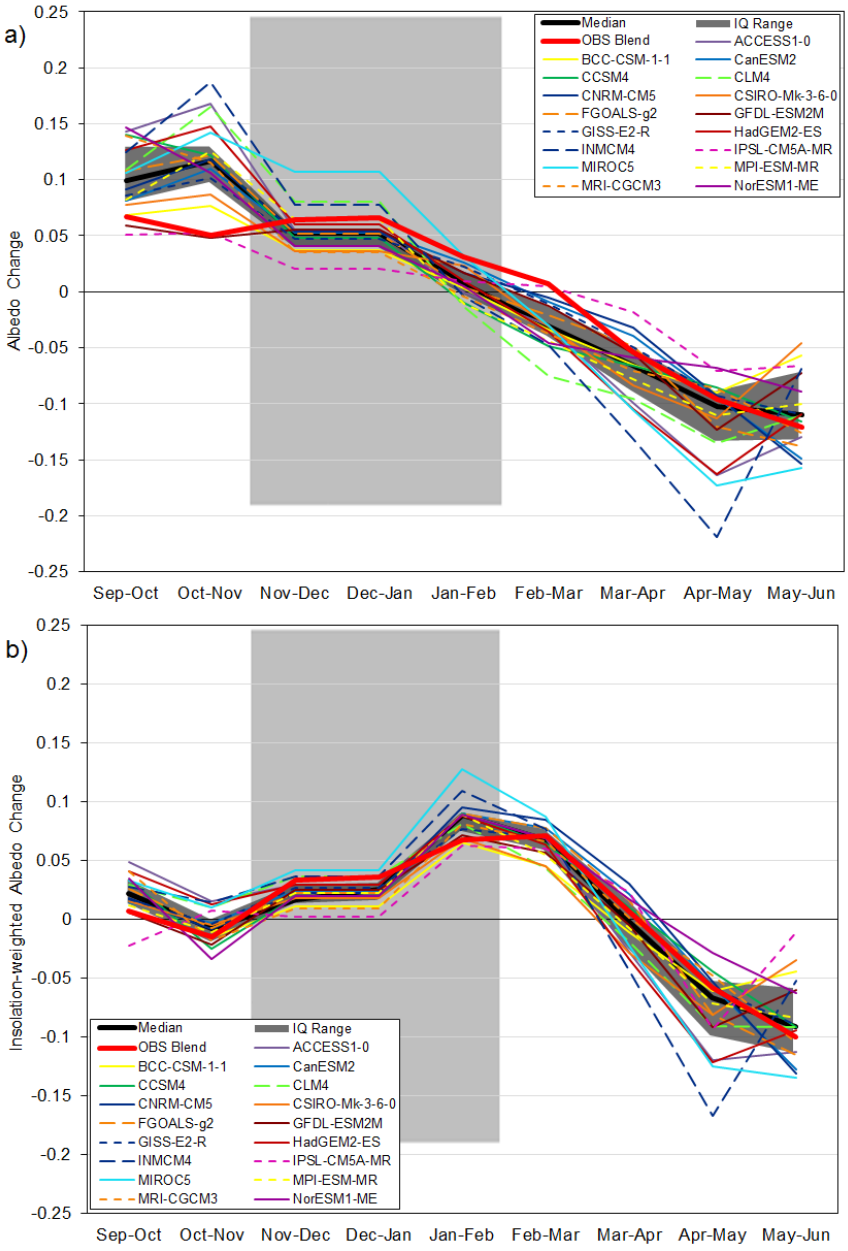

Figure 3-4: (a) Monthly change in albedo for Northern Hemisphere snow-covered land (excluding Greenland). (b) Monthly change in insolation-weighted albedo for NH snow-covered land. Monthly changes are climatologies over the 1980–2005 period for CMIP5 models. The ensemble median (black line) is the median albedo change amongst all CMIP5 models, while the dark-gray region captures the interquartile range. The light-gray shaded region indicates months of the year when observational uncertainty is high due to large solar zenith angles (>75°).

This metric reveals that the overestimation of fall albedo change by the CMIP5 models occurs across much of the NH, as indicated by the areas with positive values in Fig. 3-5a.

The models show less bias when simulating the mean albedo change during the mid-winter (DJF- mean albedo change bias over Nov-Dec, Dec-Jan, and Jan-Feb; Fig. 3-5b), but once again show greater bias during the March-April-May-June (MAMJ) melt period, on average showing slightly stronger albedo changes than the observations (Fig. 3-5c). Errors during this melt period are of particular importance because this is the time when snow albedo feedback is at its strongest, due to increasing insolation and extensive snow cover (Hall, 2004; Qu and Hall, 2006). In order to determine the climatic importance of these biases, similar to the approach of Fletcher et al. (2012) we recalculate the climatological albedo quantities weighted by the fractional local contribution (relative to the mean over the NH land) of incoming shortwave radiation at the top of the atmosphere. This reduces the influence of more uncertain observations from high latitude regions where SZA is large in winter, and emphasizes more southerly regions with lower SZA. Insolation-weighting also reduces the importance of albedo biases during SON (Fig. 3-4b) as this is a time when incident radiation is decreasing over the NH_{snow} region. The model bias and intermodel spread during the melt period remain largely similar after the weighting is applied, further illustrating the importance of springtime albedo for the surface energy balance (Qu and Hall, 2007; Fletcher et al. 2012).

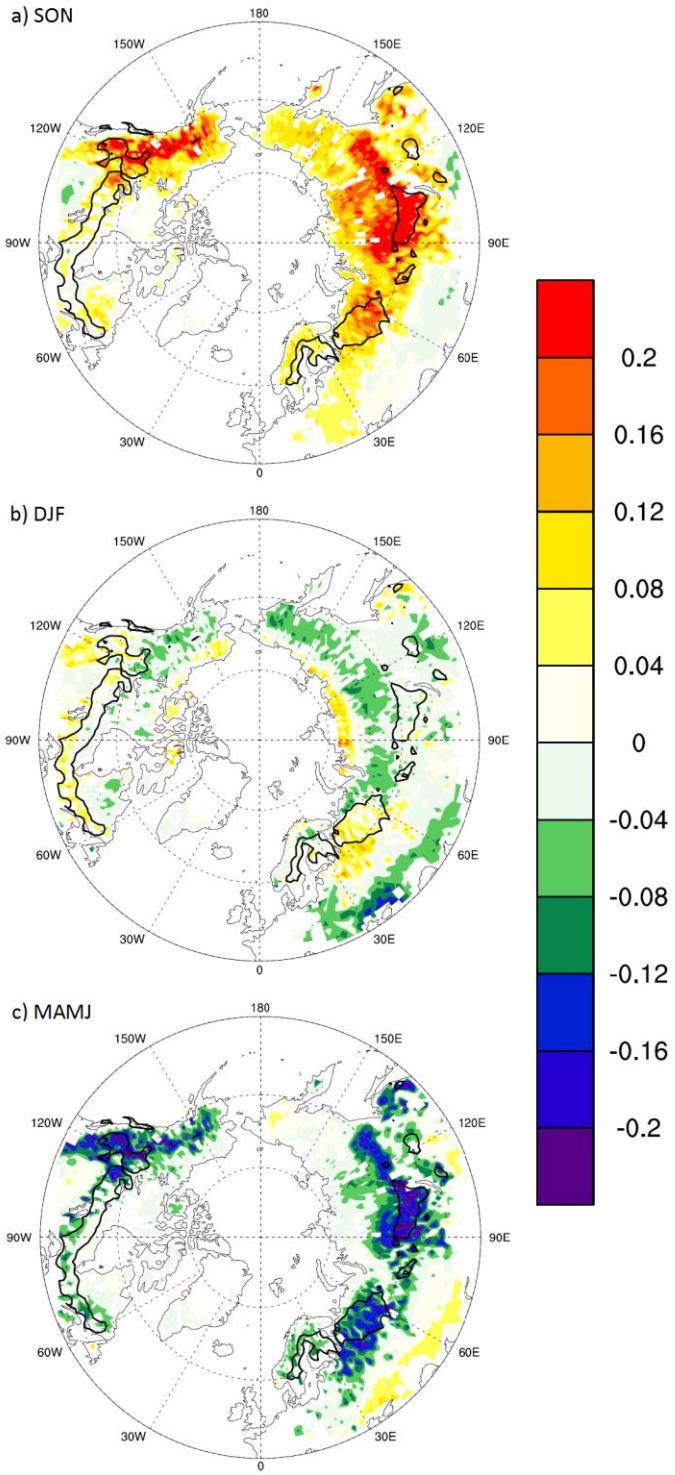

Figure 3-5: Maps of normalized model bias (CMIP5 mean - OBS)/OBS in seasonal mean albedo change for (a) SON (b) DJF and (c) MAMJ. Normalized by peak albedo to account for variations in land cover (maximum albedo is land cover dependent). The boreal region (>75%) is outlined in black.

3.4.3 Regional Albedo Change Biases

In order to better understand model bias, it is critical to first determine where the model uncertainty is largest. First, we focus on the boreal forest, a known problem area for simulated albedo (Thackeray et al., 2014) (the boundary of the boreal region is outlined in black in Figs. 3-5a-c). Models that fall outside of the zone of model consensus tend to suffer from deficiencies in the timing and/or magnitude of boreal albedo changes (Fig. 3-6a). As is the case for the NH_{snow} region as a whole, there is a clear overestimation of albedo change among the majority of models in fall, and a similar compensatory overestimation of the opposite sign during spring. This indicates that the amplitude of the range of albedo—from snow-free to snow-covered—is larger in the models than in observations, despite the amplitude of simulated SCF being less than observed (Fig. 3-3). Just as for the NH as a whole, month-to-month changes in insolation-weighted albedo over the boreal region show that the biases in SON are minimized in terms of importance to the energy budget (Fig. 3-6b). The MM_{Med} reproduces observations throughout the snow season, but a positively skewed model distribution causes the multi-model mean to be biased high (not shown).

There is also a discrepancy in the timing of the decrease in albedo that occurs during the winter-to-spring transition (Fig. 3-6a), which in a majority of CMIP5 models begins one month earlier than in observations. This provides evidence, consistent with Thackeray et al. (2014), that the treatment of snow on the boreal forest canopy is a likely source of the albedo transition bias. However, we note that the one-month bias for the larger CMIP5 group of models represents a less significant bias in timing than the two-month discrepancy that was reported by Thackeray et al. (2014) for CCSM4, suggesting that CCSM4 is an outlier.

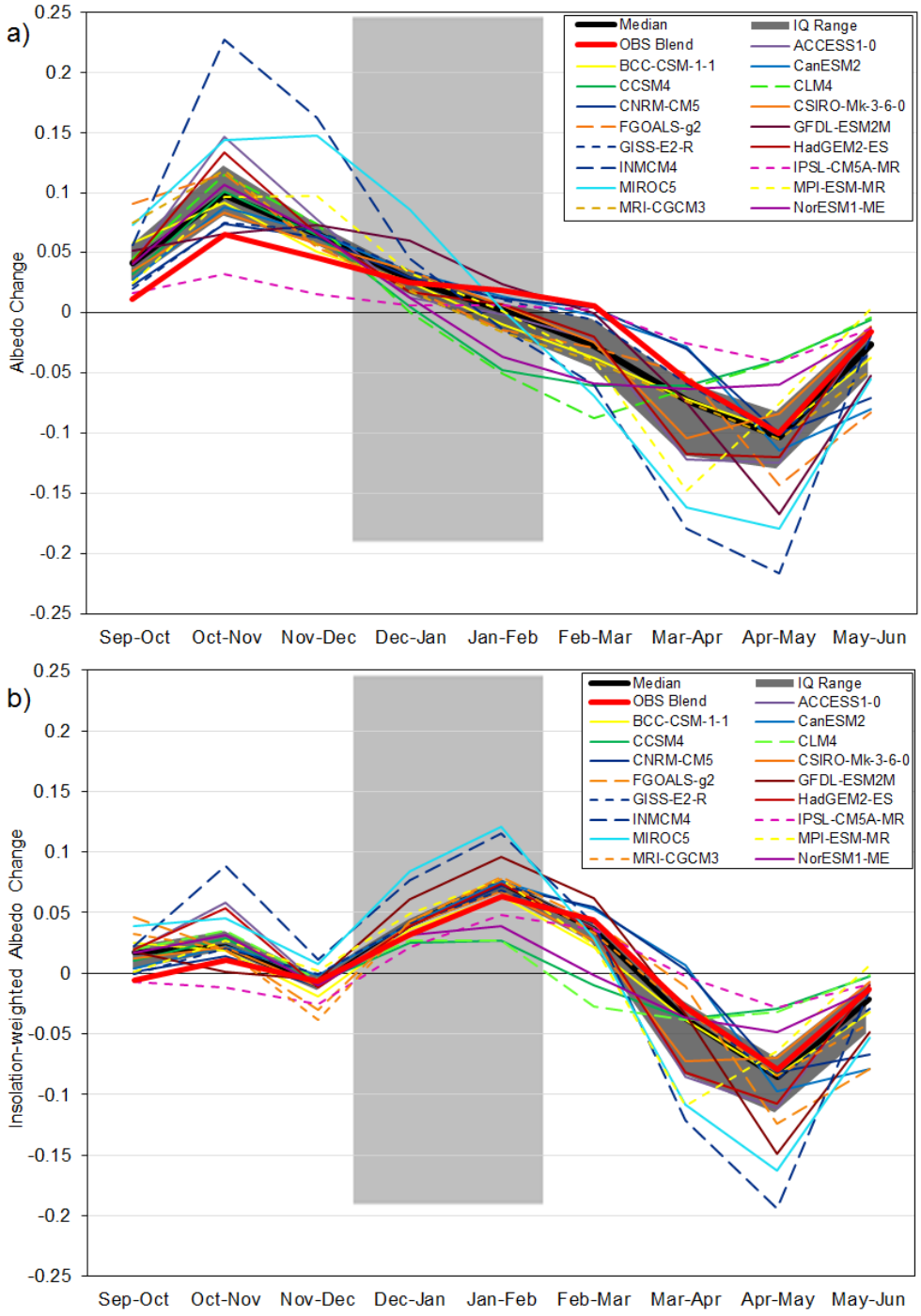

Figure 3-6: Same as Fig. 3-4, but for the boreal forest region.

Only the NorESM model shows the same two-month discrepancy that exists in CCSM4, and this model uses the same land model (CLM4) as in CCSM4 (Bentsen et al., 2013). Research

is ongoing to reduce these model biases in CCSM through the development of a new canopy snow offloading scheme (J. Perket, personal communication, 2015).

In general, over the boreal forest the models show a stronger albedo change than observations during the melt period, a result that agrees with Loranty et al. (2014). We find that 14/16 models overestimate the amplitude of the seasonal cycle of albedo (Fig. 3-6a). Our principle finding is that model biases in the seasonal evolution of albedo are caused by deficiencies in the timing and magnitude of peak α_{sfc_snow}. The knock-on effect is that an overly strong albedo decrease during spring is necessary to balance the overly large albedo increase during fall. It is worthwhile to point out that this overestimate of albedo is not driven by the simulation of terrestrial snow cover, which we have shown does not persist in the models for significantly longer than in OBS_{blend} (Section 3.4.1). Instead, we find that the bias in the timing of the albedo changes is related to errors in the simulated peak α_{sfc_snow}. Models that poorly simulate the monthly evolution in albedo over the snow season fail to accurately represent the maximum observed monthly mean α_{sfc_snow} over the boreal region and/or the timing of its occurrence (Fig. 3-7a). A majority of models (14/16) overestimate peak α_{sfc_snow}—by more than 50% in some cases—and the peak α_{sfc_snow} tends to occur in Jan or Feb, whereas in observations it occurs in Mar. There is also greater model uncertainty (as indicated by a larger IQR) during the melt period (Mar-Apr IQR = 0.062, Oct-Nov IQR = 0.042), illustrating a general lack of model consensus over the boreal forest during the spring melt season (Fig. 3-6a).

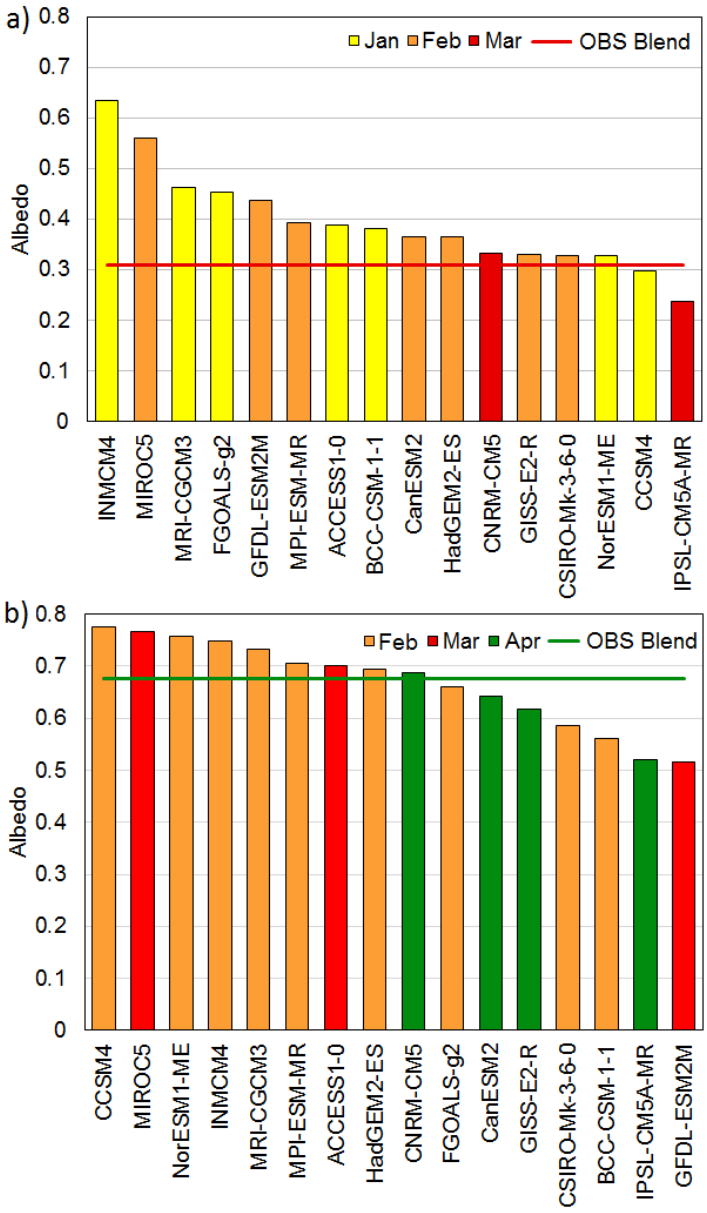

Figure 3-7: Maximum monthly mean surface albedo of CMIP5 models over (a) the boreal region and (b) the non-boreal Arctic region. Color coded to show which month the peak albedo occurs during. The individual observational products (not shown) all fall within 0.02 of the OBS Blend mean for both cases. The color of the observational line is the month in which the OBS Blend reaches its maximum.

For the non-boreal Arctic region, comparison of the multi-model ensemble mean and observations reveals close agreement in terms of the maximum monthly mean albedo (CMIP5: 0.66, OBS_{blend}: 0.67). This is because of an equal spread of models above and

below the observed peak α_{sfc_snow} (Fig. 3-7b). However, 75% of models incorrectly simulate earlier timing of peak albedo over this Arctic region (9 models identify Feb as the peak and 3 identify Mar), which observations show to be April. This bias means that, on average, the simulated albedo starts to decrease in Mar-Apr (Fig. 3-8a) because of stronger snow melt in the models during the early portion of the melt period (Section 3.4.1). This causes a low bias in albedo change during the melt phase, contrary to the situation over the boreal region. As for the insolation-weighted albedo, the MM_{Med} matches observations very well throughout the snow season until May-Jun when a bias exists as the observations show a much stronger decrease in insolation-weighted albedo.

3.5 Bias Quantification

3.5.1 Skill Metric

To quantify uncertainty in model performance and track model development, benchmarking metrics are needed to assess model bias (Model – OBS) (Hargreaves et al., 2013). The representation of the seasonal cycle of SCF and α_{sfc} in the CMIP5 models was evaluated using a normalized skill score that, to our knowledge, has not been applied in this context before. SCF is an important variable to evaluate because it is directly linked to the calculation of surface albedo in many models. We first applied a skill calculation (SS; Eq. 3-2) based on Eq. 4 from Taylor (2001), which was adapted for the temporal rather than spatial domain, to the monthly mean changes in SCF and albedo area-averaged over our analysis regions

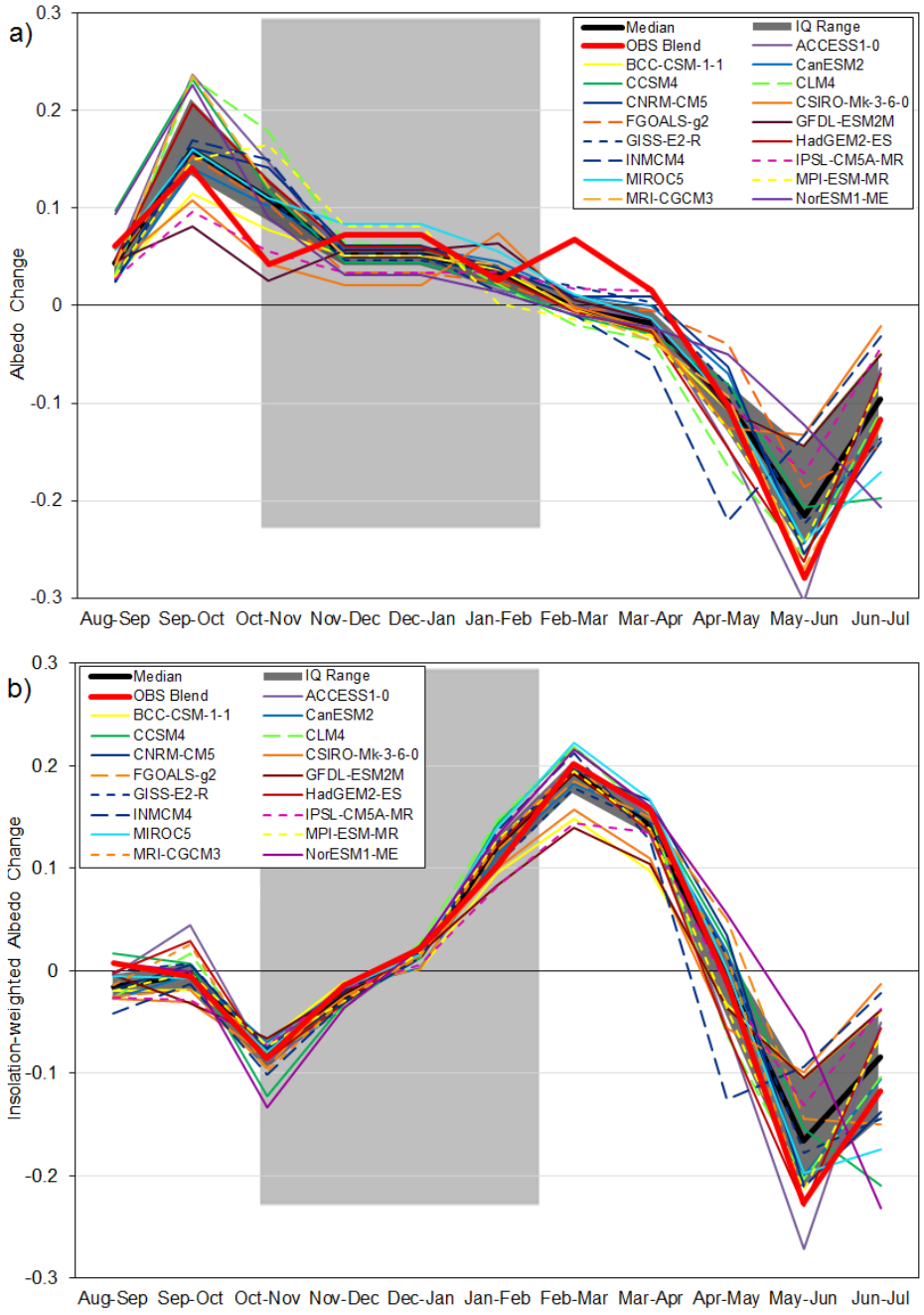

Figure 3-8: Same as Fig. 3-4, but for the non-boreal Arctic region (>75%). The observational period is extended to include the whole snow season (August-July).

(Section 3.3.3). We simplified this calculation by assuming that the maximum correlation between two datasets (the R_o term in Eq. 4 of Taylor (2001)) was unity (rather than 0.9976 as

calculated for Taylor's example), thus removing R_o from the equation (this has a negligible impact on SS). This method provides a statistical synopsis of how well two datasets agree, taking into account their correlation, and the ratio of their variances.

$$SS = \frac{2(1+R)}{(\hat{\sigma}_f + 1/\hat{\sigma}_f)^2} \quad (3\text{-}2)$$

where R is the correlation between the model output and observations, and $\hat{\sigma}_f$ is the ratio of standard deviations (model / observed). We averaged the skill scores computed separately for albedo (SS_{alb}) and for SCF (SS_{scf}) to yield a total skill score (SS_{tot}).

$$SS_{tot} = (SS_{alb} + SS_{scf}) / 2 , \quad (3\text{-}3)$$

We calculated SS for each of our analysis regions, and over multiple time periods, to highlight areas and times where model biases are strongest and the most model development is required. This metric penalizes incorrect simulation of pattern variance (seasonal cycle amplitude) and correlation (seasonal cycle timing), but it does not penalize mean bias. However, mean biases do not impact SS because it is calculated using the month-to-month change in bounded variables (i.e., albedo and SCF both start and end the snow season at similar values). Similar to Taylor diagrams (Taylor, 2001), this normalized skill metric could be applied to directly compare other bounded variables, unrelated to the cryosphere, to quantify the ability of models to simulate their time evolution against observations.

3.5.2 CMIP5 Skill Score Results

When SS_{tot} is computed for the entire NH_{snow} region, the models agree well with observations. This is best demonstrated by the multi-model mean SS_{tot} of 0.86 (Fig. 3-9a), and a range of only 0.72-0.92 across models (SS_{tot} = 1.00 would represent a perfect score).

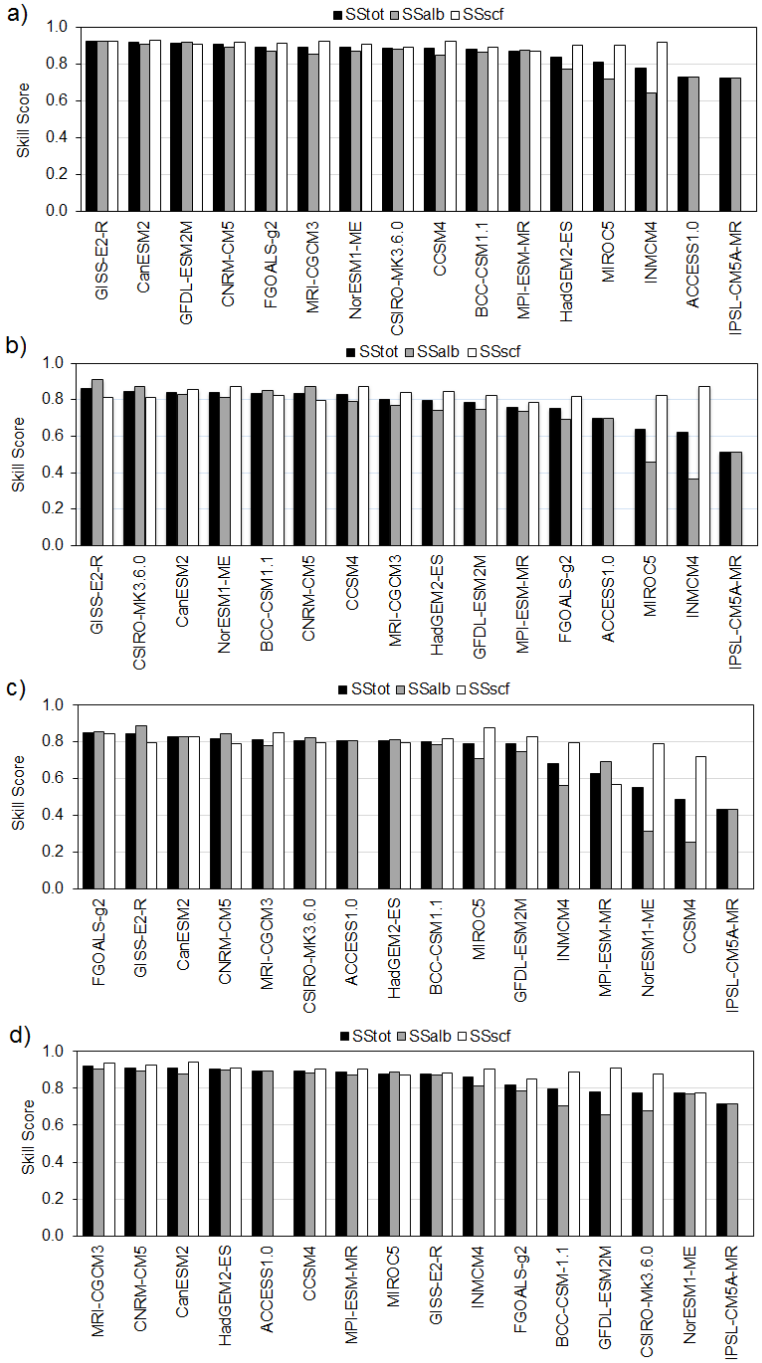

Figure 3-9: (a) Clustered bar plot showing Northern Hemisphere skill scores (Sep-Jun) in descending order of SS_{tot}. There are three scores for each model (total, albedo, scf) represented by the different bars. There are certain model configurations for which SS_{scf} could not be calculated ($SS_{tot} = SS_{alb}$ in these cases). (b) same as a for Boreal Region (c) same as b but isolating for the melt period (only Jan-Jun) (d) same as a for non-boreal Arctic.

This implies that there is a small degree of bias over snow-covered regions in a majority of the models. In comparison, over the boreal region there is greater model uncertainty with a mean SS_{tot} of 0.76 and a range of 0.51-0.86 (Fig. 3-9b). This decrease of 0.10 in the mean total score indicates that the boreal forest is a problem area for the models when it comes to simulating the seasonal evolution of the cryosphere. During the boreal melt period the scores are even lower for SS_{tot} (mean SS_{tot} = 0.73, range = 0.48–0.85; Fig. 3-9c), which is related to weaker performance in a number of models, not only outliers. The non-boreal Arctic region is better simulated than the boreal region, with SS_{tot} close to the NH_{snow} average at 0.85, and with a similar range (0.71-0.92; Fig. 3-9d).

To better determine the source of the model biases, we decompose SS_{tot} into contributions from SCF and albedo. On average the models simulate SCF evolution (Sep-Jun) very well over the NH_{snow} region (mean SS_{scf} = 0.91, with a range 0.87-0.93; Fig. 3-9a) with lower skill over the boreal forest region (mean SS_{scf} = 0.83; range 0.79-0.88; Fig. 3-9b). This appears to be related to canopy snow processes: the mean SS_{scf} computed over the melt season alone (Jan-Jun) decreases relative to the Sep-Jun values (0.79, with a range of 0.57–0.87). There are smaller biases over the non-boreal Arctic region, where snow resides from Sep-Jul. For consistency, we also calculated the skill there over the Sep-Jun period, which showed that the models agree well with observations with a mean SS_{scf} of 0.89 and a range of 0.77–0.94 (Fig. 3-9d).

The results in Section 3.4.2 illustrated larger biases in albedo than SCF over the NH_{snow} region in fall and spring. The skill metric for albedo (SS_{alb}) supports this conclusion, with a mean of 0.83 and a large spread (0.64-0.92; Fig. 3-9a). Over the boreal region, the

average score declines to 0.73, and with even larger spread (0.36–0.91; Fig. 3-9b). Isolating the melt period reveals an even lower mean SS_{alb} (0.69), with a larger spread (0.25–0.86; Fig. 3-9c), presumably related to the same canopy melt issues that affect SS_{scf}. The non-boreal Arctic has some of the largest absolute albedo change biases in the NH (Fig. 3-8), yet its fractional contribution to the total albedo is diminished because the α_{sfc_snow} at these latitudes is also the largest (~0.70). On average, the models show smaller biases when simulating the monthly changes in albedo over this region (mean SS_{alb} = 0.82, range = 0.65–0.91; Fig. 3-9d). Therefore, for the vast majority of models, and in all regions analyzed, the evolution of albedo is more poorly simulated than that of SCF throughout the snow season. This conclusion is aligned with how the models traditionally calculate albedo (see Section 3.4.2), with a certain amount of dependence on SCF, but with a greater number of degrees of freedom (i.e., how to deal with vegetation masking, the time evolution of pure snow albedo, snowpack contamination).

3.5.3 Case Study: The Community Climate System Model

Prior research has shown that the CCSM4 model underestimates SAF over the boreal forest because of issues related to the parameterization of canopy snow in the land model (CLM4) (Thackeray et al., 2014). Interestingly, the CCSM4 model is an outlier within the CMIP5 ensemble for the boreal forest region (Section 3.4.3). To separate climate forcing biases from the land model process-level errors we here examine offline simulations of CLM4 (CLM4-OFF) forced by observed temperature, precipitation, and other atmospheric variables (Section 3.3.1). Compared to CCSM4, which includes a freely-varying ocean and atmosphere, CLM4-OFF produces larger positive biases in both SCF and albedo in fall across the NH_{snow} (Figs.

Table 3-2: Skill scores for the Northern Hemisphere snow-covered region from the three CLM offline simulations.

Model (Forcing)	SS_{tot}	SS_{alb}	SS_{scf}
CLM4 (Qian)	0.83	0.74	0.93
CLM4.5 (Qian)	0.83	0.73	0.93
CLM4.5 (CRUNCEP)	0.85	0.77	0.94

3-2, 3-4a) and boreal regions (Figs. 3-3a, 3-6a). However, during the melt period SCF is better simulated across the NH_{snow} and boreal regions in CLM4-OFF (Figs. 3-2, 3-3a), but despite this, the albedo biases over this time period are larger than in CCSM4 (Figs. 3-4, 3-6a).

The latest update of the CLM (version 4.5) includes an improved SCF parameterization (Swenson and Lawrence, 2012). To quantify the effect of this change on model skill, we compared SS_{tot} over the NH_{snow} region in two simulations using CLM4.5 with one simulation using the previous version (CLM4; Table 3-1). CLM4.5-CRUNCEP has the highest SS_{tot} (Table 3-2), largely due to a lower peak snow-covered surface albedo (although still 24% higher than observed; OBS_{blend}: 0.46) and a later snow melt (less SCF loss in Feb-Apr, more in May-Jun). The CLM4.5-Qian simulation scores slightly lower than CLM4 because of a greater overestimate of peak α_{sfc_snow}, while CLM4.5-CRUNCEP has the best score (0.85). Therefore, differences in the atmospheric forcing result in scores that are as different as those due to parameterization improvements. In both CLM4.5 simulations, the SS_{scf} increases relative to CLM4, but continuing albedo transition issues (see Section 3.4.3) affect the total score. This further supports our earlier conclusion that factors other than SCF are primarily responsible for the albedo biases. Potential future improvements should focus

on the seasonal cycle of albedo, as this is where model biases related to the terrestrial cryosphere are largest.

3.6 Discussion and Conclusions

This study used multiple satellite-derived datasets to quantify the skill of CMIP5 model simulations of month-to-month changes to the Northern Hemisphere terrestrial snow cover (mean SS_{tot} = 0.86). Results show that the models tend to be better at simulating the monthly change in SCF (mean SS_{scf} = 0.91) than the change in albedo (mean SS_{alb} = 0.83). The MM_{Med} overestimates the seasonal mean albedo change over the NH_{snow} region in both the accumulation and melt periods. However, the biases in fall are of much less importance to the surface energy balance because of low solar insolation during that season across the NH. On average, the models realistically reproduce SCF over the NH, which points to albedo errors being not primarily related to misrepresentation of simulated snow extent. Instead, model biases are related to the magnitude and timing of peak α_{sfc_snow}, as demonstrated in Fig. 3-7.

Over the boreal forest the simulated seasonal albedo cycle is biased high in 14/16 of models because they overestimate the peak snow-covered albedo of the forest (by more than 50% in some cases). One of the biggest outlier models in terms of α_{sfc_snow} over the boreal region is MIROC5, which has a type 1 albedo scheme (see Section 3.2). Qu and Hall (2007) showed that the predecessor to the MIROC5 model had the highest α_{sfc_snow} of its category, only exceeded by the type 4 models that calculate α_{sfc_snow} independent of land cover (i.e., INMCM4). The α_{sfc_snow} value is also important because a model that is biased high (low) will likely have a SAF that is too strong (weak) (Fletcher et al., 2015). As a result, almost all

of the models perform more poorly over the boreal region (mean SS_{tot} = 0.76) than they do over the larger study region, and as expected, isolating for only the melt period lowers these scores even further (mean SS_{tot} = 0.73). This finding is not that surprising, given that prior research has identified serious deficiencies in simulated albedo during the melt period over the boreal forest (Thackeray et al., 2014; Loranty et al., 2014). This is largely due to the complex processes involving snow interception, residence time of snow on the canopy, and snow/vegetation masking (Essery, 2013). The boreal albedo skill score (Jan-Jun; Fig. 3-9c) shows that the timing issue with CLM4's canopy snow parameterization (Thackeray et al., 2014) does not exist to the same extent in any other CMIP5 land surface models. Despite this, a number of models still perform poorly over the melt period because they dramatically overestimate (INMCM4, MIROC5) or underestimate (IPSL) the peak α_{sfc_snow}. One implication of this result is that canopy snow and vegetation masking parameterizations continue to be a source of uncertainty, and fundamentally contribute to biases in the simulation of albedo over the boreal forest.

Over the Arctic, the models score higher (mean SS_{tot} = 0.85) and the multi-model ensemble mean peak α_{sfc_snow} agrees better with observations. However, the scores are still limited by an Arctic warm bias in a subset of models that causes snow melt to occur too early in spring, which results in mistiming the seasonal albedo decline. Note that there would be lower agreement in spring SCF between models and observations if recent years (2006-2014) had been included, as this period includes large model biases with respect to observed snow extent (Derksen and Brown, 2012). However, we here restrict our analysis to the time period of the CMIP5 historical simulations, which end in 2005.

The cumulative change in insolation-weighted albedo (Figs. 3-4b, 3-6b, 3-8b) over the melt period can be used as an analog for SAF because SAF strength is strongly correlated with the climatological α_{sfc_snow} (Qu and Hall, 2007; Qu and Hall, 2014). Our findings support previous research showing that SAF in the CMIP5 models is on average biased high over the boreal forest (due to a peak albedo that is too high) and biased low over the Arctic (65-75°N) (Fletcher et al., 2015). Unlike the rest of the CMIP5 models, Thackeray et al. (2014) showed that SAF in CCSM4 was weaker than observations, not because of an underestimated peak albedo, but due to bias in the timing of albedo changes due to the parameterization of interactions between snow and the forest canopy.

It is clear that the CMIP5 models have a number of different issues related to their performance, so it is challenging to make specific recommendations. Some models have a small bias in α_{sfc_snow}, but show biases in the timing of its peak; in this case a correction to delay the decline in albedo should increase SS_{alb}. The model biases that appear to be the most urgent are in peak α_{sfc_snow}, where seemingly straightforward corrections could yield significant improvements to simulated snow processes including snow albedo feedbacks. Correcting these albedo biases might be expected to reduce biases in NH_{snow} surface air temperature (SS_{tas} = 0.92; applying Eq. 3-2 to surface air temperature data from ERA-Interim (Dee et al., 2011)). There is also the possibility that the α_{sfc_snow} has been tuned either too high, or too low, in order to best simulate large scale climate and compensate for model biases elsewhere (Koenigk et al., 2014), in which case changes in α_{sfc_snow} could have the reverse effect by inducing further temperature bias. However, if improving the α_{sfc_snow} and seasonality results in greater temperature biases, then one should interpret this as revealing

some other bias in the model, meaning that the good initial temperature simulation must have been due to compensating errors. In an effort to further diagnose and reduce biases within the land modules, we believe that offline simulations from a broader set of models would help dramatically. We also agree with Essery (2013) and Qu and Hall (2014) in concluding that a rather simple correction to constrain simulated albedo based on observations could be applied to reduce the spread in snow-covered surface albedo and in turn SAF. Reducing the intermodel spread in these two quantities could help narrow the uncertainty in projections of warming over Northern Hemisphere land.

3.7 Acknowledgements

CMIP5 output can be downloaded from the CMIP5 archive (cmip-pcmdi.llnl.gov/cmip5/). Offline simulations of CLM are available on the Earth System Grid (www.earthsystemgrid.org). MODIS albedo and snow cover data was obtained from the online Data Pool at the NASA Land Processes Distributed Active Archive Center (LP DAAC; https://lpdaac.usgs.gov/data_access). GlobSnow snow water equivalent data can be found at the GlobSnow archive (http://www.globsnow.info/swe/). APP-x data were obtained from the University of Wisconsin, Madison (ftp://stratus.ssec.wisc.edu/pub/appx). Albedo data from GlobAlbedo can be found at the GlobAlbedo archive (http://www.globalbedo.org/global.php). We acknowledge funding from the Natural Sciences and Engineering Research Council of Canada's Climate Change and Atmospheric Research Initiative via the Canadian Sea Ice and Snow Evolution (CanSISE) Network. We are thankful to David Lawrence for providing detailed feedback on an earlier version of the manuscript and to three anonymous reviewers for their constructive comments.

Chapter 4

The impact of simulated surface albedo biases on climate

4.1 Overview

Several recent studies have noted substantial biases in surface albedo amongst the current generation of global climate models (GCMs), primarily across snow-covered areas. Various model parameterization issues have been suggested as potentially relevant to this problem (i.e., leaf area index, canopy snow, forest type, subgrid-scale lakes). There is however, little understanding of how albedo biases are potentially influencing simulated climate because of difficulty in isolating them from other complex processes and feedbacks. A number of novel simulations are conducted here using the Community Earth System Model (which itself has a substantial albedo bias) to improve knowledge related to biases in surface albedo. The model's (biased) internal calculation of albedo is replaced with prescribed albedo data, derived from satellite observations, or from another model. Results show that by correcting the albedo in CESM, simulated temperature is perturbed further away from observations (implying the presence of other biases), with robust cooling during winter and spring. It does however, induce a pattern reversal of climatological biases in winter sea level pressure, partially correcting the model's tendency towards a positive Arctic Oscillation. Furthermore, biases across the boreal forest region are found to be influential for both local and remote climate features, while models with large biases in maximum snow-covered surface albedo are vulnerable to even greater climate impacts than CESM.

4.2 Introduction

Surface albedo, a measure of reflectivity, is quantified as the ratio of outgoing to incoming shortwave radiation. It is an important characteristic of the Earth's energy balance and therefore a key parameter in global climate models (GCMs). Much of the seasonal variability in Northern Hemisphere (NH) land surface albedo is due to changes in the presence of snow cover (Roesch, 2006). Its influence is exerted across much of the mid-high latitudes and in areas of high elevation, covering approximately 40% of NH land during late winter (Robinson and Frei, 2000). The highly reflective nature of snow acts to cool the climate by reducing incident radiation absorbed at the surface, enhancing thermal emissivity and latent heat fluxes due to melting of snow (Gong et al., 2004; Flanner et al., 2011). Furthermore, Dutra et al. (2011) show that interannual variability in snow cover explains much of the variability in winter near-surface temperatures across snow-covered regions. Anomalous snow cover can also indirectly influence large-scale atmospheric circulation and NH winter climate (Gong et al., 2004; Fletcher et al., 2009; Allen and Zender, 2011; Cohen et al., 2012). In extratropical land areas, surface albedo increases from its snow-free value (~0.08-0.15) in early fall to a maximum value in late winter (~0.3-0.8), followed by a rapid decline during spring melt (i.e., He et al., 2014). The peak surface albedo over a region is strongly tied to its land cover, with lower values (more energy absorption) across heavily vegetated forests even in the presence of snow, and higher values (less energy absorption) in areas of low-lying or no vegetation (grasslands, croplands, tundra).

Capturing the seasonal evolution of land cover specific aspects of snow-covered surface albedo has proven challenging for many climate models. The coarse nature of GCMs

(~100-200 km horizontal resolution) causes issues with the representation of topography, land cover, and snow distribution/properties, all of which are influential in determining surface albedo. Prior research has shown that several climate models have trouble with the magnitude and/or timing of seasonal changes in land surface albedo over the NH extratropics (Thackeray et al., 2014, 2015; Li et al., 2016; Wang et al., 2016). This albedo bias (relative to satellite-derived observations) is largely attributed to the over-simplified representation of key snow processes, which drive errors in simulated snow cover extent and snow-covered surface albedo. One area with particularly large biases is the boreal evergreen forest, where nearly all CMIP5 models overestimate peak winter albedo (Loranty et al., 2014; Thackeray et al., 2015). Simulating albedo can be difficult in this environment because of complex interactions between snow processes and forest cover, including the masking effect that the canopy has on underlying snow (Qu and Hall, 2007; Essery, 2013), and its role in intercepting snowfall (Thackeray et al., 2014; Bartlett and Verseghy, 2015). Several models also exhibit substantial biases in their leaf area index (LAI), which is a key factor in determining snow-covered surface albedo over forests (Loranty et al., 2014; Wang et al., 2016). Models with an LAI that is too low tend to also have a snow-covered surface albedo that is biased high (and vice versa) because of a larger canopy gap fraction. Furthermore, there is also a large spread in peak albedo over non-forested regions such as grasslands, shrublands, and tundra. In these landscapes, snow can completely cover most surface vegetation, resulting in a very high peak surface albedo values (~0.6-0.8). Biases in maximum albedo create a follow-on effect whereby the simulation of albedo through the melt period is negatively impacted, with implications for snow albedo feedback (SAF). This

is because SAF strength is largely controlled by the spring surface albedo contrast (snow-covered surface albedo – snow-free albedo) (Qu and Hall, 2007; Fletcher et al., 2015). It is important to better understand model processes related to SAF because it remains a significant source of uncertainty (40-50%) in model projections of future warming over NH land (Qu and Hall, 2014).

In this study, we directly perturb simulated albedo using climatological albedo derived from satellite observations, to quantify the influence of albedo biases on climate. The land model used here (Community Land Model, version 4; Lawrence et al., 2011) has known issues related to the seasonality of changes in albedo over the boreal forest (Thackeray et al., 2014). This problem is largely the result of how forest canopy hydrology is parameterized in the model. Notably, the model removes all snow from the canopy when temperatures exceed the freezing point, which causes an early transition from a snow-covered to snow-free environment. Model development to improve this issue in the latest version (CLM5) has resulted in an improved seasonal cycle of albedo (not shown). However, several other models exhibit similar, but less significant, biases in the timing of albedo changes. On the other hand, biases in albedo magnitude could be even more problematic for simulated climate. As a means of improving our understanding of these processes, we examine the importance of albedo biases through a series of model experiments.

Similar approaches to the one used here (Section 4.3.3) are well documented as a suitable method for decoupling the land surface from the atmosphere to investigate land-atmosphere interactions. These studies predominantly prescribe soil moisture (e.g., Koster et al., 2000; Seneviratne et al., 2006) or snow cover (Gong et al., 2002, 2004; Fletcher et al.,

2007; Allen and Zender, 2010; Sobolowski et al., 2010; Dutra et al., 2011). Many of these prescribed snow experiments attempt to identify linkages between fall snow cover and broad-scale atmospheric circulation patterns (such as the Arctic Oscillation) during winter (Gong et al., 2002; Fletcher et al., 2007, 2009; Orsolini and Kvamsto, 2009; Allen and Zender 2011). In some cases, observational snow cover was used to perturb the model (Orsolini and Kvamsto, 2009; Douville, 2010; Allen and Zender, 2011), which one may expect results in an improved albedo. A more realistic representation of the seasonal evolution of snow cover does not, however, account for differences between simulated and observed snow-covered surface albedo. In particular, albedo biases driven by poor vegetation masking or land cover data are still present when simulated snow cover is replaced with observations.

The primary goal of this work is to determine the influence of albedo biases on simulated Northern Hemisphere climate. This research addresses the importance of previously identified albedo biases, while also answering the question of whether correcting these biases will move temperature and snow simulations closer to or further from observations. The importance of regional albedo biases are also investigated through a series of experiments. We also establish the framework for performing similar simulations that will be run as a part of the ESM-SnowMIP project (http://www.climate-cryosphere.org/activities/targeted/esm-snowmip), which seeks to better understand the variability in Earth system model simulations of snow. The data and methods are described in Section 4.3. In Section 4.4, we present the results from a series of uncoupled and coupled climate experiments. Lastly, Section 4.5 highlights the key findings of this research and provides a discussion of how our findings relate to current literature.

4.3 Data and Methods

4.3.1 Model Description

The model used in this study is the Community Earth System Model (CESM; Gent et al., 2011), version 1.04. CESM is composed of atmosphere (Community Atmosphere Model, CAM; Neale et al., 2013), land (CLM; Lawrence et al., 2011), ocean (Parallel Ocean Program, POP; Danabasoglu et al., 2012), and sea ice (CICE; Holland et al., 2012) components. The horizontal resolution of the model is approximately 1° (0.9° latitude x 1.25° longitude), while the vertical structure is made up of 26 levels. The land surface component is relatively sophisticated with detailed representations of key biogeophysical processes. CLM4 also simulates snow accumulation and melt processes along with compaction, aging, and the radiative impact of aerosols on snow. It has a multi-level snow scheme with up to 5 snowpack layers, depending on snow depth (Oleson et al., 2010). Because of the dominant role that snow cover plays in the seasonal cycle of NH surface albedo, it is important that snow processes are well represented.

4.3.2 Observational Data

A blend of satellite-derived albedo products is used to perturb model simulations. The blended product (henceforth, OBSblend) is a linear combination of climatological monthly surface albedo from the Moderate Resolution Imaging Spectroradiometer (MODIS; Schaaf et al., 2002), the extended advanced very high resolution radiometer (AVHRR) Polar Pathfinder (APP-x) project (Wang and Key, 2005) and GlobAlbedo (Muller, 2013) over the APP-x domain between approximately 45-50°N and 90°N (as described in Thackeray et al., 2015),

and only MODIS elsewhere. Since, we are primarily interested in the Northern Hemisphere extratropics, the limited domain for the blended observations is not a concern. We find that in daily albedo products there exists a trade-off between higher temporal resolution and the number of missing observations (primarily due to cloud cover obscuring the optical sensors), so monthly mean observational values are used to limit missing values. The datasets are also averaged over different temporal ranges (MODIS/GlobAlbedo: 2000-2005, APP-x: 1982-2005), but their climatological values are not very sensitive to the time frame selected (Thackeray et al., 2015). Several other observation-based estimates are used to evaluate CESM's control climate. This includes surface air temperature and sea level pressure from NCEP-II reanalysis (Kanamitsu et al., 2002), and snow water equivalent (SWE) from the Blended-5 dataset (Mudryk et al., 2015).

4.3.3 Experimental Design

Here, we conduct a novel set of model experiments to determine the impact of simulated albedo biases on climate. The experimental design overrides the model's (biased) internal calculation of albedo and replaces it with prescribed albedo data, derived from satellite observations, or from another model (see below). By explicitly correcting the model biases using prescribed satellite data, we can directly relate the change in a model variable (e.g., surface air temperature) relative to the uncorrected model, to the albedo perturbation applied. The override procedure is analogous to imposing prescribed sea surface temperatures (SSTs) to the atmospheric model, with the prescribed value passed to the radiation code. Changes to albedo are implemented before other modules call this variable (i.e., for surface radiation

calculations). It should be noted that we only discuss the NH extratropics because albedo elsewhere is well simulated by CLM.

We perform sensitivity experiments using two configurations of the land surface model CLM4: one is driven by prescribed atmospheric forcing derived from reanalysis data (hereafter 'CLM-off'), and one where CLM4 is coupled to the atmospheric model CAM4 with prescribed sea ice conditions (thickness and area) and ocean surface temperatures (hereafter 'CLM-CAM'). The first set of simulations are run in offline mode (not coupled to atmosphere/ocean), meaning that there is an active land component with atmospheric input (temperature, precipitation, solar radiation, wind, pressure, and humidity). An ensemble of simulations is not required because of the consistent atmospheric state. We initially ran the model for 30 years (1982-2012) with the start date coinciding with the availability of observational albedo data from APP-x (1982). The first set of offline simulations are forced by CRUNCEP (version 7) data (Viovy, 2011), while subsequent shorter simulations (1999-2004) use the Qian dataset (Qian et al., 2006). This allows the impact of discrepancies in the forcing data to be examined, an important measure because the choice of forcing data is capable of dominating the response generated by land models (Menard et al., 2015).

There are three offline cases, each containing different surface albedo fields. The control simulation is unperturbed, meaning that it has the standard albedo from CLM4. Next, observationally-derived albedo (OBSblend) is used to determine the effect of correcting for model biases in albedo. Lastly, we seek to determine the maximum realistic impact of albedo biases on climate. To do so, we perturb CLM4 with climatological monthly mean albedo (1980-2005) from the Model for Interdisciplinary Research on Climate, version 5

(MIROC5), which is one of the CMIP5 models with the highest Northern Hemisphere surface albedo. This tests the importance that a different type of albedo bias (primarily related to magnitude rather than timing) can have on model simulations. It should be noted that because we are using the albedo from this model, it is likely susceptible to biases in the simulated snow cover. In the case of MIROC5, there is a tendency for snow cover to lag behind observations (and other models) in the fall due to a slow onset (see Fig. 3-2). Another notable difference is the percent of snow cover over portions of the NH when snow is present (65-85%), which in this model is considerably lower than CLM (95-100%). This could be part of the reason why albedo in MIROC5 is slightly lower than CLM4 over sparsely vegetated regions.

Several CLM-CAM simulations are also carried out, in which both the land and atmosphere are fully interactive (Table 4-1). The ocean and sea ice conditions are prescribed in a similar manner to the Atmosphere Model Intercomparison Project (AMIP; Gates et al., 1999). The ocean state uses climatological (1982-2001) sea surface temperatures (SSTs) from the Hadley Centre Sea Ice and Sea Surface Temperature data set (HadISST; Rayner et al., 2003). Because these runs allow for land-atmosphere interactions, it is suspected that this will enhance the response to albedo perturbations. The same three albedo experiments described above are run in this CLM-CAM setup. We also produce three simulations with regional albedo perturbations in an effort to determine regional influences on the model response. Each simulation uses OBSblend albedo over the area of interest: defined as the boreal evergreen forest (BOR; >50% plant functional type in CESM), western Eurasian boreal (WEU; 5-85°E, 50-70°N), and North American boreal (NA; 50-160°W, 45-65°N).

Table 4-1: Summary of land-atmosphere coupling experiments. The MAMJ mean albedo over land areas polewards of 45N is shown for CTRL, while other experiments are referenced as a percent albedo change in relation to this value. Note that the lowering of albedo over grasslands and tundra dominates the increased boreal albedo in OBS.

Experiment	Albedo	SST	Length (years)	NH45 MAMJ Albedo and Percent Change from CTRL
CTRL	CLM4	HADISST	20	**0.33**
OBS	OBSBlend	HADISST	20	-3%
MIROC	MIROC5	HADISST	20	13%
BOR	OBSBlend+CTRL	HADISST	20	4%
WEU	OBSBlend+CTRL	HADISST	20	1%
NA	OBSBlend+CTRL	HADISST	20	2%

Albedo outside of these regions is equal to that of the CLM-CAM control case. As a measure of the perturbation strength for each case, we evaluate the percent change in albedo relative to the MAMJ mean control albedo over land areas polewards of 45°N (NH45). All simulations begin on January 1 and run for 20 years and 1 month; the additional month is generated because we discard the start of each simulation. It should be noted that there may be some issues with energy conservation under this setup.

4.4 Results

4.4.1 Offline Model Simulations (CLM-OFF)

4.4.1.1 Climatological Mean Climate

First, we briefly describe some aspects of the land model's climate (and its biases) that will be helpful for interpreting the results of later experiments. CLM4 overestimates albedo at high latitudes in fall and winter (SON, DJF), and underestimates MAM albedo across the

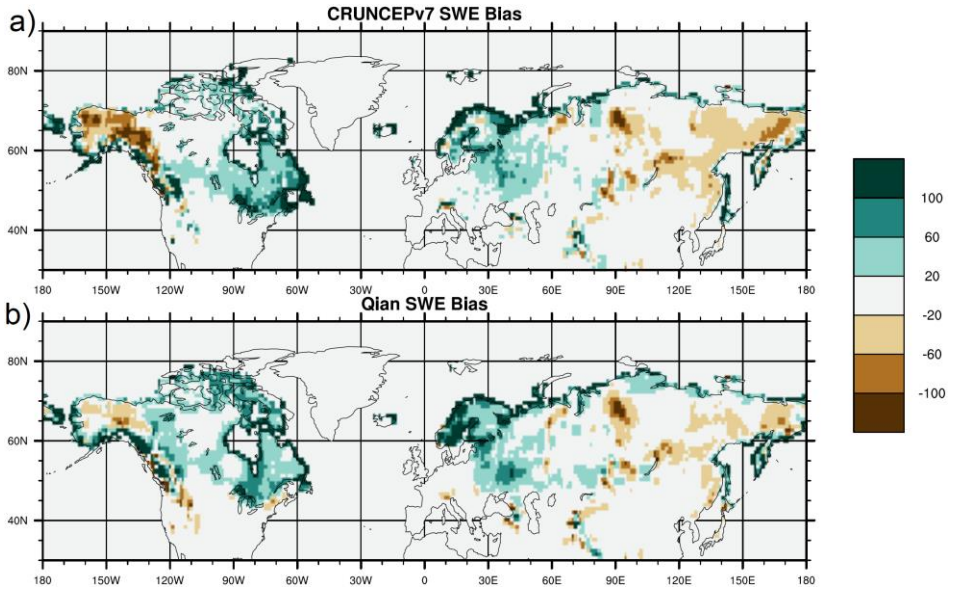

Figure 4-1: Bias in simulated climatological March SWE (units: mm) two simulations of CLM4 with different forcing (a) CRUNCEPv7, (b) Qian. Bias is calculated with regards to the Blended-5 dataset (Mudryk et al., 2015).

boreal forest region (largely due to the timing of canopy snowmelt) (Thackeray et al., 2015). Annual mean climatological surface air temperature from CLM4 has a significant cold bias at high latitudes (~2-4°C locally), with more pronounced biases in the winter and spring (not shown). As shown in Figure 4-1a, there are also large regional biases in climatological spring SWE that exceed 100 mm compared to the Blended-5 product of Mudryk et al., (2015). The model accumulates too much SWE across midlatitude and northeastern North America and western Eurasia, with a low SWE bias across Alaska/Yukon and eastern Siberia. Notably, there is so little snow over Alaska/Yukon (due to a lack of cold season precipitation over Alaska/Yukon in CRUNCEP) that a gap exists in snow cover extent, which could have repercussions on simulated albedo. Uncertainty in Arctic precipitation is a common issue due to sparse meteorological stations at high latitudes (Brown, 2000). A second control simulation derived from different atmospheric forcing (Qian) shows a reduction in this bias,

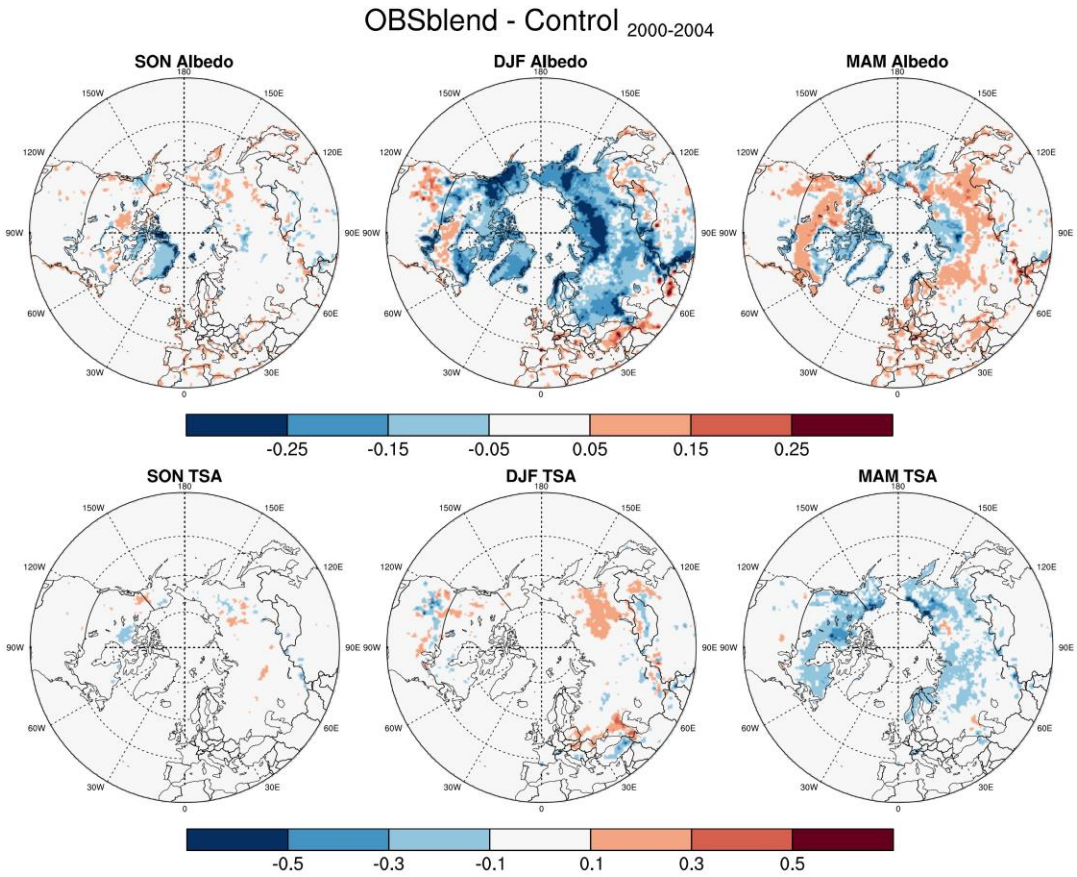

Figure 4-2: Difference in seasonal mean albedo (top) and surface temperature (bottom) between offline OBS and Control cases (using Qian forcing). Seasonal means for the fall (SON), winter (DJF), and spring (MAM) are shown.

although the spatial pattern is largely the same (Fig. 4-1b). Further analysis focuses on the Qian-driven simulations. Results from this batch of runs showed very strong similarities to the prior simulations in areas not affected by the aforementioned precipitation biases (not shown). It is of interest to know whether correcting model biases in albedo will move temperature and snow simulations closer to or further from observations.

4.4.1.2 Response to Albedo Perturbations

First, the simulated albedo from CLM4 is replaced with prescribed observational albedo (OBSblend). Following on from the biases described in Section 4.4.1.1, the perturbation

corresponds to albedo being reduced in winter (DJF) over much of the extratropics, and increased in spring (MAM) across the boreal forest region (Fig. 4-2). Although the changes to albedo are largest in DJF, they have little impact on simulated wintertime temperature (Fig. 4-2). This is due to very low incoming radiation over much of the Northern Hemisphere high-latitudes during winter. On the other hand, the increased albedo in spring leads to a surface cooling that locally ranges from -0.1 to -0.5K, and minor increases in late-spring snow cover (not shown).

These results show the impact of small changes to snow-covered surface albedo in CLM4 by using satellite albedo products. In fact, the percent change in NH45 MAMJ albedo is slightly negative (-3%) because the lowering of albedo over grasslands and tundra outweighs the increased boreal albedo here. Next, we apply a stronger perturbation (+13% NH45 MAMJ albedo) to further evaluate model sensitivity. The climatological mean albedo in the MIROC5 model is unrealistically high across the boreal forest region in DJF, and all snow-covered areas in MAM (Fig. 4-3). There is not much to note about the fall results in either case (or for subsequent experiments), so mean winter and spring climate are primarily discussed going forward. Winter and spring cooling covers a much larger spatial extent in this case, and is nearly double the magnitude of what was identified using satellite derived albedo. On the other hand, MIROC5 albedo is lower in winter over areas of sparse (or low-lying) vegetation south of the boreal forest; this produces weak local warming, but the dominant response is in the form of a cooling associated with the high bias to the north (Fig. 4-3). However, the offline experimental configuration in CLM-off prevents land-atmosphere processes from affecting the response to albedo perturbations over time, hence, the response

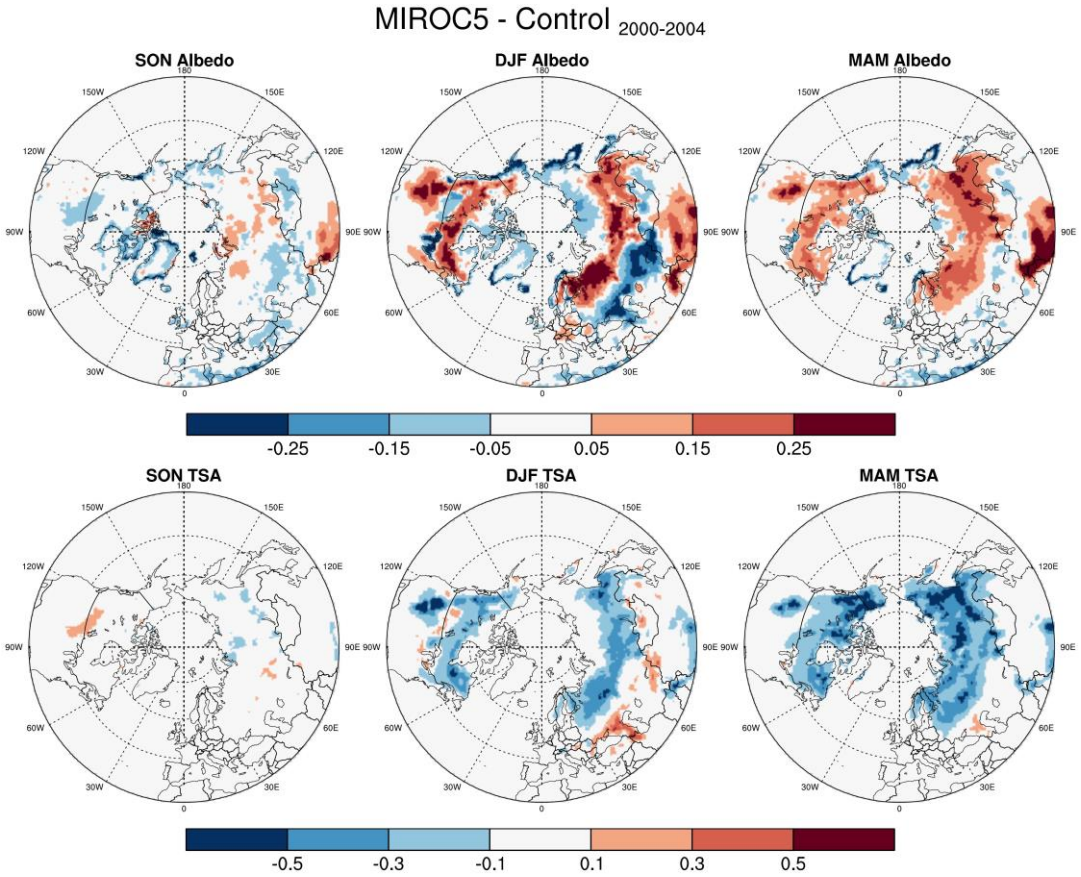

Figure 4-3: Difference in seasonal mean albedo (top) and surface temperature (bottom) between offline MIROC and Control cases (using Qian forcing). Seasonal means for the fall (SON), winter (DJF), and spring (MAM) are shown.

over most extratropical regions remains weak, even in this case with stronger forcing. In the following section, we quantify the impact of atmospheric coupling on the response through the CLM-CAM simulations.

4.4.2 Land-Atmosphere Simulations (CLM-CAM)

4.4.2.1 Climatological Mean Climate

Here we briefly examine the climate produced by an AMIP-type simulation of CESM1-CAM4. This model also exhibits biases in near-surface air temperature (relative to NCEP-II

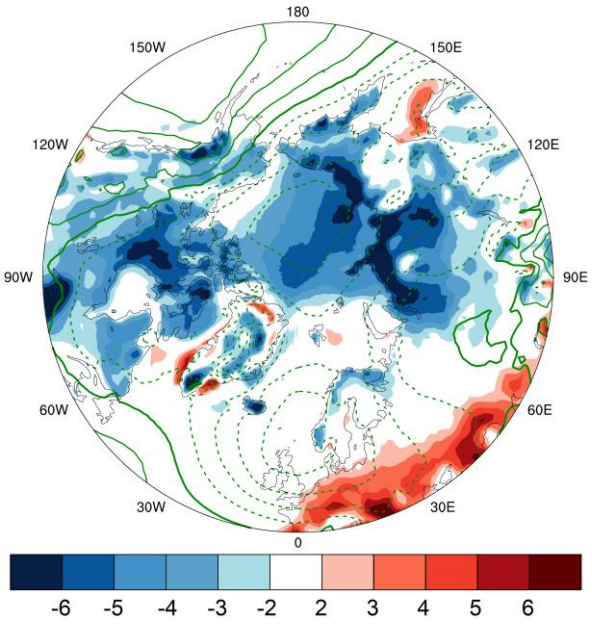

Figure 4-4: Difference in climatological mean winter (DJF) 2m air temperature (shading; K) and sea level pressure (contours; hPa) between the CESM AMIP control simulation (years 1-20) and NCEP-II reanalysis (1982-2001). The contour interval is 2 hPa, with negative contours dashed.

reanalysis; varies slightly with the choice of observational dataset), while DJF cold biases of between 2-6°C persist over northern Siberia, Arctic Canada/Alaska, and the central Arctic basin (Fig. 4-4). The control simulation also has notable biases in its general circulation patterns over high-latitudes in winter, when compared to reanalysis data: there is a pronounced negative bias in sea level pressure (SLP) over the polar cap (Fig. 4-4). Three NH regions stand out with particularly large biases in winter SLP: the polar cap (-9 hPa), Iceland low (-9 hPa), and Aleutian low (+7 hPa). This finding is consistent with other studies using the same atmospheric model (CAM4) (Xie et al., 2012; De Boer et al., 2012). Weakened SLP over the polar cap is also a feature of all six realizations of the 20-year AMIP experiment performed using the CESM-CAM4 model[1]. This seems to imply that the model favors a positive Arctic Oscillation (AO) setup by default. Biases in SWE over land remain large (in

[1] Available at http://www.cesm.ucar.edu/experiments/cesm1.0/#amip.

both directions) when compared to the Blended-5 dataset (up to 100 mm; not shown), this is somewhat expected because precipitation is no longer being prescribed (as in offline cases). A more detailed description of the model's climate is given by Neale et al. (2013).

4.4.2.2 Climatological Response in the OBS Experiment

In the OBS case, the albedo perturbation slightly reduces the non-forested albedo value (affecting the plains and tundra) and prolongs the peak albedo value over the boreal forest region (to prevent its early decline). The albedo perturbations (consistent with the CLM-off simulations in Section 4.4.1) drive a strong reduction in net shortwave radiation over the boreal forest, and an increase across the plains to the south and tundra to the north. These surface radiative changes drive the following climate response in climatological mean 2m air temperature, net shortwave radiation (downward minus upward), net longwave radiation (upward minus downward), and sensible plus latent heat (positive upward) (Fig. 4-5). Cooling of between 1-3 degrees is evident across much of the NH extratropics in both DJF and MAM (Fig. 4-5ab). This is somewhat surprising because there is a small increase in net shortwave radiation at the surface (averaged across NH45 region) during winter (~2 Wm^{-2}) and negligible change in fall and spring (~0.5 Wm^{-2}). The lack of radiative change in fall (not shown) is a result of only a slight albedo perturbation, whereas in spring it is a balance of contrasting areas with more and less absorbed radiation (Fig. 4-5d). There are also minor reductions in the net longwave radiative flux during winter (-1 Wm^{-2}; Fig. 4-5e) and spring (-2.5 Wm^{-2}; Fig. 4-5f). Turbulent sensible (-5 Wm^{-2}) and latent heat (-3 Wm^{-2}) fluxes away from the surface are also decreased during spring (Fig. 4-5h), and near-zero during winter.

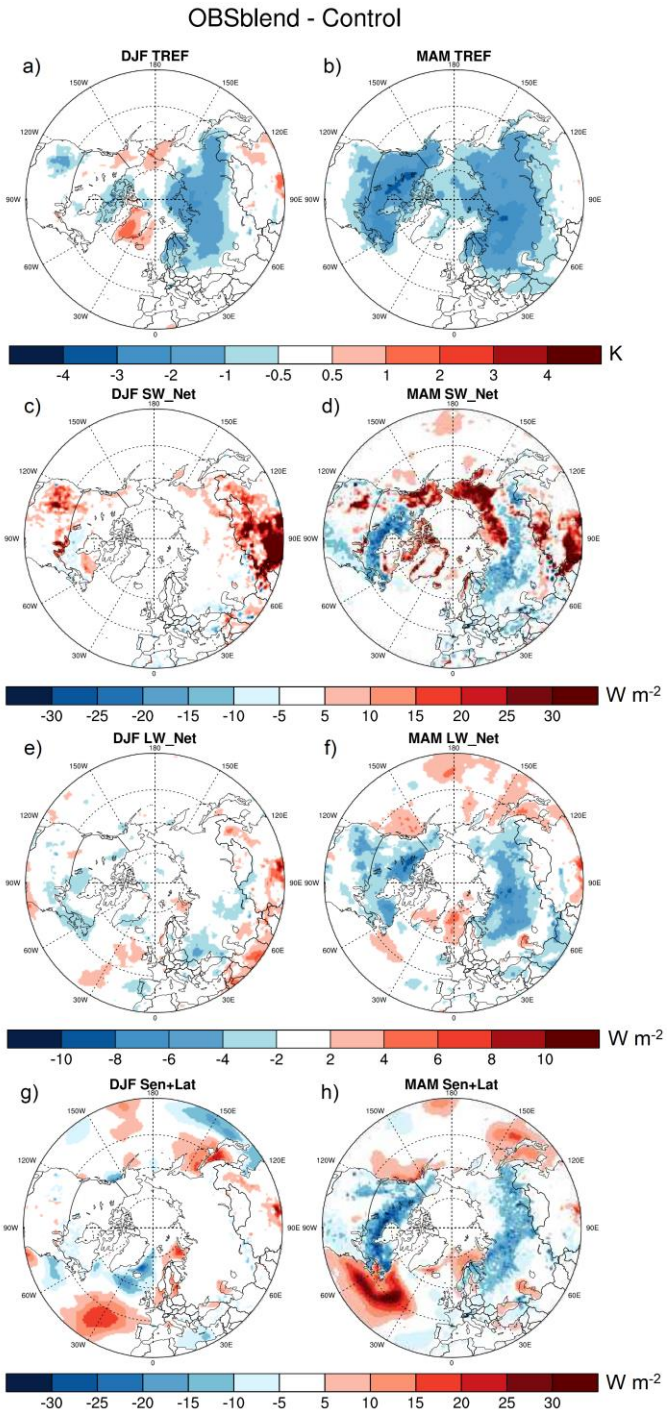

Figure 4-5: Response to OBS albedo forcing in seasonal mean (a, b) 2m air temperature (K), (c, d) net shortwave radiation at the surface (W m^{-2}), (e, f) net longwave radiation at the surface (W m^{-2}), and (g, h) sensible plus latent turbulent heat fluxes (W m^{-2}). Seasonal means for the winter, and spring are shown, while summer and fall are excluded because of less albedo perturbation. Net shortwave radiation is positive down, while other fluxes are the opposite.

Because we apply perturbations to the surface albedo, the land surface temperature response is generally greater (colder) than atmospheric temperature response, thus causing negative turbulent heat fluxes. A decrease in sensible heat flux acts to directly cool the lower atmosphere. Spring cooling corresponds to concurrent reductions in the surface energy budget (described above), but in winter there is very little change in the energy balance.

The lack of a surface shortwave signal in winter means that other processes are likely driving the cooling of the continent, and changes to large-scale atmospheric circulation appear to play a key role. The albedo perturbation is associated with a strengthening low pressure system over the polar cap during winter (Fig. 4-6a), weaker zonal mean zonal winds around 60°N, and an equatorward shift of North Atlantic jet and storm track (Fig. 4-6c). These changes, coupled with reductions in meridional heat transport (not shown), result in greater movement of cold air to the mid-latitudes. This pattern is similar to the typical general circulation associated with a negative AO (Thompson and Wallace, 1998). It should be noted that this setup resembles a reversal of the SLP biases in the control climate (Fig. 4-4), but weaker in magnitude. Therefore, correcting albedo in CLM-CAM pushes the simulated winter temperatures further away from observations (implying the presence of other biases), but partially corrects the model's tendency towards a positive AO.

Increasing the spring albedo in CLM over the boreal forest region naturally reduces snow melt by limiting shortwave radiation absorbed by the snowpack. This change coupled with cooler near-surface air temperature (Fig. 4-5) leads to spring snow cover fraction (SCF) anomalies that exceed +25% for a given month (Fig. 4-7a-c). Prolonged snow cover duration influences the model's upper-layer soil moisture during summer months (Fig. 4-7d-f). Soil

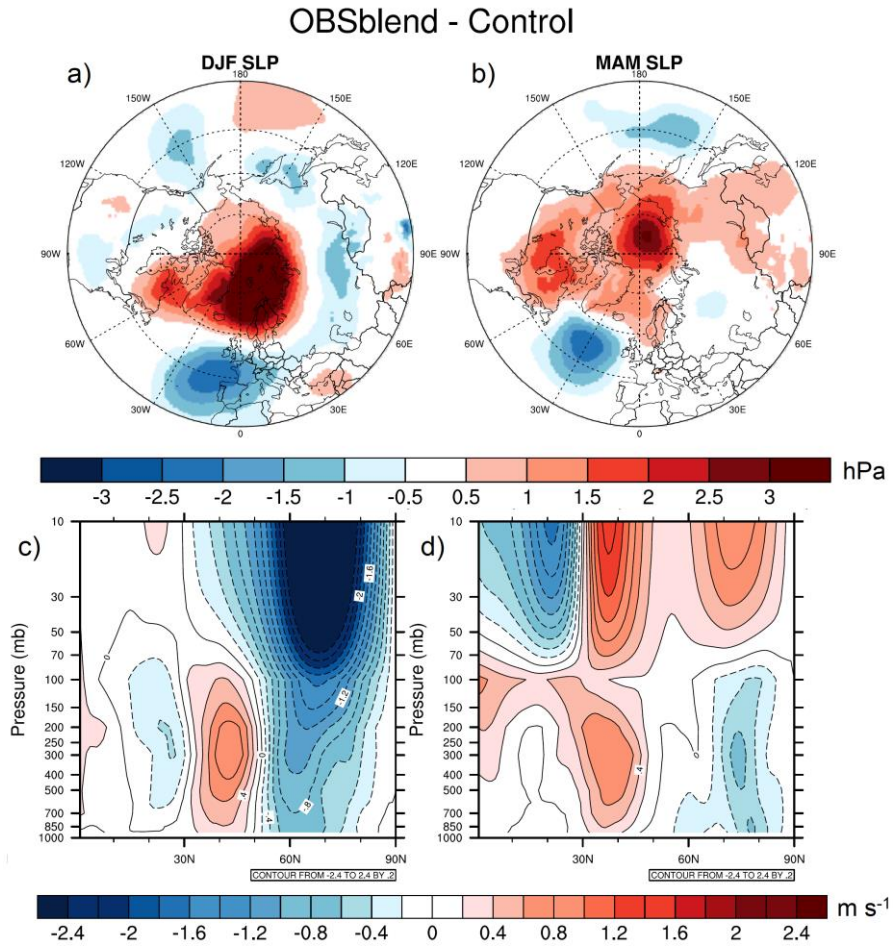

Figure 4-6: Climatological seasonal mean difference in sea level pressure (a, b) and zonal mean zonal wind (c, d) between the OBS and control cases.

moisture anomalies can affect moisture and heat exchange, and contribute to long-term atmospheric variability because of their slowly developing nature (Eltahir, 1998; Liu, 2003). Prior studies have shown that anomalously wet soils can cause decreased 500 hPa geopotential heights (GPH) (Ju et al., 2005), while dry soils can invoke the opposite response (Fischer et al., 2007; Pal and Eltahir, 2003). Therefore, it is possible that the anomalously wet soils across the NH extratropics are playing a role in the persistent cooling that occurs throughout summer (not shown). It should be noted that correcting the albedo biases of CLM

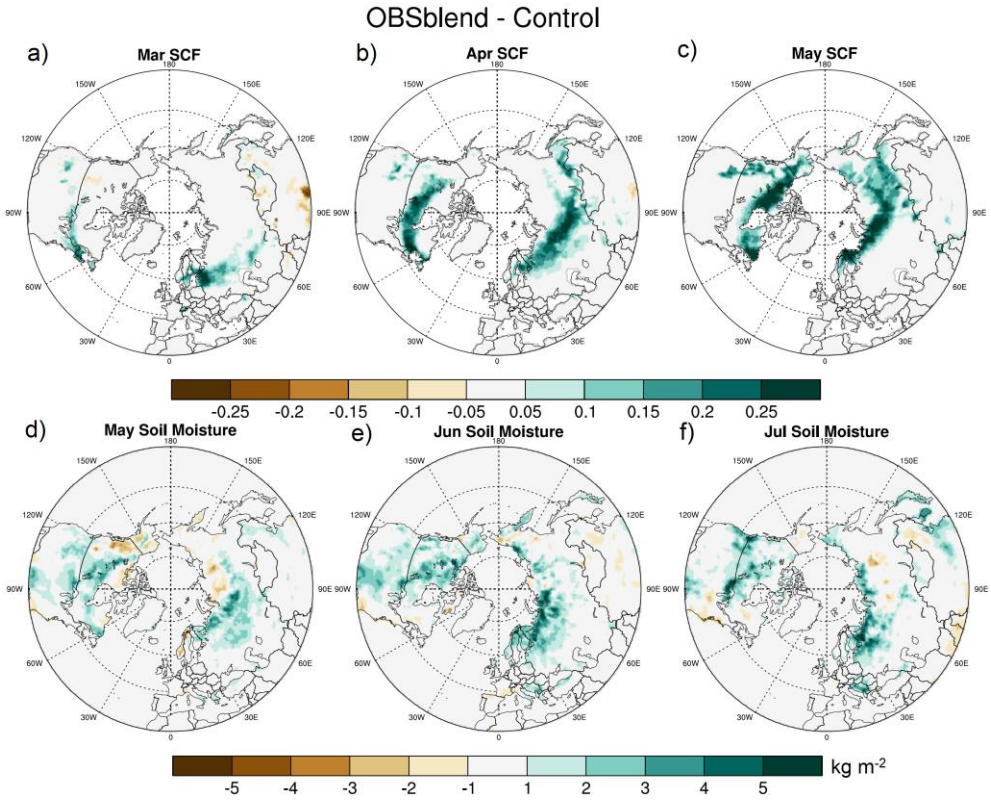

Figure 4-7: Climatological seasonal mean difference in spring snow cover fraction (a, b, c) and May-Jun-Jul soil moisture (d, e, f) between OBS and Control.

involves slightly increasing the extratropical snow-free albedo, because the model's default vegetation albedo is lower than observed.

The continental cooling response in spring also has knock-on implications for the Arctic summer/fall. Although sea-ice properties (area and thickness) are fixed, the atmosphere over the ice, and in turn, snow on sea-ice are free to evolve and potentially impact radiative and turbulent heat fluxes. We find that cooling in the Arctic basin, due to reduced meridional heat transport and advection of cold air, limits the melting of snow on sea-ice in May-Jun (Fig. 4-8a). This leads to a thicker (10-20 cm; Fig. 4-8b) and more reflective (~10-30%; increase in albedo by 0.05-0.20; Fig. 4-8c) Jul-Aug snowpack on the ice (versus control). Enhanced snow on sea-ice drives a concurrent reduction in the net surface

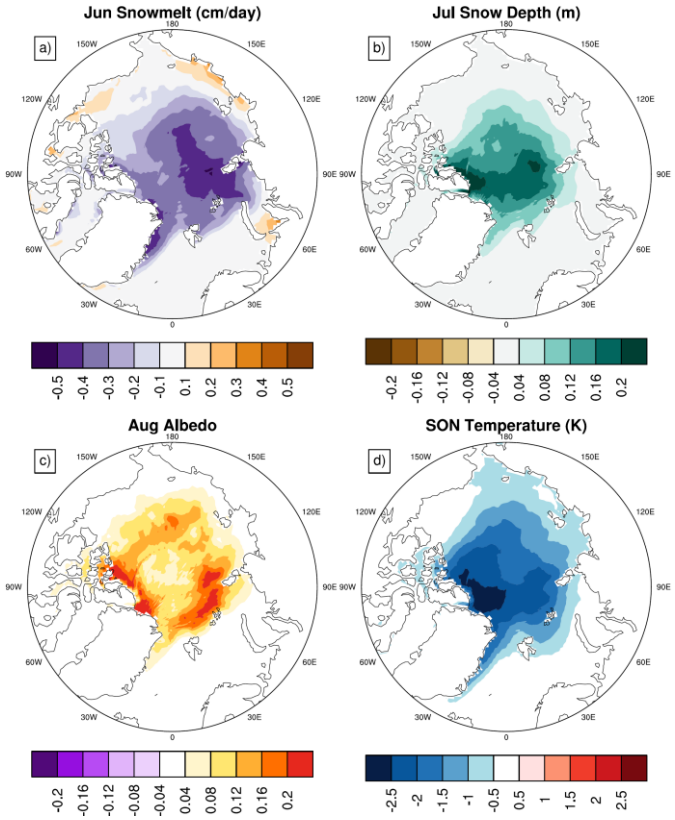

Figure 4-8: Response to OBS albedo forcing in climatological sea ice variables (a) June snowmelt (cm/day), (b) July snow depth (m), (c) August surface albedo (no units), and (d) fall surface temperature (K).

heat flux, and increased sensible and latent heat fluxes over the ice in Aug-Sep. The resulting ~-2 K temperature anomaly is apparent in the mean fall temperature response (Fig. 4-8d). Consistent with this cold polar cap there is a lowered 500 hPa GPH and stronger 60°N winds in fall. Therefore, anomalous snow on sea-ice acts as a bridge linking the changes applied to spring albedo with the atmospheric response generated in fall/winter.

4.4.2.3 Climatological Response in the MIROC Experiment

Here we substantially increase snow-covered surface albedo over much of the mid-high latitudes, and decrease it in areas just south of the boreal forest region during winter (Fig. 4-3). The albedo-induced radiative perturbation is largest across the boreal forest region,

approximately double that of the OBS experiment during spring, and more than four times stronger during winter. By spring, the albedo is largely only increased over the NH extratropics and it is this period when the radiative response is most dominant. Anomalous cooling of 2-5 K is produced across the NH extratropics in winter (NH45 land: -1.3 K) and spring (NH45 land: -2.6 K) (Fig. 4-9ab). In this case, winter cooling isn't limited to the Eurasian continent as before. This is likely associated with decreased net shortwave across much of southern Canada (Fig. 4-9c), which is far enough south that albedo perturbations have a radiative impact. The spring temperature response is also largely driven by decreased shortwave radiation (-9.5 W m^{-2}). In response to shortwave forcing, net longwave is also reduced (-4 W m^{-2} in spring), with the largest changes across the boreal latitudes (Fig. 4-9f). This is coupled with much weaker sensible (-7.5 W m^{-2}) and latent heat (-4 W m^{-2}) fluxes over land (Fig. 4-9h). Differences in radiative fluxes in fall are relatively weak over much of the NH extratropics once again because albedo perturbations during this period are small (due to slow snow onset in MIROC5). The largest radiative differences during fall stem from changes to cloud cover (not shown).

The enhanced NH cooling generated in the MIROC case is also linked to changes in large-scale atmospheric circulation. During winter, we see the development of an annular SLP pattern that largely resembles Fig. 4-6a, with a positive anomaly over the polar cap and negative anomalies over the Aleutian Islands and western Europe (Fig. 4-10a). This pattern persists through spring (Fig. 4-10b), noticeably with a greater magnitude than generated by OBS. In both seasons, there is a significant weakening of the polar winds (Fig. 4-10cd). These two circulation features enhance the albedo-induced temperature change over Eurasia.

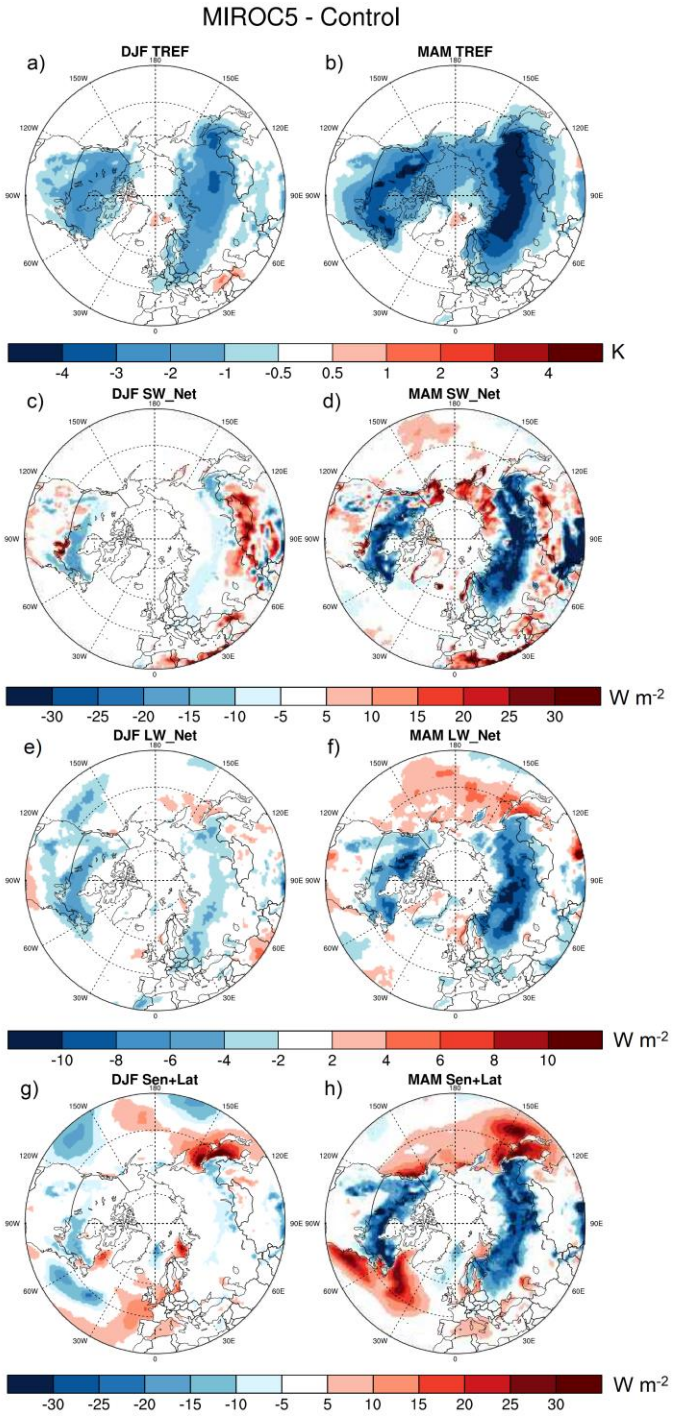

Figure 4-9: Response to MIROC albedo forcing in seasonal mean (a, b) 2m air temperature (K), (c, d) net shortwave radiation at the surface (W m^{-2}), (e, f) net longwave radiation at the surface (W m^{-2}), and (g, h) sensible plus latent turbulent heat fluxes (W m^{-2}). Seasonal means for the winter, and spring are shown, while summer and fall are excluded because of less albedo perturbation. Net shortwave radiation is positive down, while other fluxes are the opposite.

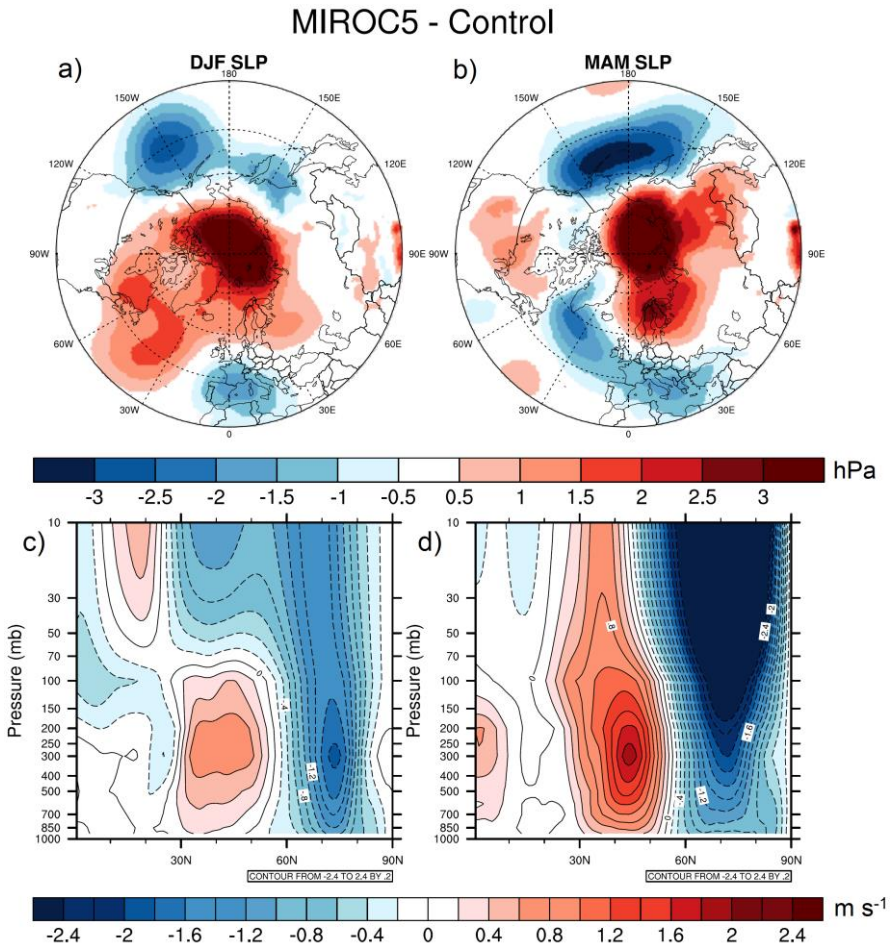

Figure 4-10: Climatological seasonal mean difference in sea level pressure (a, b) and zonal mean zonal wind (c, d) between the MIROC and control cases.

The knock-on effects of continental cold anomalies once again include extended spring snow cover duration, anomalous summer soil moisture, and thicker snow on sea-ice. The spatial pattern of SCF anomalies largely resemble the prior results, but are intensified (up to 50% larger than control across melt zone; not shown). Therefore, in both albedo perturbations cases (OBS and MIROC), we see robust climate impacts.

The hemispheric response discussed in the prior subsections is broken down here to better understand regional dynamics. For consistency with motivating studies, we look at the mean response averaged over two main physiographic regions: the NH boreal forest and the

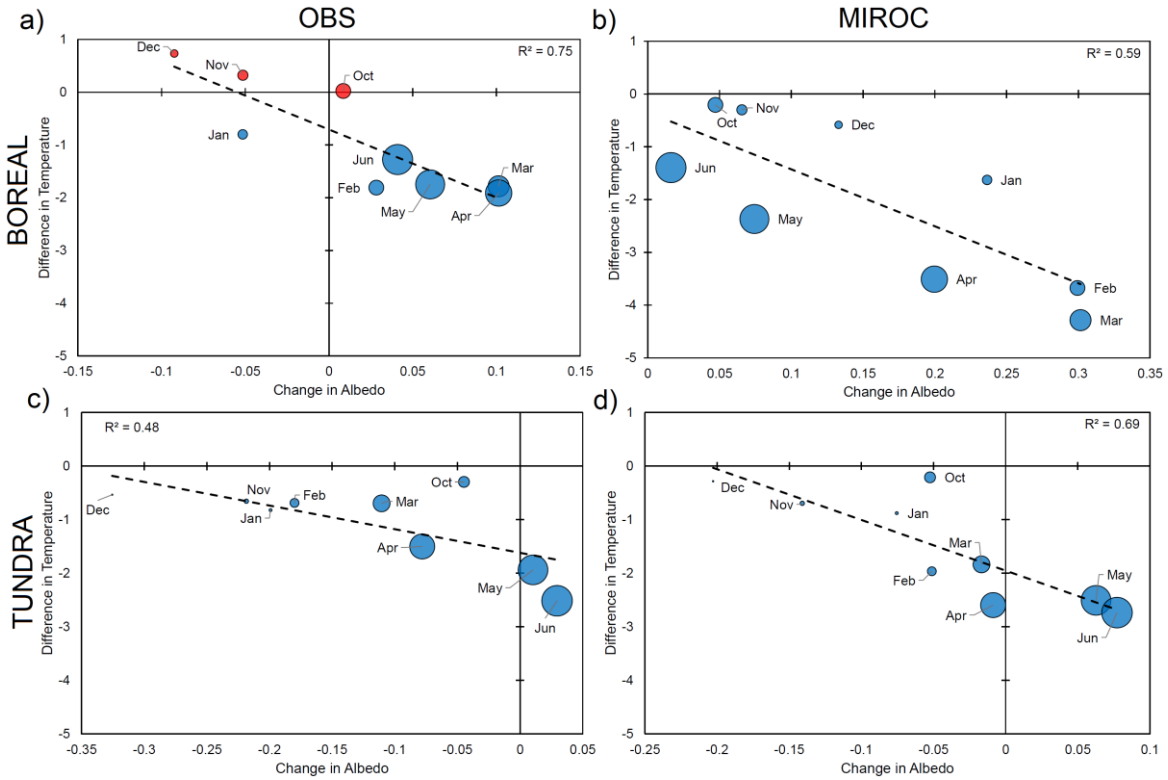

Figure 4-11: Relationship between monthly albedo changes and the corresponding temperature response across the boreal forest region (top) and the non-boreal tundra (bottom) in OBS (left) and MIROC (right). The size of each point is related to the amount of incoming solar radiation during that month.

non-boreal tundra. Across the boreal forest region, spring albedo was increased by 0.09 in OBS, and 0.19 in MIROC. These perturbations result in 1.8 K and 3.4 K of cooling over this region, respectively. Albedo changes across the region are generally weaker in magnitude during the rest of the year, apart from winter when a lack of incident radiation limits temperature impacts (Fig. 4-11ab). Across the non-boreal tundra, albedo changes are largest in the OBS case, during winter. However, the more northern location of this region restricts albedo biases from having much of a climate impact until March. This explains why decreasing the DJF albedo in both cases (OBS: -0.23, MIROC: -0.11) does not result in regional warming (OBS: -0.7 K, MIROC: -1 K). The albedo changes across this region seem

to be largely dominated by remote effects (i.e., Eurasian cooling due to SLP pattern). During the rest of the year, there is much better agreement between the models and observations so albedo changes are smaller. Decomposing the regional structure of these simulations highlights previously illustrated albedo biases over the boreal (spring albedo is too low in CESM) (Thackeray et al., 2014) and tundra regions (winter albedo is higher than observations) (Thackeray et al., 2015) in CLM4. From this we can conclude that albedo biases in the snow-covered surface albedo over the boreal forest region are more important for the models evaluated here.

4.4.3 Isolating Regional Drivers

Because of the nature of our prior experiments (changing albedo over much of the NH extratropics), it is difficult to pinpoint what may be important in driving the responses that were generated. Here, we attempt to isolate the role that different regions may play in influencing our prior results. Our initial focus is on the boreal evergreen forest (>50% plant functional type in CESM). In this case (BOR), we only perturb albedo over this region (to observed), while albedo elsewhere is equal to that of the CLM-CAM control case (+4% NH45 MAMJ albedo). Results from BOR are compared with control and OBS. The temperature response in BOR is highlighted by 1-3 degree cold anomalies (compared to control; Fig 4-12bc) over Eurasia (in winter and spring) and North America (in spring). This is largely consistent with the cooling pattern from our OBS case (Fig. 4-5a). Furthermore, we once again see the development of a strengthening winter polar cap (Fig. 4-12e) and associated weakening of the 60°N zonal mean zonal winds (Fig. 4-12h). Therefore, by only

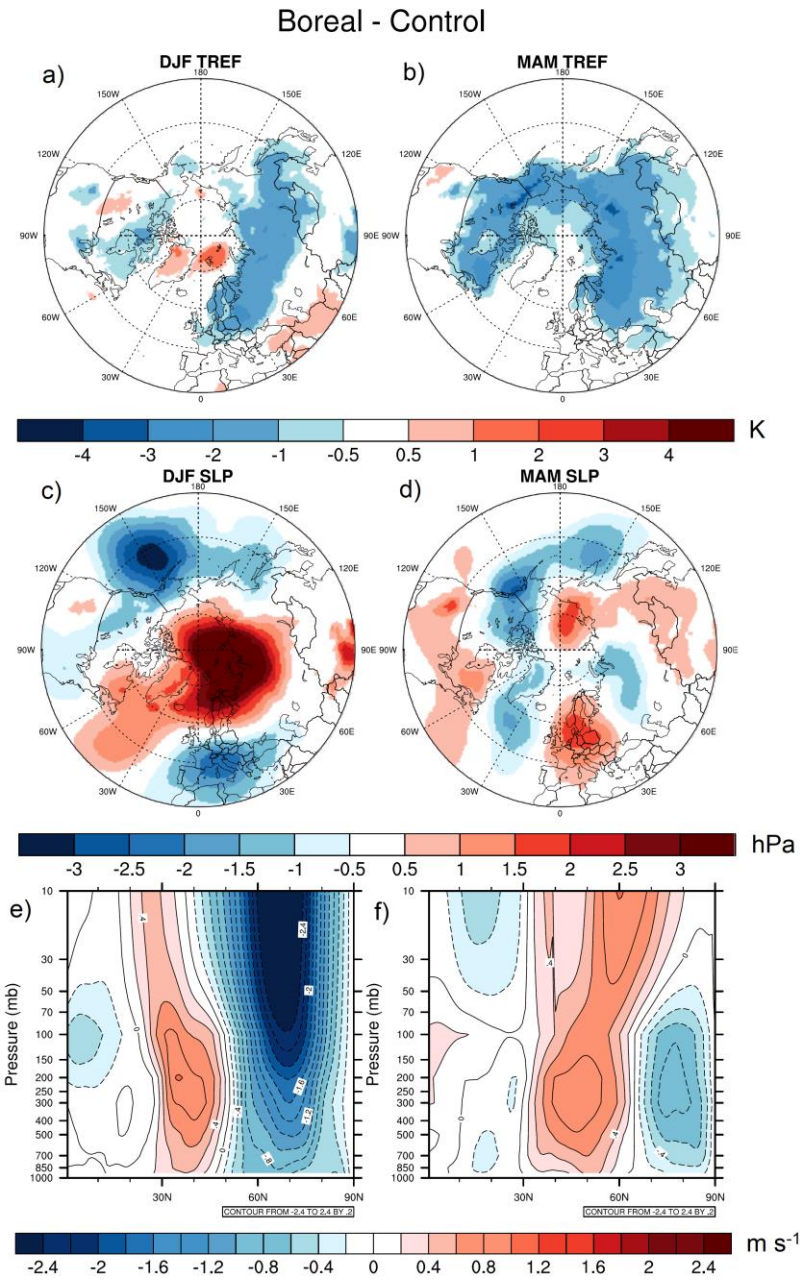

Figure 4-12: Climatological seasonal mean difference in 2m air temperature (a, b), sea level pressure (c, d), and zonal mean zonal wind (e, f) between the boreal and control cases.

correcting the spring albedo over the boreal forest we generate substantial climate impacts many months later.

To further understand the development of consistent large scale atmospheric circulation patterns in winter we run two additional cases. This final test examines the role of albedo anomalies over the boreal forests of North America and Eurasia separately. Several recent studies have suggested that changes in northwestern Eurasian climate can impact the AO, particularly through the loss of sea ice in the Barents and Kara Seas (i.e., Inoue et al., 2012; Mori et al., 2014) and the expansion of October snow cover (i.e., Cohen et al., 2012; Furtado et al., 2015; Yeo et al., 2017). Surface temperature and circulation anomalies in this region may stimulate the propagation of significant wave activity out of the lower troposphere (Saito et al., 2001; Kolstad and Charlton-Perez, 2011) and the development of atmospheric blocking events over the Urals, driving persistent cold anomalies over Eurasia (Luo et al., 2016; Yao et al., 2017; Luo et al., 2017). To investigate this, we perturb albedo over the western Eurasia boreal forest in one case (WEU), and over the North American boreal forest in another simulation (NA). An important distinction is that the boreal forest tends to be located at lower latitudes in NA. Therefore, the impact on the surface energy budget from albedo perturbations applied in NA begins roughly one month earlier than for WEU.

We find that the WEU case produces a similar, but weaker seasonal temperature response to that of the full NH extratropical boreal albedo perturbation in the BOR experiment (Fig. 4-12ab), mostly limited in extent to eastern Eurasia (not shown). This appears to be largely associated with a weaker positive SLP anomaly over the polar cap, which also has its center shifted closer to Siberia. In contrast, the NA case generates Eurasian cooling that spans from Scandinavia to eastern Siberia, which is very similar to the BOR

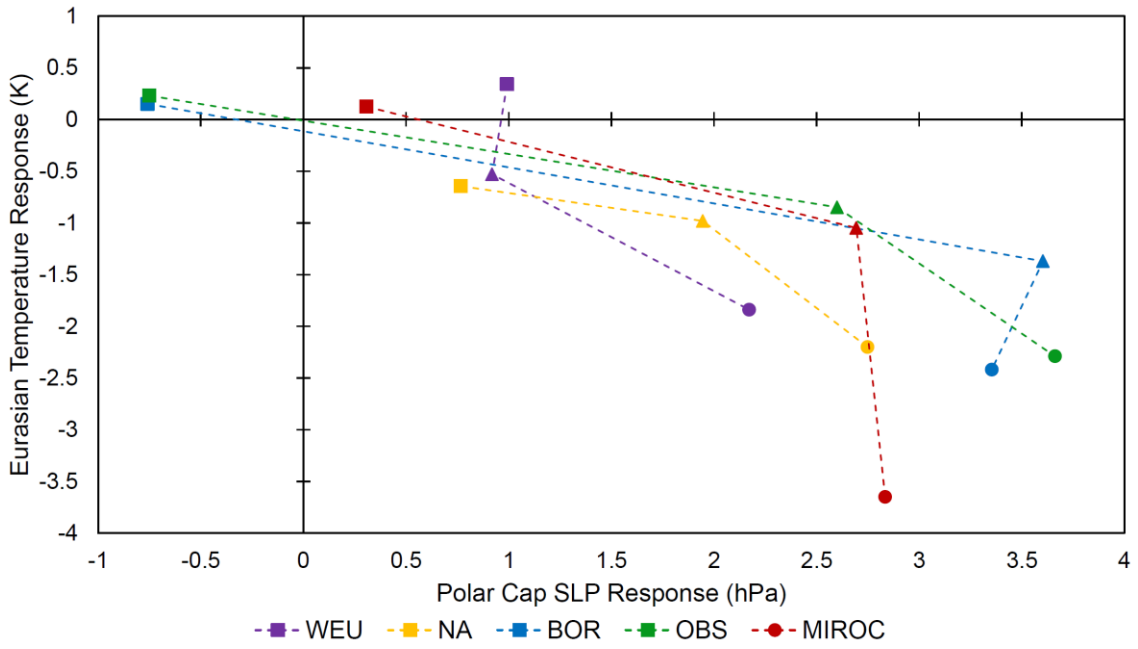

Figure 4-13: Seasonal evolution of climatological anomalies (referenced to control) in Eurasian (5-160E, 50-70N) temperature and polar cap (65-90N) sea level pressure throughout winter. Values for December (squares), January (triangles), and February (circles) are shown. A general strengthening of the polar cap occurs throughout the winter (left to right).

experiment. This is accompanied by a circulation response reminiscent of a negative AO (stronger polar cap and weaker zonal mean zonal winds). Prior studies have shown that snow cover anomalies over North America can produce remote responses in temperature and sea level pressure (Gong et al., 2003; Sobolowski et al., 2010). Breaking down the seasonal evolution of this relationship between Eurasian temperatures and polar cap SLP shows us that the WEU case has a different winter trajectory than the other experiments (Fig. 4-13). Notably, all cases except WEU exhibit a strengthening polar cap from Dec to Jan, which may be tied to a lack of stratospheric warming in this case (not shown). Also, the weaker forcing in WEU (smaller boreal area than NA) does not generate a very strong snow on sea-ice response in summer/fall (not shown), perhaps limiting the ability for spring perturbations to impact NH fall/winter climate. Therefore, we find that applying observational albedo forcing

over North America's boreal forest is sufficient to generate a very similar winter climate response to cases where albedo was perturbed everywhere. It should be noted that the spring cooling in these continental cases is weaker because they do not have the same radiative potential.

4.5 Discussion and Conclusions

This study examines several novel simulations, which prescribe surface albedo in an effort to better understand the potential impacts that albedo biases can have on simulated climate. We find that although winter albedo biases can be large, they have very little direct influence on simulations of climate because of low incoming radiation. Instead it is spring albedo bias that can generate significant local and remote NH climate responses in the form of temperature, snow cover, and large-scale atmospheric circulation. Changes to temperature and snow are greatly enhanced when land-atmosphere coupling is enabled. Correcting the albedo in CESM towards satellite derived values pushes the model further away from observed temperature (implying the presence of other biases), with robust cooling during winter and spring (1-3 K) and induces a pattern reversal of the climatological biases in winter sea level pressure, partially correcting the model tendency towards a positive AO. CMIP5 models with large albedo magnitude biases (i.e. MIROC5) are susceptible to even greater impacts on simulated climate. We find an approximately 4-5 K swing in seasonal mean air surface temperature over the mid-high latitudes from the low albedo of CESM to the high albedo of MIROC5.

We find that albedo-induced cold anomalies prolong spring snow cover duration, which has knock-on effects on summer soil moisture and summer/fall snow on sea-ice. This series of mechanisms bridges the changes we apply in spring to the formation of robust

atmospheric features in the following winter (as our simulations start in January). Anomalous snow cover has previously been tied to seasonally lagged climate features, but these studies all focused on October snow (i.e., Gong et al., 2004; Fletcher et al., 2007, 2009). Both anomalous snow cover and snow albedo (Allen and Zender, 2010) across the NH during the fall can encourage the development of a negative AO pattern in winter through enhanced propagation of wave activity to the stratosphere. Here we show that changes in spring albedo and its associated cooling can generate a similar response in the NH climate many months later.

The AO is naturally strongest during winter when it can extend out of the troposphere and is linked to changes in the polar jet (Thompson and Wallace, 2000; Cohen et al., 2014). Studies have shown that winter cold surges across Eurasia are greatly enhanced when the AO is in its negative phase (Jeong and Ho, 2005; He et al., 2017). In observations, recent Eurasian cooling during winter is characterized by a Warm Arctic-Cold Eurasia (WACE) pattern (Overland et al., 2011; Inoue et al., 2012; Cohen et al., 2014). This reduces the temperature gradient between the high and mid-latitudes, which can lead to more frequent atmospheric blocking events (and more persistent weather), particularly in the Ural mountain region (Luo et al., 2016; Yao et al., 2017). WACE has been tied to the loss of sea ice over the Barents and Kara Seas in fall-winter (Honda et al., 2009; Petoukhov and Semenov, 2010; Inoue et al., 2012; Mori et al., 2014; Sato et al., 2014). There is some question as to whether this warming is primarily due to anomalous turbulent fluxes (Honda et al., 2009) or changes in temperature advection (Mori et al., 2014). The nature of our simulations limits the potential for Arctic warming because sea-ice area and thickness are held fixed in both cases.

Also, because SSTs are prescribed, atmospheric fluxes can only influence temperature over land or sea-ice. Despite this, results show near-surface warming of 1-2 K from east of Greenland to the north Barents Sea in Jan-Feb (when Eurasian cooling is strongest). There are still questions as to what prompts the transition from a cold Arctic in fall to a cold Eurasia in winter. One potential trigger is a stratospheric warming that develops in November-December and largely persists within the atmosphere throughout the winter in all of our simulations except WEU (Fig. 4-14). It is accompanied by a stratospheric reduction in 60°N zonal wind (polar night jet) that doesn't affect the lower atmosphere until Jan-Feb (not shown; consistent with what Cohen et al., 2014 proposes). The detection of winter stratospheric warming as a precursor for a negative AO has been noted by prior studies (Kolstad and Charlton-Perez, 2011; Cohen et al., 2011; Cohen et al., 2014). This mechanism could possibly connect the cooling applied in spring to the formation of strong winter atmospheric responses. It is generally thought that stratospheric warming events are caused by greater vertical propagation of Rossby waves (possibly linked to sea-ice loss and Eurasian snow) that act to weaken the polar vortex (Cohen et al., 2014). Further investigation into the tropospheric precursors to stratospheric warming is outside the scope of this study, as several others have extensively covered this (Garfinkel et al., 2010; Kolstad and Charlton-Perez, 2011; Cohen et al., 2011).

Since we are interested in the sensitivity of the model to albedo biases, the brute force nature of our approach is effective. More elegant methodologies for incorporating observational constraints in models for example, could involve data assimilation, but that more complex approach would not directly address the goals of this study. It should also be

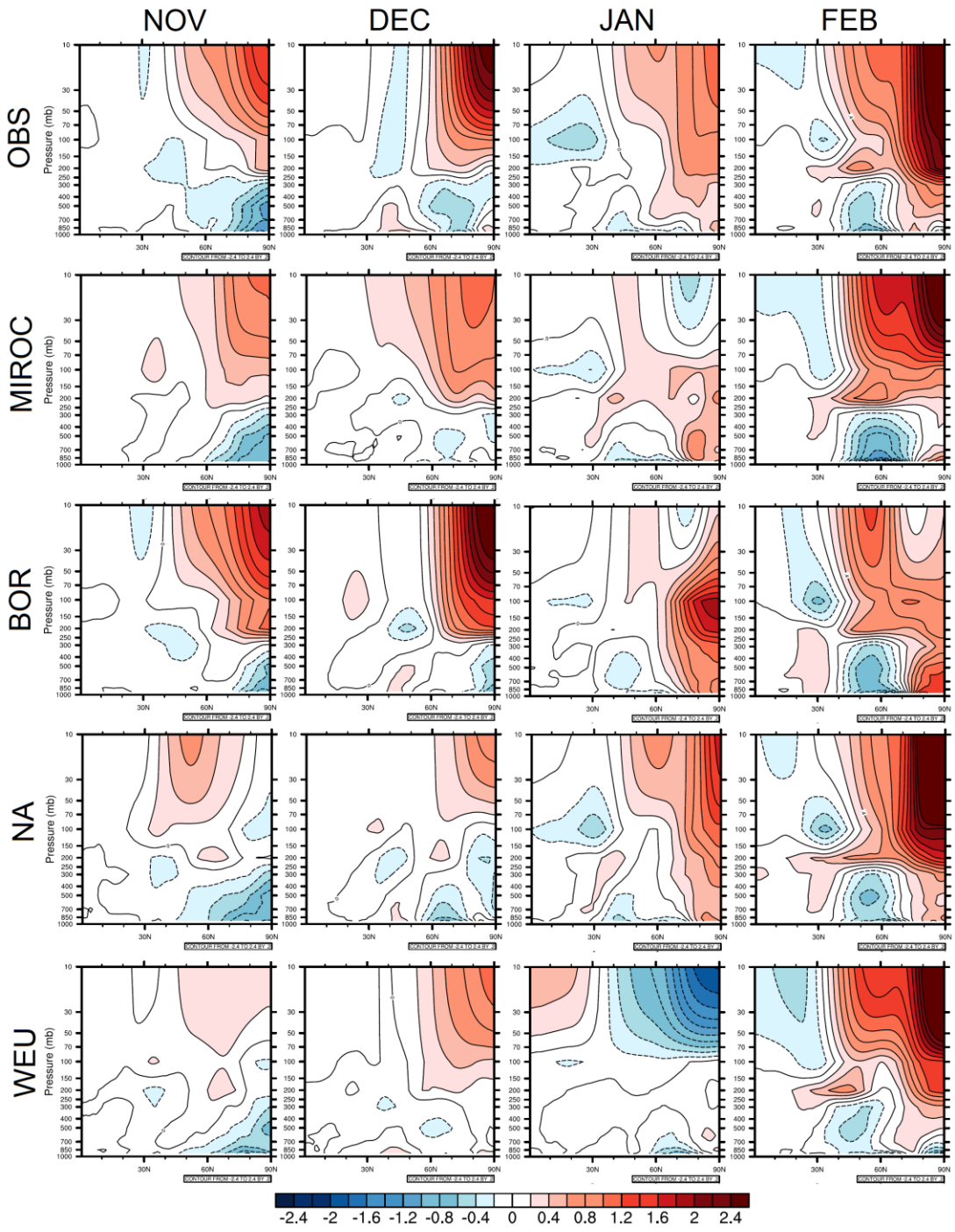

Figure 4-14: Difference in climatological zonal mean air temperature (K) throughout the atmosphere between each experiment (OBS, MIROC, BOR, NA, WEU) and the control case for November through February. The contour interval is 0.2.

noted that the relationship between albedo and climate-relevant variables is likely different in every GCM, but we are limited to community models such as CESM. Lastly, although the prescribed albedo evolves in a smoother nature (linearly from one monthly value to the next) than what would naturally occur, we do not believe this influences the long-term climate because the monthly mean radiation balance at the surface remains the same.

The results shown here attempt to improve our understanding of simulated snow-covered surface albedo biases, which several recent studies have pointed out in the current generation of GCMs (Loranty et al., 2014; Thackeray et al., 2014, 2015; Li et al., 2016; Wang et al., 2016). We find that spring albedo biases across the boreal forest from the CMIP5 ensemble can be influential for both local and remote climate features. Moving forward it is important for model development to reduce biases in spring albedo, for both its role in snow albedo feedback (Qu and Hall, 2014; Fletcher et al., 2015) and the direct climate impacts discussed here. For some models this means improving parameterizations of snow to reduce bias in snow cover (or canopy hydrology), while others may require reworking of how subgrid-scale lakes are treated (Verseghy et al., 2017) or changes to regional vegetation characteristics such as LAI or tree cover fraction. Interestingly, the results shown here suggest that correcting the albedo biases in CESM would actually reinforce simulated cold biases. Therefore, making albedo more realistic may not have the desired effect of correcting temperature, but in this event, one should interpret this as uncovering some other bias in the model.

4.6 Acknowledgements

We acknowledge funding from the Natural Sciences and Engineering Research Council of Canada through the Alexander Graham Bell Canada Graduate Scholarships-Doctoral Program and NSERC's Climate Change and Atmospheric Research Initiative via the Canadian Sea Ice and Snow Evolution (CanSISE) Network.

Chapter 5

Quantifying the uncertainty in historical and future simulations of Northern Hemisphere spring snow cover

5.1 Overview

Projections of 21st century Northern Hemisphere (NH) spring snow cover extent (SCE) from two climate model ensembles are analyzed to characterize their uncertainty. The Fifth Coupled Model Intercomparison Project (CMIP5) multi-model ensemble exhibits variability due to both model differences and internal climate variability, whereas spread generated from a Canadian Earth System Model large ensemble (CanESM-LE) experiment is solely due to internal variability. The analysis shows that simulated 1981-2010 spring SCE trends are slightly weaker than observed (using an ensemble of snow products). Spring SCE is projected to decrease by -3.7 ± 1.1% decade^{-1} within the CMIP5 ensemble over the 21st century. SCE loss is projected to accelerate for all spring months over the 21st century, with the exception of June (because most snow in this month has melted by the latter half of the 21st century). For 30-year spring SCE trends over the 21st century, internal variability estimated from CanESM-LE is substantial, but smaller than inter-model spread from CMIP5. Additionally, internal variability in NH extratropical land warming trends can affect SCE trends in the near-future (R^2 = 0.45), while variability in winter precipitation can also have a significant (but lesser) impact on SCE trends. On the other hand, a majority of the inter-model spread is driven by differences in simulated warming (dominant in March, April, May), and snow cover available for melt (dominant in June). The strong temperature/SCE

linkage suggests that model uncertainty in projections of SCE could be potentially reduced through improved simulation of spring season warming over land.

5.2 Introduction

Seasonal snow cover is a crucial component of the climate system, with major impacts on the surface energy budget and water balance. At its peak, snow covers approximately 47 million km^2 of Northern Hemisphere (NH) land (about 40% of the land area) each year (Hall 1988; Robinson and Frei 2000). The reflective properties of snow mean that it has a very strong influence on land surface albedo, controlling its seasonal evolution. This high albedo has a cooling influence on climate, with the contribution from terrestrial snow to cryospheric cooling being roughly equal to that of sea ice (Flanner et al. 2011). Furthermore, snow cover can indirectly impact atmospheric circulation (Fletcher et al. 2009; Cohen et al. 2012). Water resources across most NH extratropical (polewards of 30°N) land areas rely on natural water storage provided by snowpack (Diffenbaugh et al. 2013), with approximately one-sixth of Earth's population dependent on snowmelt for a portion of their water supply (Barnett et al. 2005; Mankin et al. 2015). Earlier spring snowmelt across the western United States has been linked to increased summer heat extremes (Diffenbaugh et al. 2005; Hall et al. 2008) and wildfires (Westerling et al. 2006). Snow cover also has a low thermal conductivity, meaning that it can have an insulating effect on soil temperatures, with important impacts on permafrost extent (Zhang 2005; Zhang et al. 2008; Lawrence and Slater 2010). Variability in snow conditions also has implications for travel and tourism (e.g., Scott et al. 2008). It is crucial, therefore, that we understand how projected warming will affect snow cover.

Extensive climatological snow cover, and relatively high insolation, make the climate system most sensitive to snow and albedo changes during spring (changes during fall and winter are less important because of decreasing insolation across the NH) (Ingram et al. 1989; Hall 2004). Snow albedo feedback (SAF) peaks during March-April-May (Qu and Hall 2014). Numerous observational studies have shown that Northern Hemisphere spring snow cover extent (henceforth, SCE) has been decreasing rapidly over recent decades (Groisman et al. 1994; Déry and Brown 2007; Flanner et al. 2009; Brown et al. 2010; Brown and Robinson 2011; Hernández-Henríquez et al. 2015). Most of the loss in snow occurs over 'temperature-sensitive regions', where changes in SCE are closely linked to temperature variability (Karl et al. 1993; Déry and Brown 2007). March-April SCE is decreasing at a rate of -3.4 ± 1.1 % decade^{-1} (1979-2005) (Brown and Robinson 2011), and June SCE has decreased by ~-18% decade^{-1} from 1979-2014 (Derksen et al. 2015). This rate of decline in SCE exceeds the well-publicised declining trend in September Arctic sea ice (-13% decade^{-1}). It should be noted that the absolute areal SCE loss in Mar-Apr is comparable to that observed during June because there is much less snow covered area in June (Section 5.4.1).

By contrast, the suite of climate models contributing to the Coupled Model Intercomparison Project phase 5 (CMIP5) simulate March-April SCE trends roughly one-third as large as observed for the same time period (-1.0 ± 0.3 % decade^{-1}) (Brutel-Vuilmet et al. 2013). This underestimation, also found for the CMIP3 models (Roesch 2006), is associated with underestimated extratropical spring warming (Brutel-Vuilmet et al. 2013). Derksen and Brown (2012) and Mudryk et al. (2014) illustrate other aspects of the observed trends that are not well captured by general circulation models (GCMs).

Northern Hemisphere SCE is expected to continue decreasing under future warming. Several studies over the past 30 years have utilized GCMs to show that SCE decreases substantially in a doubled CO_2 climate (Manabe and Wetherald 1987; Boer et al. 1993; Essery 1997). More recently, the Intergovernmental Panel on Climate Change's Fifth Assessment Report (IPCC AR5) stated that early spring (March-April) SCE is likely to decrease by 7-25% (RCP2.6-RCP8.5) by 2100 (Collins et al. 2013; Brutel-Vuilmet et al. 2013). However, this projection was only assigned a medium confidence level because of a large inter-model spread, and a lack of sophistication in the representation of snow processes in many models (e.g., single layer snowpacks, and snow schemes that assume an equal distribution of snow mass across a grid cell (Collins et al. 2013; Slater et al. 2001). Furthermore, no projections of SCE were provided for late spring (May-June), when snow cover is largely restricted to the Arctic, but still represents a significant area (mean 1982-2002 Arctic SCE for May and June was 11.0 and 3.9 million km^2, respectively (Brown et al. 2010)). The Arctic has experienced the greatest warming in recent decades (Bekryaev et al. 2010), and that trend is expected to continue due to positive feedback mechanisms such as the lapse rate and albedo feedbacks (Pithan and Mauritsen 2014) with implications for spring snow cover.

CMIP (Meehl et al. 2007; Flato et al. 2013) and SnowMIP (Etchevers et al. 2004; Rutter et al. 2009) studies have demonstrated that a large inter-model spread exists when simulating snow properties (extent and mass). This limits our confidence in future projections, and is likely to be caused by a combination of internal climate variability, and model uncertainty (inter-model variability among GCMs in response to the same forcing)

from physical processes that are either missing, or oversimplified (Hawkins and Sutton 2011). For example, simulated snow mass (and similarly SCE) is sensitive to different parameterizations for snowfall, albedo, snow-vegetation masking, and snow cover fraction (see Slater et al. 2001; Bartlett et al. 2006; Dai 2008; Rutter et al. 2009; Essery et al. 2013).

Internal climate variability arises primarily from naturally-occurring non-linear atmospheric and oceanic processes, and their interactions (Deser et al. 2012b; Kay et al. 2015). The processes can be nearly instantaneous, or take several years (Hegerl et al. 2007). Internal variability influences projected regional trends in temperature and precipitation, even in the presence of a background trend in CO_2 forcing (Hawkins and Sutton 2009, 2011; Deser et al. 2012b), both of which are crucial factors for future winter snow accumulation patterns (Räisänen 2008; Krasting et al. 2013; Mankin and Diffenbaugh 2015; Shi and Wang 2015). Therefore, it is likely that internal climate variability could also influence projected trends for spring SCE.

The primary goal of this work is to investigate the spread in 21st century changes to spring snow cover as projected by the CMIP5 suite of climate models. We use the recent past to help understand the spread in trend strength between simulations and observations. We also seek to determine the influences of both internal variability and model uncertainty in these simulations, to answer the following research questions: (i) what impact does the representation of snow/climate processes (e.g., the sensitivity of snow cover to warming (henceforth, snowmelt sensitivity)) have on simulations of SCE?; and (ii) what are the respective roles of temperature and precipitation changes in governing SCE trends? The data and methods are described in Section 5.3. In Section 5.4, we present historical and projected

SCE trends, and diagnose the respective roles of model uncertainty and internal variability. Lastly, Section 5.5 highlights the key findings of this research and provides a discussion of how our findings relate to previous research.

5.3 Data and Methods

5.3.1 Climate Model Data

We use monthly mean output from the suite of *historical* (1850-2005) and *future* (2006-2100) simulations from the CMIP5 archive (Taylor et al. 2012; cmip-pcmdi.llnl.gov/cmip5/) to evaluate snow cover in 15 models (Table 5-1). Only models that archived the variable *snc* (snow cover fraction; SCF) are included in this analysis so as to avoid introducing uncertainty through the estimate of SCE from snow water equivalent (snow mass - *snw*) as done in previous studies (e.g. Roesch 2006). Future snow cover projections are forced using the RCP8.5 scenario because it most closely resembles the observed emissions pathway over the past decade (*Peters et al.*, 2013). We use all available realizations (n = 1-10) from each of the 15 CMIP5 models for a total of 61 historical runs and 41 runs for the RCP8.5 scenario. We compute individual trends/averages for each realization, then take the inter-realization average across each model to calculate ensemble means. These values are then used to determine the CMIP5 multimodel mean values.

We also use output (variables: *snc*, *snw*, *tas*, *psl*) from a large (50 realization) ensemble of the second generation Canadian Earth System Model, CanESM2 (Arora et al. 2011). To produce the 50-member large ensemble, (henceforth, CanESM-LE) ten realizations are initiated in 1950 from each of the five original realizations of CanESM2

Table 5-1: List of CMIP5 models analyzed in this study with reference letters for each model, the native resolution, the number of realizations contributed for both the historical and future periods, and spring SCE trends (10^6 km^2 decade^{-1}) for the recent past (1981-2010). Trend values that are not significant (according to a Mann-Kendall test) are marked with an asterisk.

	Model name	Institute	Resolution (°lat x °lon)	Realizations (Historical/ RCP8.5)	MAMJ SCE Trend (1981-2010)
A	Beijing Climate Center-Climate System Model version 1.1 (BCC-CSM1.1)	BCC	2.8 x 2.8	3/1	-0.53
B	Beijing Normal University Earth System Model (BNU-ESM)	BNU	2.8 x 2.8	1/1	-0.47
C	Canadian Earth System Model version 2 (CanESM2)	CCCMA	2.8 x 2.8	5/5 (+50)	-0.78
D	Community Climate System Model version 4 (CCSM4)	NCAR	0.9 x 1.25	6/6	-0.55
E	Centre National de Recherches Météorologiques-Climate Model (CNRM-CM5)	CNRM-CERFACS	1.4 x 1.4	10/5	-0.44
F	Commonwealth Scientific and Industrial Research Organization Mark 3.6 (CSIRO-Mk3.6.0)	CSIRO-QCCCE	1.875 x 1.875	10/10	-0.27
G	Flexible Global Ocean-Atmosphere-Land System model, Grid-point version 2 (FGOALS-g2)	LASG-CESS	2.8 x 2.8	5/1	-0.50
H	Goddard Institute for Space Studies Model E with Russell Ocean Model (GISS-E2-R)	NASA GISS	2.0 x 2.5	6/1	-0.42
I	Institute for Numerical Mathematics Climate Model version 4 (INM-CM4)	INM	1.5 x 2.0	1/1	-0.07*
J	Model for Interdisciplinary Research on Climate version 5 (MIROC5)	MIROC	1.4 x 1.4	5/3	-0.52
K	MIROC Earth System Model (MIROC-ESM)	MIROC	2.8 x 2.8	3/1	-0.56
L	Max Planck Institute Earth System Model low resolution (MPI-ESM-LR)	MPI-M	1.875 x 1.875	3/3	-0.27
M	Meteorological Research Institute Coupled General Circulation Model version 3 (MRI-CGCM3)	MRI	1.121 x 1.125	3/1	-0.20*
N	Norwegian Earth System Model intermediate resolution + biogeochemical cycling (NorESM1-ME)	NCC	1.89 x 2.5	1/1	-0.49
O	NorESM intermediate resolution (NorESM1-M)	NCC	1.89 x 2.5	3/1	-0.42

submitted to CMIP5. Each new ensemble member is perturbed by changing the seed of a random number generator used in the parameterization of radiative transfer through clouds. Following the CMIP5 design, historical forcing is applied from 1950 to 2005, followed by RCP8.5 from 2006 to 2100. This methodology is appropriate for sampling the statistics of climate variability within CanESM2, because the initial ocean conditions down to 300m depth have very little influence on the simulation after 5-10 years (Branstator and Teng 2012). This implies that, by the time our analysis period begins in 1981, CanESM-LE represents 50 statistically independent climate states.

As a result, CanESM-LE is used to quantify the component of internal variability within future projections from a single GCM, while the CMIP5 ensemble includes a combination of model uncertainty and internal variability. Similar large ensembles have previously been used to separate the components of future climate patterns related to forced and internal variability (Deser et al. 2012a,b; Wettstein and Deser 2014; Swart et al. 2015). Consistent with previous research (Deser et al. 2012b; Deser et al. 2014), we estimate the *forced response* to greenhouse gas (GHG) forcing as the ensemble mean response from all 50 realizations of CanESM-LE. As in Hawkins and Sutton (2011) we estimate the contribution of *internal variability* to each realization by subtracting the ensemble mean of a particular quantity from the values in that realization. This approach is effective when there are enough simulations so that climate noise can be sufficiently diluted (Deser et al. 2012b; Deser et al. 2016).

5.3.2 Observational Data

Seven observation-based estimates (Table 5-2) are used to evaluate the CMIP5 models during recent decades (1981-2010). The use of an observational ensemble reduces the chance of incorrectly identifying a model bias due to errors in a single observational analysis. The seven observation-based estimates are derived from reanalyses, satellite data, and *in situ* measurements. Each dataset must have complete Northern Hemisphere coverage, and a data record spanning the 1981-2010 period. Those datasets that meet this criteria are: (1) the NOAA snow chart climate data record (NOAA CDR) (Brown and Robinson 2011; ftp://eclipse.ncdc.noaa.gov/cdr/snowcover/), (2) the Brown snow cover product derived from a combination of climate station data and a simple snow model (Brown et al. 2003), (3) the combined in situ and satellite passive microwave derived GlobSnow SWE product (Takala et al. 2011; www.globsnow.info), (4) SWE from the Modern Era Retrospective Analysis for Research and Applications (MERRA) (Rienecker et al. 2011), (5) SWE from the European Centre for Medium-Range Forecasts Interim Land Reanalysis (ERA-I-Land) (Balsamo et al. 2015), (6) SWE from the Global Land Data Assimilation System Version 2 (GLDAS-2) product (Rodell et al. 2004), and (7) SWE output from the Crocus snowpack model driven by ERA-I meteorology (Brun et al. 2013). Three of the snow products use the same atmospheric forcing data from ERA-Interim (Brown, Crocus, and ERA-I-Land). However, despite this similarity, they exhibit very different SCE trends due to differences in the snow parameterizations between Crocus and HTESSEL (ERA-I-Land), while the Brown dataset only uses temperature and precipitation to force a simple snow model (Table 5-2).

Table 5-2: List of observational-derived snow data products analyzed in this study, the native resolution, respective climatological SCE (10^6 km^2) and spring SCE trends (10^6 km^2 $decade^{-1}$; % $decade^{-1}$). Trend values that are not significant are marked with an asterisk.

	Data Product	Resolution	MAMJ SCE Trend (1981-2010)	MAMJ Percent Loss (1981-2010)	MAMJ Mean Snow Extent (1981-2010)
1	Brown (Brown et al. 2003)	0.75° x 0.75°	-0.74	-3.9	19.0
2	CROCUS (Brun et al. 2013)	1° x 1°	-0.63	-3.8	16.6
3	European Centre for Medium-Range Forecasts Interim Land Reanalysis (ERA-I-Land) (Balsamo et al. 2015)	0.75° x 0.75°	-0.38	-2.2	17.9
4	Global Land Data Assimilation System Version 2 (GLDAS-2) (Rodell et al. 2004)	1° x 1°	-0.22*	-1.6	14.1
5	GlobSnow (Takala et al. 2011)	25 km	-0.55	-3.4	16.2
6	Modern Era Retrospective Analysis for Research and Applications (MERRA) (Rienecker et al. 2011)	0.5° x 0.66°	-0.50	-3.3	15.1
7	NOAA Climate Data Record (Brown and Robinson 2011)	190 km	-0.82	-4.2	19.3
	CMIP5 Mean		-0.43 ± 0.17	-2.5 ± 1.0	17.0 ± 3.4
	CanESM-LE	2.8° x 2.8°	-0.62 ± 0.18	-3.0 ± 0.9	20.6 ± 0.2

The NOAA CDR is derived primarily from optical satellite data (Brown and Robinson 2011). This dataset provides monthly fractional snow cover, which is calculated as the percent of days per month that a grid cell is at least 50% snow covered. The Brown dataset (Brown et al. 2003) uses ground-based snow measurements and a simple snowpack model to produce SCF from daily SWE thresholds exceeding 4mm. The five remaining datasets (MERRA, ERA-I-Land, GLDAS-2, GlobSnow, and CROCUS) were used in the SWE product inter-comparison described in Mudryk et al. (2015). For these products, SWE is initially interpolated to a 1° by 1° grid and SCF is then derived from daily SWE thresholds

exceeding 4 mm. The 1981-2010 time period is a shorter record than available from individual datasets (for example the NOAA CDR starts in 1967) but the compromise in time series length is mitigated by the advantages of a multi-dataset perspective which has typically not been used in previous snow-climate studies.

An observational ensemble of temperature is used to determine spring snow extent sensitivity. We select five datasets for temperature: the Climatic Research Unit land station temperature database (CRU) (Jones et al. 1999; 2012), the Goddard Institute for Space Studies (GISS) surface temperature analysis (Hansen et al. 2010), the National Climatic Data Center (NCDC) temperature product (Smith et al. 2008), and the National Centers for Environmental Prediction (NCEP) surface and 2m (NCEP2m) temperature datasets (Kalnay et al. 1996).

5.3.3 Analysis Methods

The CMIP5 models output data at a variety of resolutions (1-3° grid boxes), and to account for this we must create a consistent land/sea mask such that land area biases are reduced (particularly in the Canadian Arctic Archipelago (CAA), where many narrow channels may not be resolved at coarser resolution (Laliberté et al. 2016)). For each CMIP5 model a land/sea mask extracted from the Modern Era Retrospective Analysis for Research and Applications (MERRA) product is remapped to the native model resolution to isolate simulated NH land-only snow cover and temperature data. This ensures that we reduce discrepancies in the amount of land area between models (mainly in the CAA). Using this mask along with the model-specific land mask reduces climatological SCE in the models, but has minimal impact on their trends (not shown). Furthermore, the study area for this analysis

is spatially restricted to the Northern Hemisphere extratropics (>30°N), with Greenland excluded, and temporally restricted to March-April-May-June (MAMJ).

SCE is calculated from model output by multiplying grid cell snow cover fraction (%) by the area of each grid cell (m^2) then taking the hemispheric sum for each month. Similarly, snow water mass (SWM) is computed by multiplying grid cell level snow water equivalent (SWE) by the area of each grid cell and summing over the NH. This is applied to SWE data from the CanESM-LE to allow for an illustration of the influence that changes in winter precipitation have on SCE trends. The pre-melt SWM is a useful measure of snowfall totals over the winter months, particularly across the Arctic, because wind-driven snow processes are not represented in current models (Turner et al. 2006; Lawrence et al. 2012). We find that 1981-2010 winter (Oct-Mar) snowfall trends are strongly correlated with March SWM trends within CanESM-LE (r=0.92; not shown). Along with measures of correlation, we also use the coefficient of determination (R^2) to recognize the contribution from precipitation and temperature to SCE variability.

Time series of SCE and SWM data are used to calculate climatologies, and linear trends. We calculate these values for each of the four 30-year climatological time frames during the study period: historical (1981-2010), near-future (2011-2040), mid-century (2041-2070), and long-term (2071-2100). In some cases, a 21st century trend (2011-2100) is used to simplify the discussion of results. Since the *historical* CMIP5 data ends in 2005, we use RCP8.5 data to complete the 1981-2010 period so that a comparison with recent observations can be made (similar to *Derksen and Brown*, 2012). SCE trends are computed as both absolute area (million km^2 $decade^{-1}$) and percent changes (% $decade^{-1}$). Absolute area

calculations are useful in the context of comparing different months, while percent changes may be more suitable for inter-ensemble comparisons because they account for potential differences in snow cover climatology. Throughout, all trend values reported are accompanied by 1 sigma standard deviations to represent uncertainty. Note that trends are calculated at each model's native resolution, and regridding to a 1°x1° grid is only used for spatial mapping of the snow cover from the CMIP5 models. Lastly, the term 'bias' will be used solely for comparing models in relation to observation-based estimates.

5.4 Results

5.4.1 Historical Spring SCE Trends

Considering first the entire spring season for the Northern Hemisphere, SCE has decreased at a mean rate of -0.55 ± 0.21 million km^2 $decade^{-1}$ from 1981-2010, according to the seven observation-based estimates evaluated here (Table 5-2). Dividing this rate by the climatological spring SCE produces a percent change of -3.3% $decade^{-1}$. The strongest trend in terms of absolute area occurs in March (mean: -0.66 ± 0.26 million km^2 $decade^{-1}$), and the weakest in June (-0.41 ± 0.30 million km^2 $decade^{-1}$) (Fig. 5-1). However, direct measures of trend magnitude do not account for the much greater total snow area in March (32.6 ± 2.5 million km^2) than June (2.6 ± 1.9 million km^2; not shown). When viewed as a percent change relative to the monthly climatology, March SCE is decreasing at a rate of -2.0 ± 0.8% $decade^{-1}$, while the rate of June SCE loss is -16 ± 11% $decade^{-1}$ (not shown). Both early spring and June trends found here are weaker than those previously reported that were based only on the NOAA CDR: Brutel-Vuilmet et al. (2013) reported trends of -3.4% $decade^{-1}$ for March-April

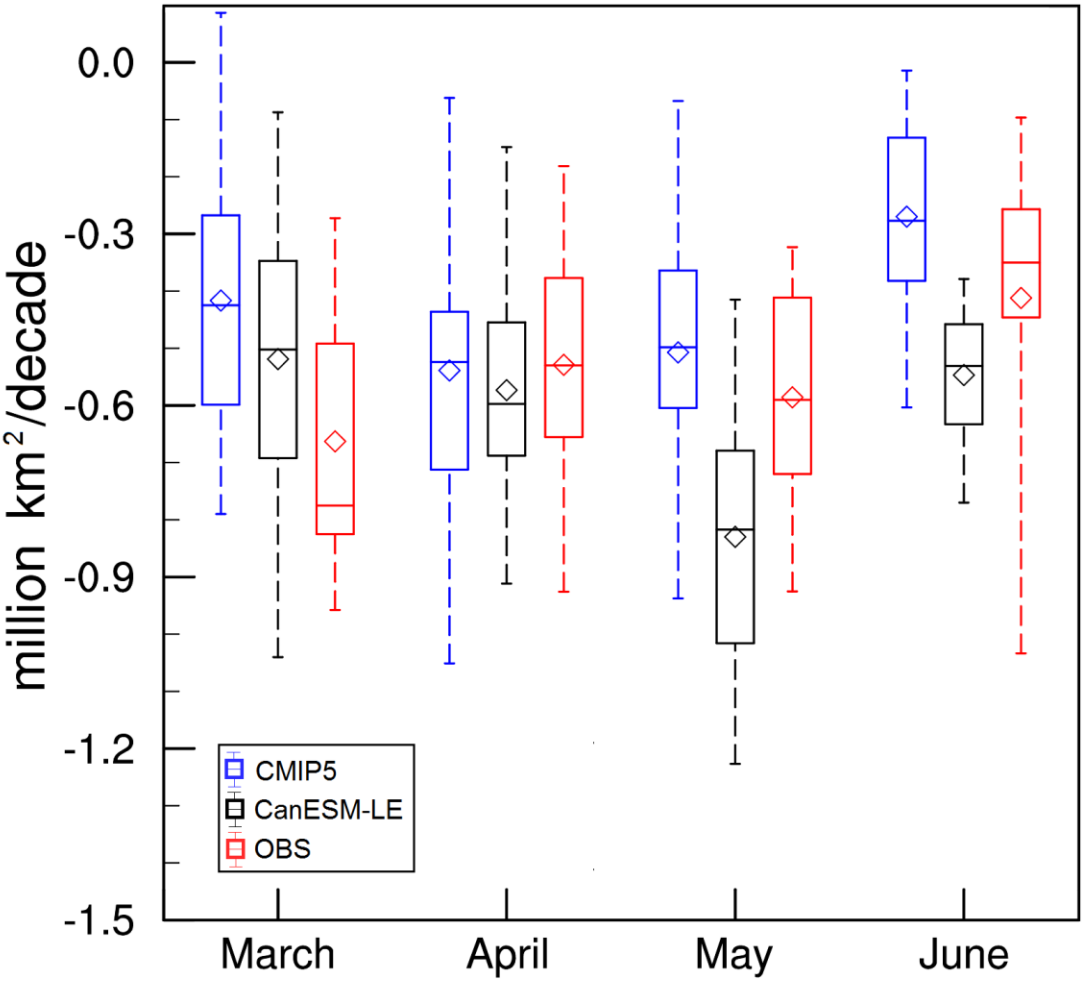

Figure 5-1: Historical (1981-2010) Northern Hemisphere extratropical snow cover extent trends among three ensembles: CMIP5, CanESM-LE, and observation-based (OBS). For each box the enclosed region shows the 25th-75th percentile range, the horizontal line shows the median, and the diamond shows the ensemble mean. The dashed fences indicate the minimum and maximum. The CMIP5 box uses the mean for each model (averaged over all available realizations).

over the 1979-2005 period, while Derksen and Brown (2012) reported trends of -18% decade^{-1} in June over the (1979-2011) period.

These reported differences result because there is a substantial spread among the observation-based estimates of SCE trends, and of the seven products evaluated here the NOAA CDR trends are the largest in magnitude (Table 5-2). Mudryk et al. (2015) have recently shown an analogously large spread in SWM trends from various snow analysis

products. Such spread likely occurs as a result of differences in methodology and the type of data used to construct each dataset (e.g., *in situ*, reanalysis, satellite-derived). Three of the four reanalysis products (GLDAS-2, ERA-I-Land and MERRA) exhibit the weakest spring SCE trends over recent decades, with GLDAS-2 losing the least SCE in each spring month. On the other hand, two of the three products which utilize either satellite-derived or *in situ* information (NOAA CDR and Brown) exhibit the strongest trends in spring SCE over the recent past.

Simulated spring trends from the CMIP5 models are approximately 22% weaker than observed on average (multimodel ensemble mean (MM): -0.43 ± 0.17 million km^2 $decade^{-1}$, or -2.5 ± 1.0% $decade^{-1}$). This is also weaker than that of the CanESM-LE (mean = -0.62 ± 0.18 million km^2 $decade^{-1}$), which demonstrates much greater late-spring snow loss. From a monthly perspective, the CMIP5 mean SCE trend is largest during April, and weakest in June (Fig. 5-1). The agreement between CMIP5 models and observations is very good during April and May, but less so during March and June, when the models have weaker trends (MM: -1.4 ± 0.8% $decade^{-1}$ and -8.4 ± 5.4% $decade^{-1}$, respectively). However, March is the only month with a statistically significant difference between the observed and simulated mean trends ($p<0.05$; using a two-sided Student's *t*-test). Furthermore, nearly all models exhibit negative SCE trends throughout the spring, except for INMCM4, which has a slight increasing trend during March. The CMIP5 models range from losing very little snow in MAMJ at 13% of the observed baseline (-0.07 million km^2 $decade^{-1}$), to 142% of observed (-0.78 million km^2 $decade^{-1}$) (Table 5-1). As a demonstration that single model contributions to the CMIP5 archive may underestimate internal variability, CanESM2 is the model with the

greatest spring snow loss of any CMIP5 model from 1981-2010, yet we find that CanESM-LE (the large ensemble produced using the same model) is much closer to the CMIP5 average (Fig. 5-2).

The variability in 30-year trends from the CMIP5 ensemble is equally large for March, April and May (standard deviation (σ) = 0.24 million km^2 decade^{-1}), and slightly lower in June (σ = 0.17). However, when we examine 10-year trends the spread widens dramatically for all spring months. For example, in May the simulated range (max-min) for decadal trends is more than seven times that for 30-year trends (-3.7 to 2.7 million km^2 decade^{-1}; Fig. 5-S1). This highlights the larger contribution to the SCE trends from internal variability, compared to the forced response to GHG increases, over shorter time periods. This result is consistent with similar findings for temperature and precipitation trends (Hawkins and Sutton 2009; 2011). The following section will investigate possible factors contributing to the large inter-model spread within *historical* simulations from the current generation of climate models.

5.4.2 Sources of Model Uncertainty: Historical Trends

5.4.2.1 Sensitivity of SCE to Warming Trends

First we evaluate how differences in warming could be affecting the simulated inter-model spread in SCE trends. Although a very important contributor (R^2 = 0.74), differences in simulated warming do not explain all of the inter-model spread in spring SCE trends for the 1981-2010 period. We use mean extratropical land warming rather than local warming because unnaturally high sensitivities can occur for some models in areas where the warming

trend is close to zero. The observed spring NH extratropical land warming trend over the 1981-2010 period is 0.34 ± 0.04 K decade^{-1}. On average, the CMIP5 models accurately capture spring warming over recent decades, with an ensemble mean of 0.36 ± 0.11 K decade^{-1} (Fig. 5-2). In contrast, the CanESM-LE has a greater mean warming trend (0.52 ± 0.08 K decade^{-1}), which overlaps with the CMIP5 warming trend but which falls outside the uncertainty range of the observed warming trend. The mean trend seen in the CanESM-LE ensemble reflects the majority of CMIP5 models (10/15) which simulate recent (1981-2010) spring warming that is greater than or equal to the warming found in observations.

Despite realistically reproducing observed temperature trends, only two models produce more snow loss than the observation-based estimates. This suggests that snow in some models tends to be less sensitive to temperature variations than in observations. To quantify this property of the models, we compute a snowmelt sensitivity $\lambda_{smelt} = \langle \Delta SCE \rangle / \langle \Delta T_s \rangle$, which measures how much SCE is reduced per degree of warming, averaged over the NH land area (averaging is denoted by the angle brackets). Observed spring λ_{smelt} during the spring months (MAMJ mean) is -1.62 ± 0.61 million km^2 K^{-1}, with the large uncertainty driven mainly by disagreement among the observed SCE trends (illustrated by the shaded rectangle in Fig. 5-2), which create a large spread among the 35 possible combinations of observed temperature (5 products) and SCE (7 products). This exceeds the estimate of λ_{smelt} that is computed for both the CanESM-LE (-1.18 ± 0.15 million km^2 K^{-1}), and the CMIP5 ensemble (MM = -1.19 ± 0.31 million km^2 K^{-1}). The 68% confidence interval for the CMIP5 estimate of λ_{smelt} overlaps that from observations, indicating that the two

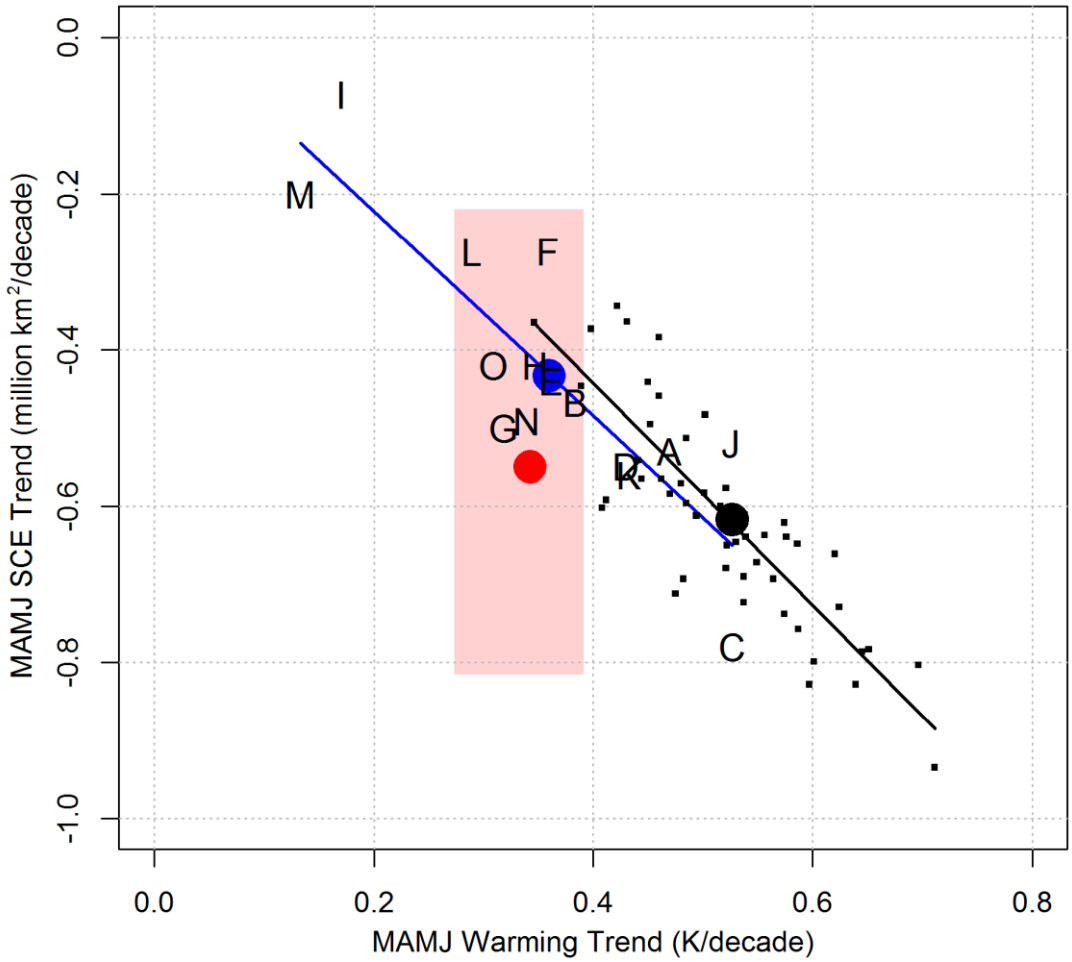

Figure 5-2: Relationship between spring SCE trends and NH extratropical land warming for the CMIP5 models during the historical period (1981-2010). Each model is represented by a letter, corresponding to the information in Table 5-1. Filled circles represent the CMIP5 mean (blue), CanESM-LE mean (black), and the observation-based mean (red). Each member of the CanESM-LE is shown as a small black square. The shaded red rectangle illustrates the range of observation-based trends. Models that fall to the bottom left portion of the plot are most sensitive to warming.

estimates of mean snowmelt sensitivity are not significantly different. However, similar to Brutel-Vuilmet et al. (2013) we find that the weaker-than-observed SCE trends from the CMIP5 ensemble are likely due in part to a weaker-than-observed snow response to warming.

5.4.2.2 Climatological Mean Snow Cover

A secondary cause of the weaker-than-observed SCE trends in CMIP5 is biases in the simulated climatological (1981-2010 mean) snow cover ($\overline{SCE}$) for a given month. The ability to accurately represent present day snow cover is important for simulated SCE trends because of a positive correlation between snow extent and SAF strength (Levis et al. 2007). This relationship indicates that models with greater SCE produce stronger SAF for a given rise in temperature, because larger SCE implies a greater potential area over which albedo can be reduced from its snow-covered to its snow-free value. In the CMIP5 multi-model mean, nearly all land poleward of 45°N is at least 50% snow covered in March (Fig. 5-3a; MM $\overline{SCE}$ of ~30.5 ± 3.5 million km^2). However, there is a significant spread in March $\overline{SCE}$ within the CMIP5 ensemble: the model with the highest $\overline{SCE}$ has 18% more snow-covered area than the mean (red line Fig. 5-3a), while the model with the lowest $\overline{SCE}$ has 28% less snow cover than the mean (green line Fig. 5-3a). Much of the disparity between these models is found across western North America, western Eurasia, and the Tibetan Plateau (similarly for April; Fig. 5-3b). Comparatively, the observation-based estimates show $\overline{SCE}$ ranging from 30 to 36 million km^2 in March, with a mean of approximately 32 million km^2. Disparity between the minimum and maximum observation-based snow cover products is greatest over eastern Eurasia and western North America (Fig. 5-3a). Of note is the good agreement over western Eurasia, where both of the extreme observation-based estimates exceed or closely resemble the maximum model extent. This implies that the CMIP5 models may be systematically underestimating early spring snow cover in this region.

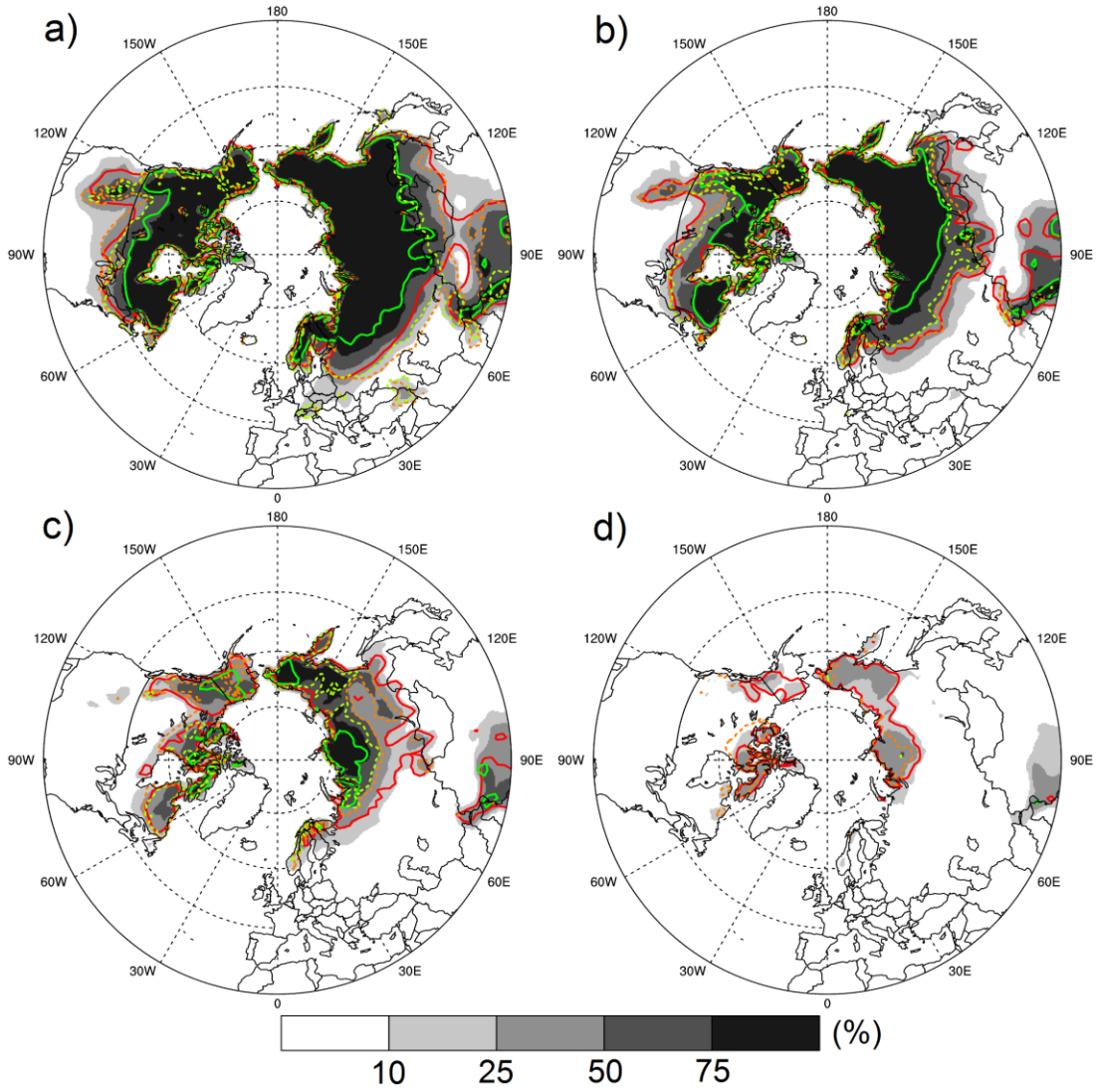

Figure 5-3: Spatial distribution of monthly mean historical (1981-2010) snow cover fraction (%) from the CMIP5 ensemble mean for (a) March (b) April (c) May and (d) June. Solid contours show the boundary of the region with >50 % SCF for the model with minimum (green line) and maximum (red line) SCE during each month. Dotted contours show the minimum (yellow) and maximum (orange) observation-based estimates of the region with >50 % SCF. The observational minimum does not appear in June because SCE is below 50 % everywhere.

Late spring (May-June) snow cover resides primarily across the Arctic (>60°N), with much of the high-latitudes still more than 50% snow-covered during May (Fig. 5-3c). On average, the CMIP5 models simulate May $\overline{SCE}$ of 11.8 ± 3.9 million km^2, while the observation-based products range from 6.9 to 14.7 million km^2, with a mean of 10.6 ± 2.6

million km^2. In June any remaining snow cover is restricted to Siberia, Arctic Canada, and Alaska and is characterized by local snow cover fractions lower than 50% (CMIP5 mean $\overline{SCE}$ is 3.2 ± 2.0 million km^2; Fig. 5-3d). Similar to the models, the observation-based estimates have a mean of 2.6 ± 1.9 million km^2, and a large spread spanning from 0.5 (GLDAS-2) to 5.9 million km^2 (NOAA CDR). Note that differences between models in their $\overline{SCE}$ is likely the result of model uncertainty, rather than internal variability, as demonstrated by a very small range within the CanESM-LE (<1 million km^2 for all spring months; not shown).

Biases in June $\overline{SCE}$ have the most significant impact on SCE trends of any month: those models with minimal SCE in June tend to show very weak SCE trends because in future there is so little snow left to melt. The models with low June $\overline{SCE}$ (e.g., BCC-CSM1.1, CSIRO-Mk3.6, INMCM4, MPI-ESM-LR; Fig. 5-S2) exhibit a mean SCE trend of only -0.06 million km^2/decade (not shown), a factor of six weaker than the other CMIP5 models (-0.35 million km^2 decade^{-1}; not shown). These same models with low June $\overline{SCE}$ have previously been shown to have mean late spring near-surface air temperatures that are substantially warmer than the other CMIP5 models (Thackeray et al. 2015). Therefore, biases in $\overline{SCE}$ can affect the SCE trend in seasons when SCE becomes limited (e.g., late spring).

There is a slightly weaker correlation (r=0.43) between trends in 1981-2010 March SWM (used as a proxy for variability in winter snowfall) and MAMJ SCE trends within the CMIP5 ensemble (not shown). A moderately strong correlation also exists between March SWM trends and λ_{smelt} (r=0.70). However, because SWM does not have the same sub-seasonal importance as $\overline{SCE}$ (there is a weak correlation with SCE trends for all months other

than March) it is not investigated further. Furthermore, although there are many other potential sources of model uncertainty in simulated SCE (e.g. model resolution, land surface scheme complexity, climatological temperature biases), we do not find any clear linkages between these parameters and spring SCE trends, so they are not discussed further.

5.4.3 Projected Trends in Spring SCE

To evaluate projections of future spring SCE, we use two model ensembles: the multi-model CMIP5 ensemble, and the CanESM-LE. As previously noted, the latter only contains (land-atmosphere-ocean induced) spread due to internal variability, so it provides a useful benchmark to compare with the estimate of inter-model spread from CMIP5. It should be noted that CanESM-LE provides one model's estimate of internal variability, which could vary for other CMIP5 models (e.g. Kay et al. 2015). First, we discuss the median projected change for the spring as a whole, followed by early (MA) and late spring (MJ). On average, the CMIP5 models project that spring SCE trends will strengthen during the 21st century relative to the recent past. The mean rate of spring snow loss over the 21st century (2011-2100 trend) is approximately -3.7 ± 1.1% decade^{-1}, 33% greater than in the period 1981-2010 (Fig. 5-S3). Similarly, the CanESM-LE exhibits a strengthening of 41% (more negative) compared to its 1981-2010 trend. However, CanESM2 exhibits the strongest 1981-2010 trend of the CMIP5 models (Table 5-1) so the median rate of 21st century spring snow loss from CanESM-LE is also larger (-4.3% decade^{-1}).

The CMIP5 models project that early spring (Mar-Apr) SCE trends will strengthen in the 21st century relative to the recent past (Figs. 5-4a,b). The mean SCE responses over the 21st century (2011-2100 trend) from CMIP5 (-0.80 ± 0.23 million km^2 decade^{-1}) and

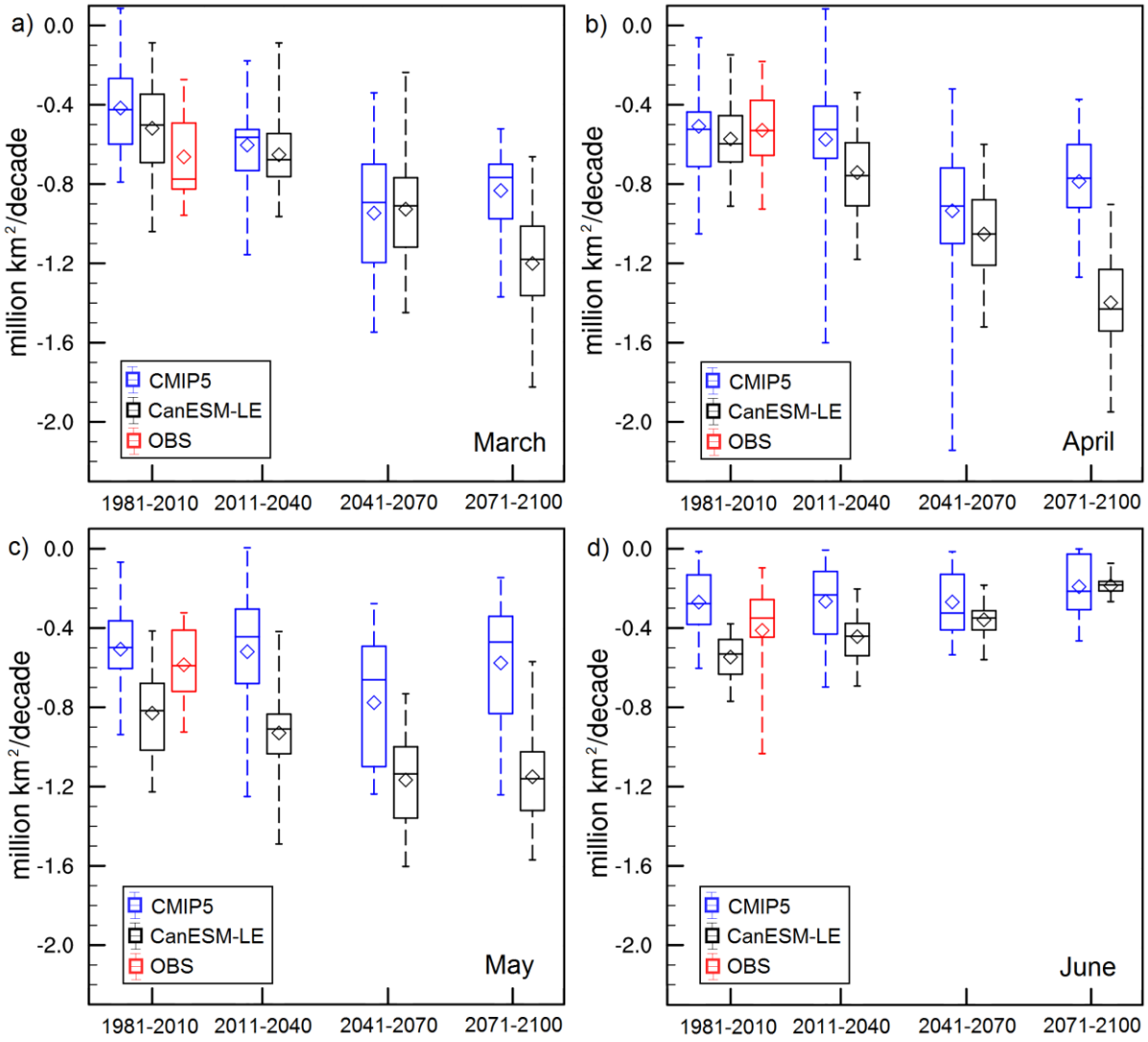

Figure 5-4: Northern Hemisphere March (a) April (b) May (c) and June (d) SCE trends over the 21st century under the RCP8.5 emissions scenario for the CMIP5, CanESM-LE, and observation-based (OBS) ensembles. As for Figure 5-1, each box shows the 25th-75th percentile range, the horizontal line shows the ensemble median, and the diamond shows the ensemble mean. The dashed fences indicate the ensemble minimum and maximum. Trends are shown in millions of km^2 per decade and split into four thirty-year climatological periods (1981-2010, 2011-2040, 2041-2070, and 2071-2100).

CanESM-LE (-1.02 ± 0.22 million km^2 decade^{-1}) are more than 65% stronger than their respective simulated rates for the period of 1981-2010. This is consistent with greater simulated rates of warming during the 21st century (not shown). Since these two ensembles have different mean $\overline{SCE}$ (Table 5-3), we also calculate the ensemble mean percentage of

Table 5-3: Projected 21st century (2011-2100) mean SCE trends (area and percent) along with 1981-2010 mean climatological SCE for each spring month. Percent loss is calculated by dividing the absolute area trend by mean SCE.

	Projected Absolute Area Trend (10^6 km^2 decade^{-1})		Projected Percent Loss Trend (% decade^{-1})		1981-2010 Mean SCE (10^6 km^2)	
	CMIP5	CanESM-LE	CMIP5	CanESM-LE	CMIP5	CanESM-LE
March	-0.80 ± 0.23	-0.96 ± 0.22	-2.6 ± 0.7	-2.8 ± 0.7	30.5 ± 3.6	33.9 ± 0.2
April	-0.80 ± 0.25	-1.08 ± 0.21	-3.6 ± 1.1	-3.9 ± 0.8	22.5 ± 4.0	27.4 ± 0.2
May	-0.64 ± 0.24	-1.10 ± 0.22	-5.5 ± 2.0	-6.5 ± 1.3	11.8 ± 3.9	16.9 ± 0.2
June	-0.26 ± 0.17	-0.35 ± 0.07	-8.1 ± 4.9	-8.7 ± 1.9	3.2 ± 2.0	4.0 ± 0.1

snow loss over the 21st century to account for differences in the amount of snow cover available for melt: the CMIP5 models lose -3.0 ± 0.9% decade^{-1}, while CanESM-LE loses 3.3 ± 0.7% decade^{-1}.

Within the CMIP5 ensemble, mean 21st century May SCE loss (2011-2100 trend) is projected to strengthen slightly (by ~25%) compared to the 1981-2010 trend. Trends in May also exhibit the greatest discrepancy between CMIP5 (-5.5 ± 2.0% decade^{-1}) and CanESM-LE (-6.5 ± 1.3% decade^{-1}) (Fig. 5-4c). Unlike the other months, June SCE trends are projected to weaken over the course of the 21st century (Fig. 5-4d). A gradual weakening within CanESM-LE is tied to a significant reduction in the amount of snow area remaining for melt (mean SCE < 0.5 million km^2 by 2071-2100). This same reasoning explains why the simulated June trends (even under the most aggressive GHG forcing scenario) of -8.1± 4.9% decade^{-1} from CMIP5 and -8.7± 1.9% decade^{-1} from CanESM-LE are weaker than observed in recent decades (-16% decade^{-1}). In summary, rates of projected snow cover loss are

expected to increase for all spring months, with the exception of June, where a relatively small SCE remains in the latter half of the 21st century.

Lastly, we consider the inter-model spread of land surface warming trends as a possible source of uncertainty for projected spring SCE trends within the CMIP5 ensemble. We estimate the uncertainty in the CMIP5 projections using the multi-model standard deviation (σ) (Hawkins and Sutton 2011), and we average σ over three different 30-year periods (2011-2040, 2041-2070, 2071-2100). This procedure yields uncertainties in SCE trends for March (σ = 0.28 million km^2 decade^{-1}), April (σ = 0.36 million km^2 decade^{-1}), May (σ = 0.34 million km^2 decade^{-1}) and June (σ = 0.18 million km^2 decade^{-1}). Taking the example of the relatively large uncertainty in April, we find a wide range of projected SCE trends for the 2011-2040 period, from a small gain in one model to a loss of -1.6 million km^2 decade^{-1} in another model (Fig. 5-S4). In this case, the model with the strongest (weakest) SCE loss also warms the most (least) over this period. Warming trends explain much of the inter-model spread in early spring SCE trends (R^2 = 0.79; Fig. 5-5), whereas June SCE trends are heavily influenced by biases in $\overline{SCE}$ (R^2 = 0.93; Fig. 5-5). For the spring as a whole, variability in 21st century NH land warming explains ~80% of the inter-model spread in SCE trends. Therefore, reducing variability in simulated future warming should in turn reduce uncertainty in SCE trends (further discussed in Section 5.5).

5.4.4 The Contribution of Internal Variability to Projected Trends in SCE

Many of the CMIP5 models that project extremely strong or weak spring SCE trends contributed only a single realization in the CMIP5 archive, while considerably better

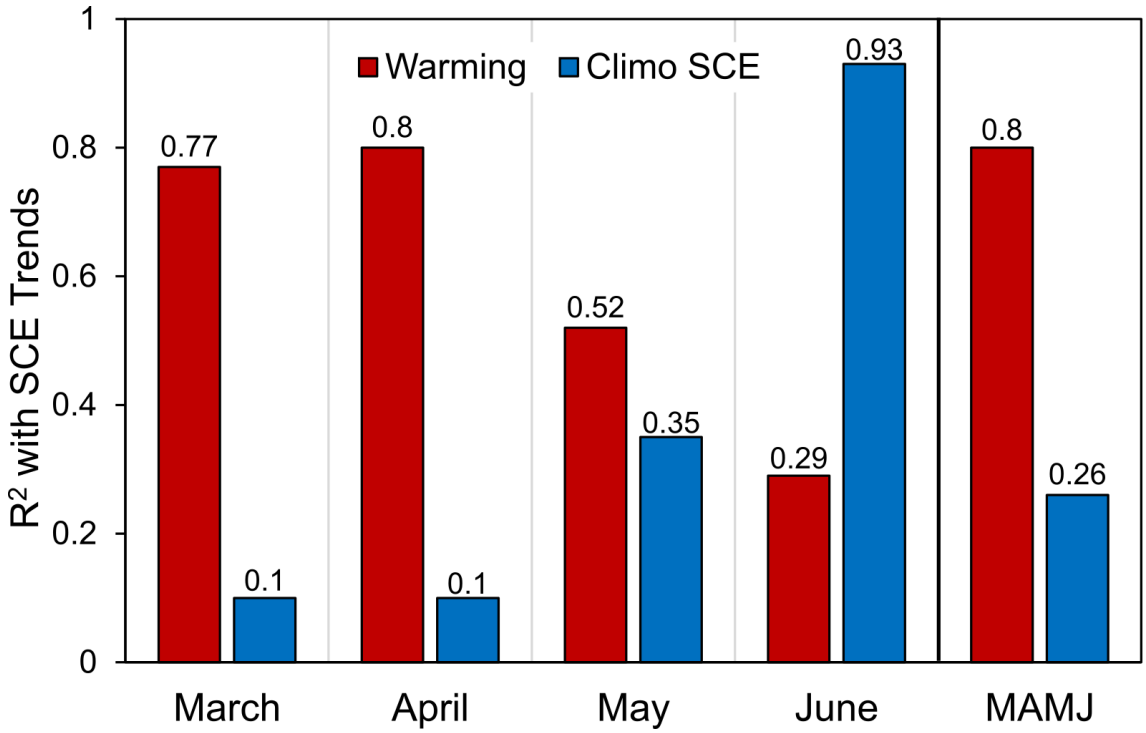

Figure 5-5: Bar plot showing the R^2 for 21st century SCE trends (2011-2100) from CMIP5 predicted based on projected NH extratropical land warming trends (red) and climatological SCE (blue) as predictors for March, April, May, and June. MAMJ values are calculated from the average seasonal trends in SCE and temperature rather than as an average of R^2 values.

agreement in projected SCE trends exists among the set of four models that contributed n≥5 realizations (particularly in early spring when warming trends dominate, not shown). This motivates an important question as to the role of internal variability in SCE trends; however, the majority of CMIP5 models completed fewer than five realizations, which is likely insufficient for estimating internal variability (Kay et al. 2015).

The 50-realization CanESM-LE exhibits a smaller spread in MAMJ SCE trends throughout the 21st century than the CMIP5 ensemble (σ = 0.18 and 0.29 million km^2 $decade^{-1}$, respectively, averaged over three epochs 2011-2040, 2041-2070, 2071-2100). Internal variability, as indicated by the shading for CanESM-LE in Fig. 5-6, is likely a very important contributor to the inter-model spread in the near-term (2011-2040), but the fraction of total

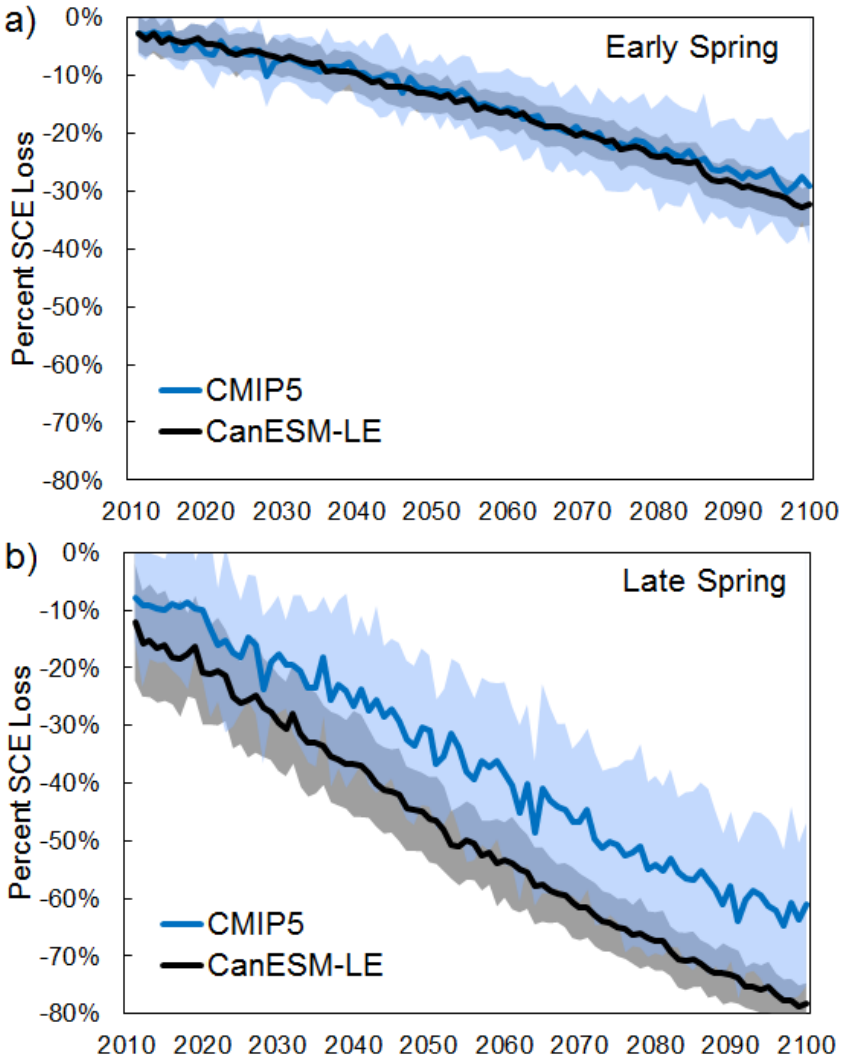

Figure 5-6: Percentage of climatological Northern Hemisphere SCE (1981-2010 mean) lost over the 21st century in CMIP5 and CanESM-LE for (a) early spring (b) late spring. Ensemble mean shown with ± 1 standard deviation shading. Note that the decreasing CanESM-LE variability in Fig. 5-6b is caused by June SCE falling closer to zero.

variance within the CMIP5 ensemble attributable to internal variability decreases on longer timescales as a relatively larger fraction is explained by model uncertainty (Fig. 5-6). This same finding has also been shown for precipitation and temperature trends, where internal variability has a greater influence in the near-future than at the end of the century (Hawkins and Sutton 2009, 2011).

Lastly, to demonstrate the interplay between internal variability and model uncertainty, we can compare the results from CanESM-LE with the intra-ensemble spread for all CMIP5 models with n≥5 realizations available for the RCP8.5 experiment (CanESM2, CCSM4, CNRM-CM5, and CSIRO-Mk3.6.0). This subset of models, which we assume provides an improved estimate of model uncertainty isolated from internal variability, contains substantial variation, both in the inter-model SCE trends (n=4, σ: 0.22 million km^2 $decade^{-1}$), and the inter-realization variability (n=26, min/max σ: 0.12/0.23 million km^2 $decade^{-1}$). The inter-realization spread of trends for each model is thus of similar magnitude to the inter-model spread, making it plausible that a significant fraction of the inter-model spread is caused by internal variability. We find considerable similarities between this analysis and the work on trends in September Arctic sea-ice extent (SIE) by Swart et al. (2015). For example, there is a remarkable similarity in the contributions from internal variability and model uncertainty to projected trends of SIE and SCE (not shown). The conclusion for near-term projections is that the large contribution from internal variability presents a challenge to determining the physical cause of 30-year SCE trends.

5.4.4.1 Case Study: May SCE Trends in CanESM-LE

In the CanESM-LE, near-future (2011-2040) springtime (MAMJ) SCE trends range from -0.26 to -1.08 million km^2 $decade^{-1}$, with the largest monthly spread occurring in May (-0.42 to -1.49 million km^2 $decade^{-1}$). For May, this represents a more than doubling of the range exhibited by the five CanESM2 runs contributed to CMIP5 (-0.69 to -1.11 million km^2 $decade^{-1}$). We will therefore use May as a case study for better understanding the primary physical factors contributing to the spread.

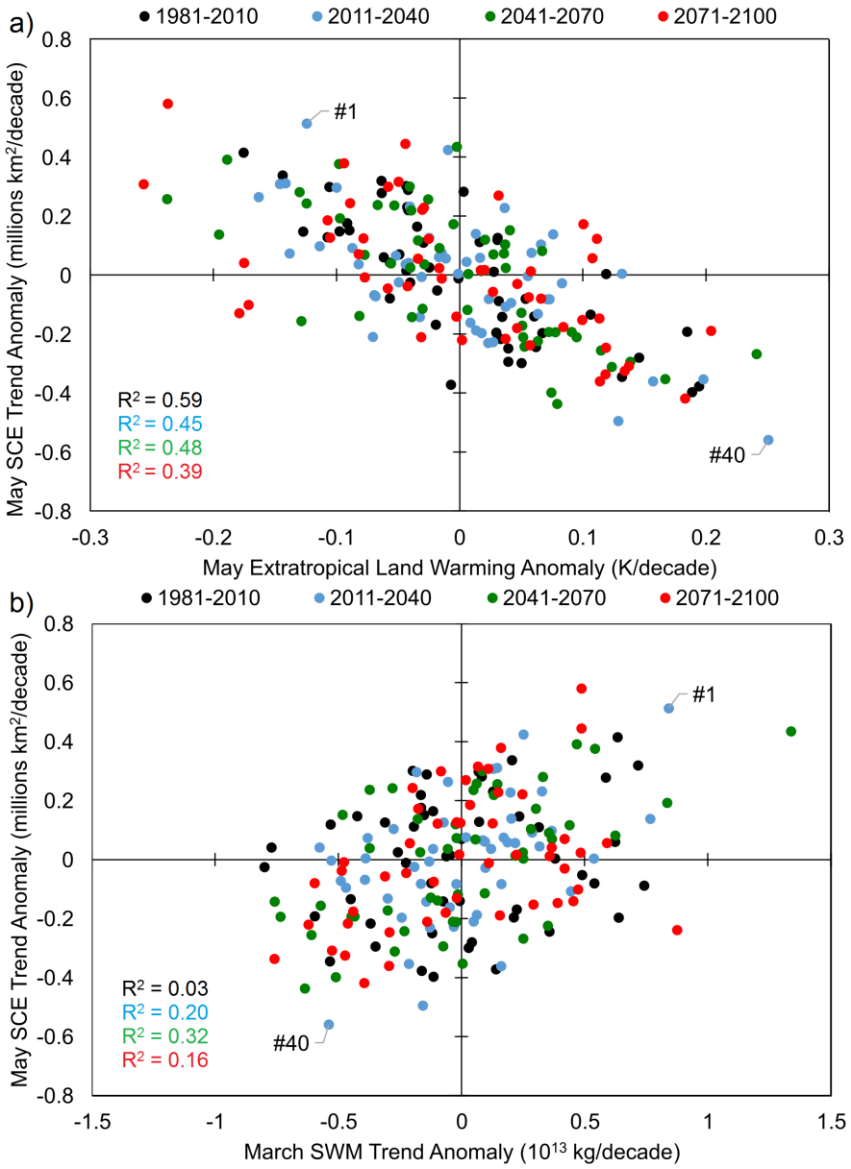

Figure 5-7: Relationship between May SCE trend anomalies within CanESM-LE and (a) May warming anomalies over NH extratropical land, (b) March snow water mass anomalies over NH extratropical land. Each realization is represented by four points, one for each of the climatological periods (color coded). Trend anomalies are calculated by removing the ensemble mean (forced component). The R^2 for each time period is shown in the bottom corner (color coded).

First, we examine the contribution from variations in trends of near-surface air temperature. Only a relatively small fraction (17%) of the inter-realization variability in CanESM-LE projected near-future May SCE trends is explained by *annual mean* global

Table 5-4: Correlation between May SCE trends (2011-2040) and global annual mean temperature, Northern Hemisphere extratropical land temperature, Arctic land temperature, and Northern Hemisphere March snow water mass within the CanESM large ensemble.

Variable	Time Period	Correlation	R-Squared
Global annual temperature	2011-2040	-0.41	0.17
NH May temperature	2011-2040	-0.67	0.45
Arctic May temperature	2011-2040	-0.69	0.47
NH March SWM	2011-2040	0.44	0.19

surface warming (land + ocean), with r= -0.41 (Table 5-4) and the negative sign implying that enhanced global warming is associated with greater snow loss. However, nearly half of the inter-realization variability (45%) is explained when we restrict the analysis to include only contemporaneous (e.g., May) and local (e.g., NH extratropical land averaged) temperatures (Fig. 5-7a; r= -0.67). The majority of May snow cover resides across the Arctic (Fig. 5-3c), so one would expect an even stronger correlation with temperature there if local warming was the only contributor to differences in SCE trends. Yet, when we restrict the temperatures to the Arctic (>60°N) region, the relationship becomes only slightly stronger (r= -0.69). This demonstrates that differences in simulated warming cannot fully account for variability within CanESM-LE SCE trends, and so next we examine the roles for changes in precipitation and atmospheric circulation.

Whereas in CMIP5 we find that June SCE trends are highly correlated with the intermodel spread in June climatological SCE (Fig. 5-5), the spread in climatological SCE in CanESM-LE is minimal (<1 million km^2) for all spring months and there is no correlation with SCE trends (not shown). However, we do find a relationship in CanESM-LE between spring SCE trends and snow accumulation during the previous winter. We use March snow

water mass (SWM) as a proxy for simulated snowfall totals over the winter months, and find a weak positive correlation (r= 0.44 for 2011-2040; Table 5-4 (The R^2 for other climatological periods are shown on Fig. 5-7b)) between 21st century trends in SWM and May SCE. To illustrate the importance of SWM for inter-realization differences in SCE trends, in Fig. 5-7 we compare May land warming, May SCE loss and March SWM loss over the NH extratropics for the period 2011-2040. Across the 50 realizations May land warming varies from 0.35 to 0.78 K decade^{-1}, and the realization that warms the most (run 40) also produces the greatest SCE loss (Fig. 5-7a). However, the realization with the weakest SCE loss (run 1) is not the realization with the least warming (run 49). The reason is that a weaker-than-average decreasing trend in March SWM in run 1 contributes to a weaker-than-average SCE trend (Fig. 5-7b). Positive SWM anomalies extend snow cover duration because greater melt energy is required to remove deeper snow.

Lastly, we explore the role of local temperature and atmospheric circulation changes in explaining the inter-realization spread in CanESM-LE SCE trends. We compute local correlations between near-future May SCF trends and contemporaneous temperature and sea level pressure (SLP) changes. Trends in temperature and snow cover have a very strong negative association over most NH areas with substantial May snow cover (Fig. 5-8a). For SLP, the relationship with snow cover is of hemispheric spatial scale, with moderate correlations of either sign that project onto the North Atlantic Oscillation (NAO) pattern (Barnston and Livezey 1987) (Fig. 5-8b). Greater Eurasian snow loss is associated with an increased meridional pressure gradient across the North Atlantic typical of a positive NAO phase, bringing enhanced warm advection into Eurasia. In contrast, contributions to changes

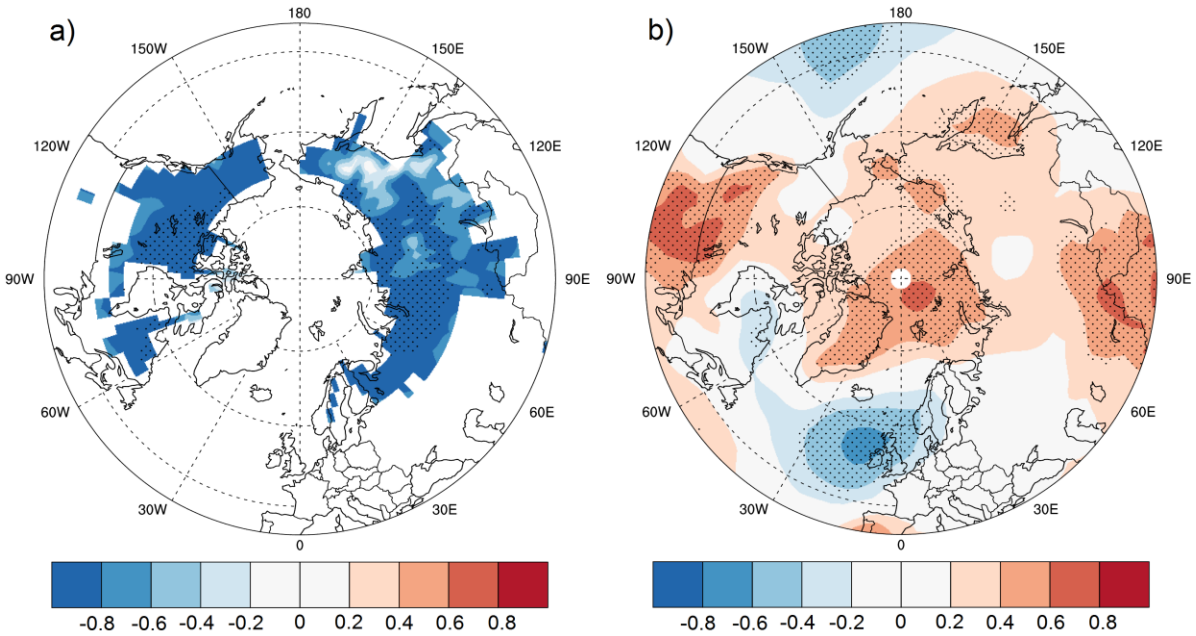

Figure 5-8: (a) Local correlation between near-future (2011-2040) May snow cover fraction anomalies and near-surface air temperature anomalies from the CanESM-LE, (b) correlation between hemispheric (NH) mean May SCF anomalies and local May sea level pressure anomalies. Stippling indicates regions of statistical significance (p = 0.05).

in western North American SCE largely stem from North Pacific SLP patterns. Figure 5-8b consequently represents a combination of several unique circulation patterns. This demonstrates that atmospheric circulation responses associated with internal variability exert an influence on near-term SCE trends over much of NH land.

5.5 Discussion and Conclusions

This study uses seven observation-based estimates of snow cover, five surface temperature datasets, and two climate model ensembles to characterize the uncertainty in simulations of NH spring snow cover extent. We find that weaker than observed historical (1981-2010) SCE trends from the CMIP5 ensemble can be partially explained by biases in climatological spring snow extent within these models. However, biases in simulated SCE trends during

recent decades are much smaller than previously shown from studies that relied on a single observation-based reference dataset (Derksen and Brown 2012; Brutel-Vuilmet et al. 2013). These studies used the NOAA CDR because of its long time series (1967-present), which we find to have the strongest spring SCE trend of the seven observation-based estimates. SCE in some models appears to lack sensitivity to warming, but the ensemble means are not significantly different.

Spring snow cover is projected to decrease by -3.7 ± 1.1% decade^{-1} within the CMIP5 ensemble over the 21st century. This represents a strengthening of 33% relative to the rate simulated over recent decades (1981-2010). Projected snow cover loss is expected to increase for all spring months over the 21st century, with the exception of June (when nearly all remaining snow has melted by the latter half of the 21st century). For 30-year spring SCE trends over three time periods in the 21st century (2011-2040, 2041-2070, 2071-2100), we find that internal variability, as estimated from the CanESM initial condition ensemble (CanESM-LE; σ = 0.18 million km^2 decade^{-1}), is substantial, but smaller than the inter-model spread from CMIP5 (σ = 0.29 million km^2 decade^{-1}). In contrast, the spread in SCE trends from CanESM-LE and CMIP5 are very similar for the historical period (Fig. 5-1). The main physical drivers of inter-model differences in projected spring SCE trends are differences in simulated warming trends (R^2 = 0.80) and biases in mean SCE, with the latter more important in late spring. In theory, a reduction in the variability of projected warming should lead to a decrease in the spread of spring SCE trends. Internal variability is a major contributor to inter-model spread (total variance) in the near-term, but the fraction of total variance attributable to internal variability decreases on longer timescales because of greater

model uncertainty. We find large internal variability in near-term (2011-2040) warming trends over NH extratropical land, which explains almost 50% of the variability in projected SCE trends, even in the presence of a strong forced trend from GHGs. Furthermore, internal variability in winter snowfall trends has a significant (but lesser) impact on SCE trends (R^2= 0.20).

There are a number of ways to potentially reduce the uncertainty in projections of NH SCE. The first involves increasing the number of realizations from each model as a part of future modeling efforts. Following the approach of Deser et al. (2012b), we calculate the minimum number of realizations (N_{min}) required to detect the near-future forced May SCF trend at the 5% significance level, given by $N_{min} = 8 / (X/\sigma)^2$, where X is the ensemble mean trend, and σ is the standard deviation of the 50 trends. Regions with stronger snow responses generally need between 3-10 realizations to detect a significant trend, whereas areas with weaker responses (eastern Siberia, Arctic Canada; Fig. 5-9a) require upwards of 50 realizations (Fig. 5-9b). The implication here is not that hundreds of realizations are necessary, but that over some regions the near-term forced response is so weak that it cannot be captured. However, a majority of the models contributing to CMIP5 provided fewer than three realizations for RCP8.5.

Secondly, there is a very strong relationship between projected spring SCE trends and warming trends (R^2 = 0.80). However, under RCP8.5 the CMIP5 models exhibit a rather large spread in 21st century spring warming (0.39 to 0.95 K decade^{-1}). Therefore, a reduction in the uncertainty of the forced component of projected warming could lead to a decrease in the spread for spring SCE trends (the component due to internal variability is essentially

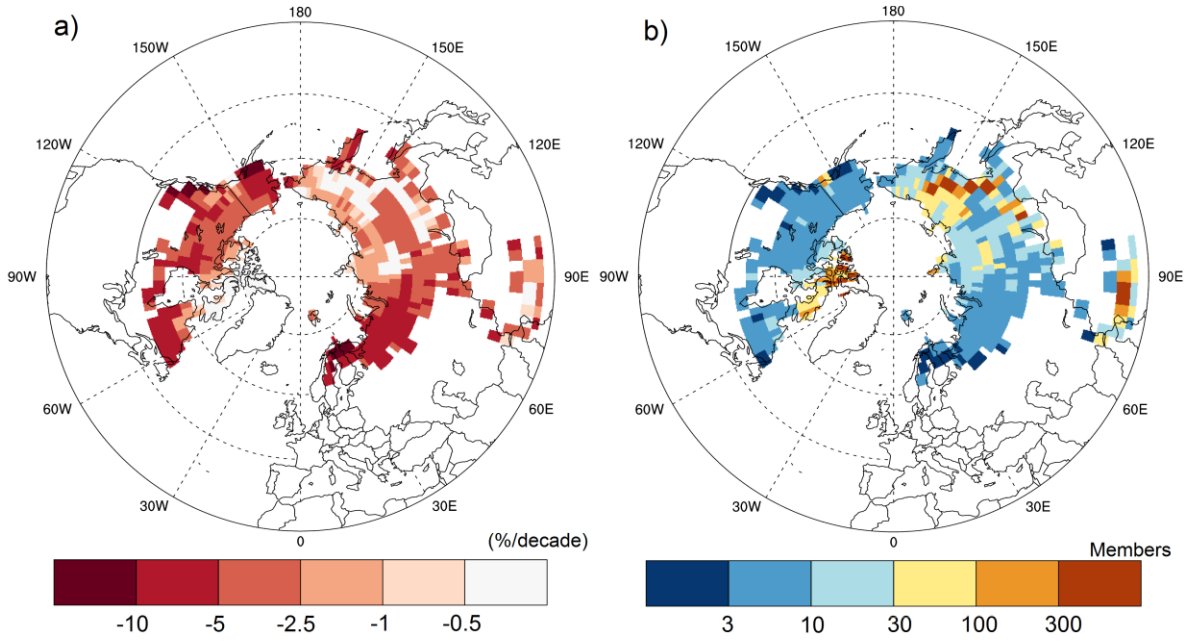

Figure 5-9: (a) Near-future (2011-2040) CanESM-LE ensemble mean May SCF trend. (b) Minimum number of realizations needed to detect a significant trend response in near-future May SCF.

random, and therefore unconstrained). Previous research has shown that 40-50% of the spread in CMIP5 21st century spring warming over NH extratropical land can be explained by variability in simulated snow albedo feedback (SAF) (Qu and Hall 2014). Furthermore, Thackeray and Fletcher (2016) demonstrated that selecting only models with SAF closest to observed estimates reduces the spread in CMIP5 21st century NH land warming by ~40%. Therefore, model development focused on alleviating process-level biases—particularly those related to SAF— could help to reduce model uncertainty in future projections of warming and snow cover.

5.6 Acknowledgements

We acknowledge funding from the Natural Sciences and Engineering Research Council of Canada's Climate Change and Atmospheric Research Initiative via the Canadian Sea Ice and

Snow Evolution (CanSISE) Network. We also acknowledge Environment and Climate Change Canada's Canadian Centre for Climate Modelling and Analysis for executing and making available the CanESM2 Large Ensemble simulations used in this study. We thank Eric Brun for providing data from the Crocus snowpack model, and Ross Brown for providing the Brown dataset. We also thank three anonymous reviewers for their helpful comments.

Supplementary Figures

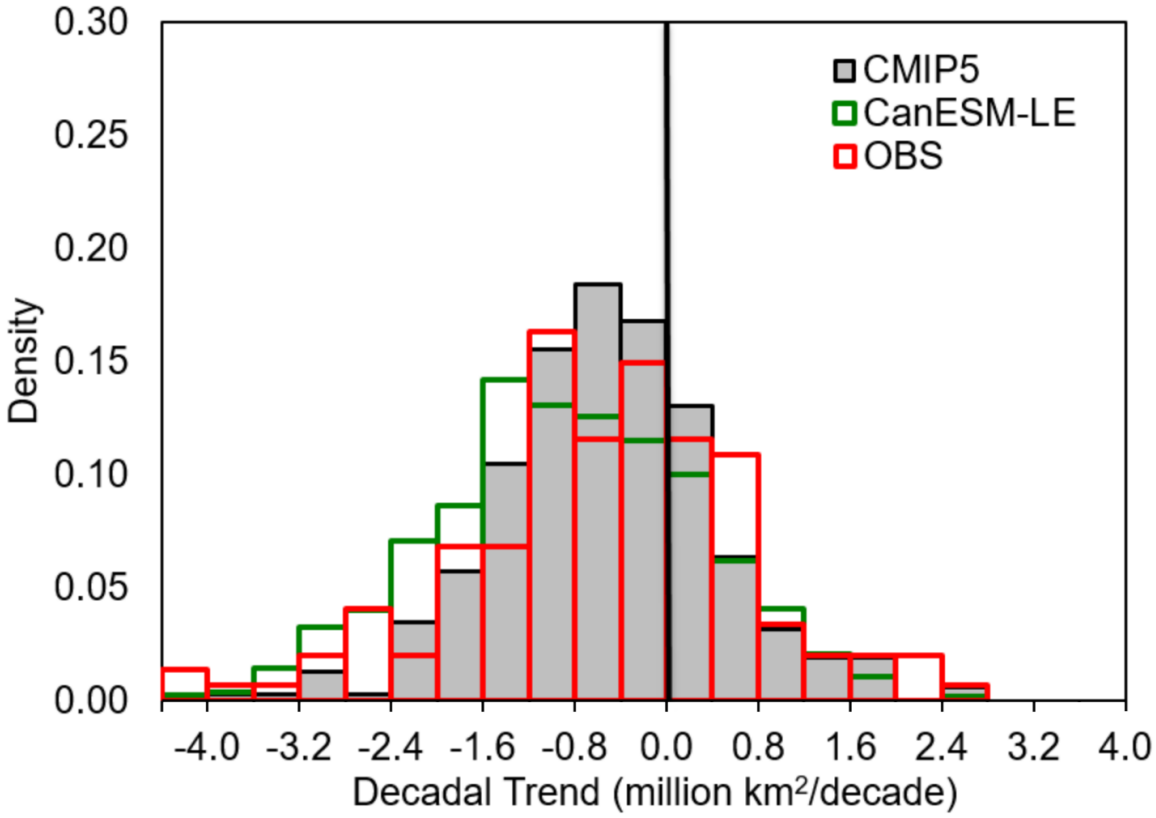

Figure 5-S1: Distribution of all 10-year May SCE trends during the historical period (1981-2010) for observations, CMIP5, and CanESM-LE.

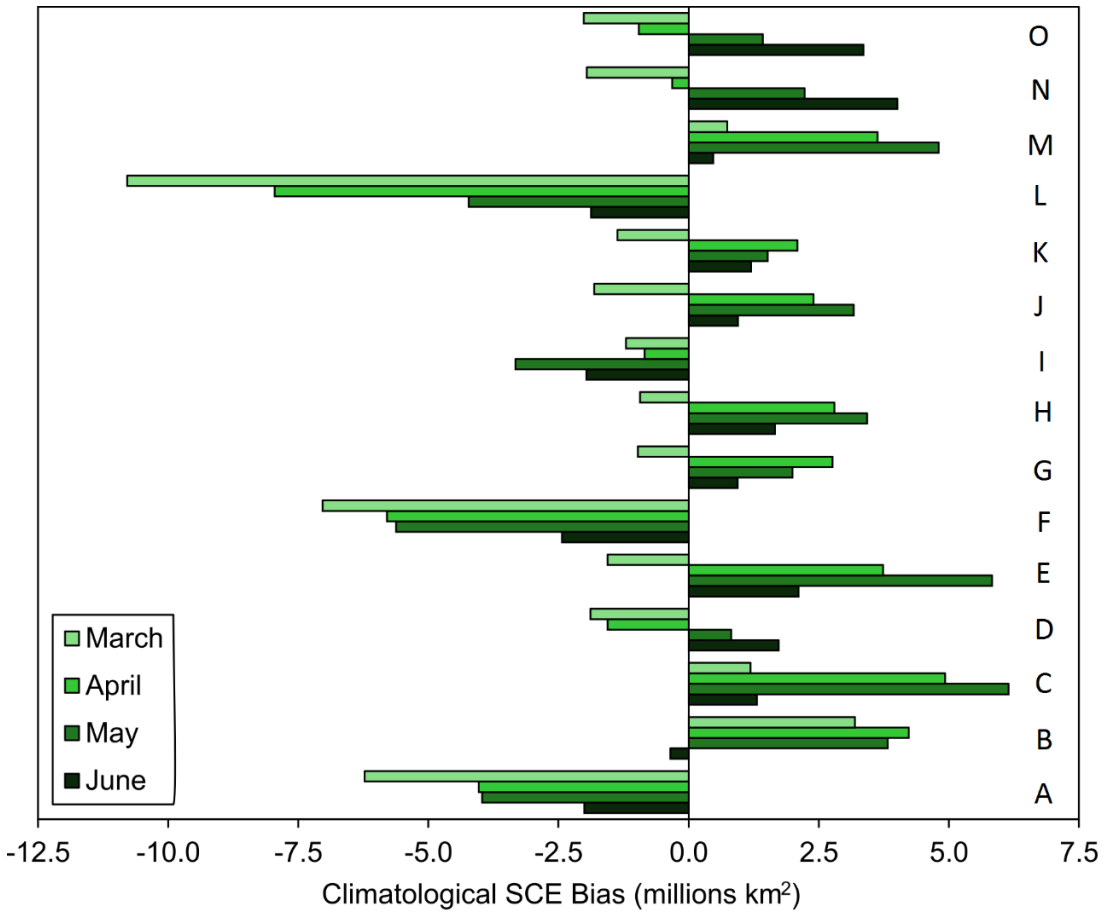

Figure 5-S2: CMIP5 historical (1981-2010) snow cover extent bias relative to the average of seven observation-based estimates for the Northern Hemisphere extratropics during March, April, May, and June. Letters correspond to individual models, as shown by Table 5-1.

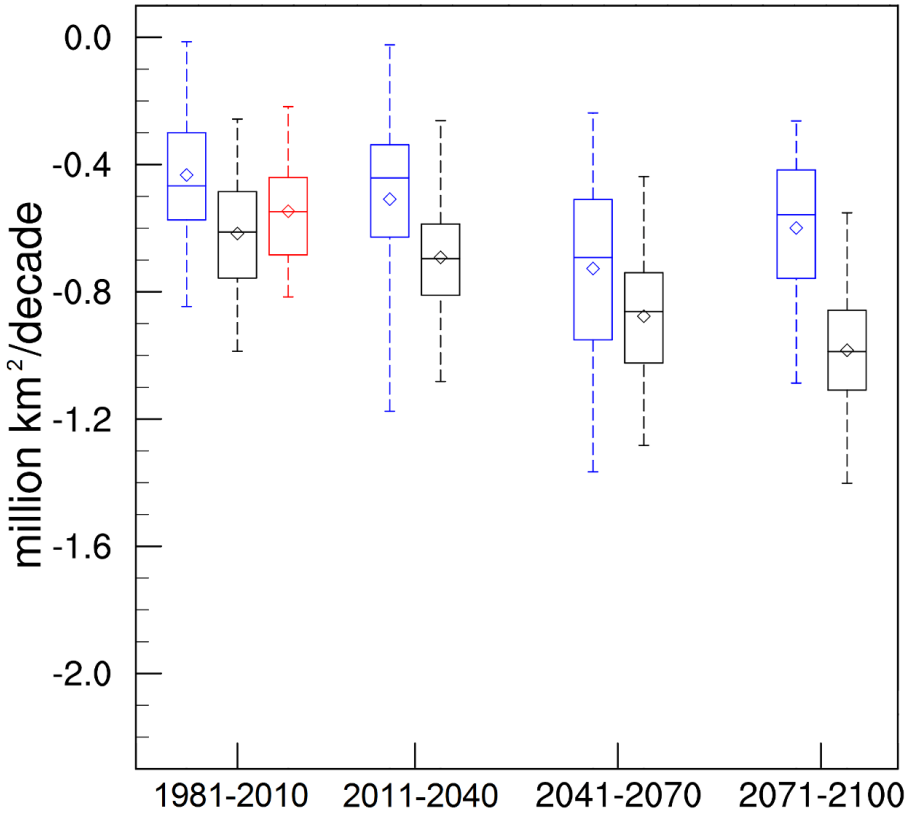

Figure 5-S3: Northern Hemisphere spring (MAMJ) SCE trends over the 21st century under the RCP8.5 emissions scenario amongst three ensembles: CMIP5 (blue), CanESM-LE (black), and observation-based (red). As for Figure 5-4, the enclosed region shows the 25th-75th percentile range, the horizontal line shows the median, and the diamond shows the ensemble mean. The dashed fences indicate the minimum and maximum.

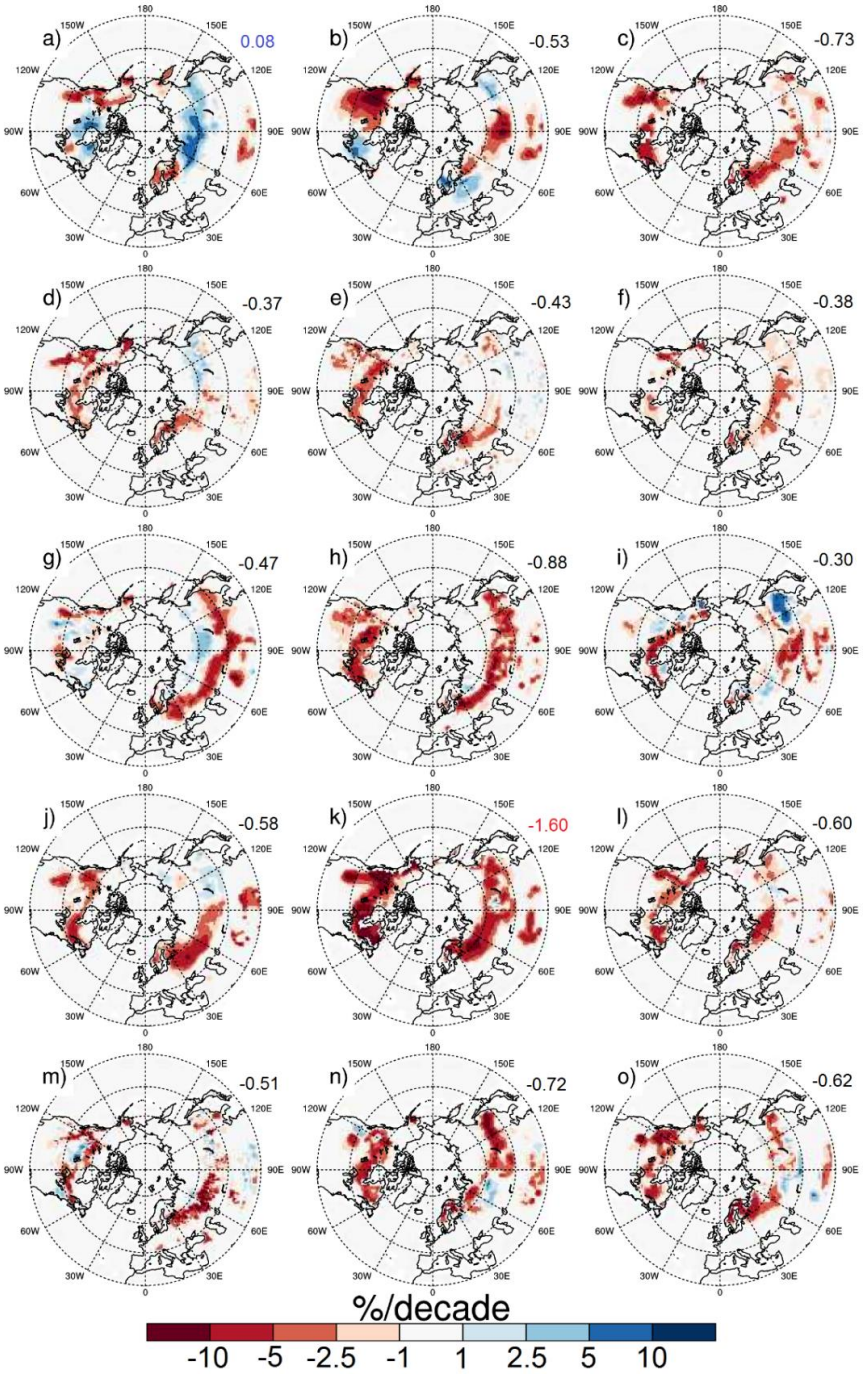

Figure 5-S4: Near-term (2011-2040) trends in April snow cover fraction (% decade^{-1}) from the CMIP5 models. Letters correspond to the model list in Table 5-1. The NH mean SCE trend is shown in the top right of each panel (units: million km^2 decade^{-1}).

Chapter 6

Conclusions

6.1 Summary

The overall aim of this research was to improve knowledge of terrestrial snow processes influencing climate through changes in albedo. This was primarily achieved through the critical evaluation of simulated snow cover (seasonality and trends) and snow-covered surface albedo (seasonality) in comparison with a collection of observation-based estimates. By highlighting deficiencies in climate model simulations of snow, we are helping to guide areas of future model development. As it pertains to snow-covered surface albedo this may involve improving parameterizations of canopy snow, vegetation characteristics (tree cover fraction, LAI), or subgrid-scale features (i.e., lake fraction). This is an important step towards reducing uncertainty in projections of land temperature and snow cover because of the strong coupling exhibited between simulated snow albedo and SAF (80%; Qu and Hall, 2007), SAF and projected land warming (40-50%; Qu and Hall, 2014), and land warming and spring snow cover (~80%; Thackeray et al., 2016). Therefore, future work to correct process-level biases related to SAF (i.e., as pointed out in Chapters three and five) should reduce the intermodel spread associated with projections of NH land temperature and snow cover. When viewed collectively with Thackeray et al. (2014), this research forms a body of literature that spans the identification of a source of model bias (canopy snow influencing boreal albedo), its discovery in other models (substantial boreal albedo biases in seasonal timing and magnitude), and the determination of climate impacts associated with it.

In Section 1.3, there were a few research questions that throughout the course of this dissertation have been considered. First, we sought to determine the current state of knowledge regarding snow albedo feedback. Chapter 2 contains a synthesis that covers four main topics: the importance of SAF to regional and global climate, estimates of SAF from various observational and model sources, factors contributing to a sizeable spread in SAF, and outstanding issues related to our knowledge of SAF. The literature agrees that although SAF is relatively weak in the global context, it plays a key role in regional climate across much of the Northern Hemisphere extratropics. Observed SAF strength is shown to vary slightly depending on a variety of methodological choices (dataset, time frame, location), but in general, its strength is characterized by a 1% reduction in albedo per degree of warming (Table 2-1). Although the multi-model mean can accurately capture this feature, there is a large intermodel spread that arises because of differences in model parameterizations (primarily tied to variability in snow albedo; Section 2.5). Several factors still limit our understanding of SAF, principally related to the availability of reliable observational measurements and the coarse nature of global climate models (Section 6.2). To combat the latter, several new studies have used regional climate simulations to better simulate snow cover, and in turn, SAF in areas of complex terrain (Minder et al., 2016; Walton et al., 2017).

Second, we expanded the analysis of Thackeray et al., (2014) to find out if issues with canopy snow influencing albedo were prevalent in the current generation of climate models. In doing so, we were also interested in quantifying the ability of models to simulate seasonal snow cover and surface albedo. Generally speaking, models were found to better simulate the seasonal cycle of snow cover than albedo. Biases in albedo were primarily related to the

magnitude and timing of peak snow-covered surface albedo rather than the possible misrepresentation of snow cover. Figure 3-6a showed that the previously identified albedo timing issues did not exist to the same extent as in CCSM4, but many models still precede the observed melt timing. The more pressing issue within the CMIP5 ensemble is related to the magnitude of peak snow-covered surface albedo over the boreal forest region as this is dramatically overestimated by several models. An important contribution from this research is a skill metric that detects model performance related to the seasonality of snow and albedo changes (important factors in SAF strength). This tool has already been used to track model improvements related to the development of a new canopy hydrology scheme in version five of the Community Land Model (not shown; J. Perket, personal communication).

Chapter 4 carried on from the findings presented in Chapter 3 in an effort to quantify the impact of simulated snow-covered surface albedo biases on climate. This involved the production of a series of novel climate simulations using the Community Earth System Model (CESM). We found that correcting the albedo in CESM (removing biases) pushes the model further away from observed temperature (implying the presence of other biases), with robust cooling during winter and spring. It also induced a pattern reversal of climatological biases in winter sea level pressure, partially correcting the model's tendency towards a positive Arctic Oscillation. Furthermore, biases across the boreal region were found to be influential for both local and remote climate features. CMIP5 models with large albedo magnitude biases (i.e. MIROC5) are vulnerable to even greater climate impacts than CESM. We find that using the albedo from models at opposite ends of the CMIP spectrum (low vs. high albedo) creates a 4-5 K swing in spring seasonal mean air surface temperature over the

NH extratropics. For perspective, that resembles the spread in projected 21st century (2080-2099 minus 2006-2025) NH extratropical warming from the CMIP5 models (4.3 K) discussed in Section 2.6.2.

Lastly, Chapter 5 sought to evaluate trends in simulated spring snow cover against an observation-based ensemble, and determine the factors controlling the large intermodel spread. Results showed that the models underestimated the observed historical trend, however, biases were much smaller than identified by previous studies (Derksen and Brown, 2012; Brutel-Vuilmet et al., 2013). In the near-future, internal variability was estimated to be substantial, but smaller than the intermodel spread from CMIP5. Internal variability in spring land warming and winter precipitation trends were shown to affect SCE trends on shorter timescales. Additionally, intermodel spread was largely driven by simulated warming trends, and the amount of snow remaining in late-spring.

Necessary steps for reducing uncertainty in projections of snow cover were also proposed here. First, we suggested to increase the number of realizations produced by each model in future modeling efforts. Because of internal variability, several simulations are needed to generate a confident projection of snow cover. Using the approach of Deser et al., (2012b) we found that where snow responses were strong, between 3-10 realizations were needed to detect a significant trend. This is noteworthy because most of the models contributing to the last CMIP provided less than three realizations for future scenarios. Second, it was suggested that the tight relationship between projected spring SCE trends and simulated warming ($R^2 = 0.80$) could be exploited, meaning that by reducing the spread in projected spring land warming (0.39 to 0.95 K decade^{-1}), reductions in projected SCE

uncertainty would follow. As previously mentioned, much of this warming spread can be explained by variability in snow albedo feedback (Qu and Hall, 2014). Therefore, correcting process-level biases related to SAF could help reduce intermodel spread in projections of temperature and snow cover.

6.2 Limitations

In the evaluation of climate models, there are many limiting factors at play. Quality long-term observational datasets are necessary for comparisons with model output, but there can be substantial uncertainty associated with them. At the point scale, records of snow for instance are sparse over much of the high-latitudes and have consistency issues associated with them. Snow monitoring at meteorological stations is susceptible to changes in both methodology or location over long time periods (Kunkel et al., 2007). Data quality issues are compounded when global coverage is needed, as most observation-based datasets on this scale have been shown to contain considerable uncertainty (Anisimov et al., 2007; Decker et al., 2012). For example, satellite-derived estimates of SWE have global coverage, but tend to be biased low in mountainous and densely vegetated regions (Hall et al., 2001; Takala et al., 2011). Monitoring of snow cover from satellites is largely done via visible sensors, but their effectiveness is often restricted by cloud cover, which can be persistent during boreal winter (Foster et al., 2005; Hall et al., 2010). When it comes to albedo, our high-latitude study area also introduces uncertainty because of large solar zenith angles during winter (Schaaf et al., 2002). Furthermore, a lack of observational data for some quantities often prevents a ‘like for like’ comparison. For example, in an ideal setting we would examine simulated canopy snow

against surface measurements of this property. However, we must adapt and instead use observed snow cover and albedo data as proxies for canopy snow presence.

To comprehensively evaluate the melt period, we would ideally want daily observational measurements. However, because of data quality issues that plague daily retrievals of albedo (i.e. more missing data), we tend to average the data over longer temporal periods. Similarly, our analysis is restricted by the length of records available from observation-based products. For example, the evaluation of historical SCE trends from models was limited to the 1981-2010 period (Chapter 5). This is because some products within the observational ensemble had not been continued or updated to present (Mudryk et al., 2017). All of these factors act to limit our confidence in the comparisons that we make between observations and models.

The modeling experiments performed here (Chapter 4) also involve several limitations. First, because of the inherent computationally expensive nature of climate models, the length and number of simulations that we can generate is somewhat constrained. We are also limited to using a single GCM to run all experiments because most models are not publicly available. This is an issue because the relationship between albedo and climate likely differs in every model. Lastly, the lack of reliable daily surface albedo measurements means that we must use monthly data for all experiments needing observed albedo. This creates an albedo that evolves in a smoother nature (linear interpolation from one monthly value to the next at each grid cell) than what would occur naturally. However, because the monthly mean radiation remains the same it shouldn't have an impact on long-term climate.

6.3 Future work

Several interesting questions have arisen following the findings of this work, providing great potential for future research. There are also several ongoing and planned modeling efforts, which bring a whole host of new opportunities to examine modeling of the cryosphere. The next generation of climate models will take part in phase 6 of the Coupled Model Intercomparison Project (CMIP6; Eyring et al., 2016), with early results from these models expected in the coming year. Two of the main World Climate Research Programme Grand Science Challenges (GCs) that are a focus of CMIP6 pertain to snow, including: evaluating the impact of warming on the cryosphere and its global consequences, and improving knowledge of factors driving water availability (Eyring et al., 2016). One project that is particularly relevant to this thesis is the Earth System Model-Snow Model Intercomparison Project (ESM-SnowMIP; http://www.climate-cryosphere.org/activities/targeted/esm-snowmip). The goal of ESM-SnowMIP is to improve the representation of snow in ESMs, conduct systematic model evaluation studies, and advance knowledge regarding the role of snow in the global climate system. The modeling framework laid out in Section 4.3.3 allows for similar prescribed observation experiments to be run as a part of this initiative. Planned experiments include prescribing observational snow cover, and prescribing snow albedo (rather than surface albedo), which leaves the models susceptible to simulated snow cover and vegetation masking parameterizations.

The interactions between snow albedo feedback and vegetation may have added complexity in CMIP6, as many models will incorporate dynamic vegetation. It is known that the boreal forest region is historically sensitive to climate change (Fischlin et al., 2007;

MacDonald et al., 2008). Future warming is projected to bring with it the northward expansion of the Arctic treeline (i.e., Chapin et al., 2005), although the relationship between global warming and vegetation changes is spatially complex (Bonan, 2008). This is likely to result in major intermodel differences in vegetation characteristics by the late 21st century. Because of the ability for forests to mask highly reflective snow cover, the expansion of the treeline into the tundra is likely to cause local warming through large reductions in surface albedo. Therefore, differences in simulated vegetation could have a major impact on projections of temperature, snow cover, and the role that SAF plays in future climate.

The research conducted in Chapter 4 involved the creation of several novel climate simulations, collectively spanning over 100 years. There are aspects of these simulations that have not been studied in great detail (i.e. clouds, subtropical regions), which could be of interest for future research. Additionally, new sensitivity experiments could be performed in a timely manner now that a methodology has been assembled. For example, to determine how the cryosphere and hydroclimate will respond to projected radiative forcing we could prescribe simulated albedo from the end of the 21st century.

The creation of model benchmarking metrics is a highly valuable contribution to the modeling community. Further work could be put into improving the snow albedo metric defined in Chapter 3 as a step towards its possible inclusion in the International Land Model Benchmarking Project (ILAMB; https://www.ilamb.org/). This could include incorporating other observational datasets (i.e., CERES albedo) or relevant variables (i.e., snow water equivalent). The latest version of the multi-sourced albedo dataset developed in this chapter (OBSblend) is being used to test development runs from CLM5 (J. Perket, personal

communication). Both the extension (longer time series) and expansion (more products) of this dataset would be valuable contributions.

Lastly, the continued advance of computing capabilities opens many possibilities for improved-resolution analysis of snow processes. In the past year, several studies have started to examine the representation of snow-climate interactions in high-resolution (or regional) climate model simulations (Minder et al., 2016; Walton et al., 2017; Berg and Hall, 2017). This is promising because snow in mountainous regions is a key water storage source, but the coarse resolution of current global models leads to a poor representation of topography, and in turn, snowfall in these areas. There are a couple of new and planned simulations that could be investigated for this purpose, including a large ensemble from the Canadian Regional Climate Model (Scinocca et al., 2016; Fyfe et al., 2017), and simulations of CESM with a nested high-resolution grid (1/8° resolution) over the western United States domain (D. Lawrence, personal communication). Therefore, there is great potential for further advancing our understanding snow-climate interactions in the coming years.

Copyright Permissions

JOHN WILEY AND SONS LICENSE
TERMS AND CONDITIONS
May 17, 2017

This Agreement between Chad Thackeray ("You") and John Wiley and Sons ("John Wiley and Sons") consists of your license details and the terms and conditions provided by John Wiley and Sons and Copyright Clearance Center.

License Number
4111521291517
License date
Licensed Content Publisher
John Wiley and Sons
Licensed Content Publication
Journal of Geophysical Research: Atmospheres
Licensed Content Title
Quantifying the skill of CMIP5 models in simulating seasonal albedo and snow cover evolution
Licensed Content Author
Chad W. Thackeray, Christopher G. Fletcher, Chris Derksen
Licensed Content Date
Jun 25, 2015
Licensed Content Pages
19
Type of use
Dissertation/Thesis
Requestor type
Author of this Wiley article
Format
Print and electronic
Portion
Full article
Will you be translating?
No
Title of your thesis / dissertation
Using a hierarchy of climate models to investigate snow processes influencing surface albedo
Expected completion date
Aug 2017
Expected size (number of pages)
170
Requestor Location
Chad Thackeray
200 University Avenue West
Waterloo, ON N2L3G1
Canada
Attn: Chad W Thackeray
Publisher Tax ID

EU826007151
Billing Type
Invoice
Billing Address
Chad W Thackeray
25 Bianca Drive
Whitby, ON L1M 2J3
Canada
Attn: Chad Thackeray
Total
0.00 CAD
Terms and Conditions

TERMS AND CONDITIONS

This copyrighted material is owned by or exclusively licensed to John Wiley & Sons, Inc. or one of its group companies (each a"Wiley Company") or handled on behalf of a society with which a Wiley Company has exclusive publishing rights in relation to a particular work (collectively "WILEY"). By clicking "accept" in connection with completing this licensing transaction, you agree that the following terms and conditions apply to this transaction (along with the billing and payment terms and conditions established by the Copyright Clearance Center Inc., ("CCC's Billing and Payment terms and conditions"), at the time that you opened your RightsLink account (these are available at any time at http://myaccount.copyright.com).

Terms and Conditions

- The materials you have requested permission to reproduce or reuse (the "Wiley Materials") are protected by copyright.
- You are hereby granted a personal, non-exclusive, non-sub licensable (on a stand-alone basis), non-transferable, worldwide, limited license to reproduce the Wiley Materials for the purpose specified in the licensing process. This license, **and any CONTENT (PDF or image file) purchased as part of your order,** is for a one-time use only and limited to any maximum distribution number specified in the license. The first instance of republication or reuse granted by this license must be completed within two years of the date of the grant of this license (although copies prepared before the end date may be distributed thereafter). The Wiley Materials shall not be used in any other manner or for any other purpose, beyond what is granted in the license. Permission is granted subject to an appropriate acknowledgement given to the author, title of the material/book/journal and the publisher. You shall also duplicate the copyright notice that appears in the Wiley publication in your use of the Wiley Material. Permission is also granted on the understanding that nowhere in the text is a previously published source acknowledged for all or part of this Wiley Material. Any third party content is expressly excluded from this permission.
- With respect to the Wiley Materials, all rights are reserved. Except as expressly granted by the terms of the license, no part of the Wiley Materials may be copied, modified, adapted (except for minor reformatting required by the new Publication), translated, reproduced, transferred or distributed, in any form or by any means, and no derivative works may be made based on the Wiley Materials without the prior permission of the respective copyright owner.**For STM Signatory Publishers clearing permission under the terms of the STM**

Permissions Guidelines only, the terms of the license are extended to include subsequent editions and for editions in other languages, provided such editions are for the work as a whole in situ and does not involve the separate exploitation of the permitted figures or extracts, You may not alter, remove or suppress in any manner any copyright, trademark or other notices displayed by the Wiley Materials. You may not license, rent, sell, loan, lease, pledge, offer as security, transfer or assign the Wiley Materials on a stand-alone basis, or any of the rights granted to you hereunder to any other person.

- The Wiley Materials and all of the intellectual property rights therein shall at all times remain the exclusive property of John Wiley & Sons Inc, the Wiley Companies, or their respective licensors, and your interest therein is only that of having possession of and the right to reproduce the Wiley Materials pursuant to Section 2 herein during the continuance of this Agreement. You agree that you own no right, title or interest in or to the Wiley Materials or any of the intellectual property rights therein. You shall have no rights hereunder other than the license as provided for above in Section 2. No right, license or interest to any trademark, trade name, service mark or other branding ("Marks") of WILEY or its licensors is granted hereunder, and you agree that you shall not assert any such right, license or interest with respect thereto

- NEITHER WILEY NOR ITS LICENSORS MAKES ANY WARRANTY OR REPRESENTATION OF ANY KIND TO YOU OR ANY THIRD PARTY, EXPRESS, IMPLIED OR STATUTORY, WITH RESPECT TO THE MATERIALS OR THE ACCURACY OF ANY INFORMATION CONTAINED IN THE MATERIALS, INCLUDING, WITHOUT LIMITATION, ANY IMPLIED WARRANTY OF MERCHANTABILITY, ACCURACY, SATISFACTORY QUALITY, FITNESS FOR A PARTICULAR PURPOSE, USABILITY, INTEGRATION OR NON-INFRINGEMENT AND ALL SUCH WARRANTIES ARE HEREBY EXCLUDED BY WILEY AND ITS LICENSORS AND WAIVED BY YOU.

- WILEY shall have the right to terminate this Agreement immediately upon breach of this Agreement by you.

- You shall indemnify, defend and hold harmless WILEY, its Licensors and their respective directors, officers, agents and employees, from and against any actual or threatened claims, demands, causes of action or proceedings arising from any breach of this Agreement by you.

- IN NO EVENT SHALL WILEY OR ITS LICENSORS BE LIABLE TO YOU OR ANY OTHER PARTY OR ANY OTHER PERSON OR ENTITY FOR ANY SPECIAL, CONSEQUENTIAL, INCIDENTAL, INDIRECT, EXEMPLARY OR PUNITIVE DAMAGES, HOWEVER CAUSED, ARISING OUT OF OR IN CONNECTION WITH THE DOWNLOADING, PROVISIONING, VIEWING OR USE OF THE MATERIALS REGARDLESS OF THE FORM OF ACTION, WHETHER FOR BREACH OF CONTRACT, BREACH OF WARRANTY, TORT, NEGLIGENCE, INFRINGEMENT OR OTHERWISE (INCLUDING, WITHOUT LIMITATION, DAMAGES BASED ON LOSS OF PROFITS, DATA, FILES, USE, BUSINESS OPPORTUNITY OR CLAIMS OF THIRD PARTIES), AND WHETHER OR NOT THE PARTY HAS BEEN ADVISED OF THE POSSIBILITY OF SUCH DAMAGES. THIS LIMITATION SHALL APPLY

NOTWITHSTANDING ANY FAILURE OF ESSENTIAL PURPOSE OF ANY LIMITED REMEDY PROVIDED HEREIN.

- Should any provision of this Agreement be held by a court of competent jurisdiction to be illegal, invalid, or unenforceable, that provision shall be deemed amended to achieve as nearly as possible the same economic effect as the original provision, and the legality, validity and enforceability of the remaining provisions of this Agreement shall not be affected or impaired thereby.

- The failure of either party to enforce any term or condition of this Agreement shall not constitute a waiver of either party's right to enforce each and every term and condition of this Agreement. No breach under this agreement shall be deemed waived or excused by either party unless such waiver or consent is in writing signed by the party granting such waiver or consent. The waiver by or consent of a party to a breach of any provision of this Agreement shall not operate or be construed as a waiver of or consent to any other or subsequent breach by such other party.

- This Agreement may not be assigned (including by operation of law or otherwise) by you without WILEY's prior written consent.

- Any fee required for this permission shall be non-refundable after thirty (30) days from receipt by the CCC.

- These terms and conditions together with CCC's Billing and Payment terms and conditions (which are incorporated herein) form the entire agreement between you and WILEY concerning this licensing transaction and (in the absence of fraud) supersedes all prior agreements and representations of the parties, oral or written. This Agreement may not be amended except in writing signed by both parties. This Agreement shall be binding upon and inure to the benefit of the parties' successors, legal representatives, and authorized assigns.

- In the event of any conflict between your obligations established by these terms and conditions and those established by CCC's Billing and Payment terms and conditions, these terms and conditions shall prevail.

- WILEY expressly reserves all rights not specifically granted in the combination of (i) the license details provided by you and accepted in the course of this licensing transaction, (ii) these terms and conditions and (iii) CCC's Billing and Payment terms and conditions.

- This Agreement will be void if the Type of Use, Format, Circulation, or Requestor Type was misrepresented during the licensing process.

- This Agreement shall be governed by and construed in accordance with the laws of the State of New York, USA, without regards to such state's conflict of law rules. Any legal action, suit or proceeding arising out of or relating to these Terms and Conditions or the breach thereof shall be instituted in a court of competent jurisdiction in New York County in the State of New York in the United States of America and each party hereby consents and submits to the personal jurisdiction of such court, waives any objection to venue in such court and consents

to service of process by registered or certified mail, return receipt requested, at the last known address of such party.

WILEY OPEN ACCESS TERMS AND CONDITIONS

Wiley Publishes Open Access Articles in fully Open Access Journals and in Subscription journals offering Online Open. Although most of the fully Open Access journals publish open access articles under the terms of the Creative Commons Attribution (CC BY) License only, the subscription journals and a few of the Open Access Journals offer a choice of Creative Commons Licenses. The license type is clearly identified on the article.

The Creative Commons Attribution License

The Creative Commons Attribution License (CC-BY) allows users to copy, distribute and transmit an article, adapt the article and make commercial use of the article. The CC-BY license permits commercial and non-

Creative Commons Attribution Non-Commercial License

The Creative Commons Attribution Non-Commercial (CC-BY-NC)License permits use, distribution and reproduction in any medium, provided the original work is properly cited and is not used for commercial purposes.(see below)

Creative Commons Attribution-Non-Commercial-NoDerivs License

The Creative Commons Attribution Non-Commercial-NoDerivs License (CC-BY-NC-ND) permits use, distribution and reproduction in any medium, provided the original work is properly cited, is not used for commercial purposes and no modifications or adaptations are made. (see below)

Use by commercial "for-profit" organizations

Use of Wiley Open Access articles for commercial, promotional, or marketing purposes requires further explicit permission from Wiley and will be subject to a fee.

Further details can be found on Wiley Online Library http://olabout.wiley.com/WileyCDA/Section/id-410895.html

Other Terms and Conditions:

v1.10 Last updated September 2015

Questions? customercare@copyright.com or +1-855-239-3415 (toll free in the US) or +1-978-646-2777.

American Meteorological Society LICENSE TERMS AND CONDITIONS

May 19, 2017

This is a License Agreement between Chad Thackeray ("You") and American Meteorological Society ("American Meteorological Society") provided by Copyright Clearance Center ("CCC"). The license consists of your order details, the terms and conditions provided by American Meteorological Society, and the payment terms and conditions.

All payments must be made in full to CCC. For payment instructions, please see information listed at the bottom of this form.

License Number	4112050785628
License date	May 17, 2017
Licensed content publisher	American Meteorological Society
Licensed content title	Journal of climate
Licensed content date	Jan 1, 1988
Type of Use	Thesis/Dissertation
Requestor type	Author of requested content
Format	Electronic
Portion	chapter/article
Title or numeric reference of the portion(s)	The whole article will be used in thesis document
Title of the article or chapter the portion is from	Quantifying the uncertainty in historical and future simulations of Northern Hemisphere spring snow cover
Editor of portion(s)	John Walsh
Author of portion(s)	Chad Thackeray
Volume of serial or monograph.	29
Issue, if republishing an article from a serial	23
Page range of the portion	
Publication date of portion	December 2016
Rights for	Main product
Duration of use	Life of current edition
Creation of copies for the disabled	no

With minor editing privileges	no
For distribution to	Worldwide
In the following language(s)	Original language of publication
With incidental promotional use	no
The lifetime unit quantity of new product	Up to 999
Made available in the following markets	Education
The requesting person/organization is:	Chad Thackeray / University of Waterloo
Order reference number	
Author/Editor	Chad Thackeray
The standard identifier of New Work	cwt2017
Title of New Work	Using a hierarchy of climate models to investigate snow processes influencing surface albedo
Publisher of New Work	University of Waterloo
Expected publication date	Aug 2017
Estimated size (pages)	170
Total (may include CCC user fee)	0.00 USD
Terms and Conditions	

TERMS AND CONDITIONS

The following terms are individual to this publisher:

None

Other Terms and Conditions:

STANDARD TERMS AND CONDITIONS

1. Description of Service; Defined Terms. This Republication License enables the User to obtain licenses for republication of one or more copyrighted works as described in detail on the relevant Order Confirmation (the "Work(s)"). Copyright Clearance Center, Inc. ("CCC") grants licenses through the Service on behalf of the rightsholder identified on the Order Confirmation (the "Rightsholder"). "Republication", as used herein, generally means the inclusion of a Work, in whole or in part, in a new work or works, also as described on the Order Confirmation. "User", as used herein, means the person or entity making such republication.

2. The terms set forth in the relevant Order Confirmation, and any terms set by the Rightsholder with respect to a particular Work, govern the terms of use of Works in connection with the Service. By using the Service, the person transacting for a republication license on behalf of the User represents and warrants that he/she/it (a) has been duly authorized by the User to accept, and hereby does accept, all such terms and conditions on behalf of User, and (b) shall inform User of all such terms and conditions. In the event such person is a "freelancer" or other third party independent of User and CCC, such party shall

be deemed jointly a “User” for purposes of these terms and conditions. In any event, User shall be deemed to have accepted and agreed to all such terms and conditions if User republishes the Work in any fashion.

3. Scope of License; Limitations and Obligations.

3.1 All Works and all rights therein, including copyright rights, remain the sole and exclusive property of the Rightsholder. The license created by the exchange of an Order Confirmation (and/or any invoice) and payment by User of the full amount set forth on that document includes only those rights expressly set forth in the Order Confirmation and in these terms and conditions, and conveys no other rights in the Work(s) to User. All rights not expressly granted are hereby reserved.

3.2 General Payment Terms: You may pay by credit card or through an account with us payable at the end of the month. If you and we agree that you may establish a standing account with CCC, then the following terms apply: Remit Payment to: Copyright Clearance Center, 29118 Network Place, Chicago, IL 60673-1291. Payments Due: Invoices are payable upon their delivery to you (or upon our notice to you that they are available to you for downloading). After 30 days, outstanding amounts will be subject to a service charge of 1-1/2% per month or, if less, the maximum rate allowed by applicable law. Unless otherwise specifically set forth in the Order Confirmation or in a separate written agreement signed by CCC, invoices are due and payable on “net 30” terms. While User may exercise the rights licensed immediately upon issuance of the Order Confirmation, the license is automatically revoked and is null and void, as if it had never been issued, if complete payment for the license is not received on a timely basis either from User directly or through a payment agent, such as a credit card company.

3.3 Unless otherwise provided in the Order Confirmation, any grant of rights to User (i) is “one-time” (including the editions and product family specified in the license), (ii) is non-exclusive and non-transferable and (iii) is subject to any and all limitations and restrictions (such as, but not limited to, limitations on duration of use or circulation) included in the Order Confirmation or invoice and/or in these terms and conditions. Upon completion of the licensed use, User shall either secure a new permission for further use of the Work(s) or immediately cease any new use of the Work(s) and shall render inaccessible (such as by deleting or by removing or severing links or other locators) any further copies of the Work (except for copies printed on paper in accordance with this license and still in User's stock at the end of such period).

3.4 In the event that the material for which a republication license is sought includes third party materials (such as photographs, illustrations, graphs, inserts and similar materials) which are identified in such material as having been used by permission, User is responsible for identifying, and seeking separate licenses (under this Service or otherwise) for, any of such third party materials; without a separate license, such third party materials may not be used.

3.5 Use of proper copyright notice for a Work is required as a condition of any license granted under the Service. Unless otherwise provided in the Order Confirmation, a proper copyright notice will read substantially as follows: “Republished with permission of [Rightsholder’s name], from [Work's title, author, volume, edition number and year of

7. Effect of Breach. Any failure by User to pay any amount when due, or any use by User of a Work beyond the scope of the license set forth in the Order Confirmation and/or these terms and conditions, shall be a material breach of the license created by the Order Confirmation and these terms and conditions. Any breach not cured within 30 days of written notice thereof shall result in immediate termination of such license without further notice. Any unauthorized (but licensable) use of a Work that is terminated immediately upon notice thereof may be liquidated by payment of the Rightsholder's ordinary license price therefor; any unauthorized (and unlicensable) use that is not terminated immediately for any reason (including, for example, because materials containing the Work cannot reasonably be recalled) will be subject to all remedies available at law or in equity, but in no event to a payment of less than three times the Rightsholder's ordinary license price for the most closely analogous licensable use plus Rightsholder's and/or CCC's costs and expenses incurred in collecting such payment.

8. **Miscellaneous.**

8.1 User acknowledges that CCC may, from time to time, make changes or additions to the Service or to these terms and conditions, and CCC reserves the right to send notice to the User by electronic mail or otherwise for the purposes of notifying User of such changes or additions; provided that any such changes or additions shall not apply to permissions already secured and paid for.

8.2 Use of User-related information collected through the Service is governed by CCC's privacy policy, available online here:http://www.copyright.com/content/cc3/en/tools/footer/privacypolicy.html.

8.3 The licensing transaction described in the Order Confirmation is personal to User. Therefore, User may not assign or transfer to any other person (whether a natural person or an organization of any kind) the license created by the Order Confirmation and these terms and conditions or any rights granted hereunder; provided, however, that User may assign such license in its entirety on written notice to CCC in the event of a transfer of all or substantially all of User's rights in the new material which includes the Work(s) licensed under this Service.

8.4 No amendment or waiver of any terms is binding unless set forth in writing and signed by the parties. The Rightsholder and CCC hereby object to any terms contained in any writing prepared by the User or its principals, employees, agents or affiliates and purporting to govern or otherwise relate to the licensing transaction described in the Order Confirmation, which terms are in any way inconsistent with any terms set forth in the Order Confirmation and/or in these terms and conditions or CCC's standard operating procedures, whether such writing is prepared prior to, simultaneously with or subsequent to the Order Confirmation, and whether such writing appears on a copy of the Order Confirmation or in a separate instrument.

8.5 The licensing transaction described in the Order Confirmation document shall be governed by and construed under the law of the State of New York, USA, without regard to the principles thereof of conflicts of law. Any case, controversy, suit, action, or proceeding arising out of, in connection with, or related to such licensing transaction shall be brought, at CCC's sole discretion, in any federal or state court located in the County of New York,

State of New York, USA, or in any federal or state court whose geographical jurisdiction covers the location of the Rightsholder set forth in the Order Confirmation. The parties expressly submit to the personal jurisdiction and venue of each such federal or state court.If you have any comments or questions about the Service or Copyright Clearance Center, please contact us at 978-750-8400 or send an e-mail to info@copyright.com.
v 1.1

Questions? customercare@copyright.com or +1-855-239-3415 (toll free in the US) or +1-978-646-2777.

References

Allen, R. J., & Zender, C. S. (2010). Effects of continental-scale snow albedo anomalies on the wintertime Arctic oscillation. *Journal of Geophysical Research Atmospheres*, *115*(23), 1–20. http://doi.org/10.1029/2010JD014490

Allen, R. J., & Zender, C. S. (2011). Forcing of the Arctic Oscillation by Eurasian snow cover. *Journal of Climate*, *24*(24), 6528–6539. http://doi.org/10.1175/2011JCLI4157.1

Anisimov, O. A., Lobanov, V. A., Reneva, S. A., Shiklomanov, N. I., Zhang, T., & Nelson, F. E. (2007). Uncertainties in gridded air temperature fields and effects on predictive active layer modeling. *Journal of Geophysical Research: Earth Surface*, *112*(2), 1–12. http://doi.org/10.1029/2006JF000593

Arora, V. K., Scinocca, J. F., Boer, G. J., Christian, J. R., Denman, K. L., Flato, G. M., … Merryfield, W. J. (2011). Carbon emission limits required to satisfy future representative concentration pathways of greenhouse gases. *Geophysical Research Letters*, *38*, 3–8. http://doi.org/10.1029/2010GL046270

Balsamo, G., Albergel, C., Beljaars, A., Boussetta, S., Brun, E., Cloke, H., … Vitart, F. (2015). ERA-Interim/Land: a global land surface reanalysis data set. *Hydrology and Earth System Sciences*, *19*(1), 389–407. http://doi.org/10.5194/hess-19-389-2015

Barlage, M., Zeng, X., Wei, H., & Mitchell, K. E. (2005). A global 0.05° maximum albedo dataset of snow-covered land based on MODIS observations. *Geophysical Research Letters*, *32*(17), L17405. doi:10.1029/2005GL022881

Barnett, T. P., Adam, J. C., & Lettenmaier, D. P. (2005). Potential impacts of a warming climate on water availability in snow-dominated regions. *Nature*, *438*(November), 303–309. http://doi.org/10.1038/nature04141

Barnett, T. P., Pierce, D. W., Hidalgo, H. G., Bonfils, C., Santer, B. D., Das, T., … Dettinger, M. D. (2008). Human-Induced Changes in the Hydrology of the Western United States. *Science*, *319*(February), 1080–1083. http://doi.org/10.1126/science.1152538

Barnston, A. G., & Livezey, R. E. (1987). Classification, Seasonality and Persistence of Low-Frequency Atmospheric Circulation Patterns. *Monthly Weather Review*. http://doi.org/10.1175/1520-0493

Bartholome, E., and A. S. Belward (2005), GLC2000: a new approach to global land cover mapping from Earth observation data, International Journal of Remote Sensing, 26(9), 1959-1977, doi:10.1080/01431160412331291297.

Bartlett, P. A., MacKay, M. D., & Verseghy, D. L. (2006). Modified snow algorithms in the Canadian land surface scheme: Model runs and sensitivity analysis at three boreal forest stands. *Atmosphere-Ocean*, *44*(3), 207–222. http://doi.org/10.3137/ao.440301

Bartlett, P. A., & Verseghy, D. L. (2015). Modified treatment of intercepted snow improves the simulated forest albedo in the Canadian Land Surface Scheme. *Hydrological Processes*, *29*, 3208–3226. http://doi.org/10.1002/hyp.10431

Bekryaev, R. V., Polyakov, I. V., & Alexeev, V. A. (2010). Role of polar amplification in long-term surface air temperature variations and modern arctic warming. *Journal of Climate*, *23*(14), 3888–3906. http://doi.org/10.1175/2010JCLI3297.1

Bentsen, M., Bethke, I., Debernard, J. B., Iversen, T., Kirkevåg, A., Seland, Ø., … Kristjánsson, J. E. (2013). The Norwegian Earth System Model, NorESM1-M – Part 1: Description and basic evaluation of the physical climate. *Geoscientific Model Development*, *6*(3), 687–720. doi:10.5194/gmd-6-687-2013

Berg, N., & Hall, A. (2017). Anthropogenic warming impacts on California snowpack during drought. *Geophysical Research Letters*, *44*(5), 2511–2518. http://doi.org/10.1002/2016GL072104

Best, M. J., Pryor, M., Clark, D. B., Rooney, G. G., Essery, R. L. H., Menard, C. B., … Harding, R. J. (2011). The Joint UK Land Environment Simulator (JULES), model description – Part 1: Energy and water fluxes. *Geoscientific Model Development Discussions*, *4*(1), 677–699. http://doi.org/10.5194/gmdd-4-641-2011

Boer, G. J. (1993). Climate change and the regulation of the surface moisture and energy budgets. *Climate Dynamics*, *8*(5), 225–239. http://doi.org/10.1007/BF00198617

Bohn, T. J., Sonessa, M. Y., & Lettenmaier, D. P. (2010). Seasonal Hydrologic Forecasting: Do Multimodel Ensemble Averages Always Yield Improvements in Forecast Skill? *Journal of Hydrometeorology*, *11*(6), 1358–1372. doi:10.1175/2010JHM1267.1

Bonan, G. B. (2008). Forests and climate change: forcings, feedbacks, and the climate benefits of forests. *Science (New York, N.Y.)*, *320*(5882), 1444–9. doi:10.1126/science.1155121

Bonan, G. B., Levis, S., Kergoat, L., & Oleson, K. W. (2002). Landscapes as patches of plant functional types: An integrating concept for climate and ecosystem models. *Global Biogeochemical Cycles*, *16*(2), 5–1–5–23. doi:10.1029/2000GB001360

Bonan, G. B., Pollard, D., & Thompson, S. (1992). Effects of boreal forest vegetation on global climate. *Nature*, *359*, 716–718.

Bony, S., Colman, R., Kattsov, V. M., Allan, R. P., Bretherton, C. S., Dufresne, J. L., … Webb, M. J. (2006). How well do we understand and evaluate climate change feedback processes? *Journal of Climate*, *19*, 3445–3482. http://doi.org/10.1175/JCLI3819.1

Boone, A., Habets, F., Noilhan, J., Clark, D., Dirmeyer, P., Fox, S., … Yang, Z.-L. (2004). The Rhône-Aggregation Land Surface Scheme intercomparison project: An overview. *Journal of Climate*, *17*(1), 187–208. http://doi.org/10.1175/1520-0442(2004)017<0187:TRLSSI>2.0.CO;2

Branstator, G., & Teng, H. (2012). Potential impact of initialization on decadal predictions as assessed for CMIP5 models. *Geophysical Research Letters*, *39*(12), 1–5. http://doi.org/10.1029/2012GL051974

Brown, R. D. (2000). Northern Hemisphere Snow Cover Variability and Change, 1915 – 97. *Journal of Climate*, *13*(2000), 2339–2355. http://doi.org/10.1175/1520-0442(2000)013<2339:NHSCVA>2.0.CO;2

Brown, R. D., Brasnett, B., & Robinson, D. (2003). Gridded North American monthly snow depth and snow water equivalent for GCM evaluation. *Atmosphere-Ocean*, *41*(1), 1–14. http://doi.org/10.3137/ao.410101

Brown, R. D., & Derksen, C. (2013). Is Eurasian October snow cover extent increasing? *Environmental Research Letters*, *8*, 024006. doi:10.1088/1748-9326/8/2/024006

Brown, R. D., Derksen, C., & Wang, L. (2010). A multi-data set analysis of variability and change in Arctic spring snow cover extent, 1967–2008. *Journal of Geophysical Research*, *115*(D16), D16111. http://doi.org/10.1029/2010JD013975

Brown, R. D., & Robinson, D. A. (2011). Northern Hemisphere spring snow cover variability and change over 1922–2010 including an assessment of uncertainty. *The Cryosphere*, *5*(1), 219–229. http://doi.org/10.5194/tc-5-219-2011

Brovkin, V., Boysen, L., Raddatz, T., Gayler, V., Loew, A., & Claussen, M. (2013). Evaluation of vegetation cover and land-surface albedo in MPI-ESM CMIP5 simulations. *Journal of Advances in Modeling Earth Systems*, *5*(1), 48–57. doi:10.1029/2012MS000169

Brun, E., Vionnet, V., Boone, A., Decharme, B., Peings, Y., Valette, R., … Morin, S. (2013). Simulation of northern Eurasian local snow depth, mass and density using a detailed snowpack model and meteorological reanalysis. *Journal of Hydrometeorology*, 203–219. http://doi.org/10.1175/JHM-D-12-012.1

Brutel-Vuilmet, C., Ménégoz, M., & Krinner, G. (2013). An analysis of present and future seasonal Northern Hemisphere land snow cover simulated by CMIP5 coupled climate models. *The Cryosphere*, *7*(1), 67–80. doi:10.5194/tc-7-67-2013

Budyko, M. I. (1969). The effect of solar radiation variations on the climate of the Earth. *Tellus A*, *7*, 611–619. http://doi.org/10.3402/tellusa.v21i5.10109

Cess, R. D., & Potter, L. (1988). A Methodology for Understanding and Intercomparing Atmospheric Climate in General Circulation Models. *Journal of Geophysical Research*, *93*(8), 8305–8314.

Cess, R. D., Potter, G. L., Zhang, M. H., Blanchet, J. ., Chalita, S., Colman, R., … Dymnikov, V. (1991). Interpretation of Snow-Climate Feedback as Produced by 17 General Circulation Models. *Science*, *253*, 888–892.

Chapin, F. S., Sturm, M., Serreze, M. C., McFadden, J. P., Key, J. R., Lloyd, A H., … Welker, J. M. (2005). Role of land-surface changes in arctic summer warming. *Science*, *310*(5748), 657–60. doi:10.1126/science.1117368

Clark, M. P., Fan, Y., Lawrence, D. M., Adam, J. C., Bolster, D., Gochis, D. J., … Zeng, X. (2015). Improving the representation of hydrologic processes in Earth System Models. *Water Resources Research*, *51*, 5929–5956. http://doi.org/10.1002/2015WR017096.Received

Cohen, J. L., Furtado, J. C., Barlow, M. A, Alexeev, V. A, & Cherry, J. E. (2012). Arctic warming, increasing snow cover and widespread boreal winter cooling. *Environmental Research Letters*, *7*(1), 14007. http://doi.org/10.1088/1748-9326/7/1/014007

Cohen, J., & Jones, J. (2011). Tropospheric precursors and stratospheric warmings. *Journal of Climate*, *25*(5), 1780–1790. http://doi.org/10.1175/JCLI-D-11-00701.1

Cohen, J. L., Screen, J. A, Furtado, J. C., Barlow, M., Whittleston, D., Coumou, D., … Jones, J. (2014). Recent Arctic amplification and extreme mid-latitude weather. *Nature Geoscience*, *7*(9), 627–637. doi:10.1038/ngeo2234

Colbeck, S.C. (1982). An overview of seasonal snow metamorphism. Reviews of Geophysics and Space Physics, 20(1), 45-61.

Collins, M., Knutti, R., Arblaster, J., Dufresne, J.-L., Fichefet, T., Friedlingstein, P., Gao, X., Gutowski, W. J., Johns, T., Krinner, G., Shongwe, M., Tebaldi, C., Weaver, A. J., & Wehner, M. (2013). Long-term Climate Change: Projections, Commitments and Irreversibility. *In: Climate Change 2013: The Physical Science Basis. Contribution of Working Group I to the Fifth Assessment Report of the Intergovernmental Panel on Climate Change* [Stocker, T.F., D. Qin, G.-K. Plattner, M. Tignor, S.K. Allen, J.

Boschung, A. Nauels, Y. Xia, V. Bex and P.M. Midgley (eds.)]. Cambridge University Press, Cambridge, United Kingdom and New York, NY, USA, 1029-1136.

Collins, W. J., Bellouin, N., Doutriaux-Boucher, M., Gedney, N., Halloran, P., Hinton, T., … Woodward, S. (2011). Development and evaluation of an Earth-System model – HadGEM2. *Geoscientific Model Development*, *4*, 1051–1075. doi:10.5194/gmd-4-1051-2011

Colman, R. A. (2003). A comparison of climate feedbacks in general circulation models. *Climate Dynamics*, *20*(January 2002), 865–873. http://doi.org/10.1007/s00382-003-0310-z

Colman, R. A. (2013). Surface albedo feedbacks from climate variability and change. *Journal of Geophysical Research: Atmospheres*, *118*(April), 2827–2834. http://doi.org/10.1002/jgrd.50230

Crook, J. A., & Forster, P. M. D. F. (2014). Comparison of surface albedo feedback in climate models and observations. *Geophysical Research Letters*, *41*(5), 1717–1723. http://doi.org/10.1002/2014GL059280.Received

Dai, A. (2008). Temperature and pressure dependence of the rain-snow phase transition over land and ocean. *Geophysical Research Letters*, *35*(12), 1–7. http://doi.org/10.1029/2008GL033295

Danabasoglu, G., Bates, S. C., Briegleb, B. P., Jayne, S. R., Jochum, M., Large, W. G., … Yeager, S. (2012). The CCSM4 Ocean Component. *Journal of Climate*, *25*, 1361–1389. http://doi.org/10.1175/JCLI-D-11-00091.1

De Boer, G., Chapman, W., Kay, J. E., Medeiros, B., Shupe, M. D., Vavrus, S., & Walsh, J. (2012). A characterization of the present-day arctic atmosphere in CCSM4. *Journal of Climate*, *25*(8), 2676–2695. http://doi.org/10.1175/JCLI-D-11-00228.1

de Rosnay, P., & Polcher, J. (1998). Modelling root water uptake in a complex land surface scheme coupled to a GCM. *Hydrology and Earth System Sciences*, *2*(2/3), 239–255. http://doi.org/10.5194/hess-2-239-1998

Decker, M., Brunke, M. A., Wang, Z., Sakaguchi, K., Zeng, X., & Bosilovich, M. G. (2012). Evaluation of the reanalysis products from GSFC, NCEP, and ECMWF using flux tower observations. *Journal of Climate*, *25*(6), 1916–1944. http://doi.org/10.1175/JCLI-D-11-00004.1

Dee, D. P., Uppala, S. M., Simmons, A. J., Berrisford, P., Poli, P., Kobayashi, S., … Vitart, F. (2011). The ERA-Interim reanalysis: Configuration and performance of the data

assimilation system. *Quarterly Journal of the Royal Meteorological Society*, *137*(April), 553–597. doi:10.1002/qj.828

Derksen, C., & Brown, R. (2012). Spring snow cover extent reductions in the 2008-2012 period exceeding climate model projections. *Geophysical Research Letters*, *39*(19), L19504. doi:10.1029/2012GL053387

Derksen, C., Brown, R., Mudryk, L., & Luojus, K. (2015). Terrestrial Snow (Arctic). In State of Climate in 2014. *Bulletins of the American Meteorological Society*, *96*, S133-S135.

Déry, S. J., & Brown, R. D. (2007). Recent Northern Hemisphere snow cover extent trends and implications for the snow-albedo feedback. *Geophysical Research Letters*, *34*(22), L22504. http://doi.org/10.1029/2007GL031474

Deser, C., Knutti, R., Solomon, S., & Phillips, A. S. (2012). Communication of the role of natural variability in future North American climate. *Nature Climate Change*, *2*(October), 775–779. http://doi.org/10.1038/nclimate1562

Deser, C., Phillips, A., Bourdette, V., & Teng, H. (2012). Uncertainty in climate change projections: The role of internal variability. *Climate Dynamics*, *38*, 527–546. http://doi.org/10.1007/s00382-010-0977-x

Deser, C., Phillips, A. S., Alexander, M. A., & Smoliak, B. V. (2014). Projecting North American climate over the next 50 years: Uncertainty due to internal variability. *Journal of Climate*, *27*, 2271–2296. http://doi.org/10.1175/JCLI-D-13-00451.1

Deser, C., Terray, L., & Phillips, A. S. (2016). Forced and Internal Components of Winter Air Temperature Trends over North America During the Past 50 Years: Mechanisms and Implications. *Journal of Climate*, *29*, 2237–2258. https://doi.org/10.1175/JCLI-D-15-0304.1

Dessler, A. E. (2013). Observations of Climate Feedbacks over 2000-10 and Comparisons to Climate Models. *Journal of Climate*, *26*, 333-342.

Diffenbaugh, N. S., Pal, J. S., Trapp, R. J., & Giorgi, F. (2005). Fine-scale processes regulate the response of extreme events to global climate change. *Proceedings of the National Academy of Sciences of the United States of America*, *102*(44), 15774–15778. http://doi.org/10.1073/pnas.0506042102

Diffenbaugh, N. S., Scherer, M., & Ashfaq, M. (2013). Response of snow-dependent hydrologic extremes to continued global warming. *Nature Climate Change*, *3*(4), 379–384. http://doi.org/10.1038/nclimate1732

Doherty, S. J., Warren, S. G., Grenfell, T. C., Clarke, A. D., & Brandt, R. E. (2010). Light-absorbing impurities in Arctic snow. *Atmospheric Chemistry and Physics*, *10*(23), 11647–11680. doi:10.5194/acp-10-11647-2010

Donohoe, A., & Battisti, D. S. (2011). Atmospheric and surface contributions to planetary albedo. *Journal of Climate*, *24*, 4402–4418. http://doi.org/10.1175/2011JCLI3946.1

Douville, H. (2010). Relative contribution of soil moisture and snow mass to seasonal climate predictability: A pilot study. *Climate Dynamics*, *34*(6), 797–818. http://doi.org/10.1007/s00382-008-0508-1

Dutra, E., Schär, C., Viterbo, P., & Miranda, P. M. A. (2011). Land-atmosphere coupling associated with snow cover. *Geophysical Research Letters*, *38*(15), 1–5. http://doi.org/10.1029/2011GL048435

Eltahir, E. A. B. (1998). A Soil Moisture-Rainfall Feedback Mechanism: 1. Theory and observations. *Water Resources Research*, *34*(4), 765–776. http://doi.org/10.1029/97WR03499

Essery, R. (1997). Seasonal snow cover and climate change in the Hadley Centre GCM. *Annals of Glaciology*, *25*, 1–5.

Essery, R. (2013). Large-scale simulations of snow albedo masking by forests. *Geophysical Research Letters*, *40*(20), 5521–5525. doi:10.1002/grl.51008

Essery, R., Morin, S., Lejeune, Y., & B Ménard, C. (2013). A comparison of 1701 snow models using observations from an alpine site. *Advances in Water Resources*, *55*, 131–148. doi:10.1016/j.advwatres.2012.07.013

Essery, R., & Pomeroy, J. (2004). Vegetation and Topographic Control of Wind-Blown Snow Distributions in Distributed and Aggregated Simulations for an Arctic Tundra Basin. *Journal of Hydrometeorology*, *5*, 735–744. doi:10.1175/1525-7541(2004)005<0735:VATCOW>2.0.CO;2

Essery, R., Rutter, N., Pomeroy, J., Baxter, R., Stahli, M., Gustafsson, D., … Elder, K. (2009). SnowMIP2: An Evaluation of Forest Snow Process Simulations. *Bulletin of the American Meteorological Society*, *90*, 1120–1135. https://doi.org/10.1175/2009BAMS2629.1

Etchevers, P., Martin, E., Brown, R., Fierz, C., Lejeune, Y., Bazile, E., … Yamazaki, T. (2004). Validation of the energy budget of an alpine snowpack simulated by several snow models (SnowMIP project). *Annals of Glaciology*, *38*, 150–158.

Eyring, V., Bony, S., Meehl, G. A., Senior, C. A., Stevens, B., Stouffer, R. J., & Taylor, K. E. (2016). Overview of the Coupled Model Intercomparison Project Phase 6 (CMIP6) experimental design and organization. *Geoscientific Model Development*, *9*(5), 1937–1958. http://doi.org/10.5194/gmd-9-1937-2016

Fang, H., Liang, S., Kim, H.-Y., Townshend, J. R., Schaaf, C. L., Strahler, A. H., & Dickinson, R. E. (2007). Developing a spatially continuous 1 km surface albedo data set over North America from Terra MODIS products. *Journal of Geophysical Research*, *112*(D20), D20206. doi:10.1029/2006JD008377

Fernandes, R., Zhao, H., Wang, X., Key, J., Qu, X., & Hall, A. (2009). Controls on Northern Hemisphere snow albedo feedback quantified using satellite Earth observations. *Geophysical Research Letters*, *36*(21), L21702. http://doi.org/10.1029/2009GL040057

Fischer, E. M., Lawrence, D. M., & Sanderson, B. M. (2011). Quantifying uncertainties in projections of extremes-a perturbed land surface parameter experiment. *Climate Dynamics*, *37*, 1381–1398. http://doi.org/10.1007/s00382-010-0915-y

Fischer, E. M., Seneviratne, S. I., Vidale, P. L., Luthi, D., & Schar, C. (2007). Soil Moisture – Atmosphere Interactions during the 2003 European Summer Heat Wave. *Journal of Climate*, *20*, 5081–5099. http://doi.org/10.1175/JCLI4288.1

Fischlin, A., Midgley, G. F., Price, J. T., Leemans, R., Gopal, B., Turley, C., Rounsevell, M. D. A., Dube, O. P., Tarazona, J., Velichko, A. A. (2007). Ecosystems, their properties, goods, and services. *Climate Change 2007: Impacts, Adaptation and Vulnerability. Contribution of Working Group II to the Fourth Assessment Report of the Intergovernmental Panel on Climate Change*, M.L. Parry, O.F. Canziani, J.P. Palutikof, P.J. van der Linden and C.E. Hanson, Eds., Cambridge University Press, Cambridge, 211-272.

Flanner, M. G., Shell, K. M., Barlage, M., Perovich, D. K., & Tschudi, M. A. (2011). Radiative forcing and albedo feedback from the Northern Hemisphere cryosphere between 1979 and 2008. *Nature Geoscience*, *4*(3), 151–155. http://doi.org/10.1038/ngeo1062

Flanner, M. G., Zender, C. S., Hess, P. G., Mahowald, N. M., Painter, T. H., Ramanathan, V., & Rasch, P. J. (2009). Springtime warming and reduced snow cover from carbonaceous particles. *Atmospheric Chemistry and Physics Discussions*, *8*, 19819–19859. http://doi.org/10.5194/acpd-8-19819-2008

Flato, G. M. (2011). Earth system models: An overview. *Wiley Interdisciplinary Reviews: Climate Change*, *2*(6), 783–800. http://doi.org/10.1002/wcc.148

Flato, G. M., Marotzke, J., Abiodun, B., Braconnot, P., Chou, S. C., Collins, W., Cox, P., Driouech, F., Emori, S., Eyring, V., Forest, C., Gleckler, P., Guilyardi, E., Jakob, C., Kattsov, V., Reason, C., & Rummukainen, M. (2013). Evaluation of Climate Models. *In: Climate Change 2013: The Physical Science Basis. Contribution of Working Group I to the Fifth Assess- ment Report of the Intergovernmental Panel on Climate Change* [Stocker, T.F., D. Qin, G.-K. Plattner, M. Tignor, S.K. Allen, J. Boschung, A. Nauels, Y. Xia, V. Bex and P.M. Midgley (eds.)]. Cambridge University Press, Cambridge, United Kingdom and New York, NY, USA, 741-866.

Fletcher, C. G., Hardiman, S. C., Kushner, P. J., & Cohen, J. (2009). The dynamical response to snow cover perturbations in a large ensemble of atmospheric GCM integrations. *Journal of Climate*, *22*(5), 1208–1222. http://doi.org/10.1175/2008JCLI2505.1

Fletcher, C. G., Kushner, P. J., & Cohen, J. (2007). Stratospheric control of the extratropical circulation response to surface forcing. *Geophysical Research Letters*, *34*(21), 3–7. http://doi.org/10.1029/2007GL031626

Fletcher, C. G., Kushner, P. J., Hall, A., & Qu, X. (2009). Circulation responses to snow albedo feedback in climate change. *Geophysical Research Letters*, *36*(April), 2–5. http://doi.org/10.1029/2009GL038011

Fletcher, C. G., Thackeray, C. W., & Burgers, T. M. (2015). Evaluating biases in simulated snow albedo feedback in two generations of climate models, *Journal of Geophysical Research: Atmospheres*, *120*(1), 12-26. doi:10.1002/2014JD022546.

Fletcher, C. G., Zhao, H., Kushner, P. J., & Fernandes, R. (2012). Using models and satellite observations to evaluate the strength of snow albedo feedback. *Journal of Geophysical Research*, *117*(D11), D11117. doi:10.1029/2012JD017724

Foster, J. L., Sun, C., Walker, J. P., Kelly, R., Chang, A., Dong, J., & Powell, H. (2005). Quantifying the uncertainty in passive microwave snow water equivalent observations. *Remote Sensing of Environment*, *94*(2), 187–203. doi:10.1016/j.rse.2004.09.012

Frei, A., & Lee, S. (2010). A comparison of optical-band based snow extent products during spring over North America. *Remote Sensing of Environment*, *114*(9), 1940–1948. http://doi.org/10.1016/j.rse.2010.03.015

Friedl, M. A., et al. (2002), Global land cover mapping from MODIS: algorithms and early results, Remote Sensing Of Environment, 83, 287–302, doi:10.1016/S0034-4257(02)00078-0.

Furtado, J. C., Cohen, J. L., Butler, A. H., Riddle, E. E., & Kumar, A. (2015). Eurasian snow cover variability and links to winter climate in the CMIP5 models. *Climate Dynamics*, *45*, 2591–2605. http://doi.org/10.1007/s00382-015-2494-4

Fyfe, J. C., Derksen, C., Mudryk, L., Flato, G. M., Santer, B. D., Swart, N. C., … Jiao, Y. (2017). Large near-term projected snowpack loss over the western United States. *Nature Communications*, *8*, 14996. http://doi.org/10.1038/ncomms14996

Fyfe, J. C., & Flato, G. (1999). Enhanced Climate Change and Its Detection over the Rocky Mountains. *Journal of Climate*, *12*, 230–243. Retrieved from http://dx.doi.org/10.1175/1520-0442(1999)012%3C0230:ECCAID%3E2.0.CO;2

Garfinkel, C. I., Hartmann, D. L., & Sassi, F. (2010). Tropospheric precursors of anomalous northern hemisphere stratospheric polar vortices. *Journal of Climate*, *23*(12), 3282–3299. http://doi.org/10.1175/2010JCLI3010.1

Gates, W. L., Boyle, J. S., Covey, C., Dease, C. G., Doutriaux, C. M., Drach, R. S., … Williams, D. N. (1999). An Overview of the Results of the Atmospheric Model Intercomparison Project (AMIP I). *Bulletin of the American Meteorological Society*, *80*(1), 29–55. http://doi.org/10.1175/1520-0477(1999)080<0029:AOOTRO>2.0.CO;2

Gent, P. R., Danabasoglu, G., Donner, L. J., Holland, M. M., Hunke, E. C., Jayne, S. R., … Zhang, M. (2011). The Community Climate System Model Version 4. *Journal of Climate*, *24*(19), 4973–4991. http://doi.org/10.1175/2011JCLI4083.1

GISTEMP Team. (2017) GISS Surface Temperature Analysis (GISTEMP). NASA Goddard Institute for Space Studies. Dataset accessed 2017-06-05 at https://data.giss.nasa.gov/gistemp/.

Gong, G., Entekhabi, D., & Cohen, J. (2002). A large-ensemble model study of the wintertime AO-NAO and the role of interannual snow perturbations. *Journal of Climate*, *15*(23), 3488–3499. http://doi.org/10.1175/1520-0442(2002)015<3488:ALEMSO>2.0.CO;2

Gong, G., Entekhabi, D., & Cohen, J. (2003). Relative impacts of Siberian and North American snow anomalies on the winter Arctic Oscillation. *Geophysical Research Letters*, *30*(16), 2–5. http://doi.org/10.1029/2003GL017749

Gong, G., Entekhabi, D., Cohen, J., & Robinson, D. (2004). Sensitivity of atmospheric response to modeled snow anomaly characteristics. *Journal of Geophysical Research: Atmospheres*, *109*(D6), n/a-n/a. http://doi.org/10.1029/2003JD004160

Graversen, R. G., Langen, P. L., & Mauritsen, T. (2014). Polar amplification in CCSM4: Contributions from the lapse rate and surface albedo feedbacks. *Journal of Climate*, *27*, 4433–4450. http://doi.org/10.1175/JCLI-D-13-00551.1

Graversen, R. G., & Wang, M. (2009). Polar amplification in a coupled climate model with locked albedo. *Climate Dynamics*, *33*(April 2008), 629–643. http://doi.org/10.1007/s00382-009-0535-6

Groisman, P., Karl, T. R., Knight, R. W., & Stenchikov, G. L. (1994). Changes of Snow Cover, Temperature, and Radiative Heat Balance over the Northern Hemisphere. *Journal of Climate*, *7*, 1633–1656.

Gunthner, A., Stuck, J., Werth, S., Doll, P., Verzano, K., & Merz, B. (2007). A global analysis of temporal and spatial variations in continental water storage, *Water Resources Research*, 43(5), W05416, doi:10.1029/2006WR005247.

Hall, A. (2004). The Role of Surface Albedo Feedback in Climate. *Journal of Climate*, *17*, 1550–1568. doi:10.1175/1520-0442(2004)017<1550:TROSAF>2.0.CO;2

Hall, A., & Qu, X. (2006). Using the current seasonal cycle to constrain snow albedo feedback in future climate change. *Geophysical Research Letters*, *33*, 1–4. http://doi.org/10.1029/2005GL025127

Hall, A., Qu, X., & Neelin, J. D. (2008). Improving predictions of summer climate change in the United States. *Geophysical Research Letters*, *35*(September 2007), 1–5. http://doi.org/10.1029/2007GL032012

Hall, D. K. (1988). Assessment of Polar Climate Change using Satellite Technology. *Reviews of Geophysics*, *26*(1), 26–39.

Hall, D. K., Foster, J. L., Salomonson, V. V, Klein, A. G., & Chien, J. Y. L. (2001). Development of a Technique to Assess Snow-Cover Mapping Errors from Space, *39*(2), 432–438.

Hall, D. K., & Riggs, G. A. (2007). Accuracy assessment of the MODIS snow products. *Hydrological Processes*, *21*, 1534–1547. http://doi.org/10.1002/hyp

Hall, D. K., Riggs, G. A., Foster, J. L., & Kumar, S. V. (2010). Development and evaluation of a cloud-gap-filled MODIS daily snow-cover product. *Remote Sensing of Environment*, *114*(3), 496–503. http://doi.org/10.1016/j.rse.2009.10.007

Hall, D. K., Riggs, G. A, Salomonson, V. V, DiGirolamo, N. E., & Bayr, K. J. (2002). MODIS snow-cover products. *Remote Sensing of Environment*, *83*(1-2), 181–194. doi:10.1016/S0034-4257(02)00095-0

Hall, D. K., Salomonson, V. V., & Riggs, G. A. (2006). MODIS/Terra Snow Cover Monthly L3 Global 0.05Deg CMG. Version 5. Boulder, Colorado USA: National Snow and Ice Data Center. http://dx.doi.org/10.5067/IPPLURB6RPCN.

Hansen, J., Ruedy, R., Sato, M., & Lo, K. (2010). Global surface temperature change. *Reviews of Geophysics*, *48*(4), RG4004. http://doi.org/10.1029/2010RG000345.1.INTRODUCTION

Hargreaves, J. C., Annan, J. D., Ohgaito, R., Paul, A., & Abe-Ouchi, A. (2013). Skill and reliability of climate model ensembles at the Last Glacial Maximum and mid-Holocene. *Climate of the Past*, *9*(2), 811–823. doi:10.5194/cp-9-811-2013

Hartmann, D. J., Klein Tank, A. M. G., Rusticucci, M., Alexander, L. V, Brönnimann, S., Charabi, Y. A.-R., … Zhai, P. (2013). Observations: Atmosphere and Surface. *Climate Change 2013: The Physical Science Basis. Contribution of Working Group I to the Fifth Assessment Report of the Intergovernmental Panel on Climate Change*. Retrieved from http://www.climatechange2013.org/report/full-report/

Hawkins, E., & Sutton, R. (2009). The potential to narrow uncertainty in regional climate predictions. *Bulletin of the American Meteorological Society*, *90*(8), 1095–1107. http://doi.org/10.1175/2009BAMS2607.1

Hawkins, E., & Sutton, R. (2011). The potential to narrow uncertainty in projections of regional precipitation change. *Climate Dynamics*, *37*(1), 407–418. http://doi.org/10.1007/s00382-010-0810-6

He, S., Gao, Y., Li, F., Wang, H., & He, Y. (2017). Impact of Arctic Oscillation on the East Asian climate: A review. *Earth-Science Reviews*, *164*, 48–62. http://doi.org/10.1016/j.earscirev.2016.10.014

He, T., Liang, S., & Song, D.-X. (2014). Analysis of global land surface albedo climatology and spatial-temporal variation during 1981-2010 from multiple satellite products. *Journal of Geophysical Research : Atmospheres*, *119*(10), 281–298. doi:10.1002/2014JD021667.

Hedstrom, N. R., & Pomeroy, J. W. (1998). Measurements and modelling of snow interception in the boreal forest. *Hydrological Processes*, *1625*(March), 1611–1625.

Hegerl, G. C., & Zwiers, F. W. (2007). Understanding and Attributing Climate Change. In: Climate Change 2007: The Physical Science Basis. Contribution of Working Group I to the Fourth Assessment Report of the Intergovernmental Panel on Climate Change [Solomon, S., D. Qin, M. Manning, Z. Chen, M. Marquis, K.B. Averyt, M. Tignor and H.L. Miller (eds.)]. Cambridge University Press, Cambridge, UK and New York, NY, USA.

Hernández-Henríquez, M. A, Déry, S. J., & Derksen, C. (2015). Polar amplification and elevation-dependence in trends of Northern Hemisphere snow cover extent, 1971–2014.

Environmental Research Letters, *10*(4), 44010. http://doi.org/10.1088/1748-9326/10/4/044010

Holland, M. M., Bailey, D. A., Briegleb, B. P., Light, B., & Hunke, E. C. (2012). Improved Sea Ice Shortwave Radiation Physics in CCSM4: The Impact of Melt Ponds and Aerosols on Arctic Sea Ice *. *Journal of Climate*, *25*, 1413–1430. http://doi.org/10.1175/JCLI-D-11-00078.1

Holland, M. M., & Bitz, C. M. (2003). Polar amplification of climate change in coupled models. *Climate Dynamics*, *21*, 221–232. http://doi.org/10.1007/s00382-003-0332-6

Honda, M., Inoue, J., & Yamane, S. (2009). Influence of low Arctic sea-ice minima on anomalously cold Eurasian winters. *Geophysical Research Letters*, *36*(8), 1–6. http://doi.org/10.1029/2008GL037079

Ingram, W. J., Wilson, C. A., & Mitchell, J. F. B. (1989). Modeling Climate Change: An Assessment of Sea Ice and Surface Albedo Feedbacks. *Journal of Geophysical Research*, *94*, 8609–8622.

Inoue, J., Hori, M. E., & Takaya, K. (2012). The role of barents sea ice in the wintertime cyclone track and emergence of a warm-Arctic cold-Siberian anomaly. *Journal of Climate*, *25*(7), 2561–2569. http://doi.org/10.1175/JCLI-D-11-00449.1

Jeong, J. H., & Ho, C. H. (2005). Changes in occurrence of cold surges over east Asia in association with Arctic Oscillation. *Geophysical Research Letters*, *32*(14), 1–4. http://doi.org/10.1029/2005GL023024

Jia, L., Yang, X., Vecchi, G. A., Gudgel, R. G., Delworth, T. L., Rosati, A., … Dixon, K. (2015). Improved seasonal prediction of temperature and precipitation over land in a high-resolution GFDL climate model. *Journal of Climate*, *28*(5), 2044–2062. http://doi.org/10.1175/JCLI-D-14-00112.1

Jianhua, J., Junmei, L., Jie, C., & Juzhang, R. (2005). Possible impacts of the arctic oscillation on the interdecadal variation of summer monsoon rainfall in East Asia. *Advances in Atmospheric Sciences*, *22*(1), 39–48. http://doi.org/10.1007/BF02930868

Jin, Y., Schaaf, C. B., Gao, F., Li, X., Strahler, A. H., Zeng, X., & Dickinson, R. E. (2002). How does snow impact the albedo of vegetated land surfaces as analyzed with MODIS data ? *Geophysical Research Letters*, *29*(10), 12–15. doi:10.1029/2001GL014132

Jones, P., New, M., & Parker, D. (1999). Surface air temperature and its changes over the past 150 years. *Reviews of Geophysics*, *37*(2), 173–199. http://doi.org/10.1029/1999RG900002

Jones, P. D., Lister, D. H., Osborn, T. J., Harpham, C., Salmon, M., & Morice, C. P. (2012). Hemispheric and large-scale land-surface air temperature variations: An extensive revision and an update to 2010. *Journal of Geophysical Research*, *117*(D5), D05127. http://doi.org/10.1029/2011JD017139

Kalnay, E., Kanamitsu, M., Kistler, R., Collins, W., Deaven, D., Gandin, L., … Joseph, D. (1996). The NCEP/NCAR 40-Year Reanalysis Project. *Bulletin of the American Meteorological Society*. http://doi.org/10.1175/1520-0477(1996)077<0437:TNYRP>2.0.CO;2

Kanamitsu, M., Ebisuzaki, W., Woollen, J., Yang, S. K., Hnilo, J. J., Fiorino, M., & Potter, G. L. (2002). NCEP-DOE AMIP-II reanalysis (R-2). *Bulletin of the American Meteorological Society*, *83*(11), 1631–1643+1559. http://doi.org/10.1175/BAMS-83-11-1631

Karl, T. R., Groisman, P. Y., Knight, R. W., & Heim, R. R. (1993). Recent variations of snow cover and snowfall in North America and their relation to precipitation and temperature variations. *Journal of Climate*. http://doi.org/10.1175/1520-0442(1993)006<1327:RVOSCA>2.0.CO;2

Kay, J. E., Deser, C., Phillips, A., Mai, A., Hannay, C., Strand, G., … Vertenstein, M. (2015). The Community Earth System Model (CESM) Large Ensemble Project: A Community Resource for Studying Climate Change in the Presence of Internal Climate Variability. *Bulletin of the American Meteorological Society*, *96*(8), 1333–1349. http://doi.org/10.1175/BAMS-D-13-00255.1

Klein, A. G., Hall, D. K., & Riggs, G. A. (1998). Improving snow cover mapping in forests through the use of a canopy reflectance model. *Hydrological Processes*, *12*, 1723–1744. doi:10.1002/(SICI)1099-1085(199808/09)12:10/11<1723::AID-HYP691>3.0.CO;2-2

Knutti, R. (2010). The end of model democracy? *Climatic Change*, *102*, 395–404. http://doi.org/10.1007/s10584-010-9800-2

Knutti, R., & Sedláček, J. (2013). Robustness and uncertainties in the new CMIP5 climate model projections. *Nature Climate Change*, *3*(4), 369–373. http://doi.org/10.1038/nclimate1716

Koenigk, T., Devasthale, A., & Karlsson, K.-G. (2014). Summer Arctic sea ice albedo in CMIP5 models. *Atmospheric Chemistry and Physics*, *14*(4), 1987–1998. doi:10.5194/acp-14-1987-2014

Kolstad, E. W., & Charlton-Perez, A. J. (2011). Observed and simulated precursors of stratospheric polar vortex anomalies in the Northern Hemisphere. *Climate Dynamics*, *37*(7–8), 1443–1456. http://doi.org/10.1007/s00382-010-0919-7

Koster, R. D., Suarez, M. J., Ducharne, A., Stieglitz, M., & Kumar, P. (2000). A catchment-based approach to modeling land surface processes in a general circulation model 1. Model structure. *Journal of Geophysical Research D: Atmospheres*, *105*(D20), 24809–24822. Retrieved from http://www.scopus.com/inward/record.url?eid=2-s2.0-0034535097&partnerID=tZOtx3y1

Kowalczyk, E. A., Stevens, L., Law, R. M., Dix, M., Wang, Y. P., Harman, I. N., … Ziehn, T. (2013). The land surface model component of ACCESS: description and impact on the simulated surface climatology. *Australian Meteorological and Oceanographic Journal*, *63*, 65–82.

Krasting, J. P., Broccoli, A. J., Dixon, K. W., & Lanzante, J. R. (2013). Future changes in northern hemisphere snowfall. *Journal of Climate*, *26*(20), 7813–7828. http://doi.org/10.1175/JCLI-D-12-00832.1

Kunkel, K. E., Palecki, M. A., Hubbard, K. G., Robinson, D. A., Redmond, K. T., & Easterling, D. R. (2007). Trend Identification in Twentieth-Century U.S. Snowfall: The Challenges. *Journal of Atmospheric and Oceanic Technology*, *24*(1), 64–73. doi:10.1175/JTECH2017.1

Kuusinen, N., Kolari, P., Levula, J., Porcar-Castell, A., Stenberg, P., & Berninger, F. (2012). Seasonal variation in boreal pine forest albedo and effects of canopy snow on forest reflectance. *Agricultural and Forest Meteorology*, *164*, 53–60. doi:10.1016/j.agrformet.2012.05.009

Laliberté, F., Howell, S. E. L., & Kushner, P. J. (2016). Regional variability of a projected sea ice-free Arctic during the summer months. *Geophysical Research Letters*, *43*, 256–263. http://doi.org/10.1002/2015GL066855.Received

Lawrence, D. M., Oleson, K. W., Flanner, M. G., Thornton, P. E., Swenson, S. C., Lawrence, P. J., … Slater, A. G. (2011). Parameterization improvements and functional and structural advances in Version 4 of the Community Land Model. *Journal of Advances in Modeling Earth Systems*, *3*(3), M03001. http://doi.org/10.1029/2011MS000045

Lawrence, D. M., & Slater, A. G. (2010). The contribution of snow condition trends to future ground climate. *Climate Dynamics*, *34*(7–8), 969–981. http://doi.org/10.1007/s00382-009-0537-4

Lawrence, D. M., Slater, A. G., & Swenson, S. C. (2012). Simulation of Present-Day and Future Permafrost and Seasonally Frozen Ground Conditions in CCSM4. *Journal of Climate*, *25*, 2207–2225. http://doi.org/10.1175/JCLI-D-11-00334.1

Levis, S., Bonan, G. B., & Lawrence, P. J. (2007). Present-day springtime high-latitude surface albedo as a predictor of simulated climate sensitivity. *Geophysical Research Letters*, *34*(August), 2–5. http://doi.org/10.1029/2007GL030775

Lewis, P., et al. (2013), GlobAlbedo: Algorithm theoretical basis document (V4.12).

Li, Y., Wang, T., Zeng, Z., Peng, S., Lian, X., & Piao, S. (2016). Evaluating biases in simulated land surface albedo from CMIP5 global climate models. *Journal of Geophysical Research: Atmospheres*. http://doi.org/10.1002/2016JD024774

Lian, M. S., & Cess, R. D. (1977). Energy Balance Climate Models: A Reappraisal of Ice-Albedo Feedback. *Journal of The Atmospheric Sciences*, *34*, 1058–1062.

Liston, G. E. (2004). Representing Subgrid Snow Cover Heterogeneities in Regional and Global Models. *Journal of Climate*, *17*, 1381–1397. doi:10.1175/1520-0442(2004)017<1381:RSSCHI>2.0.CO;2

Liu, Y. (2003). Spatial patterns of soil moisture connected to monthly-seasonal precipitation variability in a monsoon region. *Journal of Geophysical Research*, *108*. http://doi.org/10.1029/2002JD003124

Loranty, M. M., Berner, L. T., Goetz, S. J., Jin, Y., & Randerson, J. T. (2014). Vegetation controls on northern high latitude snow-albedo feedback: observations and CMIP5 model simulations. *Global Change Biology*, *20*(2), 594–606. doi:10.1111/gcb.12391

Loth, B., Graf, H., & Oberhuber, J. M. (1993). Snow Cover Model for Global Climate Simulations. *Journal of Geophysical Research*, *98*(1), 10451–10464.

Luo, D., Xiao, Y., Diao, Y., Dai, A., Franzke, C. L. E., & Simmonds, I. (2016). Impact of Ural Blocking on Winter Warm Arctic – Cold Eurasian Anomalies. Part II: The Link to the North Atlantic Oscillation. *Journal of Climate*, *29*, 3949–3971. http://doi.org/10.1175/JCLI-D-15-0612.1

Luo, D., Yao, Y., Dai, A., Simmonds, I., & Zhong, L. (2017). Increased Quasi Stationarity and Persistence of Winter Ural Blocking and Eurasian Extreme Cold Events in Response to Arctic Warming. Part II: A Theoretical Explanation. *Journal of Climate*, *30*, 3569–3587. http://doi.org/10.1175/JCLI-D-16-0262.1

MacDonald, G. M., Kremenetski, K. V, & Beilman, D. W. (2008). Climate change and the northern Russian treeline zone. *Philosophical Transactions of the Royal Society B: Biological Sciences*, *363*(1501), 2283–2299. http://doi.org/10.1098/rstb.2007.2200

MacKay, M. D., Bartlett, P. A., Chan, E., Derksen, C., Guo, S., & Leighton, H. (2006). On the simulation of regional scale sublimation over boreal and agricultural landscapes in a climate model. *Atmosphere-Ocean*, *44*(3), 289–304. doi:10.3137/ao.440306

Manabe, S., & Stouffer, R. J. (1980). Sensitivity of a global climate model to an increase of CO 2 concentration in the atmosphere. *Journal of Geophysical Research*, *85*(80), 5529–5554. http://doi.org/10.1029/JC085iC10p05529

Manabe, S., & Wetherald, R. (1975). The effects of doubling the CO2 concentration on the climate of a general circulation model. *Journal of Atmospheric Sciences*, *32*, 3–15. http://doi.org/10.1175/1520-0469(1975)032<0003:TEODTC>2.0.CO;2

Manabe, S., & Wetherald, R. T. (1987). Large-Scale Changes of Soil Wetness Induced by an Increase in Atmospheric Carbon Dioxide. *Journal of the Atmospheric Sciences*, *44*(8), 1211–1235.

Mankin, J. S., & Diffenbaugh, N. S. (2015). Influence of temperature and precipitation variability on near-term snow trends. *Climate Dynamics*. http://doi.org/10.1007/s00382-014-2357-4

Mankin, J. S., Viviroli, D., Singh, D., Hoekstra, A. Y., & Diffenbaugh, N. S. (2015). The potential for snow to supply human water demand in the present and future. *Environmental Research Letters*, *10*(11), 114016. http://doi.org/10.1088/1748-9326/10/11/114016

Meehl, G. A., & Stocker, T. F. (2007). Global Climate Projections. In: Climate Change 2007: The Physical Science Basis. Contribution of Working Group I to the Fourth Assessment Report of the Intergovernmental Panel on Climate Change [Solomon, S., D. Qin, M. Manning, Z. Chen, M. Marquis, K.B. Averyt, M. Tignor and H.L. Miller (eds.)]. Cambridge University Press, Cambridge, UK and New York, NY, USA.

Ménard, C. B., Ikonen, J., Rautiainen, K., Aurela, M., Arslan, A. N., & Pulliainen, J. (2015). Effects of Meteorological and Ancillary Data, Temporal Averaging, and Evaluation Methods on Model Performance and Uncertainty in a Land Surface Model. *Journal of Hydrometeorology*, *16*(6), 2559–2576. http://doi.org/10.1175/JHM-D-15-0013.1

Minder, J. R., Letcher, T. W., & Skiles, S. M. K. (2016). An evaluation of high-resolution regional climate model simulations of snow cover and albedo over the Rocky Mountains, with implications for the simulated snow-albedo feedback. *Journal of Geophysical Research: Atmospheres*, *121*(15), 9069–9088. http://doi.org/10.1002/2016JD024995

Mori, M., Watanabe, M., Shiogama, H., Inoue, J., & Kimoto, M. (2014). Robust Arctic sea-ice influence on the frequent Eurasian cold winters in past decades. *Nature Geoscience*, *7*, 869–874. http://doi.org/10.1038/NGEO2277

Mortin, J., Graversen, R. G., & Svensson, G. (2014). Evaluation of pan-Arctic melt-freeze onset in CMIP5 climate models and reanalyses using surface observations. *Climate Dynamics*, *42*, 2239–2257. http://doi.org/10.1007/s00382-013-1811-z

Moss, R. H., Edmonds, J. a, Hibbard, K. A, Manning, M. R., Rose, S. K., van Vuuren, D. P., … Wilbanks, T. J. (2010). The next generation of scenarios for climate change research and assessment. *Nature*, *463*(7282), 747–756. http://doi.org/10.1038/nature08823

Mudryk, L. R., Derksen, C., Kushner, P. J., & Brown, R. (2015). Characterization of Northern Hemisphere snow water equivalent datasets, 1981-2010. *Journal of Climate*, *28*(20), 8037–8051. http://doi.org/10.1175/JCLI-D-15-0229.1

Mudryk, L. R., Kushner, P. J., & Derksen, C. (2014). Interpreting observed northern hemisphere snow trends with large ensembles of climate simulations. *Climate Dynamics*, *43*, 345–359. http://doi.org/10.1007/s00382-013-1954-y

Mudryk, L. R., Kushner, P. J., Derksen, C., & Thackeray, C. (2017). Snow cover response to temperature in observational and climate model ensembles. *Geophysical Research Letters*, *44*. http://doi.org/10.1002/2016GL071789

Muller, J.-P. (2013), GlobAlbedo final validation report. Rep., University College London. [Available at http://www.globalbedo.org/docs/ GlobAlbedo_FVR_V1_2_web.pdf.]

Neale, R. B., Richter, J., Park, S., Lauritzen, P. H., Vavrus, S. J., Rasch, P. J., & Zhang, M. (2013). The Mean Climate of the Community Atmosphere Model (CAM4) in Forced SST and Fully Coupled Experiments. *Journal of Climate*, *26*(14), 5150–5168. http://doi.org/10.1175/JCLI-D-12-00236.1

Oleson, K. W., Lawrence, D. M., Gordon, B., Flanner, M. G., Kluzek, E., Peter, J., Zeng, X. (2010). Technical Description of version 4.0 of the Community Land Model (CLM). NCAR Technical Note NCAR/TN-478+STR, National Center for Atmospheric Research, Boulder, CO, 257 pp.

Oleson, K. W., Lawrence, D. M., Bonan, G. B., Drewniak, B., Huang, M., Koven, C. D., Levis, S., Li, F., Riley, W. J., Subin, Z. M., Swenson, S. C., Thornton, P. E., Bozbiyik, A., Fisher, R., Heald, C. L., Kluzek, E., Lamarque, J.-F., Lawrence, P. J., Leung, L. R., Lipscomb, W., Muszala, S., Ricciuto, D. M., Sacks, W., Sun, Y., Tang, J., and Yang, Z.-L. (2013). Technical description of version 4.5 of the Community Land Model (CLM), NCAR Technical Note NCAR/TN-503+STR, National Center for Atmospheric Research, Boulder, CO, 434 pp.

Orsolini, Y. J., & Nils, G. K. (2009). Role of Eurasian snow cover in wintertime circulation: Decadal simulations forced with satellite observations. *Journal of Geophysical Research Atmospheres*, *114*(19), 1–12. http://doi.org/10.1029/2009JD012253

Overland, J. E., Wood, K. R., & Wang, M. (2011). Warm Arctic-cold continents: Climate impacts of the newly open arctic sea. *Polar Research*, *30*(SUPPL.1). http://doi.org/10.3402/polar.v30i0.15787

Pal, J. S., & Eltahir, E. A. B. (2003). A feedback mechanism between soil-moisture distribution and storm tracks. *Quarterly Journal of the Royal Meteorological Society*, *129*(592), 2279–2297. http://doi.org/10.1256/qj.01.201

Pedersen, C. A., & Winther, J. G. (2005). Intercomparison and validation of snow albedo parameterization schemes in climate models. *Climate Dynamics*, *25*, 351–362. http://doi.org/10.1007/s00382-005-0037-0

Peters, G. P., Andrew, R. M., Boden, T., Canadell, J. G., Ciais, P., Le Quéré, C., … Wilson, C. (2013). The challenge to keep global warming below 2 °C. *Nature Climate Change*, *3*(1), 4–6. http://doi.org/10.1038/nclimate1783

Petoukhov, V., & Semenov, V. A. (2010). A link between reduced Barents-Kara sea ice and cold winter extremes over northern continents. *Journal of Geophysical Research Atmospheres*, *115*(21), 1–11. http://doi.org/10.1029/2009JD013568

Pithan, F., & Mauritsen, T. (2014). Arctic amplification dominated by temperature feedbacks in contemporary climate models. *Nature Geoscience*, *7*(February), 181–184. http://doi.org/10.1038/NGEO2071

Pitman, A. J. (2003). The evolution of, and revolution in, land surface schemes designed for climate models. *International Journal of Climatology*, *23*(5), 479–510. http://doi.org/10.1002/joc.893

Pomeroy, J. W., & Schmidt, R. A. (1993). The use of fractal geometry in modelling intercepted snow accumulation and sublimation. *Proc. 50th Eastern Snow Conf., Quebec City, QC, Canada, ESC*,1–10.

Prentice, I. C., Liang, X., Medlyn, B. E., & Wang, Y. P. (2015). Reliable, robust and realistic: The three R's of next-generation land-surface modelling. *Atmospheric Chemistry and Physics*, *15*(10), 5987–6005. http://doi.org/10.5194/acp-15-5987-2015

Qian, T., Dai, A., Trenberth, K. E., & Oleson, K. W. (2006). Simulation of Global Land Surface Conditions from 1948 to 2004. Part I: Forcing Data and Evaluations. *Journal of Hydrometeorology*, *7*(5), 953–975. doi:10.1175/JHM540.1

Qu, X., & Hall, A. (2006). Assessing Snow Albedo Feedback in Simulated Climate Change. *Journal of Climate*, *19*, 2617–2630. doi:10.1175/JCLI3750.1

Qu, X., & Hall, A. (2007). What Controls the Strength of Snow-Albedo Feedback? *Journal of Climate*, *20*(15), 3971–3981. doi:10.1175/JCLI4186.1

Qu, X., & Hall, A. (2014). On the persistent spread in snow-albedo feedback. *Climate Dynamics*, *42*(1-2), 69–81. doi:10.1007/s00382-013-1774-0

Räisänen, J. (2008). Warmer climate: Less or more snow? *Climate Dynamics*, *30*(2–3), 307–319. http://doi.org/10.1007/s00382-007-0289-y

Randall, D. A., Cess, R. D., Blanchet, J. P., Chalita, S., Colman, R., Dazlich, D. A., … Le Treut, H. (1994). Analysis of snow feedbacks in 14 general circulation models. *Journal of Geophysical Research*, *99*(94), 757–771. http://doi.org/10.1029/94JD01633

Randall, D. A., & Wood, R. A. (2007). Climate Models and Their Evaluation. *In: Climate Change 2007: The Physical Science Basis. Contribution of Working Group I to the Fourth Assessment Report of the Intergovernmental Panel on Climate Change* [Solomon, S., D. Qin, M. Manning, Z. Chen, M. Marquis, K.B. Averyt, M. Tignor and H.L. Miller (eds.)]. Cambridge University Press, Cambridge, UK and New York, NY, USA.

Rayner, N. A., Parker, D. E., Horton, E. B., Folland, C. K., Alexander, L. V., Rowell, D. P., … Kaplan, A. (2003). Global analyses of sea surface temperature, sea ice, and night marine air temperature since the late nineteenth century. *Journal of Geophysical Research*, *108*(D14), 4407. http://doi.org/10.1029/2002JD002670

Rienecker, M. M., Suarez, M. J., Gelaro, R., Todling, R., Bacmeister, J., Liu, E., … Woollen, J. (2011). MERRA: NASA's Modern-Era Retrospective Analysis for Research and Applications. *Journal of Climate*, *24*(14), 3624–3648. http://doi.org/10.1175/JCLI-D-11-00015.1

Rigor, I. G., Colony, R. L., & Martin, S. (2000). Variations in surface air temperature observations in the Arctic, 1979-97. *Journal of Climate*, *13*, 896–914. http://doi.org/10.1175/1520-0442(2000)013<0896:VISATO>2.0.CO;2

Roberts, M. J., Vidale, P. L., Mizielinski, M. S., Demory, M. E., Schiemann, R., Strachan, J., … Camp, J. (2015). Tropical cyclones in the UPSCALE ensemble of high-resolution global climate models. *Journal of Climate*, *28*(2), 574–596. http://doi.org/10.1175/JCLI-D-14-00131.1

Robinson, D. A., Dewey, K. F., & Heim, R. R. (1993). Global Snow Cover Monitoring: An Update. *Bulletin of the American Meteorological Society*, *74*, 1689–1696. http://doi.org/10.1175/1520-0477(1993)074<1689:GSCMAU>2.0.CO;2

Robinson, D. A., & Frei, A. (2000). Seasonal Variability of Northern Hemisphere Snow Extent Using Visible Satellite Data. *The Professional Geographer*, *52*(2), 307–315. http://doi.org/10.1111/0033-0124.00226

Robock, A. (1980). The Seasonal Cycle of Snow Cover, Sea Ice and Surface Albedo.*Monthly Weather Review*, *108*, 267–285. http://doi.org/10.1175/1520-0493(1980)108<0267:TSCOSC>2.0.CO;2

Robock, A. (1983). Ice and Snow Feedbacks and the Latitudinal and Seasonal Distribution of Climate Sensitivity. *Journal of the Atmospheric Sciences*, *40*, 986–997. http://doi.org/10.1175/1520-0469(1983)040<0986:IASFAT>2.0.CO;2

Rodell, M., Houser, P. R., Jambor, U., Gottschalck, J., Mitchell, K., Meng, C.-J., … Toll, D. (2004). The Global Land Data Assimilation System. *Bulletin of the American Meteorological Society*, *85*(3), 381–394. http://doi.org/10.1175/BAMS-85-3-381

Roesch, A. (2006). Evaluation of surface albedo and snow cover in AR4 coupled climate models. *Journal of Geophysical Research*, *111*(August), 1–18. http://doi.org/10.1029/2005JD006473

Rutter, N., Essery, R., Pomeroy, J., Altimir, N., Andreadis, K., Baker, I., Barr, A., et al. (2009). Evaluation of forest snow processes models (SnowMIP2). *Journal of Geophysical Research*, *114*(D6). doi:10.1029/2008JD011063

Saito, K., & Cohen, J. (2003). The potential role of snow cover in forcing interannual variability of the major Northern Hemisphere mode. *Geophysical Research Letters*, *30*(6), 1–4. http://doi.org/10.1029/2002GL016341

Sanderson, B. M. (2011). A multimodel study of parametric uncertainty in predictions of climate response to rising greenhouse gas concentrations. *Journal of Climate*, *24*, 1362–1377. http://doi.org/10.1175/2010JCLI3498.1

Sato, K., Inoue, J., & Watanabe, M. (2014). Influence of the Gulf Stream on the Barents Sea ice retreat and Eurasian coldness during early winter. *Environmental Research Letters*, *9*(8), 84009. http://doi.org/10.1088/1748-9326/9/8/084009

Schaaf, C., Strahler, A., Gao, F. G. F., Lucht, W., Jin, Y. J. Y., Li, X. L. X., … Privette, J. (2002). Global albedo, BRDF and nadir BRDF-adjusted reflectance products from MODIS. *Remote Sensing of Environment*, *2*, 135–148. doi:10.1109/IGARSS.2002.1025877

Schneider, S. H., & Dickinson, R. E. (1974). Climate modeling. *Reviews of Geophysics*, *12*(3), 447. http://doi.org/10.1029/RG012i003p00447

Schmidt, G. A., Ruedy, R., Hansen, J. E., Aleinov, I., Bell, N., Bauer, M., … Yao, M.-S. (2006). Present-Day Atmospheric Simulations Using GISS ModelE: Comparison to In Situ, Satellite, and Reanalysis Data. *Journal of Climate*, *19*, 153–192.

Scinocca, J. F., Kharin, V. V., Jiao, Y., Qian, M. W., Lazare, M., Solheim, L., … Dugas, B. (2016). Coordinated global and regional climate modeling. *Journal of Climate*, *29*(1), 17–35. http://doi.org/10.1175/JCLI-D-15-0161.1

Scott, D., Dawson, J., & Jones, B. (2008). Climate change vulnerability of the US Northeast winter recreation- tourism sector. *Mitigation and Adaptation Strategies for Global Change*, *13*(5–6), 577–596. http://doi.org/10.1007/s11027-007-9136-z

Screen, J. A., Deser, C., Simmonds, I., & Tomas, R. (2014). Atmospheric impacts of Arctic sea-ice loss, 1979-2009: Separating forced change from atmospheric internal variability. *Climate Dynamics*, *43*, 333–344. http://doi.org/10.1007/s00382-013-1830-9

Sellers, W. D. (1969). A Global climatic model based on the energy balance of the earth-atmosphere system. *Journal of Applied Meteorology*, *8*, 392–400.

Seneviratne, S. I., Lüthi, D., Litschi, M., & Schär, C. (2006). Land-atmosphere coupling and climate change in Europe. *Nature*, *443*(7108), 205–209. http://doi.org/10.1038/nature05095

Serreze, M. C., & Barry, R. G. (2011). Processes and impacts of Arctic amplification: A research synthesis. *Global and Planetary Change*, *77*(1–2), 85–96. http://doi.org/10.1016/j.gloplacha.2011.03.004

Shell, K. M., Kiehl, J. T., & Shields, C. A. (2008). Using the radiative kernel technique to calculate climate feedbacks in NCAR's Community Atmospheric Model. *Journal of Climate*, *21*, 2269–2282. http://doi.org/10.1175/2007JCLI2044.1

Shi, H. X., & Wang, C. H. (2015). Projected 21st century changes in snow water equivalent over Northern Hemisphere landmasses from the CMIP5 model ensemble. *The Cryosphere*, *9*(5), 1943–1953. http://doi.org/10.5194/tc-9-1943-2015

Slater, A. G., Lawrence, D. M., & Koven, C. D. (2017). Process-level model evaluation: A Snow and Heat Transfer Metric. *The Cryosphere*, *11*, 989–996. http://doi.org/10.5194/tc-2016-258

Slater, A. G., Schlosser, A., Desborough, C. E., Pitman, A. J., Henderson-Sellers, A., Robock, A., … Zeng, Q. (2001). The Representation of Snow in Land Surface Schemes:

Results from PILPS 2 (d). *Journal of Hydrometeorology*, *2*(1), 7–25. doi:10.1175/1525-7541(2001)002<0007:TROSIL>2.0.CO;2

Smith, T. M., Reynolds, R. W., Peterson, T. C., & Lawrimore, J. (2008). Improvements to NOAA's historical merged land-ocean surface temperature analysis (1880-2006). *Journal of Climate*, *21*(10), 2283–2296. http://doi.org/10.1175/2007JCLI2100.1

Snyder, P. K., Delire, C., & Foley, J. A. (2004). Evaluating the influence of different vegetation biomes on the global climate. *Climate Dynamics*, *23*(3-4), 279–302. doi:10.1007/s00382-004-0430-0

Sobolowski, S., Gong, G., & Ting, M. (2010). Modeled climate state and dynamic responses to anomalous north American snow cover. *Journal of Climate*, *23*(3), 785–799. http://doi.org/10.1175/2009JCLI3219.1

Soden, B., & Held, I. (2006). An Assessment of Climate Feedbacks in Coupled Ocean – Atmosphere Models. *Journal of Climate*, *19*(2003), 3354–3360. http://doi.org/10.1175/JCLI9028.1

Soden, B. J., Held, I. M., Colman, R. C., Shell, K. M., Kiehl, J. T., & Shields, C. A. (2008). Quantifying climate feedbacks using radiative kernels. *Journal of Climate*, *21*(1988), 3504–3520. http://doi.org/10.1175/2007JCLI2110.1

Storck, P., Lettenmaier, D. P., & Bolton, S. M. (2002), Measurement of snow interception and canopy effects on snow accumulation and melt in a mountainous maritime climate, Oregon, United States, *Water Resources Research, 38(11), 1223*, doi:10.1029/2002WR001281

Stroeve, J. C., Kattsov, V., Barrett, A., Serreze, M., Pavlova, T., Holland, M., & Meier, W. N. (2012). Trends in Arctic sea ice extent from CMIP5, CMIP3 and observations. *Geophysical Research Letters*, *39*, 1–7. http://doi.org/10.1029/2012GL052676

Stroeve, J., Holland, M. M., Meier, W., Scambos, T., & Serreze, M. (2007). Arctic sea ice decline: Faster than forecast. *Geophysical Research Letters*, *34*, 1–5. http://doi.org/10.1029/2007GL029703

Strugnell, N. C., & Lucht, W. (2001). An Algorithm to Infer Continental-Scale Albedo from AVHRR Data, Land Cover Class, and Field Observations of Typical BRDFs. *Journal of Climate*, *14*, 1360–1376. doi:10.1175/1520-0442(2001)014<1360:AATICS>2.0.CO;2

Swart, N. C., Fyfe, J. C., Hawkins, E., Kay, J. E., & Jahn, A. (2015). Influence of internal variability on Arctic sea-ice trends. *Nature Climate Change*, *5*(February), 86–89.

Swenson, S. C., & Lawrence, D. M. (2012). A new fractional snow-covered area parameterization for the Community Land Model and its effect on the surface energy balance. *Journal of Geophysical Research: Atmospheres*, *117*(D21). doi:10.1029/2012JD018178

Takala, M., Luojus, K., Pulliainen, J., Derksen, C., Lemmetyinen, J., Kärnä, J.-P., Bojkov, B. (2011). Estimating northern hemisphere snow water equivalent for climate research through assimilation of space-borne radiometer data and ground-based measurements. *Remote Sensing of Environment*, *115*(12), 3517–3529. doi:10.1016/j.rse.2011.08.014

Taylor, K. E. (2001). Summarizing multiple aspects of model performance in a single diagram. *Journal of Geophysical Research*, *106*(D7), 7183–7192. doi:10.1029/2000JD900719

Taylor, K. E., Stouffer, R. J., & Meehl, G. A. (2012). An Overview of CMIP5 and the Experiment Design. *Bulletin of the American Meteorological Society*, *93*(4), 485–498. doi:10.1175/BAMS-D-11-00094.1

Thackeray, C. W. (2014). *Assessing the influence of canopy snow parameterizations on snow albedo feedback in boreal forest regions* (master's thesis). University of Waterloo, Waterloo, Canada. Retrieved from https://uwspace.uwaterloo.ca/bitstream/handle/10012/8430/Thackeray_Chad.pdf?sequence=1

Thackeray, C. W., & Fletcher, C. G. (2016). Snow albedo feedback: Current knowledge, importance, outstanding issues and future directions. *Progress in Physical Geography*, *40*(3), 392–408. http://doi.org/10.1177/0309133315620999

Thackeray, C. W., Fletcher, C. G., & Derksen, C. (2014). The influence of canopy snow parameterizations on snow albedo feedback in boreal forest regions. *Journal of Geophysical Research: Atmospheres*, *119*(16), 9810–9821. doi:10.1002/2014JD021858

Thackeray, C. W., Fletcher, C. G., & Derksen, C. (2015). Quantifying the skill of CMIP5 models in simulating seasonal albedo and snow cover evolution. *Journal of Geophysical Research: Atmospheres*, *120*(12), 5831–5849. http://doi.org/10.1002/2015JD023325

Thackeray, C. W., Fletcher, C. G., Mudryk, L. R., & Derksen, C. (2016). Quantifying the Uncertainty in Historical and Future Simulations of Northern Hemisphere Spring Snow Cover. *Journal of Climate*, *29*(23), 8647–8663. http://doi.org/10.1175/JCLI-D-16-0341.1

Thomas, G., & Rowntree, P. R. (1992). The Boreal Forests and Climate. *Quarterly Journal of the Royal Meteorological Society*, 118: 469–497. doi: 10.1002/qj.49711850505

Thompson, D. W. J., & Wallace, J. M. (1998). The Arctic Oscillation signature in the wintertime geopotential height and temperature fields. *Geophysical Research Letters, 25*(9), 1297–1300.

Thompson, D. W. J., & Wallace, J. M. (2000). Annular Mode in the Extratropical Circulation. Part I : Month-to-Month Variability. *Journal of Climate*, *13*(1999), 1000–1016. http://doi.org/http://dx.doi.org/10.1175/1520-0442(2000)013<1000:AMITEC>2.0.CO;2

Trenberth, K. E., & Fasullo, J. T. (2013). An apparent hiatus in global warming? *Earth's Future*, *1*(1), 19–32. http://doi.org/10.1002/2013EF000165.Received

Turner, J., Connolley, W. M., Lachlan-Cope, T. A., & Marshall, G. J. (2006). The performance of the Hadley Centre Climate Model (HadCM3) in high southern latitudes. *International Journal of Climatology*, *26*(1), 91–112. doi:10.1002/joc.1260

Vaughan, D.G., Comiso, J. C., Allison, I., Carrasco, J., Kaser, G., Kwok, R., Mote, P., Murray, T., Paul, F., Ren, J., Rignot, E., Solomina, O., Steffen K., & Zhang, T. (2013). Observations: Cryosphere. *In: Climate Change 2013: The Physical Science Basis. Contribution of Working Group I to the Fifth Assessment Report of the Intergovernmental Panel on Climate Change* [Stocker, T.F., D. Qin, G.-K. Plattner, M. Tignor, S.K. Allen, J. Boschung, A. Nauels, Y. Xia, V. Bex and P.M. Midgley (eds.)]. Cambridge University Press, Cambridge, United Kingdom and New York, NY, USA.

Vavrus, S., M. M. Holland, A. Jahn, D. A. Bailey, and B. A. Blazey (2012). 21st-century Arctic climate change in CCSM4. *Journal of Climate*, 25, 2696-271. doi:10.1175/JCLI-D-11-00220.1

Verseghy, D., Brown, R., & Wang, L. (2017). Evaluation of CLASS Snow Simulation over Eastern Canada. *Journal of Hydrometeorology*, *18*(5), 1205–1225. http://doi.org/10.1175/JHM-D-16-0153.1

Viovy, N. (2011). CRUNCEP dataset. [Description available at http://dods.extra.cea.fr/data/p529viov/cruncep/readme.htm. Data available at http://dods.extra.cea.fr/store/p529viov/cruncep/V4_1901_2011/].

Voldoire, A., Sanchez-Gomez, E., Salas y Melia, D., Decharme, B., & Cassou, C. (2013). The CNRM-CM5.1 global climate model: description and basic evaluation. *Climate Dynamics*, *40*, 2091–2121. http://doi.org/10.1007/s00382-011-1259-y

Walton, D. B., Hall, A., Berg, N., Schwartz, M., & Sun, F. (2017). Incorporating snow albedo feedback into downscaled temperature and snow cover projections for California's Sierra Nevada. *Journal of Climate*, *30*, 1417-1438. http://doi.org/10.1175/JCLI-D-16-0168.1

Wang, L., Cole, J. N. S., Bartlett, P., Verseghy, D., Derksen, C., Brown, R., & von Salzen, K. (2016). Investigating the spread in surface albedo for snow-covered forests in CMIP5 models. *Journal of Geophysical Research: Atmospheres*, *121*, 1–16. http://doi.org/10.1002/2015JD023824.Received

Wang, X., & Key, J. R. (2005). Arctic surface, cloud, and radiation properties based on the AVHRR polar pathfinder dataset. Part I: spatial and temporal characteristics. *Journal of Climate*, *18*, 2575–2593. doi:10.1175/JCLI3439.1

Wang, Z., Schaaf, C. B., Strahler, A. H., Chopping, M. J., Román, M. O., Shuai, Y., … Fitzjarrald, D. R. (2014). Evaluation of MODIS albedo product (MCD43A) over grassland, agriculture and forest surface types during dormant and snow-covered periods. *Remote Sensing of Environment*, *140*, 60–77. http://doi.org/10.1016/j.rse.2013.08.025

Wang, Z., Zeng, X., Barlage, M., Dickinson, R. E., Gao, F., & Schaaf, C. B. (2004). Using MODIS BRDF and albedo data to evaluate global model land surface albedo. *Journal of Hydrometeorology*, *5*, 3–14. doi:10.1175/1525-7541(2004)005<0003:UMBAAD>2.0.CO;2

Warren, S. G. (1984). Impurities in Snow: Effects on Albedo and Snowmelt. *Annals of Glaciology*, *5*, 177-179.

Warren, S. G., Brandt, R. E., & O'Rawe Hinton, P. (1998). Effect of surface roughness on bidirectional reflectance of Antarctic snow. *Journal of Geophysical Research*, *103*, 25789–25807.

Westerling, A. L., Hidalgo, H. G., Cayan, D. R., & Swetnam, T. W. (2006). Warming and earlier spring increase western U.S. forest wildfire activity. *Science (New York, N.Y.)*, *313*(5789), 940–943. http://doi.org/10.1126/science.1128834

Wetherald, R., & Manabe, S. (1975). The Effects of Changing the Solar Constant on the Climate of a General Circulation Model. *Journal of the Atmospheric Sciences*, *32*, 2044–2059.

Wettstein, J. J., & Deser, C. (2014). Internal variability in projections of twenty-first century Arctic sea ice loss: Role of the large-scale atmospheric circulation. *Journal of Climate*, *27*, 527-550.

Wexler, H. (1953). Radiation balance of the Earth as a factor in climatic change. In: Shapley, H. (ed) *Climatic Change*. Cambridge: Harvard University Press, 73-105, Harvard Univ. Press, Cambridge, Mass.

Winton, M. (2006). Surface albedo feedback estimates for the AR4 climate models. *Journal of Climate, 19*, 359–365. http://doi.org/10.1175/JCLI3624.1

Wiscombe, W. J., & Warren, S. G. (1980). A Model for the Spectral Albedo of Snow I: Pure Snow. *Journal of The Atmospheric Sciences*, *37*(12), 2712–2733.

Xie, S., Ma, H. Y., Boyle, J. S., Klein, S. A., & Zhang, Y. (2012). On the Correspondence between short- and long-time-scale systematic errors in CAM4/CAM5 for the year of tropical convection. *Journal of Climate*, *25*(22), 7937–7955. http://doi.org/10.1175/JCLI-D-12-00134.1

Yao, Y., Luo, D., & Simmonds, I. (2017). Increased Quasi Stationarity and Persistence of Winter Ural Blocking and Eurasian Extreme Cold Events in Response to Arctic Warming. Part I: Insights from Observational Analyses. *Journal of Climate*, *30*, 3549–3568. http://doi.org/10.1175/JCLI-D-16-0261.1

Yeo, S. R., Kim, W. M., & Kim, K. Y. (2017). Eurasian snow cover variability in relation to warming trend and Arctic Oscillation. *Climate Dynamics*, *48*(1), 1–13. http://doi.org/10.1007/s00382-016-3089-4

Zelinka, M. D., & Hartmann, D. L. (2012). Climate feedbacks and their implications for poleward energy flux changes in a warming climate. *Journal of Climate*, *25*, 608–624. http://doi.org/10.1175/JCLI-D-11-00096.1

Zhang, T. (2005). Influence of the seasonal snow cover on the ground thermal regime: An overview. *Reviews of Geophysics*, *43*, RG4002.

Zhang, T., Barry, R. G., Knowles, K., Heginbottom, J., & Brown, J. (2008). Statistics and characteristics of permafrost and ground-ice distribution in the Northern Hemisphere. *Polar Geography*, *31*, 47-68. doi:10.1080/10889370802175985.

Zhao, H., & Fernandes, R. (2009). Daily snow cover estimation from Advanced Very High Resolution Radiometer Polar Pathfinder data over Northern Hemisphere land surfaces during 1982-2004. *Journal of Geophysical Research: Atmospheres*, *114*, 1–14. http://doi.org/10.1029/2008JD011272